MODELLING THE SEASONAL VARIATION OF THE FLORIDA CURRENT

by R.A.Corry B.A.

St.John's College.

A thesis submitted to the Faculty of Physical Sciences for the degree of Doctor of Philosophy in the University of Oxford.

Department of Atmospheric Physics,

Clarendon Laboratory,

Oxford.

June 1985

Abstract:

The linear response of a two layer ocean model to a periodic wind stress curl in the presence of bottom topography has been investigated. For periods much less than the time taken for the wind generated baroclinic Rossby waves to pass over the topography (i.e. 'short' periods), the ocean response is primarily that for a homogeneous ocean and thus strongly modified by topography. For periods much longer than this time (i.e. 'long' periods), the Rossby waves compensate for the effect of topography and the non-topographic Sverdrup balance holds. For the Atlantic at 25°N, the long period limit is of the order of years to decades,so at annual period the non-topographic Sverdrup balance is not applicable. Variations in transport can be forced by a wind stress over varying topography, and by the passage of a coastal baroclinic Kelvin wave over varying topography.

The relative importance of the above dynamical considerations for the Florida Current can only be determined from a model calculation involving realistic winds, topography and geography. Such a model calculation has been done with observed Bunker wind stress over a two layer ocean. The predicted variation has a Summer maximum and a Fall minimum, in agreement with the measurements of Niiler and Richardson [1973] and more recent STACS data.

The one layer model has been forced by monthly means of ATOLL wind stress for the years 1981-1984. The predicted variation was found not to be in agreement with concurrent STACS measurements. A comparison was made between the Bunker winds and

the ATOLL winds via various diagnostics. It was found that the meridional component of the wind, which is crucial to the overall Bunker Summer maximum, is of much reduced importance for the ATOLL winds. This could account for the lack of predicted Summer maxima.

Acknowledgements

I would like to thank Dr.F.W.Taylor for accepting me as a N.E.R.C research student.

I am particularly grateful to my supervisor, Dr.D.L.T.Anderson, for his constant help, advice and encouragement, and for reading this thesis and suggesting improvements.

I would like to thank Mr.R.J.Wells for his invaluable assistance with computing problems.

Financial support was given by the National Environment Research Council and St.John's College, to whom I am grateful.

Contents

CHAPTER ONE

Introduction

1.1: The Florida Current

1.1.1 Introduction.

The Florida Current is a part of the Gulf Stream system, and flows through the Florida Straits. The Gulf Stream is downstream of the Florida Current, and extends to the tail of the Grand Banks. Farther downstream is the North Atlantic Current, which reaches across the rest of the north Atlantic. These and other surface currents of the North Atlantic are shown on a schematic chart (Fig 1.1). The factor that distinguishes the Florida Current and the Gulf Stream from the other currents on Fig 1.1 is their intensity. The surface flow of the Florida Current can reach over 2 m/s. This intensity is due to the rotation and spherical nature of the earth (Stommel [1948]). The winds force a meridional transport over mid-ocean, and the return flow flows as an intense western boundary current.

The true reasons for the existence of intense western boundary currents were not known until this century, and from the discovery of the Florida Current in 1513 to the present day many theories have been advanced as explanations. Some of these theories, together with an historical introduction, are in the first chapter of Henry Stommel's book 'The Gulf Stream', and will not be reproduced here.

The measured vertically integrated transport (the transport)

through the Florida Straits provides a test for theories of the transport of western boundary currents. Most importantly, it is relatively easy, although still difficult, to measure (maximum depth is about 800 m, compared to a depth in the Gulf Stream area of about 4000 m). The transport is also well defined, since there is land both sides of the current. The transport of the Florida Current has therefore been measured over the years, both directly and indirectly, so that there is now a large data base, with a well defined mean transport, and rather less well defined variations about the mean which nevertheless display features which require explanation. It is the purpose of this thesis to explain the physics behind the Florida Current transport variations. This chapter continues with the direct transport measurements of Niiler and Richardson [1973], and then gives the main results to date of the STACS measurement program.

1.1.2 The direct technique of transport measurement.

Consider an instrument that falls freely to a preselected depth, where it releases its ballast weights and returns to the surface under its own buoyancy. If the speeds of rise and fall are constant (not necessarily equal), and if stationary conditions over the time and space intervals of the instruments fall and rise are assumed, it is easily shown that, for any distribution of horizontal water velocity $\underline{v}$ with depth, z,

$$\underline{T} = \int_0^D \underline{v}\, dz = \underline{R}D/t$$

where $\underline{T}$ is the transport per unit width to depth D, $\underline{R}$ is the horizontal separation of the drop and surfacing points, and t is the total time of the run. It is clear that this type of

Fig 1.1 Chart showing the chief features of the surface-water circulation of the North Atlantic. In general, the chart is much oversimplified, and it should be regarded as essentially schematic. (From 'The Gulf Stream' by H.Stommel).

Fig 1.2
Station locations.
From Niiler and Richardson [1973].

measurement will be neither instantaneous in time nor localised at a point in space.

The transport can then be measured with an instrument that attains terminal velocity within a few meters after release, records pressure (depth) internally as a function of time, and casts off ballast at the bottom (or some prescribed mid-depth) by means of a release mechanism. Of course , the instrument must be used with a navigation system that is capable of measuring the horizontal deflection to the desired accuracy. The navigation system, the instrument, and the analysis of the data are described in greater detail in Richardson and Schmitz [1965].

1.1.3 The seasonal variability of the Florida Current.

The seasonal variability of the transport of the Florida Current was investigated by Niiler and Richardson [1973] using their direct technique of transport measurement. The surface current, the average horizontal velocity to a number of depths, and a record of temperature versus depth were obtained at 13 closely spaced stations along the transect from Miami to Bimini (Fig 1.2). Ninety transects of the Florida Current were made over a period of seven years [1964-1971] to measure both the mean and seasonal variation of the transport. The maximum measured value was 38.2 Sverdrups, in the Summer of 1965, and the minimum value was 19 Sverdrups, in the Winter of 1970. The mean transport was found to be 29.5 Sverdrups, and the values of northward transport in several series of cruises are plotted in Fig 1.3.

Niiler and Richardson fitted the annual harmonic to the data and found an amplitude of 4.1 Sverdrups with a maximum in early June. Although a harmonic was fitted to the data, the annual

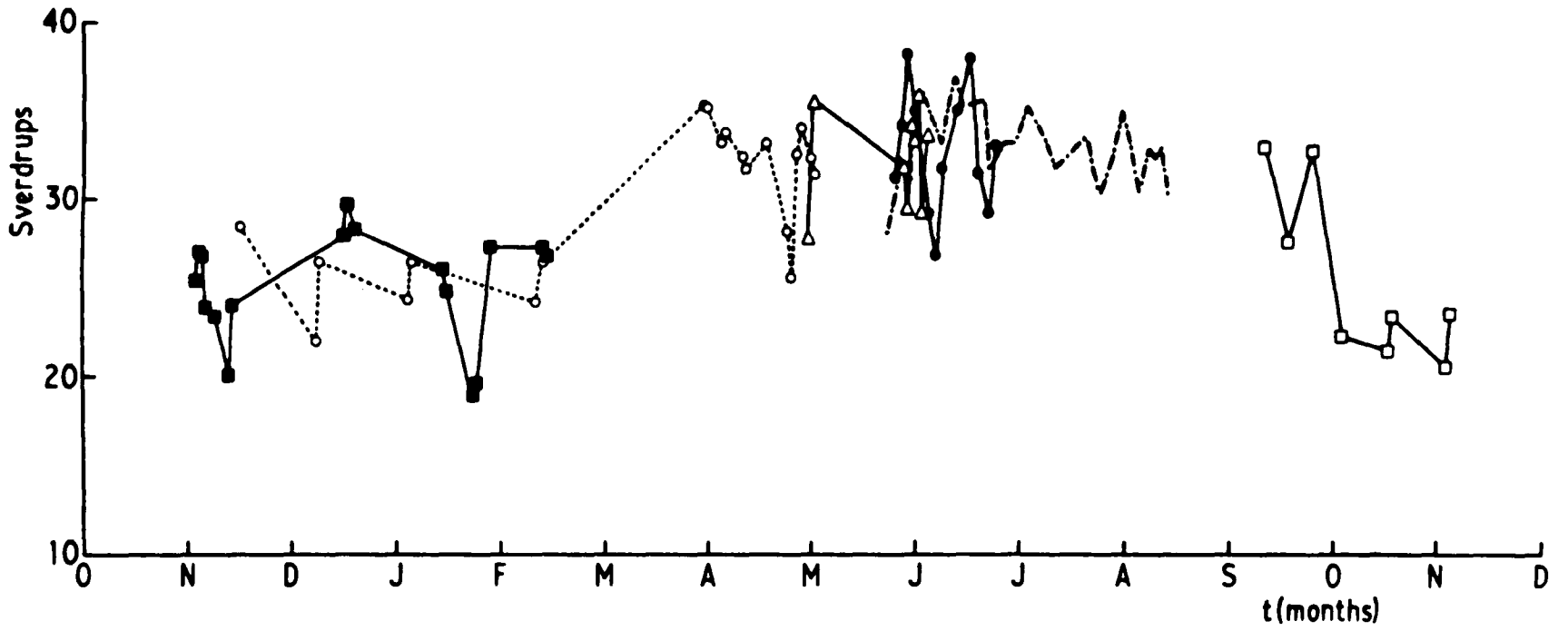

Fig 1.3 A replot of the Niiler and Richardson [1973] data aimed at visually maximising the seasonal effect. Later data from Brooks [1979] are also included on the dot-dash line. The other symbols correspond to data sequences. The labels on the time axis correspond to the beginning of each month.

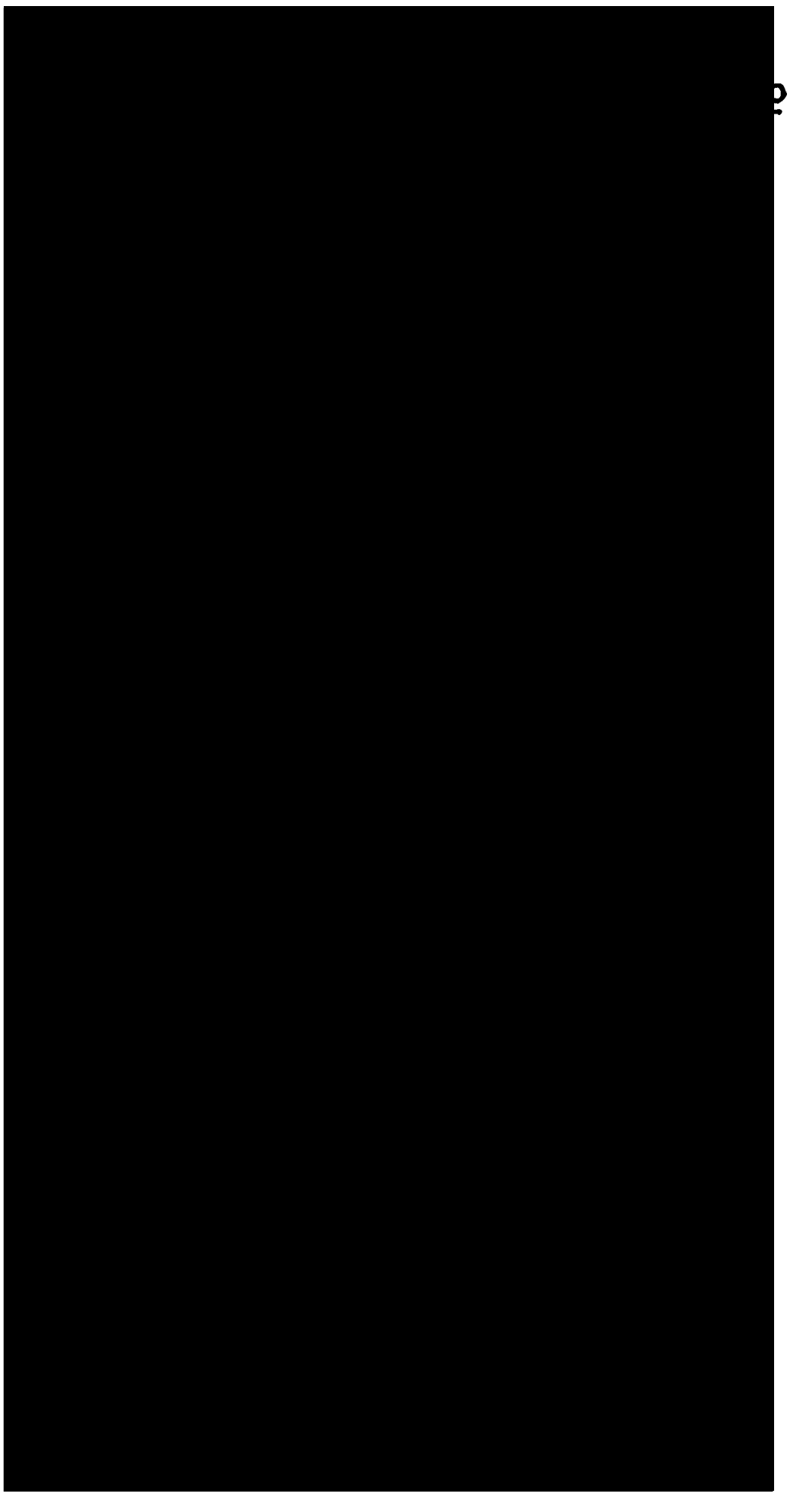

Fig 1.4 Velocity structure (northward component, cm/sec): Summertime (a), and Wintertime (b). From Niiler and Richardson [1973].

variation is not necessarily of this form. The Summer maximum can be seen on Fig 1.3, which also includes measurements made by Brooks [1979] during July and August (the dot-dash line).

Variations with depth:

Figs 1.4(a) and 1.4(b) show, respectively, the early Summer and early Winter seasonal pattern of the northward flow in vertical cross-section. A detailed comparison of the distribution of the northward component of velocity with depth has also been made from three stations. Fig 1.5 shows the seasonal contrasts of northward velocity at stations 5, 8, and 12 (solid lines for Summer, dashed lines for Winter). The most remarkable feature of the pattern is apparent at stations 8 and 12: the seasonal changes in the northward component of the velocity below the mixed layer are independent of depth. It is shown in Niiler and Richardson [1973] that the seasonal changes in the transport of the Florida Current penetrate to the bottom, while the changes in the density field are confined primarily to the upper 100 m of the water column.

1.1.4 The Sverdrup theory

We have seen that the seasonal variation of the Florida Straits transport is small ($\pm$ 4 Sverdrups) compared to the mean (30 Sverdrups). The variation also appears to have a Summer maximum. Neither of these features is reproduced by the simplest theory of transport generation, i.e. the Sverdrup theory. This theory states that:

$$\beta \frac{\partial \Psi}{\partial x} = \mathrm{curl}_z(\underline{\tau})$$

Fig 1.5 Northward velocity versus depth at stations 5, 8, and 12: Summer, solid line; Winter, broken line. From Niiler and Richardson [1973].

Fig 1.7 Mean downstream currents (in cm/sec) for June to December 1982; dots indicate current meter positions. From Lee, Schott and Zantopp [1985].

where β has its conventional meaning, Ψ is the mass transport stream function, x is the eastward coordinate, z is the vertical coordinate and τ is the wind stress. This balance applies in mid-ocean away from large currents, and leads to a southward transport in mid-ocean for the North Atlantic subtropical gyre. This is then closed by a western boundary current with northward transport, such as the Florida Current and the Gulf Stream.

Application of the Sverdrup theory using the mean wind stress leads to a prediction of mean transport. At the latitude of the Florida Straits the prediction is about thirty Sverdrups, in line with the transport measurements of Niiler and Richardson [1973]. However, in the Gulf Stream region, transports of over 100 Sverdrups have been measured, whereas the Sverdrup transport is still about thirty Sverdrups. This is a large discrepancy which is not yet fully understood, but a full explanation is likely to include the effects of bottom torques (Holland and Hirschman [1972]) and eddy driven mean flows (Holland and Rhines [1980]). However, the circulation of the North Atlantic subtropical gyre can be understood in terms of a basin scale gyre which is concentrated in the upper few hundred metres, and which contains the Sverdrup transport (about thirty Sverdrups), and a smaller deep gyre in the North-West Atlantic which accounts for all the increase in transport of the Gulf Stream, but which is driven by processes other than the wind stress curl. This is the approach taken by Leetmaa, Niiler and Stommel [1977], who conclude that the Sverdrup relationship does account for the mid-Atlantic circulation.

When, however, the Sverdrup relationship is applied to the monthly mean wind stresses, it is found (Leetmaa and Bunker [1978]) that the maximum predicted transport occurs in the Winter, with a minimum in the Fall, and that the amplitude of the

variation exceeds 15 Sverdrups. As we have seen, the actual maximum occurs during the Summer, and the amplitude of the measured seasonal variation is much smaller (about 4 Sverdrups). The Sverdrup relationship thus appears to apply for the mean flow of the Florida Current (Leetmaa, Niiler and Stommel [1977]), but not for the seasonal variation. It is the purpose of this thesis to investigate the dynamics which do apply for the seasonal variation, and to explain the apparently anomalous nature of the seasonal signal of the Florida Current.

1.2: The STACS measurement program

1.2.1 Introduction

The following description of the objectives and results to date of the STACS program comes from a series of reports published in Science for the week beginning Jan 18 1985. The main results are included in this chapter because of their particular relevance to the model calculations of Chapter 5, where a comparison of model results with STACS data is attempted.

The Subtropical Atlantic Climate Studies (STACS) program was conceived to increase our understanding of oceanic circulation and its role in establishing global climate (Molinari et al [1985]). The initial objectives are to develop the capability to monitor the annual cycle and interannual variability of the volume and temperature transport of the Florida Current and to understand the relation of the Current's variability to regional and basinwide circulation patterns (that is, is the Florida Current volume transport an important 'index' for basinwide air-sea interaction?)

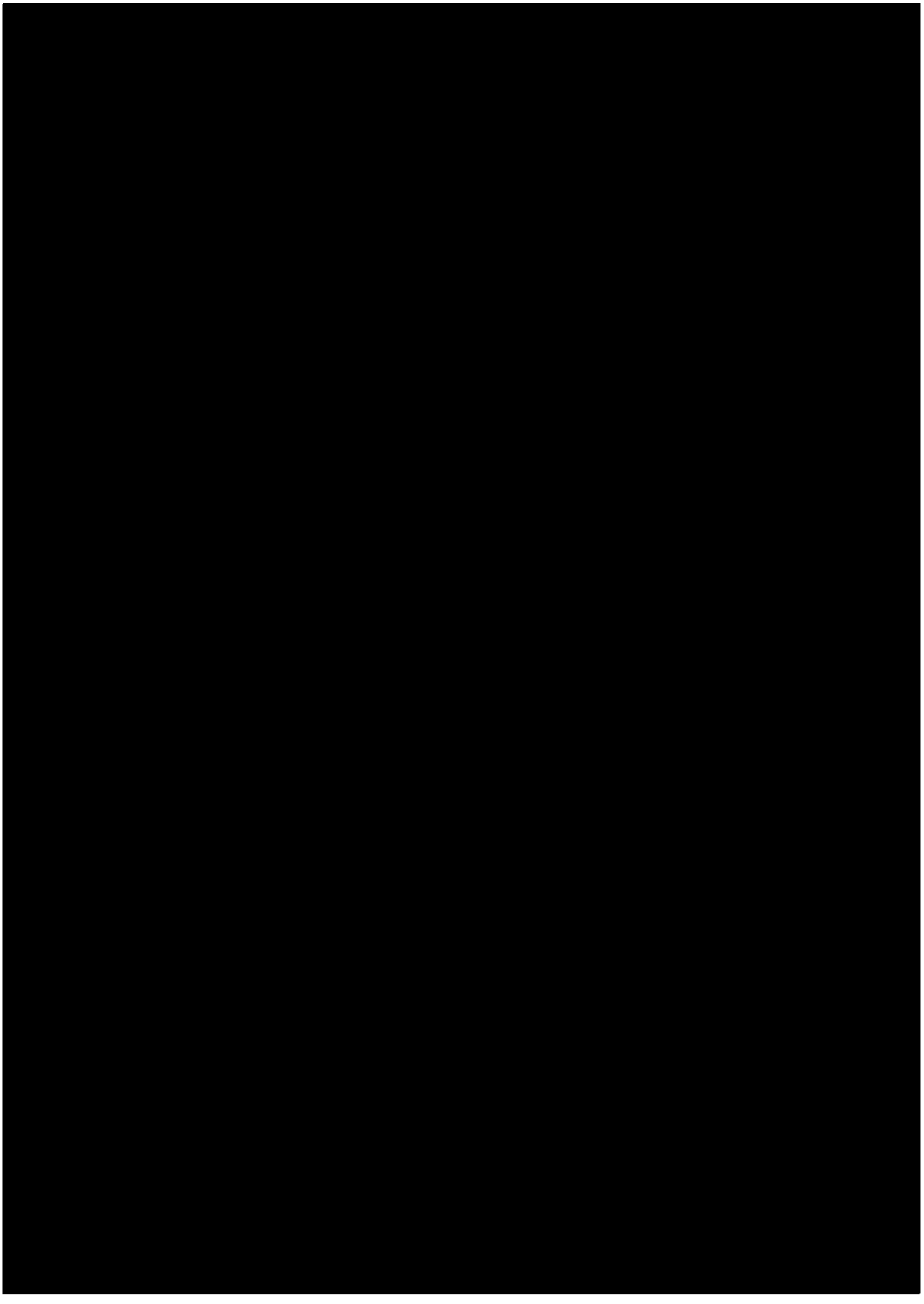

Fig 1.6 Distribution of sampling strategies in the Straits of Florida. The insert shows how the direct observations were used as standards to verify and calibrate the indirect techniques. From Molinari et al [1985].

To meet the initial objectives of STACS of developing a Florida Current monitoring scheme in the Straits of Florida, a two year intensive observing period was initiated in April 1982. Both direct and indirect observing systems were deployed to determine which system or mix of systems will provide the most accurate and efficient monitoring array. The location of all the systems is shown in Fig 1.6.

Direct observations of Florida Current temperature and volume transport were provided by ship-deployed current profilers and moored current meter arrays. Profilers provide fine resolution of temperature and horizontal velocity components in the vertical, but coarse resolution in time and horizontal space. These measurements represented the primary standard against which other systems were verified and calibrated. Data from current meters are frequent in time but sparse in the vertical and horizontal. In particular, because of technical limitations, current meters cannot be placed near the surface in the Florida Current. Thus an algorithm was required to obtain total water column transport from these data. However, once an algorithm is developed, the current meter data can provide a valuable secondary standard for verifying and calibrating the indirect techniques.

The indirect systems include coastal tide gauge stations, bottom pressure gauge arrays, a submarine cable that measures potential difference across the Straits of Florida, acoustic arrays that measure travel times between sources and receivers, and radar installations that measure surface currents. The utility of these systems is a function of how well the observed variable tracks either mass or temperature transport as determined by comparison with the direct observations. In what follows, the profiler, current meter, submarine cable and tide

gauge data are considered with emphasis on the volume transport observations. The results presented by Molinari Wilson and Leaman [1985], Lee, Schott and Zantopp [1985], Larsen and Sanford [1985] and Maul, Chew, Bushnell and Mayer [1985] show for the first time that submarine cable, coastal tide gauge and bottom pressure gauge data can provide calibrated and continuous observations of Florida Current volume transport. Because the cable measures volume transport with an apparent error of less than one Sverdrup, the cable will provide the foundation for an ongoing monitoring effort. Coastal tide gauge data obtained as part of the United States national tide gauge network will also be analysed as part of a transport monitoring effort to provide an independent backup data source. Consequently direct observations may be phased out.

1.2.2 The PEGASUS transport measurements.

Vertical profiles of horizontal velocity components and temperature were collected with a current profiler called Pegasus (Spain, Dorson and Rossby [1981]). A series of nine Pegasus stations is maintained across the Straits of Florida at 27°N (Fig 1.6). Data from nine cruises were analysed in Molinari, Wilson and Leaman [1985]. The typical cruise length was 8 to 14 days. A complete crossing of the section typically required 16 hours. Sampling and instrument errors are present in the various transport estimates. Maximum uncertainties in the total transport are estimated as about 2.5 Sverdrups (Molinari, Wilson and Leaman [1985]). However, as noted by Larsen and Sanford [1985] comparisons of Pegasus and cable estimates of transport suggest that the actual errors are probably of the order of one Sverdrup. The mean annual transport values observed during 1982

and 1983 are, within these uncertainties, equivalent to the mean annual transport given by Niiler and Richardson [1973]. The seasonal pattern of transports during 1982 and 1983 is similar to the climatological pattern in that highest transports occur in the late Spring and early Summer and lowest transports in the late Fall and early Winter (see Fig 1.8).

1.2.3 Transport measured by moored current meters

The current meter array consisted of five moorings deployed in a saw-toothed pattern (Fig 1.6) between West Palm Beach, Florida, and the Bahamas, bracketing the submarine cable used by Larsen and Sanford [1985]. The first array (STACS-I) was deployed in April 1982 and was maintained for two months. In this array, the top instruments were at 50 m for the western station, mooring 146; at 150 m for moorings 147 and 148 and at 100 m for the two eastern stations, moorings 149 and 150. In subsequent arrays (STACS-II from June to December 1982 and STACS-III from February to June 1983) the depth of the top instrument at the western station was increased to 100 m because of extreme wear on this mooring during STACS-I.

A total of 25 current meters was deployed in each of the moored arrays. The instrument configuration for STACS-II is shown on Fig 1.7, superimposed on the mean downstream flow derived from the current meter data.

For the transport calculations, the northward current components were first filtered with a 40-hour Lanczos low-pass filter, which effectively removed the tides and other high frequency fluctuations. There are three problems in determining transports from the five moored stations. (i) The current meter moorings covered only part of the water column, and current

Fig 1.8 Time series of transports determined from the five moorings (solid line), from cable voltages calibrated by Pegasus (dashed line), and from Pegasus sections (dots). From Lee, Schott and Zantopp [1985].

Fig 1.9 (a) Annual cycles of sea-level differences: line A1, Bimini to Miami (1965 to 1972); line A2, Cat Cay to Miami (1938 to 1941, 1950 to 1951). (b) Annual cycles: curve 1, STACS transports from moored current meter measurements (with standard deviations of the monthly means), the gap in December to February was filled with STACS cable transports; curve 2 cable voltages for 1970 to 1972. From Schott and Zantopp [1985].

profiles had to be extrapolated to the surface and bottom. (ii) Mooring tilt due to current drag resulted in varying instrument depths. (iii) With only five stations, the resolution across the Florida Current was quite coarse; two of the stations were displaced upstream by about 20 km.

The mooring motion problem turned out to be not as severe as expected. Standard deviations of the instrument depths were less than 5 m. These depth changes were accounted for by using the pressures recorded to determine the actual depth of the individual current measurements.

Pegasus and current meter profiles of downstream velocities show near linear distributions over most of the Florida Current, except for the eastern site where a subsurface maximum and reversal of the velocity gradient in the vertical is often observed at about 250 m (Fig 1.7). Therefore, several simple schemes were tried to extrapolate the current to the surface and bottom. The method that gave the best results in comparison with Pegasus transports was to linearly interpolate between the measured downstream velocities at the different depths and zero at the bottom and extrapolate a linear fit to the surface. This technique was used for the four western moorings. For the eastern mooring, the linear gradient was extrapolated to the surface if no gradient reversal occurred; otherwise, the gradient reversal determined from Pegasus data was used for the upper level. The surface velocities determined by vertical extrapolation at each mooring site were used to estimate the surface velocities at the western and eastern boundaries by horizontal linear extrapolation. The boundary surface velocities were linearly decreased to zero at the bottom. Total volume transport was then determined by integration in the x and z directions of the extrapolated vertical velocity profiles at each

mooring plus the boundaries.

The transport time series derived from moored current meters is shown in Fig 1.8 for April 1982 to June 1983, together with the Pegasus transports and those derived from the cable voltages. More recent (unpublished) STACS transport data are shown in Fig 5.2.

Neither the moored current meter transports nor the cable transports show a simple sinusoidal annual cycle. Rather, the continuous measurements show an event dominated record with large transport bursts in August 1982 and May 1983 lasting less than 1 month and several minima occurring in the Fall and Winter. Monthly averages of the current meter derived transports for the 14-month transport time series are shown in Fig 1.9(b), together with sea level data in Fig 1.9(a). These data reveal the significant asymmetry of the annual cycle as found in historical cable voltages and sea level differences across the Straits of Florida, which show a maximum in July-August and a minimum in October-November. The annual mean transport for May 1982 to April 1983 is 30.1 Sverdrups with a standard deviation of 3 Sverdrups in good agreement with historical estimates for the Florida Straits (Niiler and Richardson [1973]).

1.2.4 Volume transport from Voltage measurements

A considerable volume of submarine cable measurements predates the more modern direct observations. Wertheim [1954] observed the potential differences between Key West, Florida, and a site outside Havana, Cuba. After early attempts to interpret the potential differences in terms of volume transport, it has been concluded that much of the fluctuation in potential is due to lateral shifts of the axis of the current over variable bottom

topography (Schmitz and Richardson [1968]) and aliased geomagnetic interference. Based on this experiment, the motional induction approach using long submarine cables has largely been discredited.

The measurements of Larsen and Sanford [1985] were on a submarine cable between Jupiter, Florida and Settlement Point, Grand Bahama Island (Fig 1.6). In contrast to the previous measurements between Key West and Cuba, these measurements were obtained in a region of the Florida Current that is more stable (having less lateral or cross-stream movement), flowing in a channel of more rectangular cross-section. Hence, these observations can be more accurately interpreted in terms of transport.

The theory of motional induction as relevant to cable measurements is presented by Longuet-Higgins [1949] and Longuet-Higgins et al [1954]. The principal theoretical approach was to model channels as having elliptical cross-sections overlying a subfloor structure of uniform electrical conductivity. Both this model and the rectangular channel, nonconducting bottom model of Malkus and Stern [1952] predict a voltage to transport relation of the form:

Eq 1.1 $$T = h \, \Delta V / E_z$$

where h is the equivalent depth, T is the transport, Δ V is the voltage difference and $F_z = -0.42 \times 10^{-4}$ tesla is the vertical component of the earth's magnetic field. The equivalent depth is dependent on real depth, channel width, seawater and seabed conductivities, and the spatial distribution of current in the channel. It may be thought of as the depth of the channel plus the thickness of the sub-bottom layer normalised to be

electrically equivalent to a layer of sea water averaged across the channel.

That the conductivity of the sea bottom can be important is clearly revealed by the measurements of Sanford [1982]. These show that the equivalent depth h is about twice the mean depth. Such large bottom conductances were not expected. It is important to emphasise that a large bottom conductance not only reduces the induced signal strength (a disadvantage) but also reduces the effects of lateral shifts of the stream over the channel depth (an advantage).

Because the cable used is now broken, there is a constant offset voltage B to account for differences in contact potential between the cable ends, and Eq 1.1 becomes:

Eq 1.2 $$T(t)=h[\Delta V(t) + B]/F_z$$

where t is time. Although this equation is found to be appropriate in the present case, this form is not generally valid (Sanford [1982]). The principal reasons for the validity of Eq 1.2 are discussed in a footnote of Larsen and Sanford [1985], but they include the absence of significant lateral current shifts and downstream variations (on the scale of the channel width), a favourable lateral distribution of the bottom conductance, and a nearly constant temperature distribution.

The cable record has been corrected for abrupt offsets in the voltage that have occurred intermittently since March 1983 and for tidal and geomagnetic fluctuations. The transport values estimated from the Pegasus profiling data and the cable voltages are compared in Larsen and Sanford [1985]. The root-mean-square deviation is 0.67 Sverdrups, which is 2.2 percent of the mean, and the correlation is 0.97. This shows that the cable voltages

track the day to day fluctuations of the Florida Current transport.

1.2.5 Sea level variation as an indicator of Florida Current Volume transport

Sea level slope is an indirect but generally accepted first order measure of ocean surface current velocity in extratropical regions. The basis for this measure is the relationship:

$$f(V - V_a) = g \frac{dh}{dx}$$

in which V is the northward surface velocity, V_a is the ageostrophic surface velocity and includes temporal and frictional effects, g is gravity, f is the Coriolis parameter, dh is the differential height of the sea above an equipotential surface, and dx is the differential east-west dimension. The average surface current across a section is:

$$\langle V \rangle = \Delta\, hg/fL + \langle V_a \rangle$$

where L is the width of the section at the surface and Δ h is the difference in the sea level height.

The extent to which the volume transport is reflected by the sea level height depends on the vertical structure of the velocity, and ageostrophic effects. If the variations of velocity are depth independent, and ageostrophic effects are unimportant, then the sea level difference will accurately reflect transport variations. It is shown by Maul et al [1985] that the processing of sea level values across the Straits of Florida to give monthly means is by itself an inadequate measure

of the Florida Straits transport variations. Cat Cay Sea Level - Miami Sea Level (Fig 1.6) has a correlation with directly measured transport of only 0.67 for 73 pairs of observations. This is much inferior to the cable transports above. Along Straits sea level difference as estimated by Key West Sea Level - Miami Sea Level, with 81 pairs and a correlation of 0.46, appears to be the least correlated with transport of all the traditional indicators (We would expect a relationship between sea level at these stations due to the Bernoulli effect (Montgomery [1941])). On the basis of these results, sea level measurements should only be used as a backup source of information.

1.3: Conclusion

Both a recent measurement program (STACS) and older direct measurements (Niiler and Richardson [1973]) show a Summer maximum in the transport through the Florida Straits, as part of an annual variation in transport which is of much lower amplitude and almost opposite phase to predictions based on Sverdrup theory. The Sverdrup theory, however, appears to be consistent with the mean transport of the Florida Current (Leetmaa, Niiler and Stommel [1977]). The difference in the dynamics between the seasonal variations of transport and the mean transport will be addressed in this thesis.

CHAPTER TWO

Most of this chapter is written up in Anderson and Corry [1985a]*

General theory

2.1: Introduction:

The motivation behind this thesis is the explanation of the apparently anomalous seasonal variation of the Florida Current, which has a far lower amplitude than one would expect from the Sverdrup balance (Niiler and Richardson [1973]). The transport of the Florida Current also has a maximum in summer (Niiler and Richardson [1973]), again contrary to expectations based on the Sverdrup balance. It therefore appears that the Sverdrup balance does not hold for the seasonal variations. The mean transport of the Florida Current, however, (about 30 Sverdrups) appears to be in remarkably good agreement with expectations based on integration of the wind stress curl (Leetmaa, Niiler and Stommel [1977]). This suggests that a normal Sverdrup balance may hold for the mean circulation. Anderson, Bryan, Gill and Pacanowski [1979], have examined the mechanisms by which the mean circulation is established and showed that initially the response is barotropic, and does not satisfy the normal (i.e. non-topographic) Sverdrup balance. It is only after a long time, when internal Rossby waves have crossed the basin, that the Sverdrup balance is established, the balance largely verified by Leetmaa et al [1977].

The theory of the seasonal variability in the open ocean has been studied by Veronis and Stommel [1956] and Gill and Niiler [1973]. They point out that the response to seasonal winds is

* Anderson, D.L.T. and R.A. Corry [1985a] Prog. Oceanogr., 14, 197 40

primarily barotropic for regions north of 30°N. In this chapter we study various processes affecting the transport of a western boundary current as a result of periodic forcing. In particular it is shown that a Sverdrup balance is unlikely to hold at annual period, and that much of the variability of the Florida Current could be barotropic. Although the problem was motivated by the seasonal variations of the Florida Current, the work reported here is of a more general nature. Subsequent chapters consider the Florida Current in particular.

In Section 2.2, results from a simple two layer model where north-south variations are treated as periodic are presented, and the boundary response is examined as a function of forcing period. It is shown that seasonal variations in western boundary current transport could be primarily barotropic for the North Atlantic. In Section 2.3, a basin model which is still two layer is used to confirm the above result and consider further the nature of the boundary response. In Section 2.4, the influence of islands on the transport variations of a western boundary current is considered, and it is shown that both islands and strong north south topography to the east of the western boundary current can act as spatial filters for seasonal variations. Finally Section 2.5 deals with fluctuations in transport generated by Kelvin waves passing over variable topography. It is shown that for variations in meridional transport the sign of the north-south gradient of bottom topography greatly influences the character of transport variations thus forced.

2.2: The two layer one dimensional model.

2.2.1 Description of the model

In this section a simple model which involves variation with longitude x will be described and results presented to show how the western boundary transport is influenced by topography and period of the forcing. The forcing is by the zonal wind stress which can be explicitly a function of longitude, but is periodic in latitude (y) (wavelength $2\pi/l$) and in time (period $2\pi/w$). The topography can vary with x, but not with y.

The vertical structure consists of two layers (see Fig B1) but it is convenient to split the vertical structure into two modes, a barotropic and a baroclinic mode, represented by the zonal velocities $\bar{u}$ and $\hat{u}$ respectively. These are defined as the modes one would expect in the absence of topography.i.e.:

$$\bar{u} = u_1 + u_2 H_2/H_1$$

$$\hat{u} = u_1 - u_2$$

where the subscripts 1 & 2 refer to the upper and lower layers, and H_1 and H_2 are the mean depths of these layers. The nondimensional form of the equations used is (Anderson and Killworth [1977]):

Eq 2.1

$$(\bar{u}_{xx} - \Lambda_0 \bar{u})_t + \bar{u}_x + T\hat{u}_t/(1-T) - iT_x(\bar{u}-\hat{u})/\epsilon(1-T) + K\bar{u}_{xx} = F\sin(wt)$$

Eq 2.2 $$(\hat{u}_{xx} - \Lambda_1 \hat{u})_t + \hat{u}_x - i\delta T_x(\hat{u}-\bar{u})/\epsilon(1-T) + K\hat{u}_{xx} = F\sin(wt)$$

The method by which these coupled equations are solved is given in Appendix A. In deriving these equations it has been assumed

that the forcing period is >> 1/f , and so gravity waves have been filtered out. f and β have their conventional meanings, x,y have been nondimensionalised by L, t by $(\beta L)^{-1}$, T by H_2, $\bar{u}$ and $\hat{u}$ by $-X_0 L l^2 (\beta H_1)^{-1}$, L is the half width of the basin, X_0 is a typical wind stress magnitude, F sin(wt) is a time dependent forcing term and T is the topography.The nondimensional parameters are $\epsilon = \beta / f l$, $\delta = H_1 / H_2$. The parameters Λ_0 and Λ_1 are given by:

$$\Lambda_0 = (Ll)^2 + f^2 L^2 / g(H_2 - T) \cong (Ll)^2 \sim 10$$

$$\Lambda_1 = f^2 L^2 / g' H_1 + (L1)^2 \cong f^2 L^2 / g' H_1 >> 10$$

If we take $f = 6 \times 10^{-5}$ s^{-1} ; $\beta = 2 \times 10^{-11}$ m^{-1} s^{-1} ; g=9.81 m s^{-2} ; g' =0.03 m s^{-2} ; H_1 = 100 m; H_2 =4000 m; L=2000 km; $l = 2\pi/(4000$ km) then ϵ =0.212; δ =0.025; $\Lambda_0 \cong 10$; $\Lambda_1 \cong 4800$.

2.2.2 Results

Eq 2.1 shows that the barotropic mode feels topography directly, as well as indirectly through the two baroclinic terms i.e. those terms involving $\hat{u}$. Baroclinic motion can therefore alter the barotropic response. By contrast, the effect of the barotropic mode on the baroclinic mode is much weaker because of the $\delta = H_1 / H_2 << 1$ factor in 2.2.

The value of κ used is 0.02. The effect of bottom friction on the quasi-steady response of a barotropic ocean in the presence of topography has been investigated by Schulman and Niiler [1970]. The effects of friction will not be investigated in this section however, since it is the qualitative influence on transport of the time dependent baroclinic mode over topography which is of interest here.

The large value of Λ_1 compared to Λ_0 means that the adjustment of the baroclinic mode will be very different from

that for the barotropic mode (Veronis and Stommel [1956]). When topography is present the western boundary transport responds differently to low and high frequency forcing. In the case of a very low frequency forcing ($w \to 0$), Eqns 2.1 and 2.2 both have a steady solution $\bar{u}_x = F$, $\hat{u}_x = F$ i.e. they have the same Sverdrup balance. This implies $u_2 = 0$, all flow is concentrated in the upper layer and the effect of topography is negligible. This balance is over-simple, and we need not expect it to apply rigorously in the real ocean. Nonetheless Leetmaa et al [1977] have made essentially this approximation for the steady solution and shown that it appears to work remarkably well. The mechanism by which the balance $\bar{u}_x = F$, $\hat{u}_x = F$ is established has been studied by Anderson, Bryan, Gill and Pacanowski [1979] and Anderson and Killworth [1977]. It involves the propagation across the basin of long baroclinic Rossby waves generated either in the ocean interior or at the eastern boundary. The time for baroclinic Rossby waves to cross the basin is (from Eq 2.2) $2\Lambda_1$. One might estimate therefore that if the period of the waves was such that a Sverdrup balance could be established across the basin within a fraction of a period of the forcing, then the baroclinic response would substantially affect the barotropic response. This suggests that low frequency means that the period of the forcing be substantially greater than $2\Lambda_1$. If the time dependent part of the wind stress is located in the western part of the basin then compensation will be possible at shorter periods since then the waves have to travel only from the eastern edge of the forcing, not the eastern boundary.

If the period of the forcing is short (but longer than that required to establish a barotropic Sverdrup balance) then the baroclinic mode will not affect the barotropic, and the barotropic response will be strongly influenced by topography.

In fact as noted above it is not until the period becomes comparable with Λ_1 that the baroclinic mode becomes big enough to affect the barotropic, so for a large range of periods, the response is likely to be barotropic.

To test the above ideas Eqs (2.1) and (2.2) were integrated first for a flat bottomed ocean and then with topography of the form:

$$T=0.75e^{-10(x+1)^2} \qquad -1 < x < 1$$

representing a western slope as shown in Fig 2.1(a). The forcing used is of the form $F(x)=1$ for $0<x<1$ and $F(x)=0$ for $-1<x<0$. Fig 2.2(a) shows the response to steady forcing for a homogeneous ocean with the above topography. What is plotted is $\tilde{u} = u_1 + (H_2-T)u_2/H_1$, the zonal transport, but because $-H_1\tilde{u} = \psi_y = il\psi$, where ψ is the streamfunction (see Appendix B), this is proportional to the streamfunction. As expected, there is a reduction in amplitude of transport near the western boundary as a result of the topography there (the dashed line gives the solution in the absence of topography). The changes in phase of the transport over the slope are due to the contributions of flow from farther north deflected equatorward by the topography to follow f/H contours (Schulman and Niiler [1970]).

In Fig 2.2(b) $\tilde{u}$ is plotted for the baroclinic ocean for the case of steady forcing at intervals of $\Lambda_1/2$. As expected, after time $2\Lambda_1$, the transport approaches the non-topographic Sverdrup balance. It was argued above that if in the case of time dependent forcing the period was $>> 2\Lambda_1$ baroclinic compensation would be substantial. In Fig 2.3(a) $\tilde{u}$ is plotted every quarter period for a forcing of period $8\Lambda_1$. It shows that while there

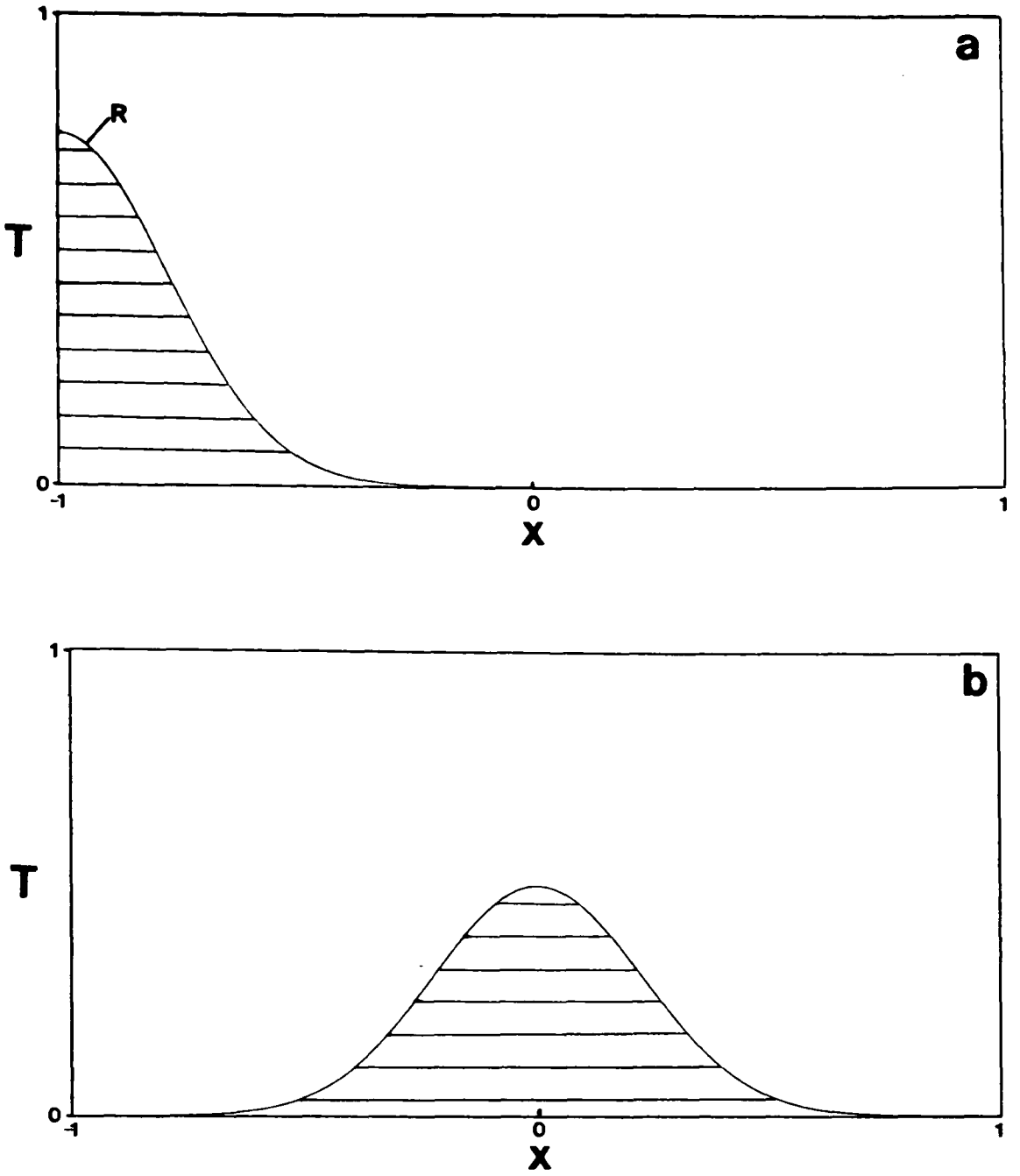

Fig 2.1(a) The Gaussian western slope topography. The measurements of Fig 2.5 are made at point R.

Fig 2.1(b) The Gaussian Mid-Atlantic ridge topography.

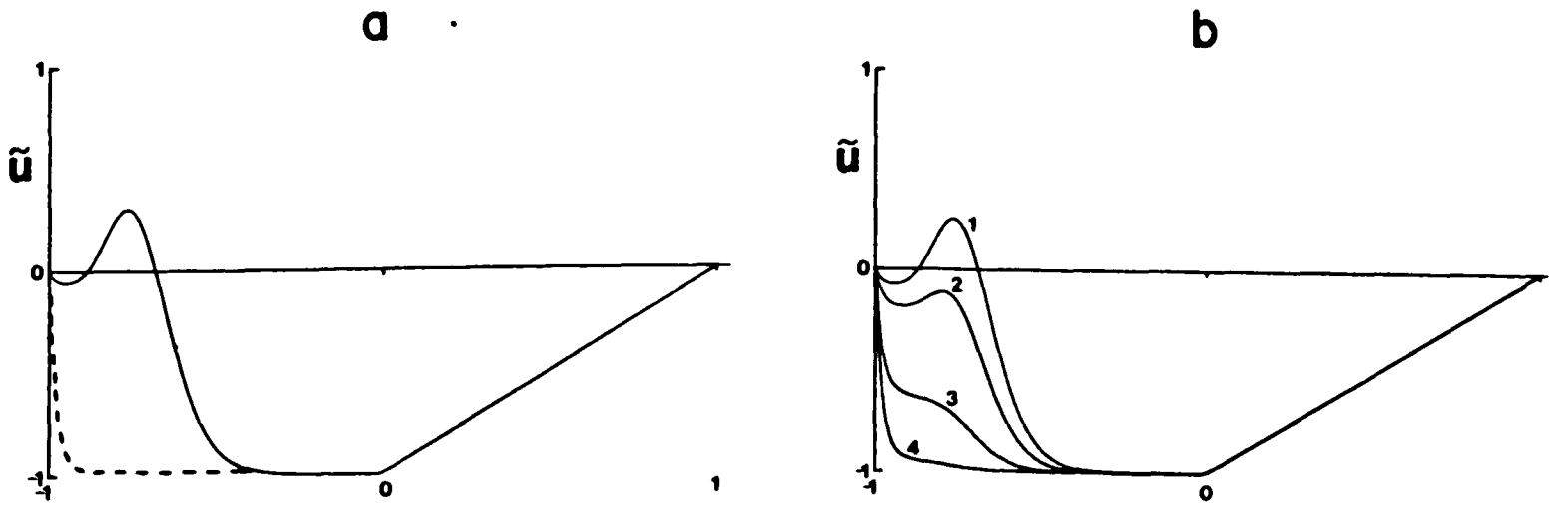

Fig 2.2(a) The equilibrium response for a homogeneous ocean to the wind forcing of Section 2.2 using the topography of Fig 2.1(a). The corresponding equilibrium response for a baroclinic ocean is shown dotted, and is also the response in the absence of topography

Fig 2.2(b) The response of a baroclinic ocean initially at rest to steady wind forcing with the topography of Fig 2.1(a) . The lines are plotted at intervals of $\Lambda_1/2$. Full compensation has nearly taken place at $2\Lambda_1$.

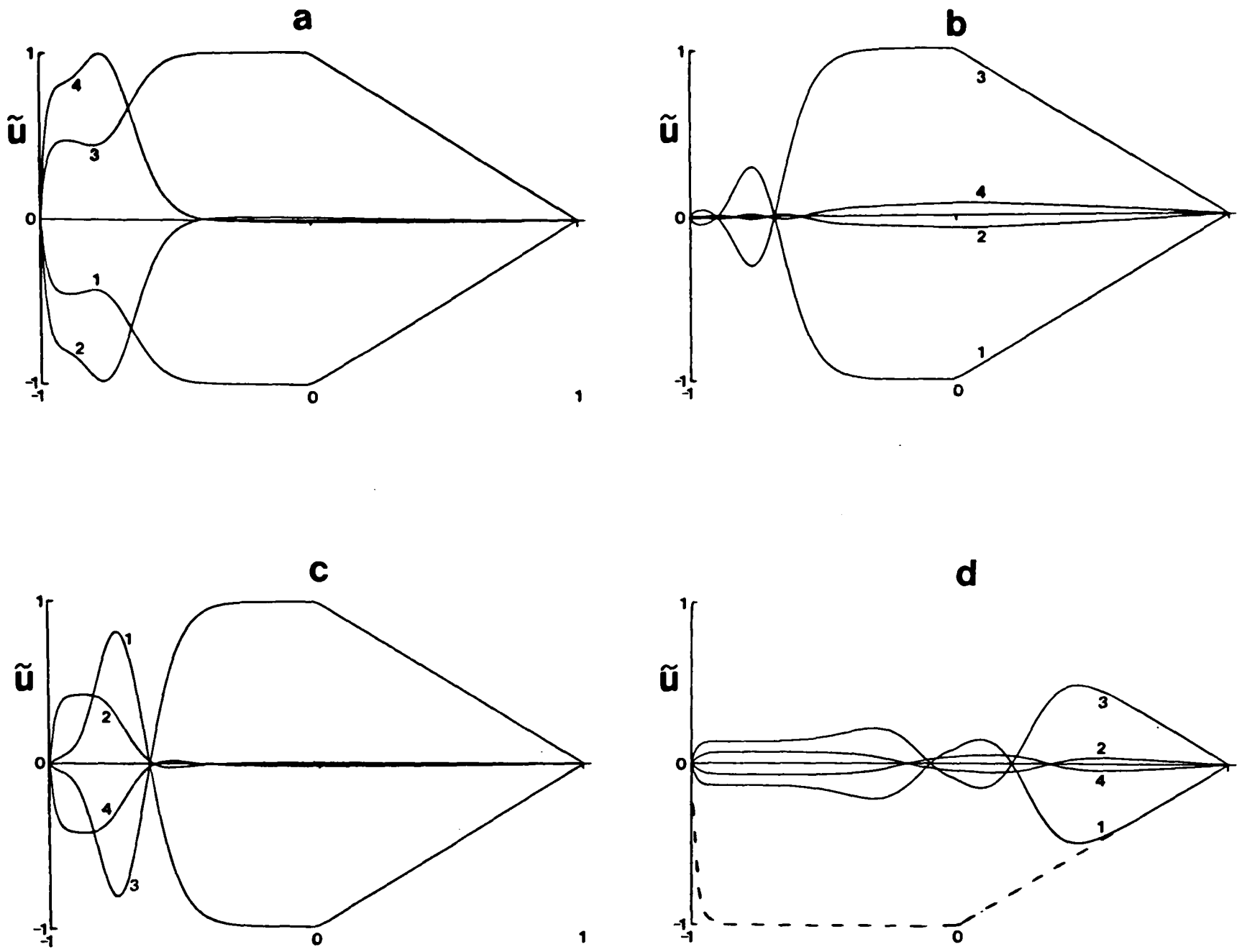

Fig 2.3(a) The response of the baroclinic ocean to harmonic forcing of period $8\Lambda_1$. Lines are plotted every quarter period. The topography of Fig 2.1(a) is used.

Fig 2.3(b) The corresponding response for a forcing period of $\Lambda_1/4$.

Fig 2.3(c) The corresponding response for a forcing period of $2\Lambda_1$.

Fig 2.3(d) The response at period $\Lambda_1/4$, but for the topography of Fig 2.1(b). The equilibrium response in the absence of topography is shown dotted, and is also the equilibrium response of a baroclinic ocean.

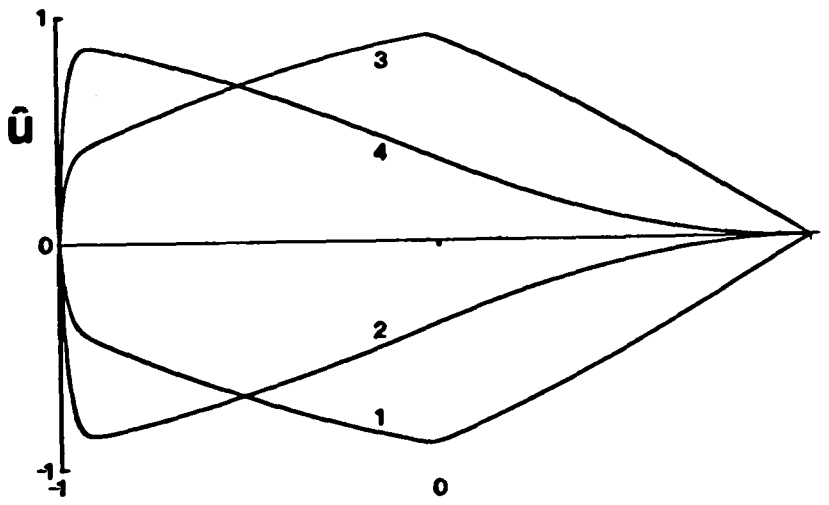

Fig 2.4 The baroclinic response $\hat{u}$ in a flat-bottomed ocean at period $8\Lambda_1$. It is not in equilibrium with the forcing.

is compensation it is not complete, there being a large phase difference between the interior solution and the response over the western continental slope. This phase difference can be explained as follows. In the case of a flat-bottomed ocean, the barotropic and baroclinic modes are independent. For period $8\Lambda_1$, the barotropic response is clearly equilibrium: at a time when the forcing is zero, so is the transport. The baroclinic response is not equilibrium however, since the period of the forcing is not much greater than the baroclinic adjustment time. Thus the baroclinic response is not zero when the forcing passes through zero. It is true that the baroclinic mode carries no transport but the point is that there will still be a large baroclinic response in the west which is not in phase with the forcing. This is shown in Fig 2.4. Now when topography is included, as anticipated earlier from 2.2, the baroclinic response is not greatly altered (not shown) . This baroclinic response induces the transport in Fig 2.3(a). In particular, even when the forcing is zero (marked 2 and 4 on Fig 2.3(a)) there is a northward transport near the boundary with a southward transport on and to the east of the continental rise. The longitudinal scale of this recirculation is determined by the scale of the topography, not by the scale of the baroclinic response, for as Fig 2.4 shows this is much larger than the recirculation scale. In order to have no western boundary transport when the forcing is zero, it is necessary to have an equilibrium baroclinic response, and this suggests periods 20 Λ_1 or longer. Practically, this means that for forcing periods of decades or less one cannot integrate the curl of the wind stress across the width of the basin and expect that to measure the western boundary transport. As Fig 2.3(a) shows, when the integrated curl across the basin is zero the transport in the

boundary layer is not. (If the forcing is farther west than that used in the above calculation, then the quoted times will also be less, since the baroclinic adjustment will be achieved sooner.)

Fig 2.3(b) shows the response to forcing of period $\Lambda_1/4$. Comparison with Fig 2.2(a) shows that the response of $\tilde{u}$ is nearly the same as for a purely barotropic ocean though a small difference from the equilibrium (barotropic Sverdrup) solution is present in the boundary layer. The case of period $2\Lambda_1$ is shown in Fig 2.3(c). This is intermediate between the 'low' and 'high' frequency limits discussed earlier, and the response is intermediate.

The amplitude variation of the boundary transport as a function of period is shown more completely in Fig 2.5, in which the value of $\tilde{u}$ at point R on Fig 2.1(a) is plotted as a function of forcing period. Transport values are low (i.e. much less than the maximum Sverdrup value of 1) for periods up to about $\Lambda_1/2$, being largely the same size as the response expected for a homogeneous ocean, and hence strongly emasculated by topography. At the other end of the range, for period $8\Lambda_1$ the transport is within 10% of the value expected in the absence of topography (0.95). The phase lag, as a fraction of period, between the maximum transport at R and the maximum of the interior response is also plotted on Fig 2.5. At long periods, as previously pointed out in connection with Fig 2.3(a), there are significant phase differences between the transport and the forcing. For example, the phase difference at a forcing period of $8\Lambda_1$ is $\sim \pi/3$, but decreases as we move to longer periods and the baroclinic response becomes more equilibrium.

Finally we consider forcing east of a ridge (such as the mid-Atlantic ridge) using the topography shown in Fig 2.1(b):

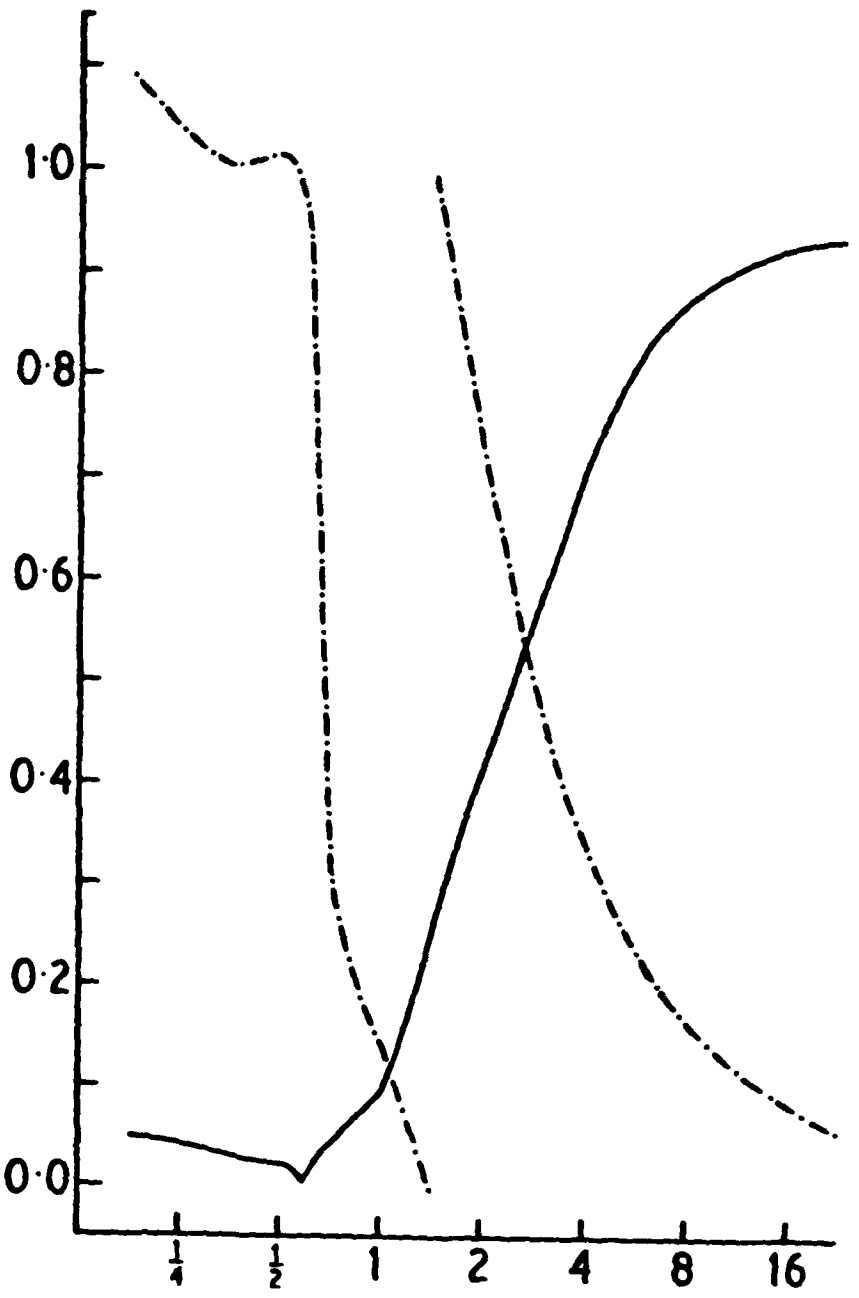

Fig 2.5 The amplitude and phase variation of $\tilde{u}$ at point R of Fig 2.1(a) for the baroclinic calculation. The amplitude is the solid line, and the phase lag with respect to the interior (as a fraction of period) is dot-dash. The x-axis is in units of Λ_1.

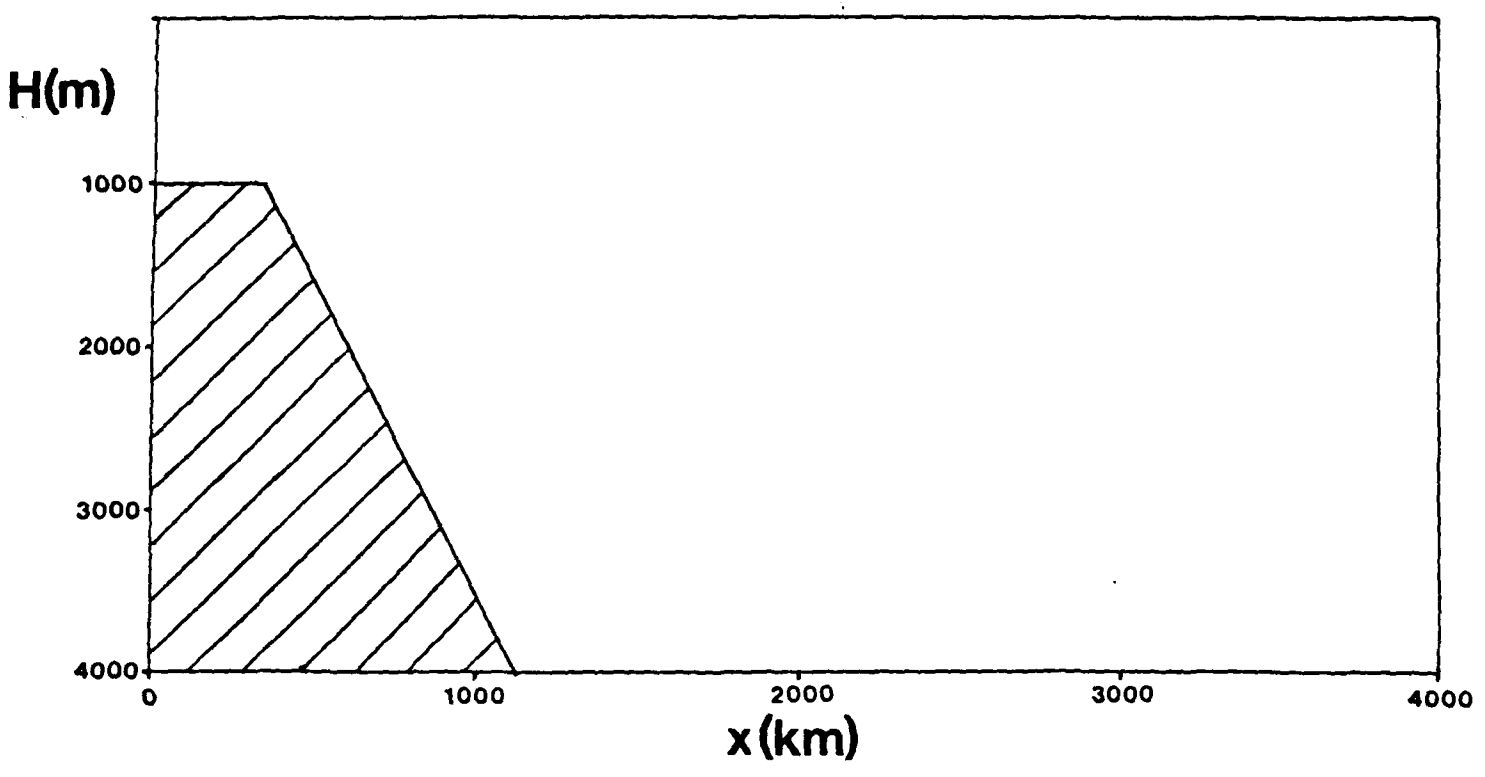

Fig 2.6 The shelf topography used for the runs throughout Section 2.3.

$$T=0.5\ e^{-10x^2} \qquad -1 < x < 1$$

$\tilde{u}$ is plotted in Fig 2.3(d) for period $\Lambda_1/4$. The equilibrium response for the baroclinic ocean is shown dotted. The response is much reduced in the western half basin from what one would expect simply from integration of the wind stress curl. This means that wind changes east of the ridge (at this period) are not very effective at influencing boundary current transport. Rather, a return circulation is established on the east of the ridge to return the flow, with a farther weaker gyre over the ridge.

2.2.3 Relevance to the North Atlantic

For baroclinic Rossby waves at 25°N the group velocity $\beta c^2/f^2$ is $\sim$ 10 cm/s. If the basin is 6000 km wide, then only for periods of 20 years or longer i.e. $> 20\Lambda_1$, would one expect the topographic reduction in transport to be almost totally compensated for. This means that only for such periods would the transport in the Florida Straits be consistent with measurements of the integral of the curl of the wind stress along the latitude of 25°N.

This necessary time will shorten if the region of wind variability is confined to the west, and provided that the wind variability is all in the western quarter of the basin one could anticipate agreement between transport and $\int curl_z(\underline{\tau})dx$ for periods greater than five years.

For the annual period, however, the results of the above section suggest that baroclinic Rossby waves can not substantially compensate for the effect of topography, and therefore that the response will be essentially barotropic and

strongly constrained by topography. It would therefore seem appropriate to think of the seasonal variation in transport for the Florida Straits as being related to the integral of $curl_z(\underline{\tau}/H)$ along f/H isolines. These deflect northwards to the east of the Bahamas suggesting that winds to the north-east may be important in determining the phase of Florida Current transport. This model, however, excludes variation of topography with y, the presence of islands, and complications due to baroclinic waves other than Rossby waves. These will be studied in later sections.

2.3: The two-dimensional, two layer model.

2.3.1 Introduction

The one dimensional model of the previous section is useful for illustrating qualitative principles. In order to include the effects of realistic topography and geography, a two dimensional model must be used. The introduction of the extra dimension also allows the effects of β -plane dispersion of baroclinic Rossby waves (Schopf, Anderson and Smith [1981]) to be evaluated, whereby baroclinic Rossby waves no longer propagate east-west but bend towards the equator. The model again has two layers in the vertical. The use of a layer model, as opposed to a level model, allows the topography to be a continuous function of (x,y) and is to be preferred for this reason to the discrete topography of a level model. The details of the model are given in Appendix B. Although the model can deal with irregular domains, in this section only simple topography and geometry will be used.

In each case the model was integrated for several years

until the solution had the periodicity of the forcing (i.e. initial transients had died away). The topography was independent of latitude and had a structure in the zonal direction of the form shown in Fig 2.6. The geometry was a simple square basin of side L=4080 km, with the southern boundary at the equator. Baroclinic Kelvin waves along the northern boundary were damped as described in Appendix B. This eliminates spurious transport variations due to the passage of these Kelvin waves over varying topography.

2.3.2 The effect of baroclinic Rossby waves

The first forcing we shall consider is a zonal wind stress confined to the eastern half basin:

$$
\begin{array}{lll}
 & X_o = \cos(2\pi\,(y-L)/L) & y > L/2 \quad x > L/2 \\
(A) & X_o = -1 & y < L/2 \quad x > L/2 \\
 & X_o = 0 & x < L/2
\end{array}
$$

In the absence of topography, the steady solution to forcing A is a single gyre in the northern half of the basin. The arguments of the previous section suggest that even with topography present the steady state response to time independent forcing for this model will also be of the above form. If now the forcing is not steady but of annual period, then the results of Section 2 suggest that the response will be largely barotropic. (For the parameters of the two dimensional model, a period of one year corresponds to a period of approximately $\Lambda_1/4$ in the one dimensional model.) Fig 2.7(a)shows the streamfunction at the time of maximum forcing. It is seen that the transport is deflected southward by the shelf. This is reminiscent of barotropic flow largely following f/H contours and hence

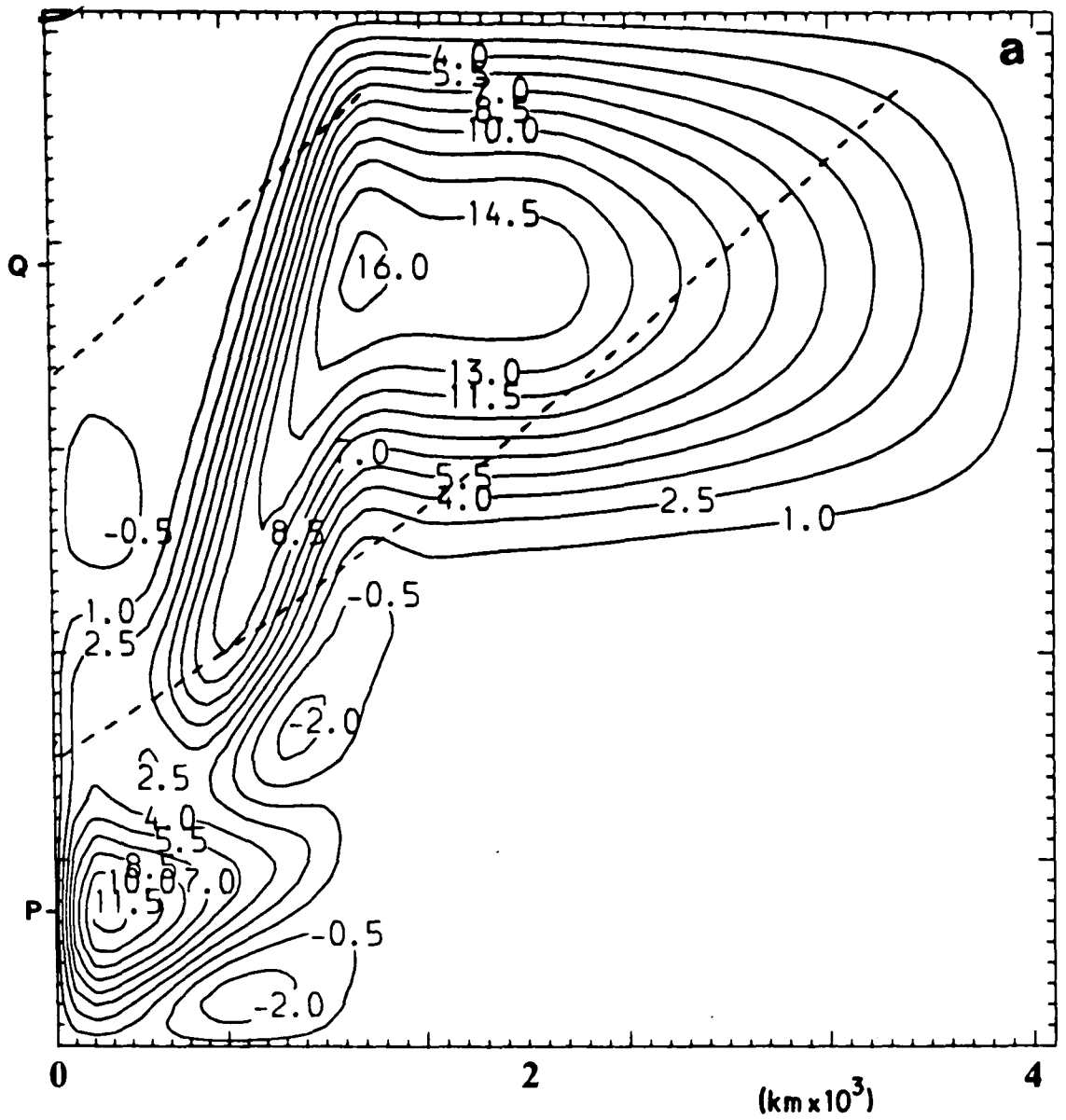

Fig 2.7(a) The streamfunction from a baroclinic calculation at the maximum of forcing A. The period is 360 days. The basin is 4080 km square. The deflection of the streamlines is reminiscent of the behaviour for a homogeneous ocean. The contours are labelled in Sverdrups. The dotted lines are caustics north of which Rossby wave activity is small. One caustic originates at the western edge of the forcing, the other at the eastern boundary.

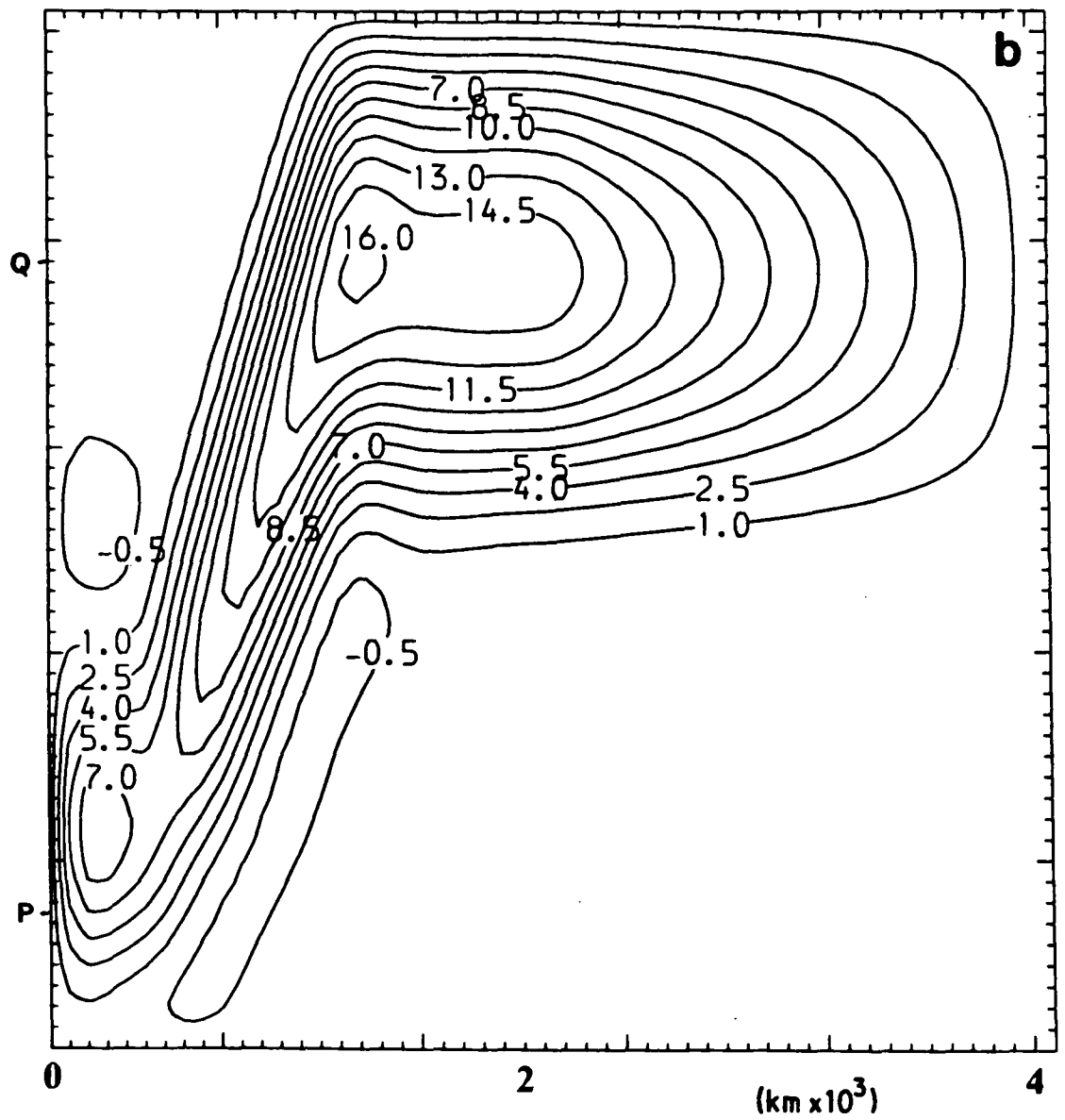

Fig 2.7(b) The streamfunction at the maximum of forcing A, but for a homogeneous ocean. Note the similarities with Fig 2.7(a). The major differences are at P.

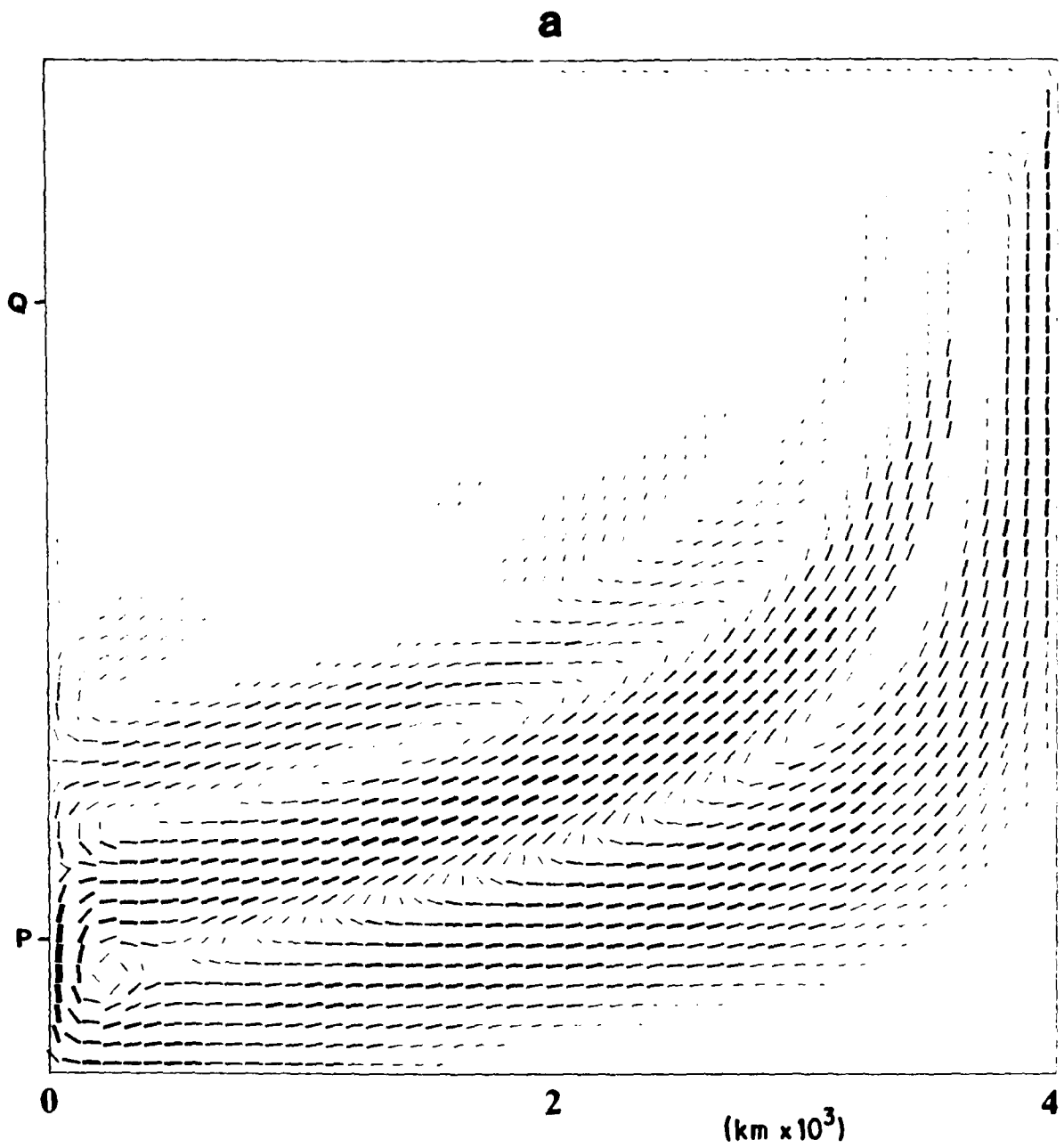

Fig 2.8(a) The upper layer transport over the basin for the run of Fig 2.7(a). A full arrowlength of single thickness corresponds to 0.8 Sverdrup. The thickness is progressively increased (without change in arrowlength) for greater transports.

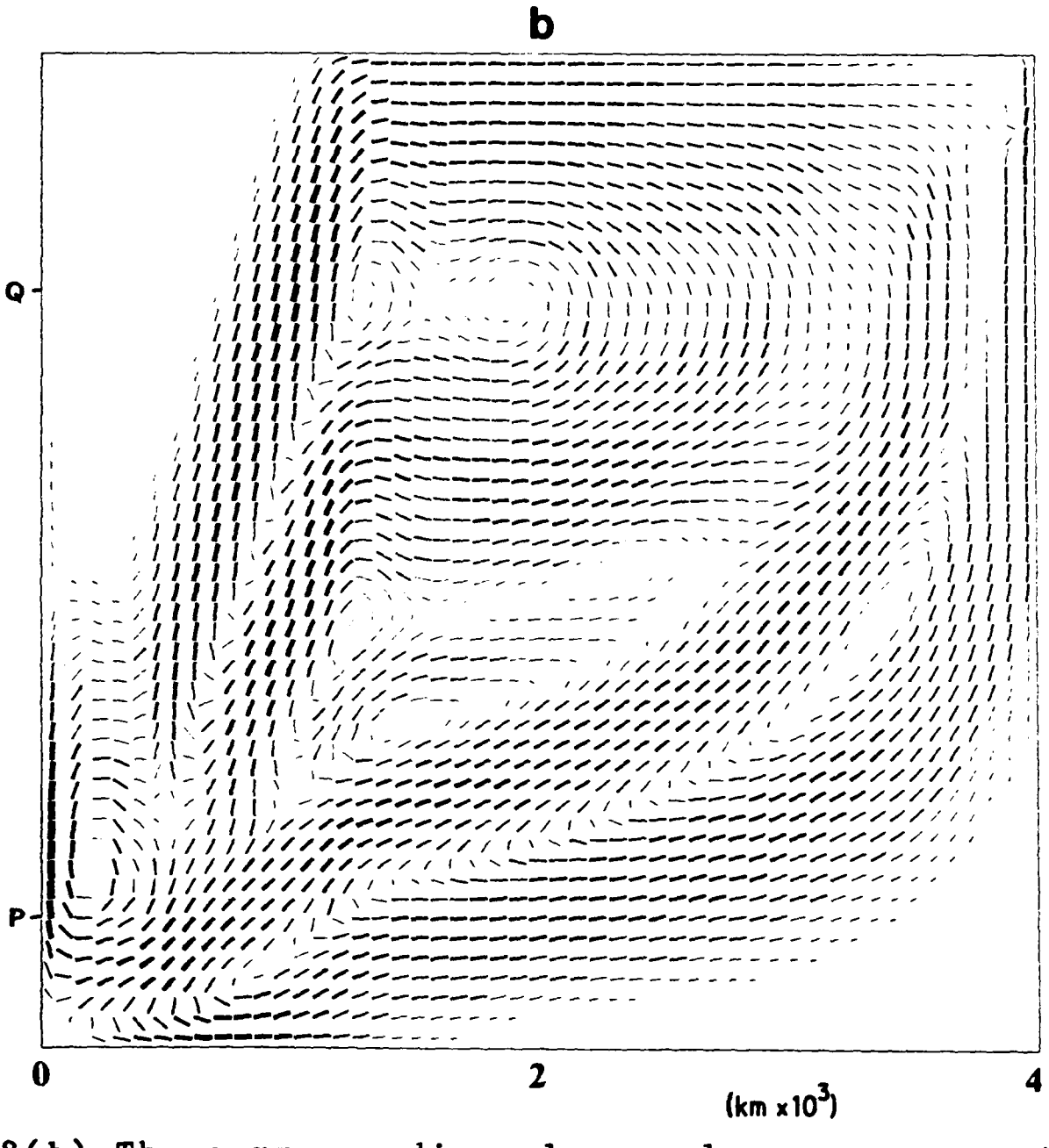

Fig 2.8(b) The corresponding lower layer transport. The presence of the northern gyre is evident.

suggestive that the response is indeed largely barotropic. To confirm this, a homogeneous model was run, and the response is shown on Fig 2.7(b). This is markedly similar to Fig 2.7(a) in gross features - the southward deflection of the streamlines over the ridge is very similar in the two cases. There are some differences, however, most noticeably in the southwestern corner of the ocean. This suggests that if we are interested in transport measurements at a latitude corresponding to P, for example, then both barotropic and baroclinic effects must be taken into account. If, however, we are interested in understanding the transport at point Q then the baroclinic effect is much weaker. The dotted lines on Fig 2.7(a) show the caustics for Rossby waves generated at the eastern and western edges of the wind forcing A (The method by which these caustics were calculated is given in Appendix C). North of this line there is negligible baroclinic wave energy, so the response is essentially purely barotropic. Just south of the dashed line, baroclinic Rossby waves are possible but, consistent with the results of Section 2 are rather ineffective at affecting the barotropic transport at this period. Still farther south, however, the Rossby waves do affect transport. Although forcing A has no curl in the southern half of the basin, energetic equatorial baroclinic Rossby waves are still excited and these can affect the transport. If a wind stress curl had been chosen that gave zero wind stress in the southern half of the basin (just add 1 to forcing A), the effect of Rossby waves at P would have been greatly reduced.

The relative importance of upper and lower layer transports over the basin is shown in Figs 2.8(a),(b). These are arrowplots of the transport in the upper and lower layers respectively for the experiment corresponding to Fig 2.7(a). At Q there is very

little transport in either layer, as expected from the above discussion. Over mid-ocean the upper layer (Fig 2.8(a)) is representative of the baroclinic response. The lack of energy in the north-west sector is a result of β -dispersion and dissipation. On Fig 2.8(b) the equal and opposite baroclinic transport is clearly visible in the south-eastern quadrant. To the north the transport in the gyre driven by the wind stress curl is evident. For a barotropic response, the transport in the two layers is in the ratio $H_1 : H_2$ which is why the gyre does not appear on Fig 2.8(a). The southward deflection of the transport over the ridge is also seen in Fig 2.8(b), consistent with the closing of streamlines in Fig 2.7(a). Near P, the proportions of total transport in the upper and lower layers follow no clear pattern: no one layer dominates in this area.

For the above numerical experiment, both the barotropic and baroclinic signals are deflected toward the equator. The mechanism by which this is done for each mode is, however, completely different. For the barotropic mode it is the influence of topography which deflects the streamlines, the extent to which this happens being dependent on the strength of the topography. For the baroclinic Rossby waves, it is the effect of β -dispersion which directs the signal equatorward, the bottom topography having little effect for small δ . It follows that at any given point, the baroclinic and barotropic signals may have totally unconnected sources. The strengths of the respective signals in an area may depend on the wind stress pattern over large areas of the ocean. It is only in the long period limit when the Sverdrup balance holds for the baroclinic mode and β -dispersion is weak that baroclinic compensation will occur and both the baroclinic and barotropic solutions can be predicted by integration of the wind stress curl along a latitude

line.

2.3.3 The generation of transport by wind stress along isobaths

Up to this point, the wind stress has been applied in a region where the bottom was flat, with topography to the west of the forcing region. But it is also possible to generate transport with a uniform wind stress over non-uniform topography. This is most clearly seen from B13 where it is $curl_z(\underline{\tau}/H)$ which drives the barotropic flow. This means that in a homogeneous ocean, transport can be generated by a steady wind even if the wind has no curl. In a baroclinic ocean this would also happen initially, but eventually compensation would occur and the transport would decrease. However, forcing of annual period in a baroclinic ocean can not achieve compensation, and so transport fluctuations in the boundary current should result. To ascertain whether this was the case, we integrated the model at annual period with meridional forcing of the form:

(B) $Y = 1$ over the whole basin

and with the same shelf as for forcing A. Over the shelf $curl_z(\underline{\tau}/H)$ is not zero.

The resulting streamfunction, at the maximum of the above forcing, is shown in Fig 2.9(a) for the case of a homogeneous ocean, while Fig 2.9(b) gives the corresponding plot for a baroclinic ocean. The similarity between Figs 2.9(a) and 2.9(b) indicates that the barotropic response is in the main little affected by baroclinic processes, especially at higher latitudes. Since the wind stress is parallel to the western boundary, a Kelvin wave is also generated there which travels southward.

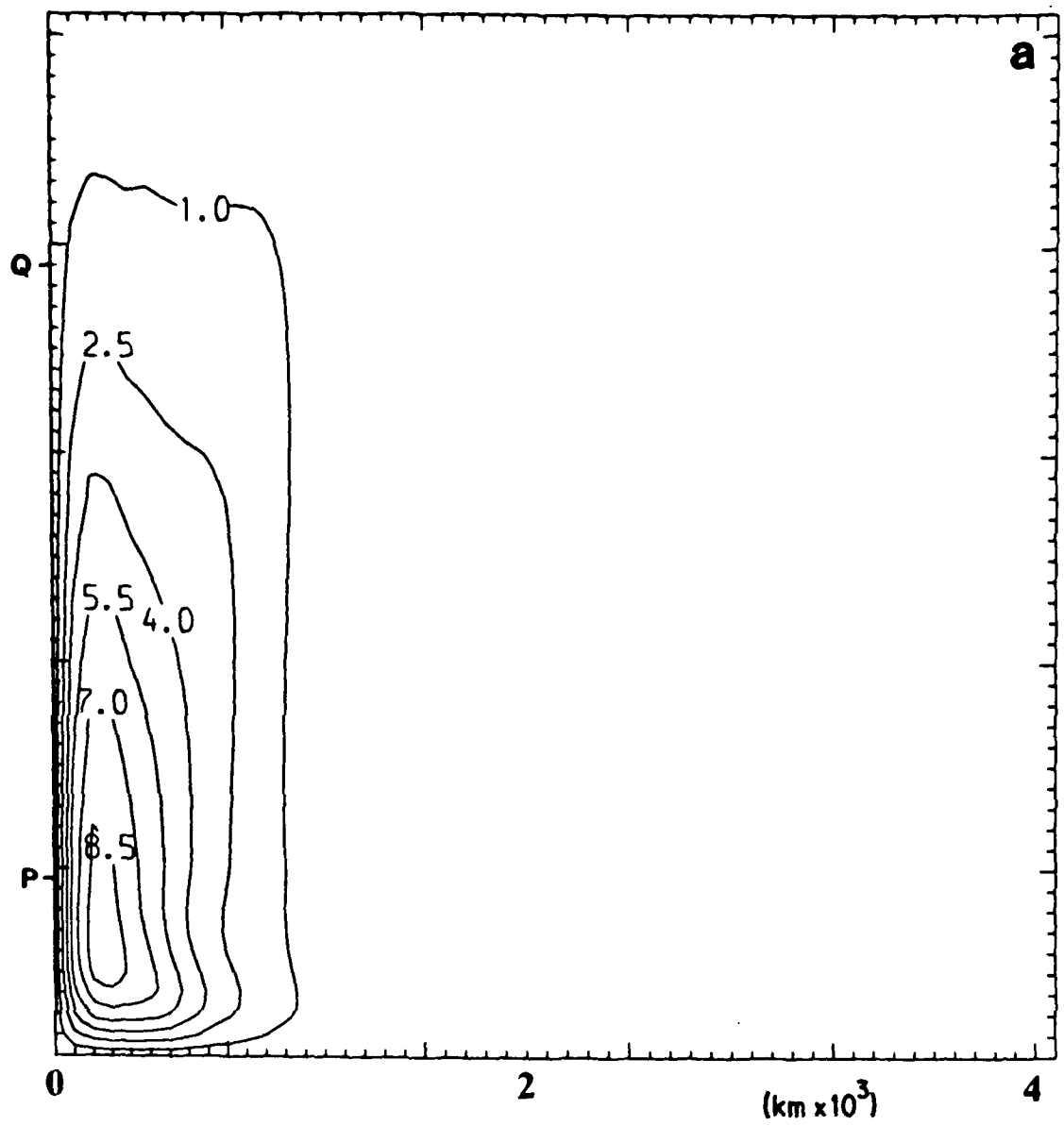

Fig 2.9(a) The streamfunction at the maximum of forcing B for a homogeneous ocean.

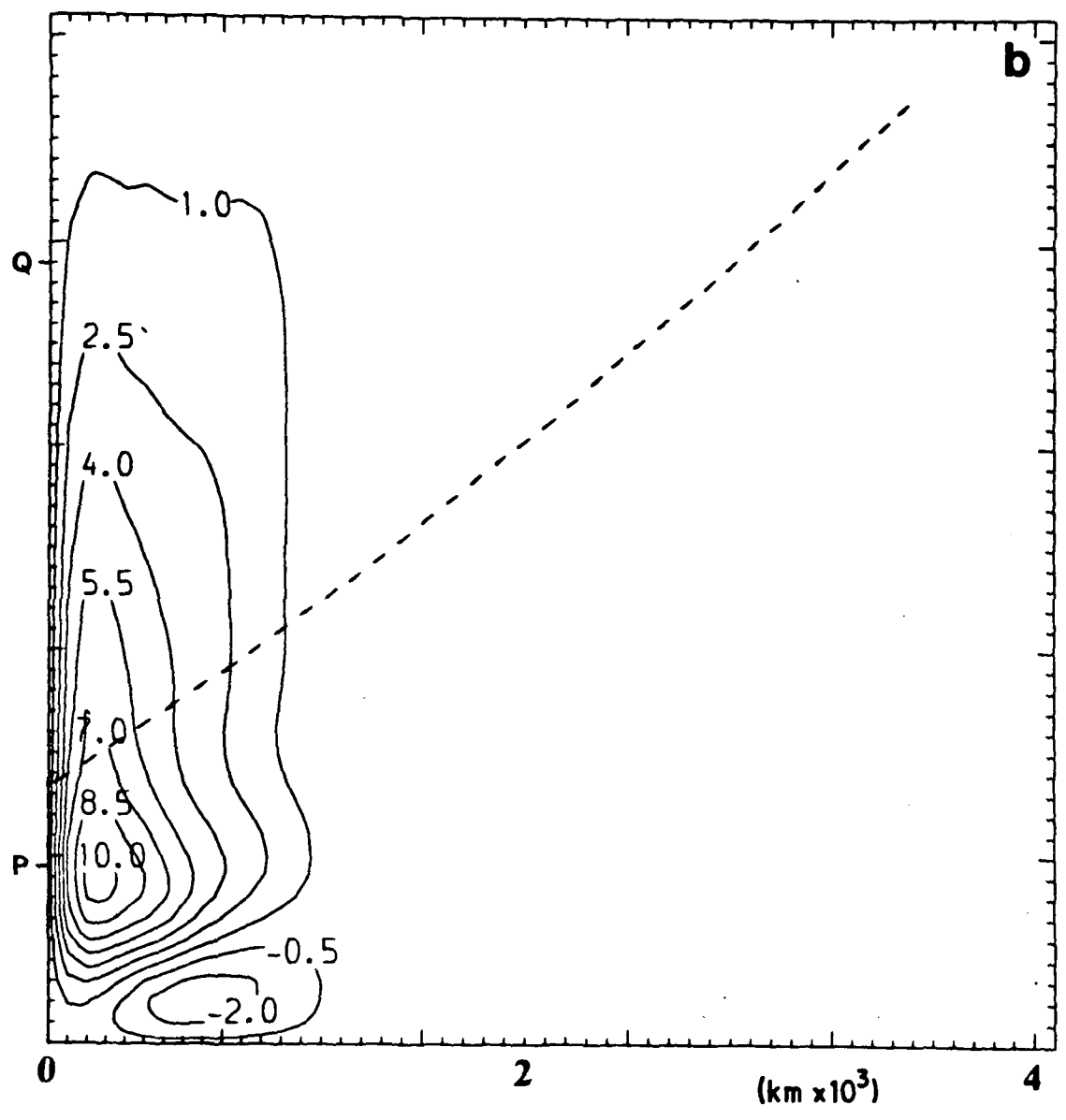

Fig 2.9(b) The streamfunction at the maximum of forcing B for the baroclinic calculation. At high latitudes there is a great similarity between Fig 2.9(a) and Fig 2.9(b). The dotted line shows the line above which Rossby wave activity is expected to be negligible.

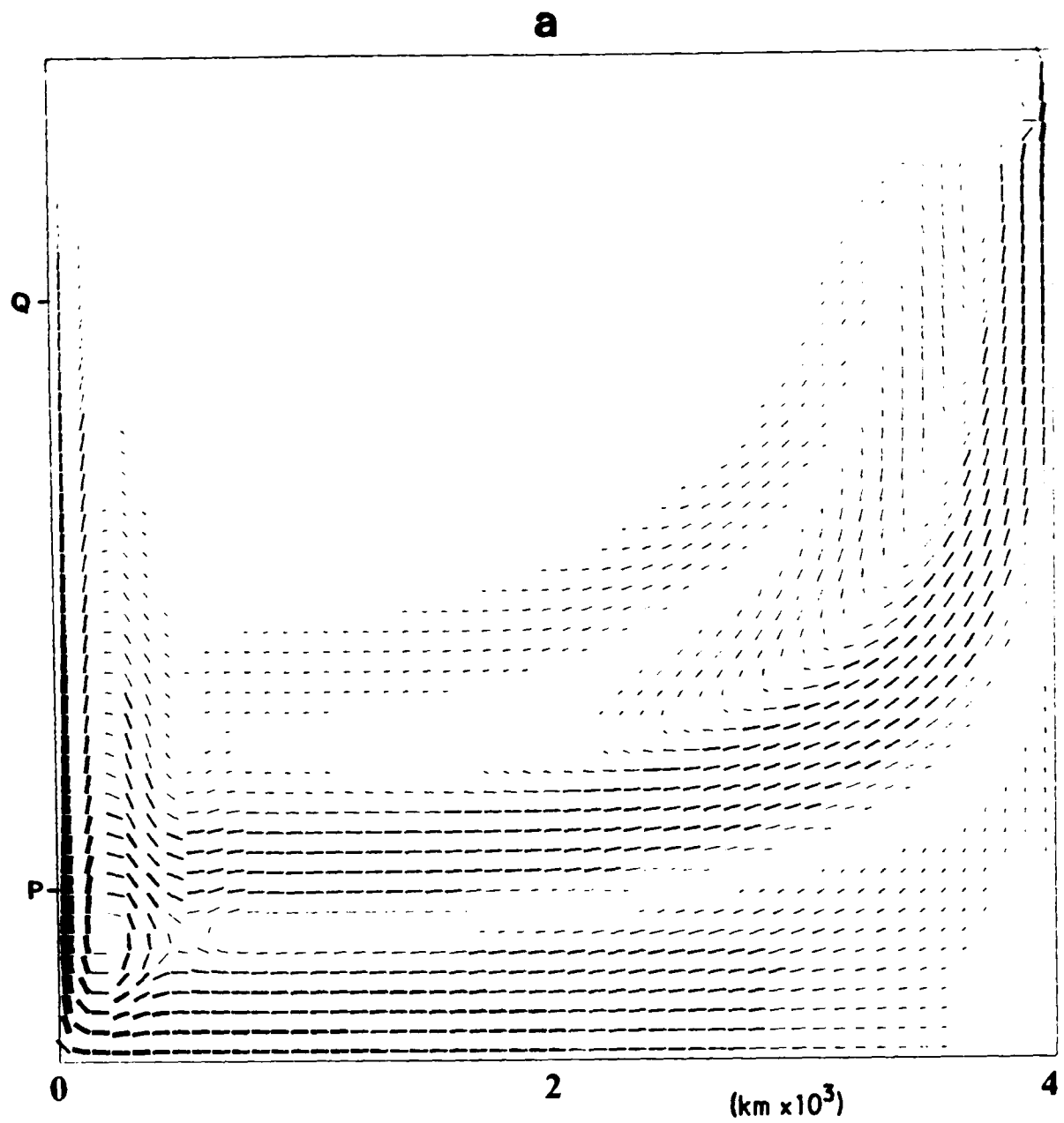

Fig 2.10(a) The upper layer transport for the run corresponding to Fig 2.9(b). It is evident on comparison with Fig 2.10(b), that the upper layer transport dominates at all latitudes near the western boundary.

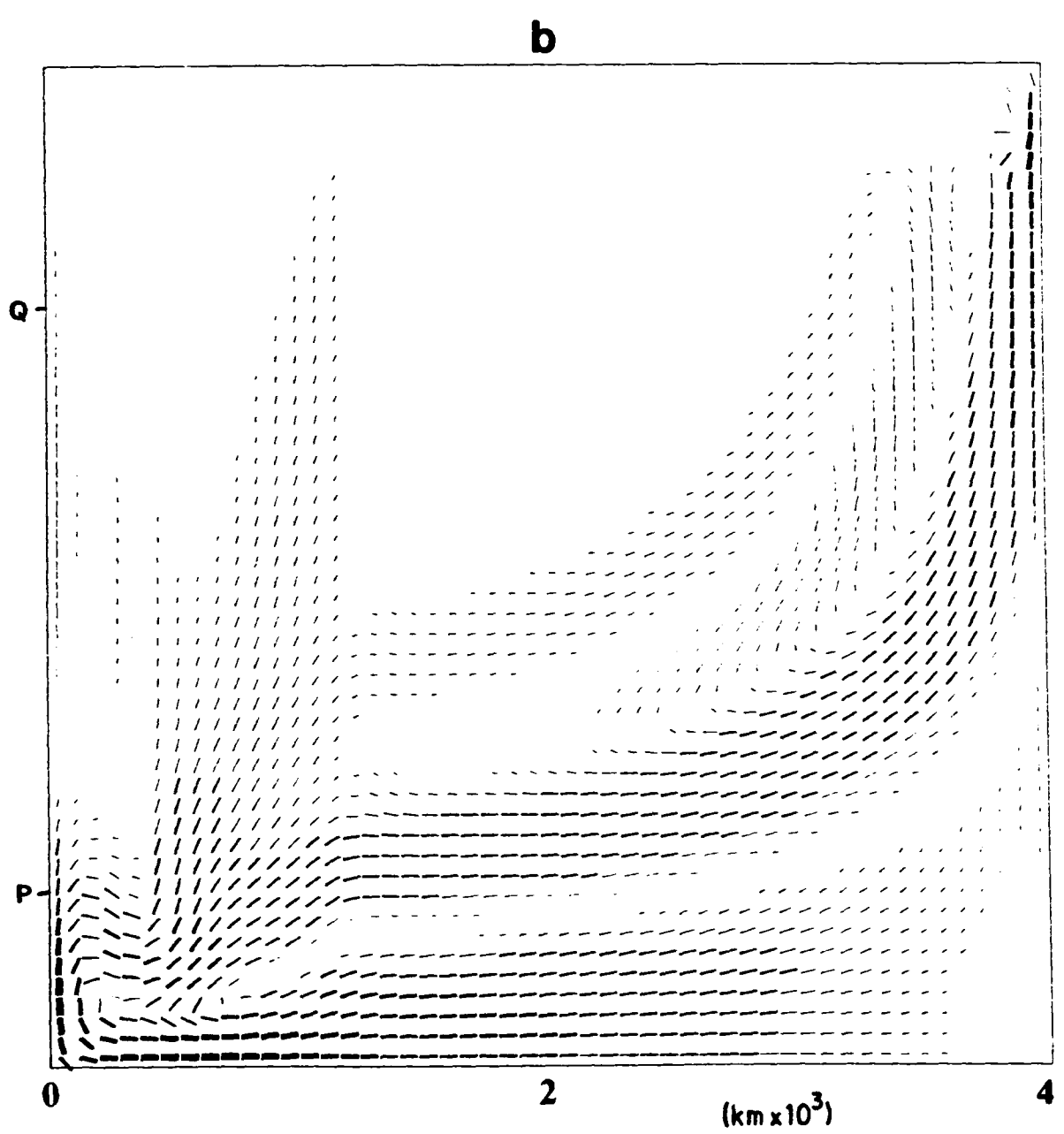

Fig 2.10(b) The lower layer transport for the run corresponding to Fig 2.9(b).

Because the topography is flat within several radii of deformation of the western boundary, this Kelvin wave does not generate any transport variations until it turns eastward near the equator to pass over the shelf. In addition to the Kelvin wave, baroclinic Rossby waves can propagate over topography. The dotted line in Fig 2.9(b) shows the caustic above which Rossby wave activity is expected to be negligible, showing that it is only near P that baroclinic Rossby waves can affect the transport.

In a homogeneous ocean, for the above topography, there is no transport induced by the wind in the eastern part of the basin, though there is a surface Ekman layer carrying a flow that is much stronger than the weak compensating flow beneath the Ekman layer. In the western boundary current, however, there is no Ekman flow, and the northward transport is depth independent. If stratification is present, then in addition to this depth independent response, the Kelvin wave along the western boundary referred to earlier can alter the velocity profile of the boundary current to make it surface intensified, without altering the total transport. On Figs 2.10(a),(b) are shown the upper and lower layer transports respectively for the experiment corresponding to Fig 2.9(b). To the east of the shelf, the barotropic response is zero, so the activity seen in the deep water in both layers is entirely baroclinic. The effects of β -dispersion and dissipation are again evident. In Figs 2.10 we see that it is the upper layer which dominates the transport variations next to the western boundary at all latitudes.

The results of this section show that changes in the component of wind stress along isobaths can be important in generating transport variations even if the wind has no curl.

2.3.4 The Ekman transport and feedback between modes over topography:

If we consider a closed basin, such as the one used above, then there is no transport across the boundaries. If a uniform wind stress is imposed, then the upper layer Ekman transport must be balanced by an opposing geostrophic transport (initially due to gradients in sea level. See Eq B12) to satisfy the boundary conditions. This means that the term Ekman transport is really a misnomer for a closed basin, there being no Ekman contribution to the total transport. The streamfunction is determined by B13, and the Ekman current is given by the baroclinic equations B14 and B15. We therefore do not expect a direct Ekman contribution to the streamfunction on Figs 2.7(a),(b) and Figs 2.9(a),(b).

For forcing A, the wind stress is in the eastern half basin, and therefore there is no Ekman response over the topography. There are, however, some Rossby waves in the area where the barotropic response is deflected south-westward by topography. In this area, there will also be forcing of the baroclinic mode by the barotropic, which in turn will force the barotropic mode; i.e. there will be feedback between the modes. The effect on the transport is expected to be small, since $\delta = H_1 / H_2 << 1$ (See Section 2.2), and if we compare Fig 2.7(a) and Fig 2.7(b), we see that this is indeed the case.

For forcing B, there is an Ekman response over the topography. How does this affect the streamfunction? The baroclinic forcing of the barotropic mode is through gradients in the interface displacement η_2. These can be generated by Ekman pumping, which is zero for Forcing B, and also by forcing of the baroclinic mode via the interaction of the bottom velocity and gradients in topography. This depends on both the barotropic

response and the Ekman velocity in the absence of baroclinic waves. Comparison of Fig 2.9(a) and Fig 2.9(b) at higher latitudes (where Rossby wave activity is expected to be low) confirms that the effect on transport of a uniform Ekman response over topography is negligible.

In a model which is forced by realistic winds the effects on transport of baroclinic Rossby waves, the Ekman flow, and the feedback between barotropic and baroclinic modes over topography will be mixed. At extratropical latitudes and at annual period, however, we have shown that these effects are small and the transport is primarily as if it were forced in a homogeneous ocean.

2.4: Geographical effects.

In the case of a baroclinic ocean, if our interest is centred on the vertically integrated transport, it is sensible to distinguish geographic and topographic effects. This is because, for a baroclinic ocean, in the steady state, the effect of topography can be compensated for by the baroclinic response, whereas the effect of geography cannot. In a homogeneous ocean, however, the distinction is much less clear, since both bottom topography and islands act in much the same way to block or deflect the flow. This similarity carries over to the case of a baroclinic ocean when the response is time dependent, provided that the frequency is not so low as to allow substantial compensation. As shown above, the response at annual period is largely barotropic for remote forcing. Hence one can anticipate that an island can be considered as an extension of bottom topography in the case of seasonal forcing. For computational

efficiency and ease of interpretation a homogeneous model will be used in this section. Baroclinic effects are thus excluded.

The interest of this section will be on the shadowing effect that an isolated island has on western boundary transport. Consider an isolated island (as shown in Fig 2.11 for example) in a rectangular box defined by the lines $x=0,2a$; $y^*=-b,b$, with a zonal wind stress again confined to the eastern half basin:

$$
\text{(C)}\qquad
\begin{aligned}
X_o &= d/d_o && y^* > d \quad x > a \\
X_o &= -d/d_o && y^* < -d \quad x > a \\
X_o &= (d/d_o)\sin(\pi\, y^*/2d) && -d < y^* < d \quad x > a
\end{aligned}
$$

where $y^*=y-2020$ km, $d_o=800$ km and d takes values of 200, 800, or 2000 km. In the absence of topography the interior flow is expected to be Sverdrup-like, and if the north-south scale of the forcing is smaller than the length of the island one might anticipate that the flow pattern would consist of a Sverdrup gyre to the east of the island, a western boundary current on the east side of the island to close the flow, and zero transport between coast and island. However, although this solution does satisfy the streamfunction equation

$$
\text{Eq 2.3}\qquad \left(\frac{\psi_{xt}}{H}\right)_x + \left(\frac{\psi_{yt}}{H}\right)_y = \mathrm{curl}_z\left[\frac{f\nabla\psi}{H} + \frac{\tau}{\rho_1 H} + F_\mu\right]
$$

(the equivalent of B13 for a homogeneous ocean), it is not a solution to the problem. This is because solutions to Eq 2.3 are not uniquely determined by the boundary conditions that $\psi=0$ at the coast, and that ψ is spatially invariant on the island. Since Eq 2.3 is rather like Poisson's equation we expect that a solution can be found for any desired value of ψ_I (the value of ψ on the island), the choice $\psi_I=0$ being only one of these. Eq

2.3 must be augmented by an equation fixing ψ_I . Such an equation can be derived from the momentum equations for a homogeneous ocean (i.e. the barotropic equivalent of B12). In an area where the wind stress is zero and the response steady this becomes:

Eq 2.4 $$[-f\bar{V} + g\eta_{1x} - F^x]\,\underline{i} + [f\bar{U} + g\eta_{1y} - F^y]\,\underline{j} = 0$$

Integrating this about any closed path in the ocean eliminates η_1 , and we find that:

Eq 2.5 $$\oint_C [\,(f\,\psi_x/H + F^x)\,\underline{i} + (f\,\psi_y/H + F^y)\,\underline{j}\,]\cdot d\underline{s} = 0$$

If the curve C is at the boundary of the island, then for the above example the wind stress is zero, and since the normal transport must vanish, the only terms that remain are the dissipative terms, and so Eq 2.5 reduces to:

Eq 2.6 $$\oint_C \underline{F}\cdot d\underline{s} = 0$$

and the dissipative scheme used will determine the appropriate value of ψ_I . If, for instance, a simple bottom friction is used the appropriate condition is:

Eq 2.7 $$\oint_C [\,\psi_y/H\,\underline{i} - \psi_x/H\,\underline{j}\,]\cdot d\underline{s} = 0$$

For a long thin rectangular island oriented north-south in a flat bottomed ocean Eq 2.7 gives the approximate numerical answer that the value of ψ_I is the average of the values immediately to the east and west of the island. Thus in general ψ_I will not be zero, even though all the forcing is to the east of the island.

It also shows that the actual value of ψ_1 and hence the northward transport between island and coast depends on the frictional scheme used. To examine this effect and to quantify how the transport between coast and island depends on the latitudinal scale of the forcing a number of calculations were run with different forcing and friction. The island was 1640 km long and 40 km wide in a basin 4040 km long and 2440 km wide. The model resolution was 40 km. In Fig 2.11(a), the equilibrium streamfunction is plotted for forcing C with d=200 km. One can see that a substantial fraction of the maximum transport (31.5 %) passes around the island and forms a western boundary current next to the western coast though a boundary current also exists to the east of the island. As d (the latitudinal scale of the forcing) increases, the fraction of the return flow which passes to the west of the island also increases, but not proportionately. For instance when d=800 km, so that the gyre is the same scale as the island, 60% of the transport is returned by the western boundary layer and only 40% by the boundary layer to the east of the island. The streamfunction for this case is shown in Fig 2.11(b) while Fig 2.11(c) shows the streamfunction for the case where d=2000 km when practically all the transport passes to the west of the island.

The above calculations applied to the case of a bottom friction with damping time scale of ten days. This frictional time scale may be rather short and the effect of such strong damping can be seen in Fig 2.11(a) where the maximum transport for the small gyre is substantially below the 11.8 Sverdrups expected from the Sverdrup balance. For comparison we repeated this calculation for a lower value of bottom friction with a timescale of about one year, but also included a lateral friction ($D=10^4$ $m^2 s^{-1}$), so that the western boundary current is still

resolved. This is the same specification of friction as was used in Section 2.3 for the time dependent calculations. Since the value of ψ_I depends on friction, changing the frictional parameters may change the proportion of maximum transport that passes to the west of the island. The streamfunction for d=200 km is plotted in Fig 2.12(a) showing that in fact the proportion of the maximum transport which passes to the west is lower (22 %) for the case of low bottom friction, but since the interior transport maximum is larger, the actual value of ψ_I hardly changes. The proportion of transport which passes to the west of the island was also lower for the calculations at larger north-south scales.

A common feature of the above runs was the sinusoidal variation of the forcing with latitude. For forcing of different shape the proportions of transport which pass to the west of the island will change. For instance, with a uniform rather than sinusoidal curl to the east of the island which generates a gyre projecting fully onto the island, all the transport will pass to the west of the island. This happens because the zonal flow passes entirely to the north and south of the island in this case, so the island boundary condition has little effect.

So far the maximum of the curl has been at the same latitude as the centre of the island. The latitudinal location of the curl relative to the island is also important. Clearly, if the curl is located entirely to the north or south of the island, then the island will have no effect (in the absence of topography). When the scale of the curl is less than the scale of the island and provided that the gyre lies within the latitude bands of the island, moving the forcing north or south relative to the island has little effect on ψ_I, and the streamfunction pattern to the west of the island is insensitive to such

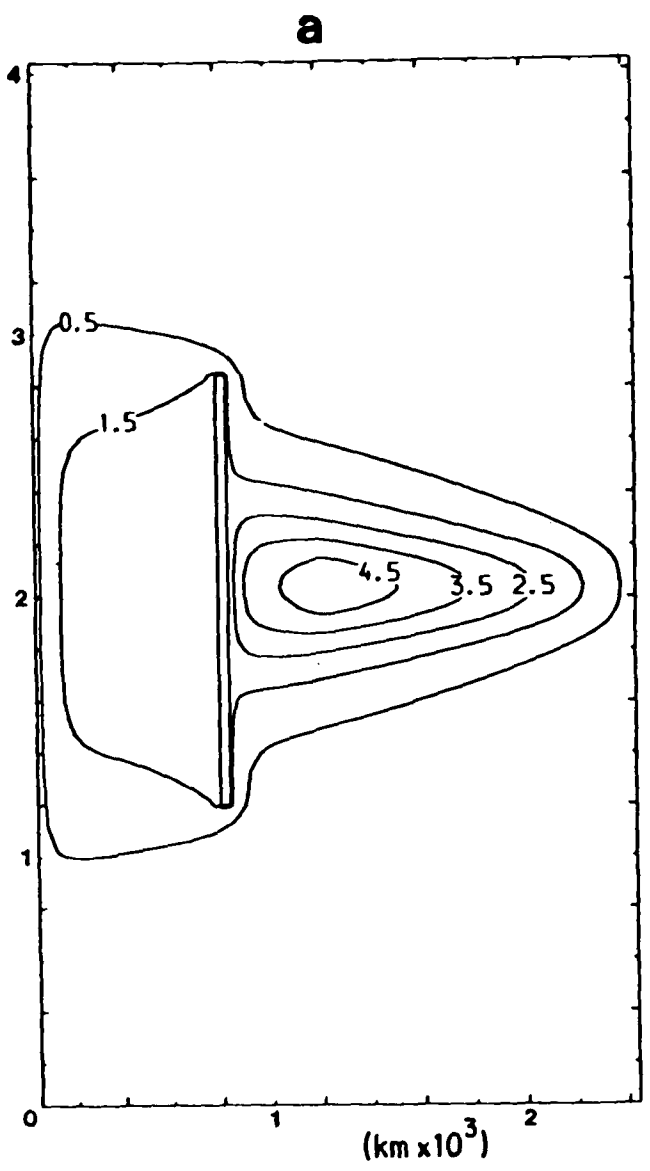

Fig 2.11(a) The streamfunction for high bottom friction and d=200 km. The basin is 2440 km wide by 4040 km long.

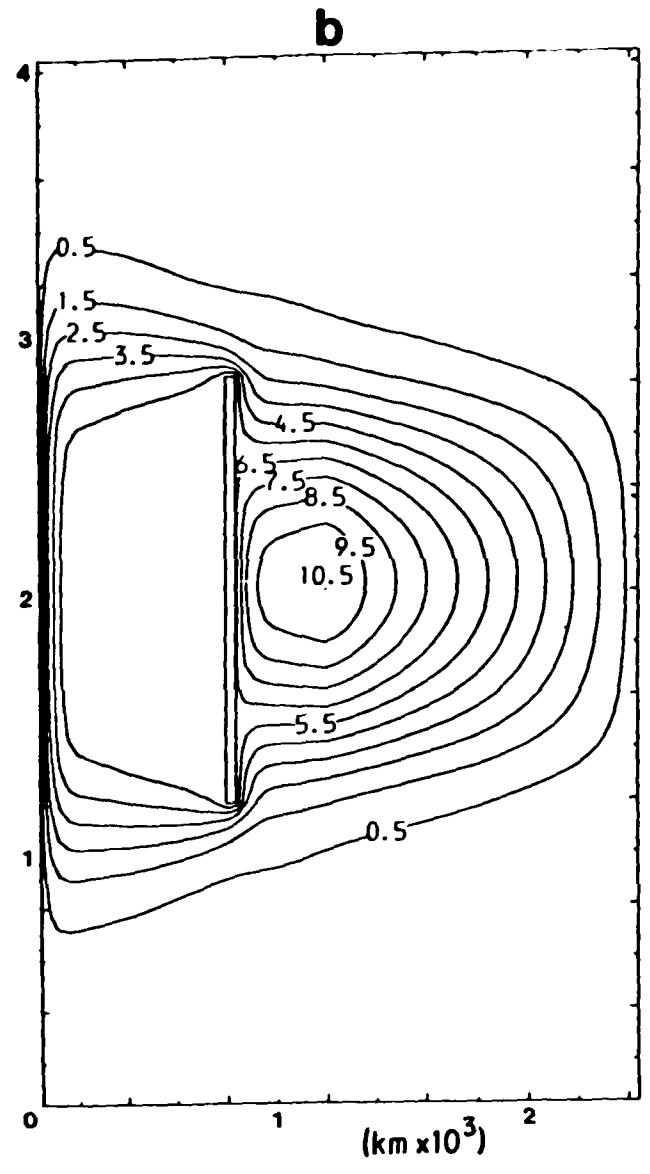

Fig 2.11(b) The streamfunction for high bottom friction and d=800 km.

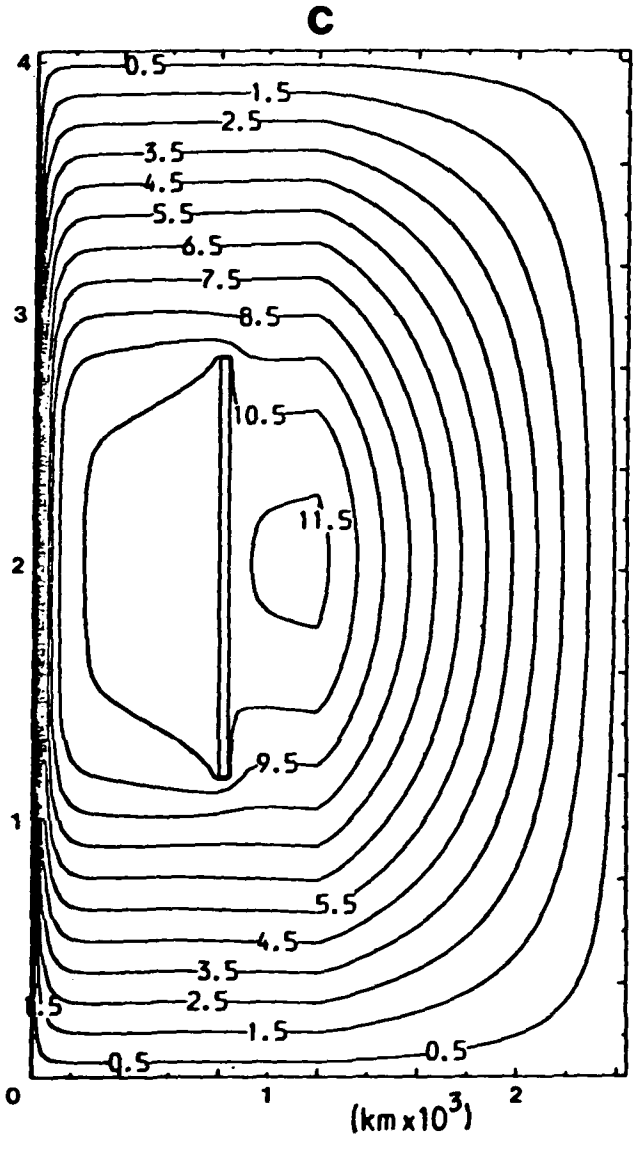

Fig 2.11(c) The streamfunction for high bottom friction and d=2000 km.

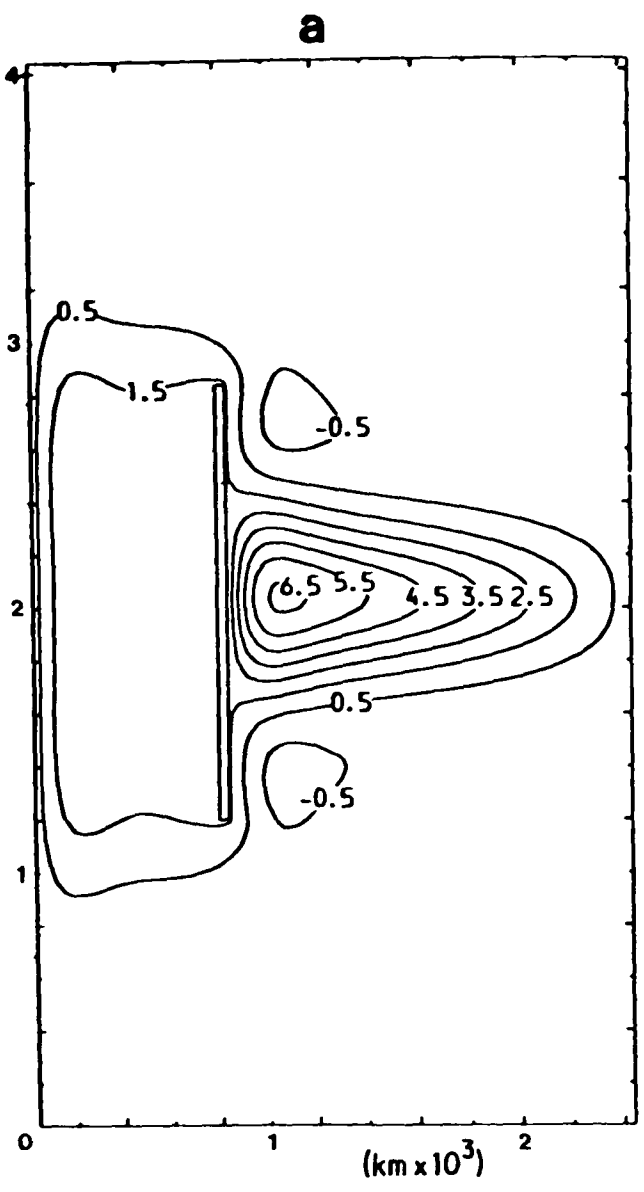

Fig 2.12(a) The streamfunction for low bottom friction and d=200 km.

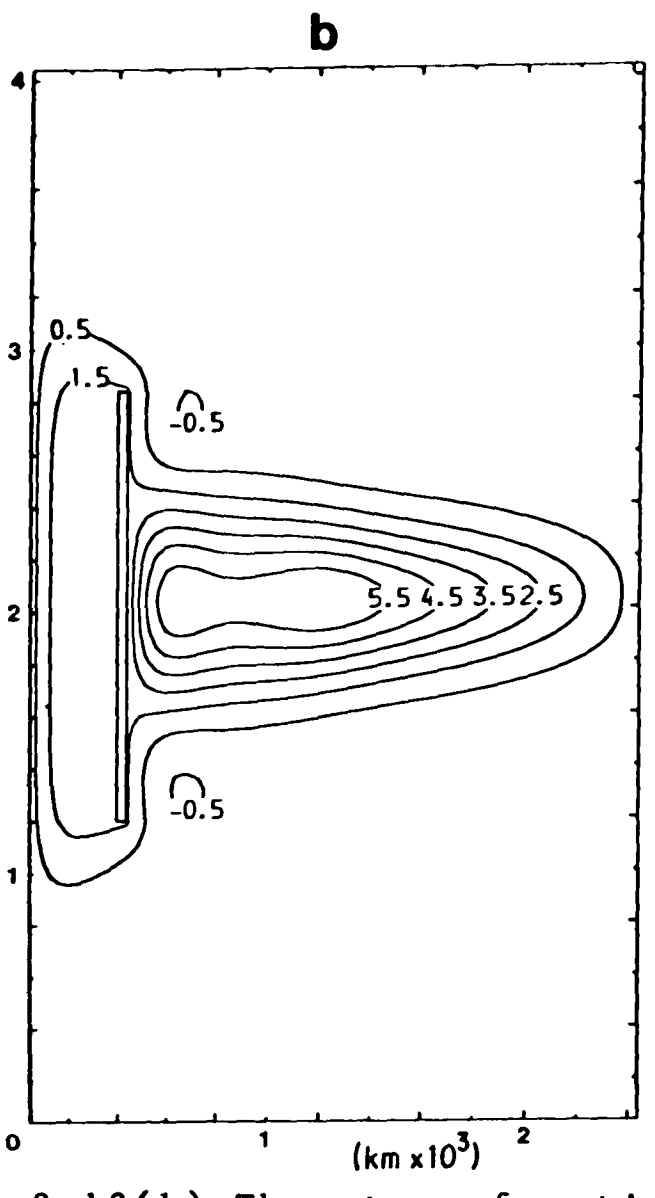

Fig 2.12(b) The streamfunction for low bottom friction and d=200 km, but the island has been moved westward.

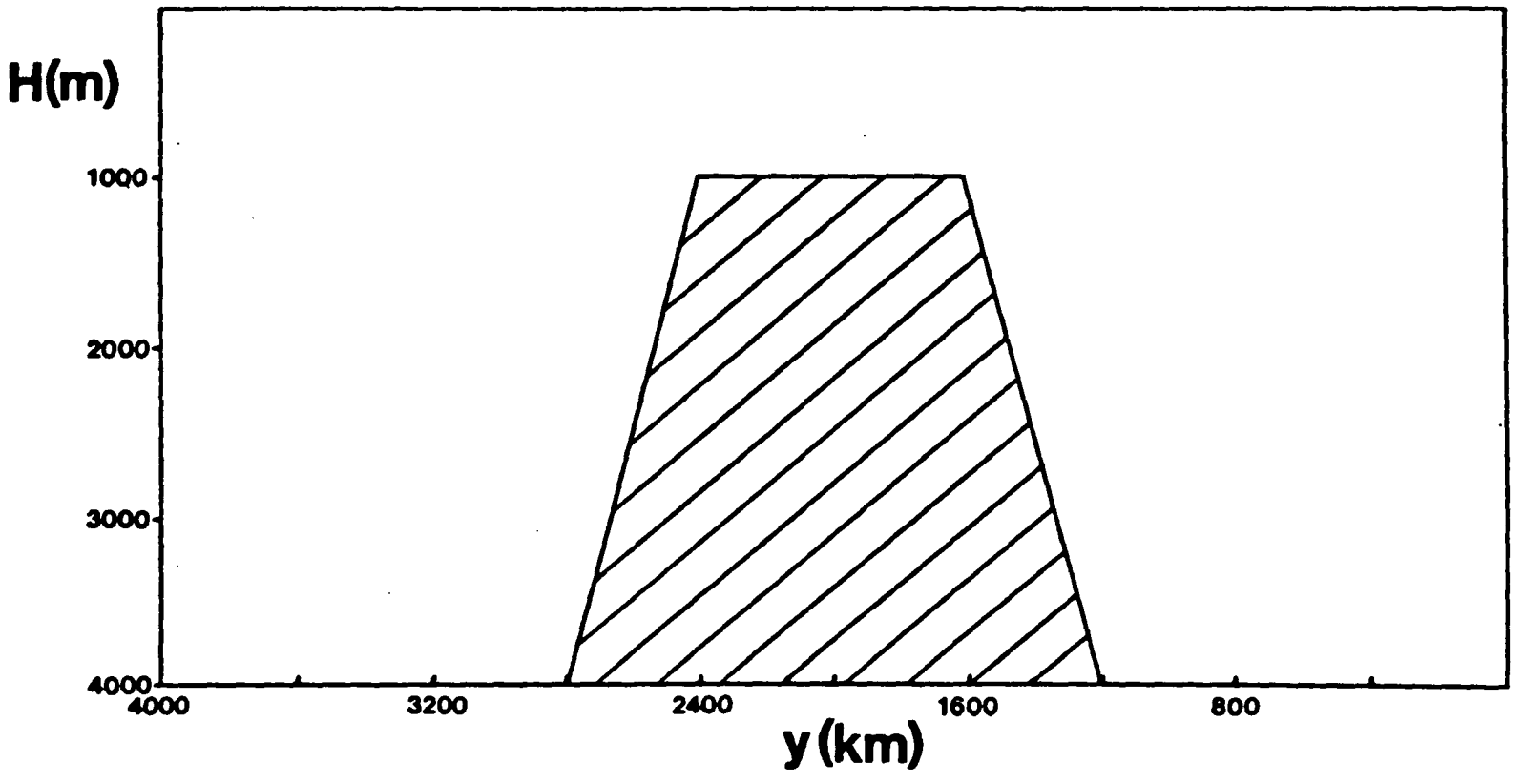

Fig 2.13 The ridge which is placed to the west of the island for the runs of Figs 2.14(a),(b), and (c).

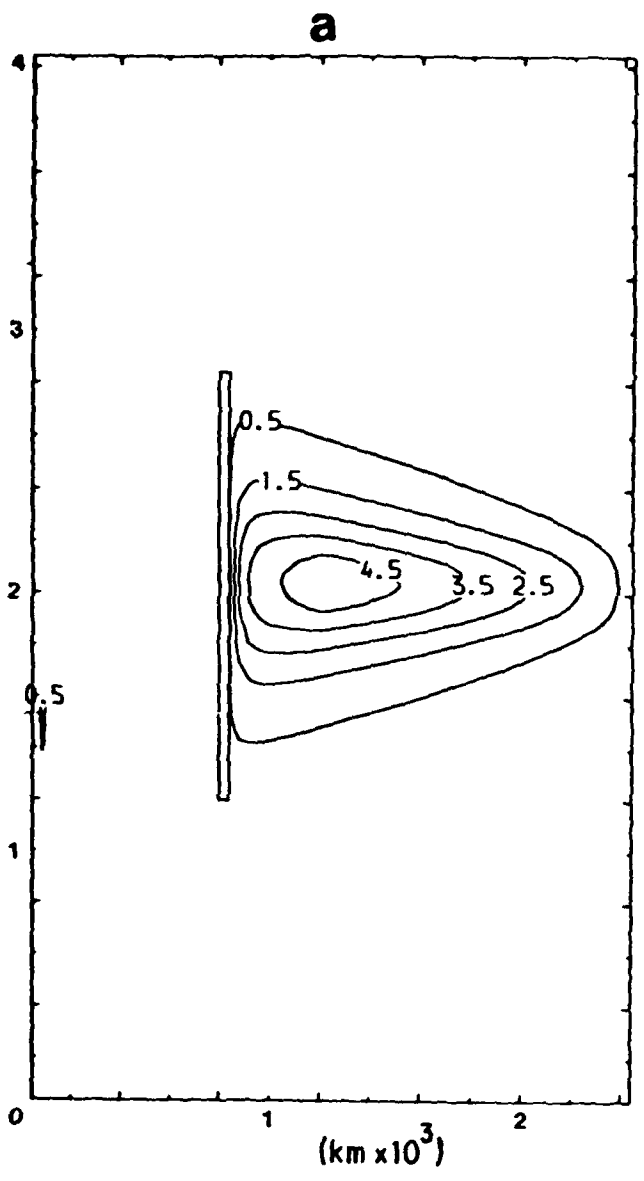

Fig 2.14(a) The streamfunction for high bottom friction, d=200 km, and the ridge of Fig 2.13.

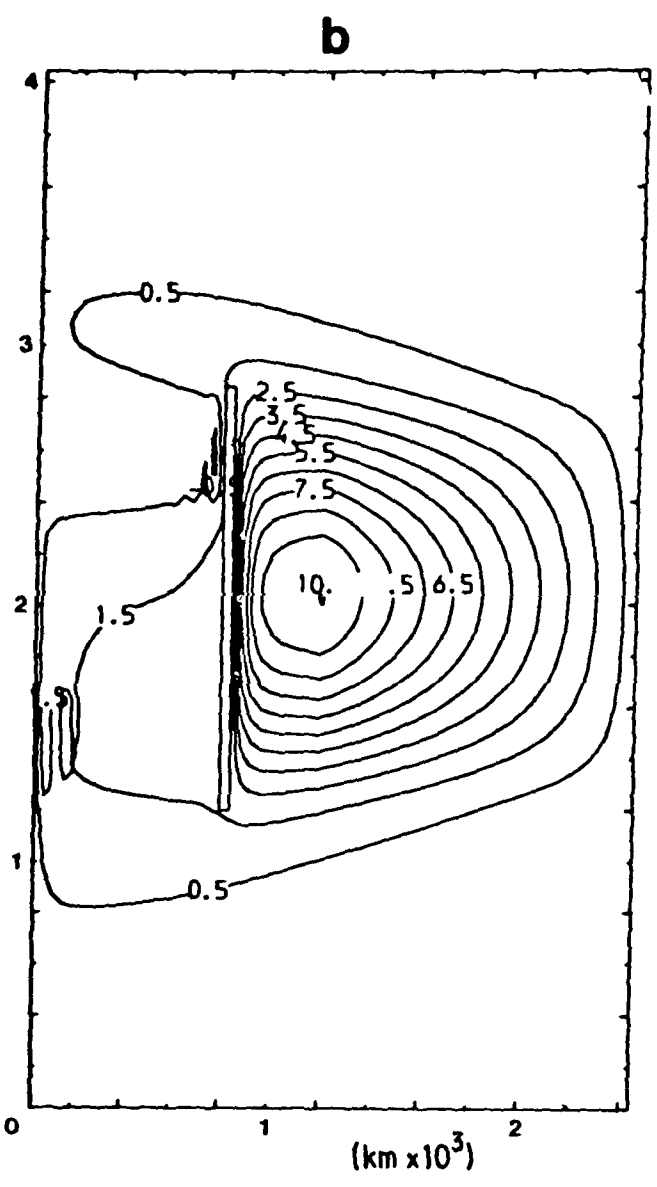

Fig 2.14(b) The streamfunction for high bottom friction, d=800 km, and the ridge of Fig 2.13.

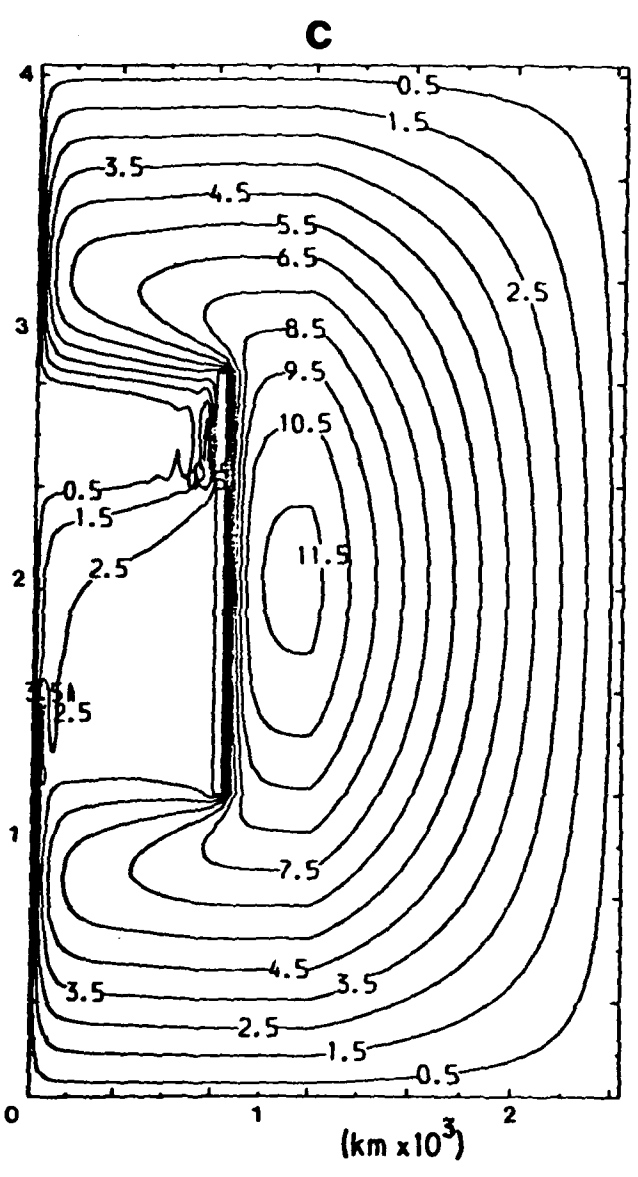

Fig 2.14(c) The streamfunction for high bottom friction, d=2000 km, and the ridge of Fig 2.13.

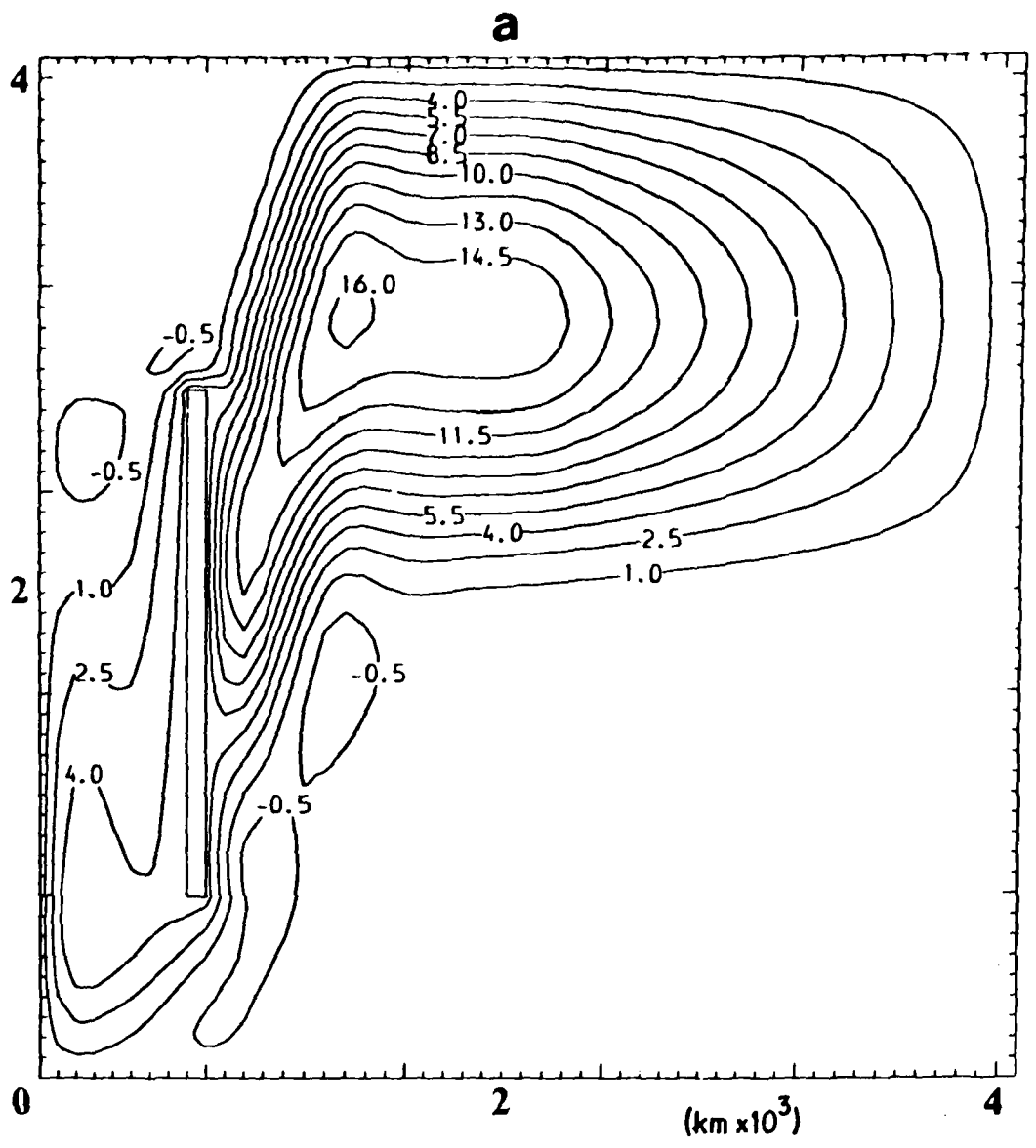

Fig 2.15(a) The streamfunction when a large island is placed on the east-west slope of Fig 2.6. Compare with Fig 2.7(b).

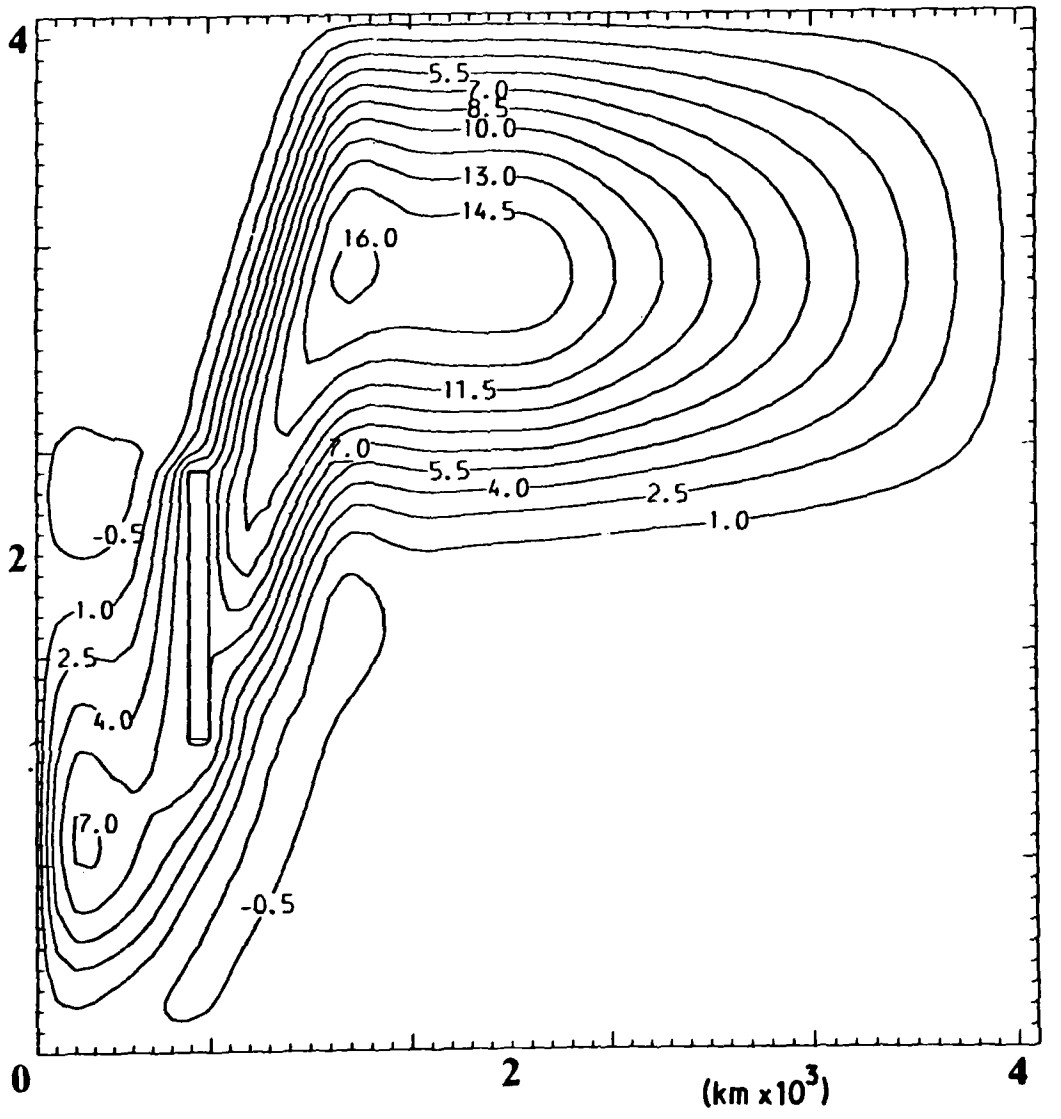

Fig 2.15(b) The streamfunction when a smaller island is placed on the east-west slope of Fig 2.6. Compare with Fig 2.7(b).

latitudinal excursions. As the gyre projects less onto the island ψ_I decreases, as one expects. Two further points are worthy of note.

(1) Movements of the wind stress forcing to north or south induce symmetrical displacements of the gyre. This is because in the absence of topography Eq 2.3 does not depend on f but only on β .

(2) Since the western boundary current is the only feature west of the island, it also follows that for the case of low bottom friction (where the interior solution does not decay substantially westward) the value of ψ_I will not change significantly as the island is displaced westward, provided that the island is not so close to the coast that it lies within the frictional boundary layer. An appropriate calculation is shown on Fig 2.12(b), which has identical friction and forcing to Fig 2.12(a), but with the island located farther west.

In the above calculations there was no bottom topography. To investigate the effect of topography a topographic barrier was put immediately to the west of the island. This had the form shown in Fig 2.13. The plots for d=200 km ;800 km ;2000 km are shown on Figs 2.14(a),(b),(c) for the case of high bottom friction for comparison with Fig 2.11. The streamfunction pattern to the west of the island shows a western boundary current where the topography has positive or zero slope, and an eastern boundary current where the topography has negative slope. This change happens because β is overpowered by the topographic

term so that the effective value of β changes sign, and topographic Rossby waves propagate eastwards. The proportions of the maximum transport value which pass to the west of the island are as expected much lower than for Fig 2.11, being respectively 7.9 %, 14.4 %, and 23.8 %. Thus, in all cases most of the transport is pushed to the east of the topography, but the proportion of transport which does pass between coast and island again increases with the ratio of the north-south scale of the forcing to the north south extent of the island.

The above topography varied in the north-south direction only. If we place an island in the middle of the shelf used in Section 2.3, then we can see the effect of an island in association with an east-west slope. Figs 2.15(a),(b) show two runs, one with a large island, and one with an island half the length. These figures are directly comparable with Fig 2.7(b). We see that again the proportion of transport which passes between coast and island increases with the ratio of the north-south scale of the forcing to the north-south extent of the island. Other calculations (not shown) indicate that the location of the island is important. If the island of Fig 2.15(b) is moved 5° north, then the pattern of ψ to the west of the island changes, and less transport passes between coast and island. For a given application (e.g. the Florida Current) location of islands, size of islands, surrounding topography and the position of wind stress curl relative to the topography may all be important. Here we merely illustrate the effect within a simple framework.

It has already been mentioned that in a homogeneous ocean the effects of islands are qualitatively similar to the effects of bottom topography. Thus, if we investigate the shadowing effect of an island, we are also investigating the shadowing

effect of strong bottom topography with shallower water to the west. The results above indicate that such bottom topography acts as a spatial filter so that the larger north-south scales of forcing have a proportionately greater effect on ψ_I. Carried over to a baroclinic ocean, this means that at 'short' periods, the larger north-south scales of forcing will have their contributions to transport variations to the west of a north-south topographic barrier weighted to a greater extent than the smaller scale forcing.

2.5: Generation of transport by baroclinic Kelvin waves.

2.5.1 Introduction

We have considered the effect of baroclinic Rossby waves over topography on transport variations, finding that at mid-latitudes and for 'short' periods baroclinic Rossby waves had little effect and transport variations were primarily barotropic. In the two dimensional model, however, a baroclinic coastal Kelvin wave can also influence boundary current transport variations, since over topography the barotropic and baroclinic modes are coupled. Anderson [1979a,b] noted that seasonal variations in the transport of the Florida Current were in phase with surface currents and suggested that one method by which this could occur was by passage over topography of a Kelvin wave, excited farther north by the longshore wind stress. In this Section we will consider this process more thoroughly.

The problem of resolution for the free Kelvin wave in a finite-difference numerical model such as the one used here has been addressed by Hsieh, Davey and Wajsowicz [1983]. They show

that for the Arakawa C-grid the phase velocity of the Kelvin wave is largely independent of resolution. For a free-slip boundary condition and the parameters used here we also find that the offshore profile of the Kelvin wave differs only slightly from the exponential.

In the following numerical experiments the only forcing of the barotropic mode will be that due to baroclinic activity. The situation we shall consider will be the case of a baroclinic Kelvin wave forced in the northern part of the basin which passes over topography that varies with latitude. A Kelvin wave is well represented on an f-plane, so we will begin the discussion of this mechanism first on an f-plane and only later consider β effects. To make sure the Kelvin wave was adequately resolved the model resolution was doubled to 40 km. H_1 was changed to 150 m, g' to 0.06 m s^{-2}, and f was taken as 5×10^{-5} s^{-1}. This choice of parameters corresponds to a Kelvin wave speed of 3 m s^{-1} and a radius of deformation of 60 km. The first grid point for η_2 is 20 km from the boundary. A north-south slope of 10^{-3} was used so that the total depth changed from 800 m to 1200 m over 400 km. The bottom friction was zero and the horizontal diffusion coefficient was taken as 10^4 $m^2 s^{-1}$. The topography as a function of latitude is shown on Fig 2.16.

2.5.2 Results

To generate the Kelvin wave, a uniform meridional wind stress of magnitude 0.1 N m^{-2} was imposed in a latitude band to the north of the topography (also shown on Fig 2.16). In an inviscid ocean this generates a time independent response south of the forcing region of the form:

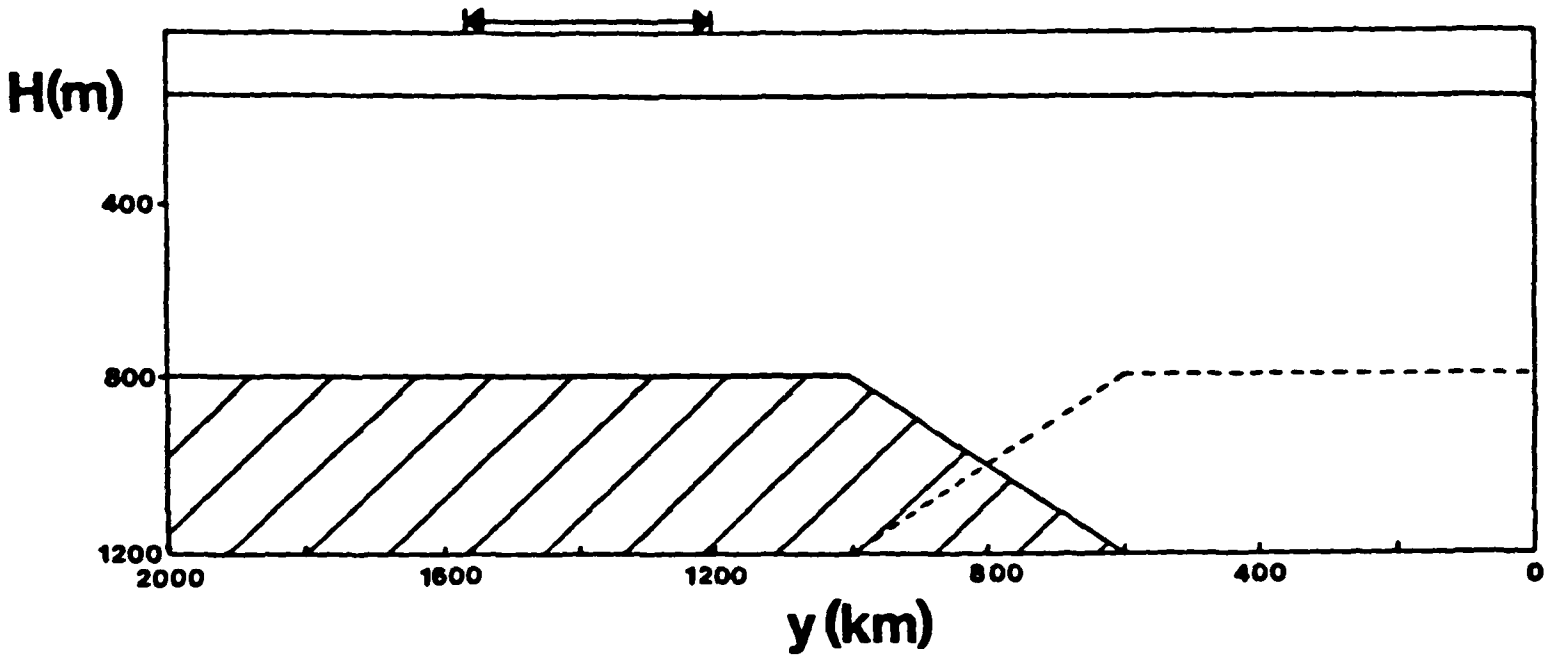

Fig 2.16 The latitudinal profile of topography used in the calculations of Section 2.5 can be either that given by the solid or dashed lines.The coastal Kelvin wave is generated by a meridional wind stress confined to the region delimited by arrows.

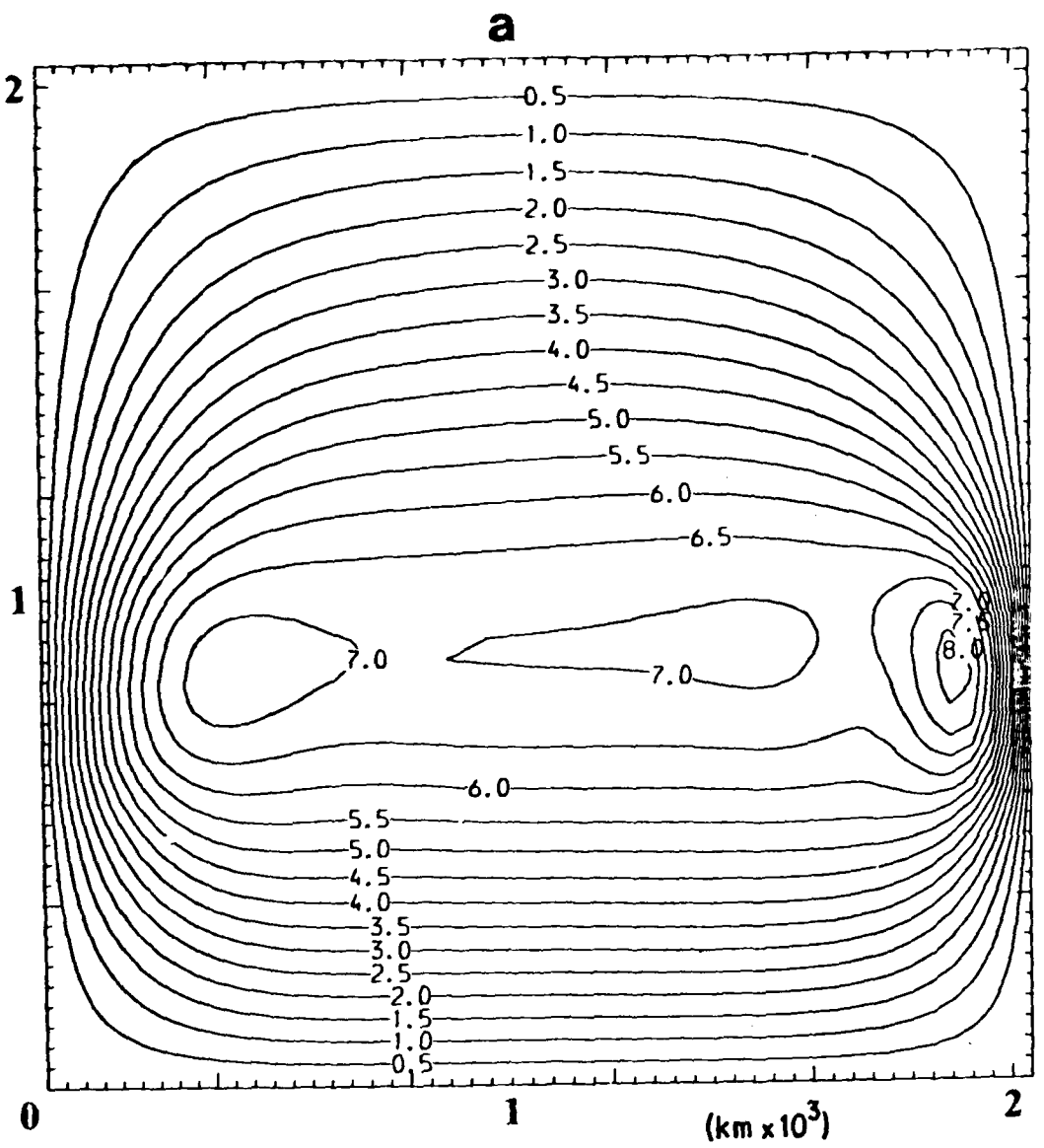

Fig 2.17(a) The streamfunction for the f-plane calculation when the negative slope topography of Fig 2.16 (i.e. dashed line) extends all the way across the basin. The contours are marked in tenths of a Sverdrup.

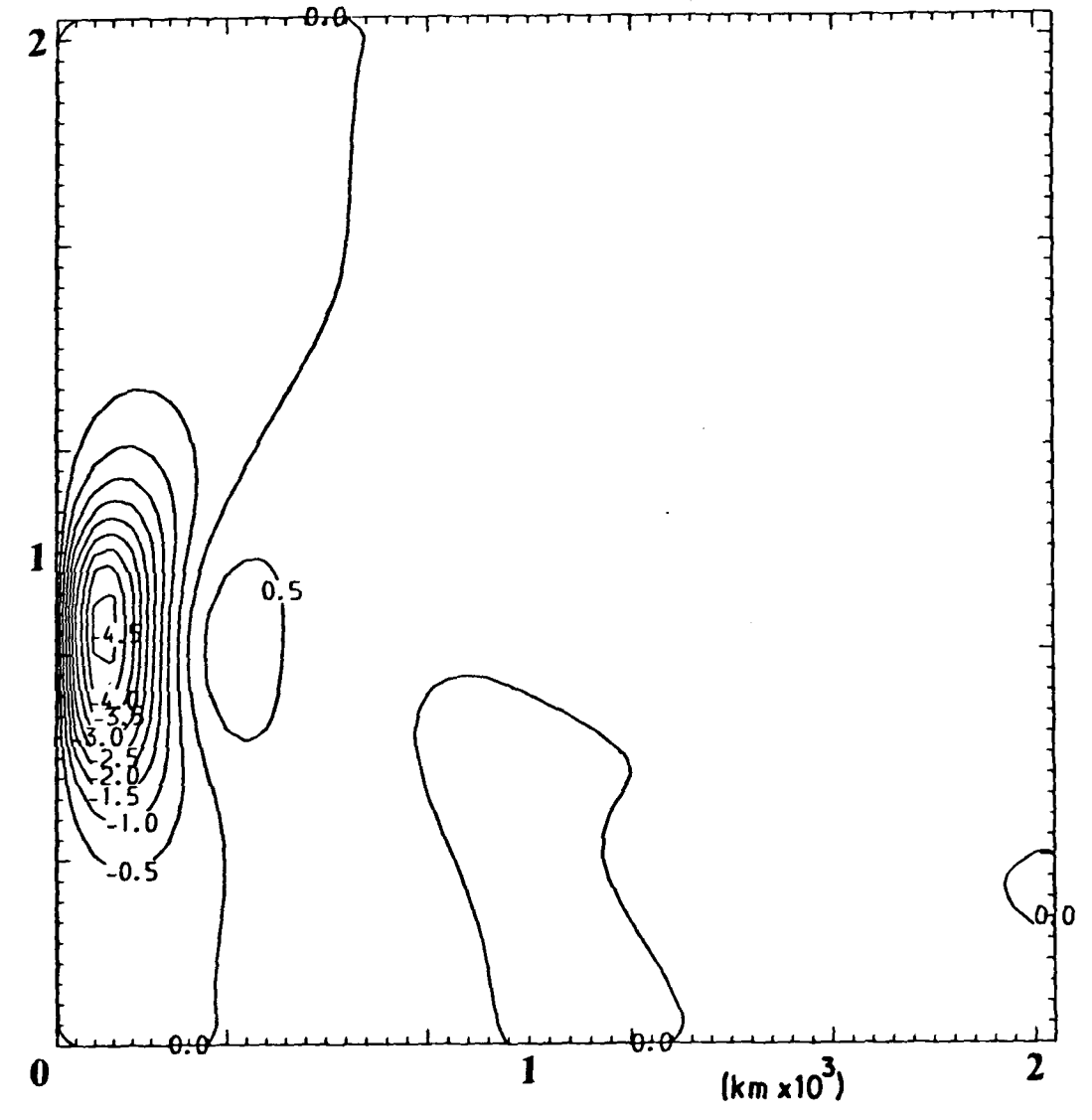

Fig 2.17(b) As for Fig 2.17(a) but with topography of positive slope (i.e. given by the solid line of Fig 2.16).

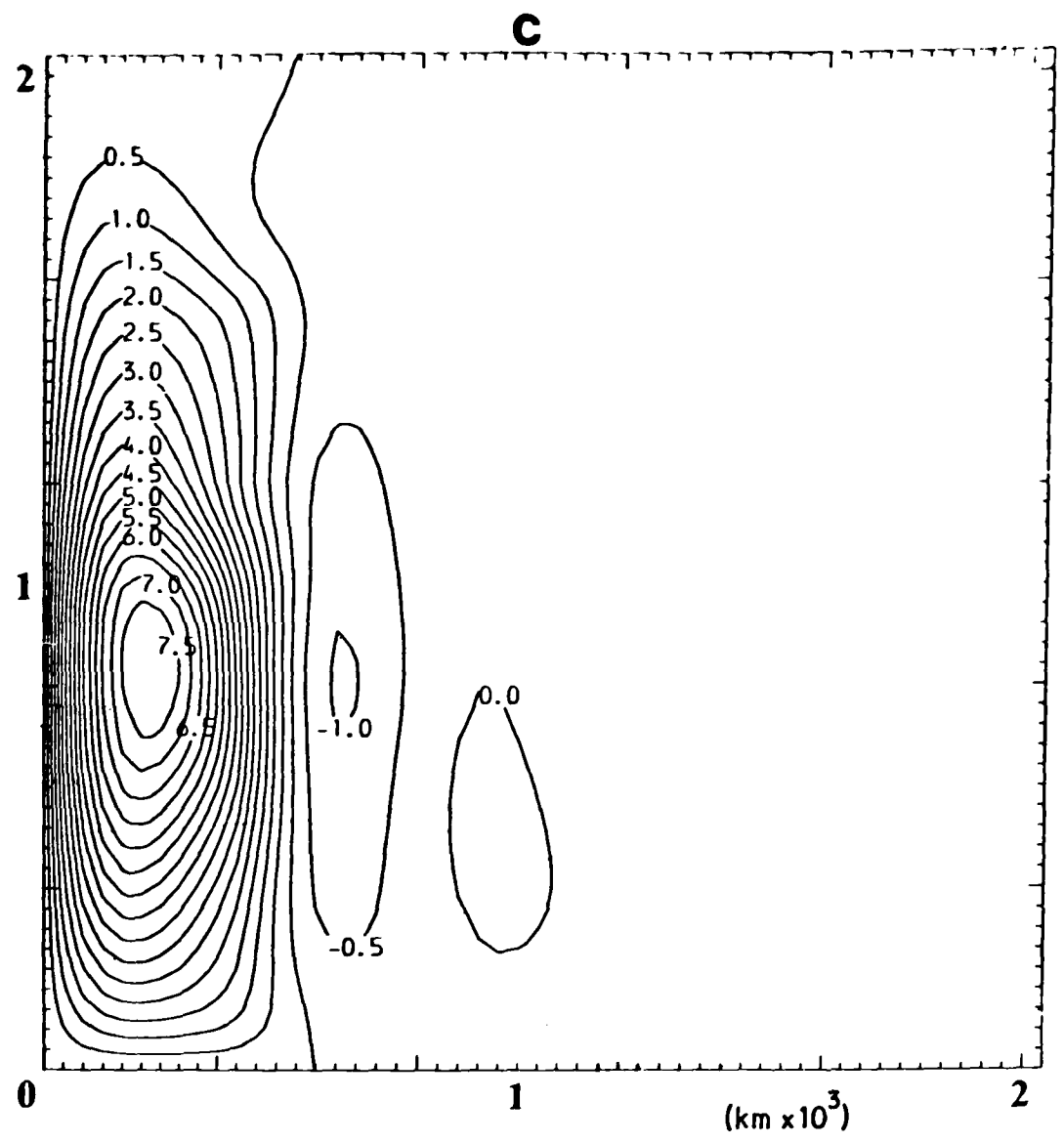

Fig 2.17(c) The streamfunction for the β-plane calculation with truncated topography. The slope is negative.

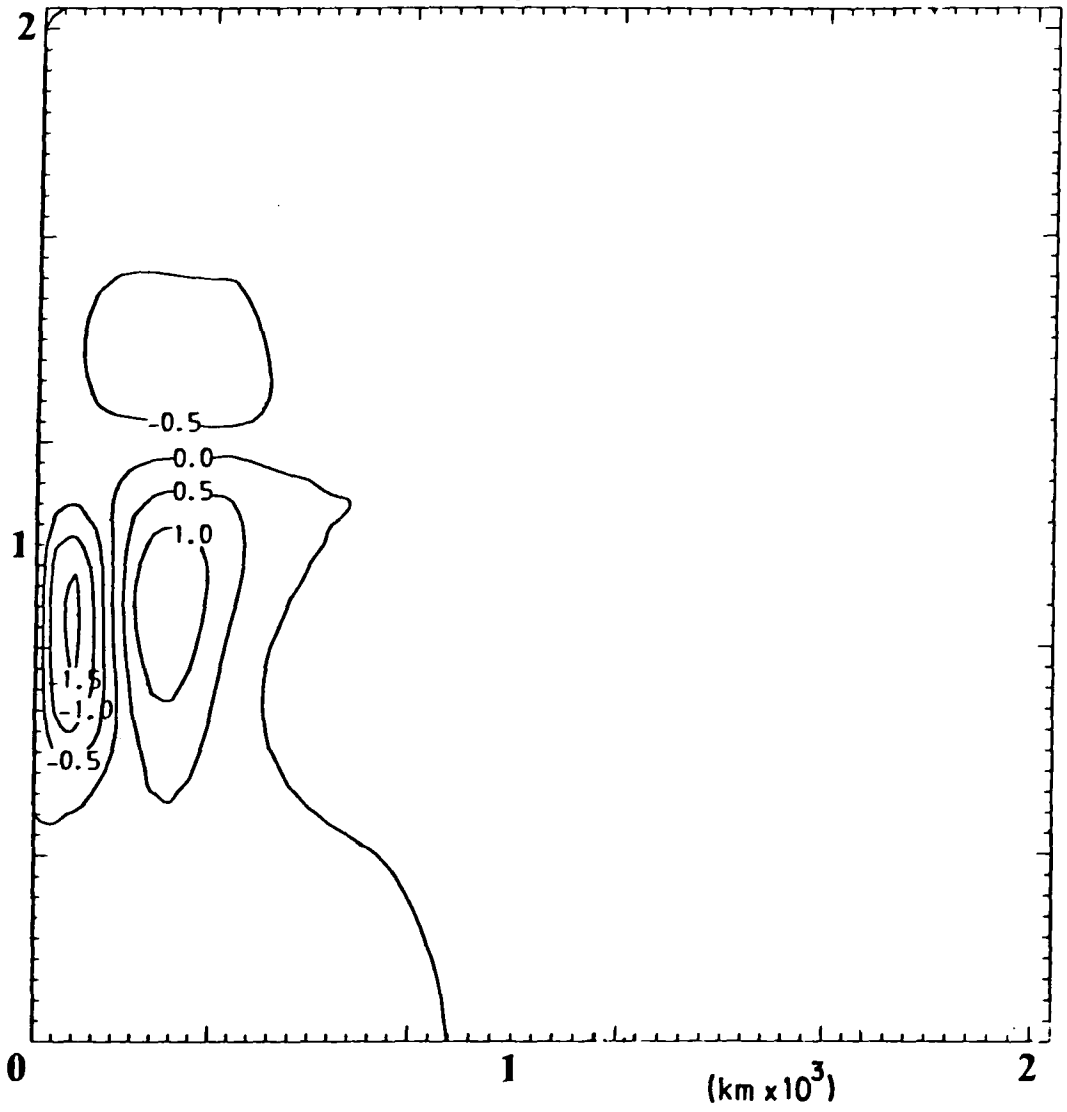

Fig 2.17(d) The streamfunction for the β-plane calculation with truncated topography. The slope is positive. Comparison with Fig 2.17(b) shows a reduced response immmediately adjacent to the western boundary.

Eq 2.8 $\eta_2 = \eta_0 e^{-x/a}$; $\eta_0 = \int Y_0 dy \ /(g' H_1)$; $a = (g' H_1)^{\frac{1}{2}}/f$

It was ensured that this was the only source of baroclinic activity over the topography to the south by damping out Kelvin waves along the northern and southern boundaries. The equation governing the streamfunction is B13 written here as Eq 2.9:

Eq 2.9 $$\left(\frac{\Psi_{xt}}{H}\right)_x + \left(\frac{\Psi_{yt}}{H}\right)_y = \mathrm{curl}_z\left[f\frac{\nabla\Psi}{H} + g'\frac{H_1\nabla\eta_2}{H} + \frac{\tau}{\rho_1 H} + F\right]$$

The term involving η_2 represents the forcing of the barotropic mode by the baroclinic. Simple scale analysis shows that at annual period and for reasonable slopes, the time dependent terms are small (i.e. the barotropic response is close to equilibrium), so only the problem of steady state forcing need be considered. Figures 2.17(a) and 2.17(b) show the streamfunction basinwide for negative and positive slope of the bottom topography ($T_y<0$ and $T_y>0$). There is a marked difference between these cases. If $T_y > 0$ it is seen that transport variations are confined to the west, while if $T_y < 0$ the streamfunction is altered basinwide, though forced only in the west. The reason for this asymmetrical response stems from the propagation of topographic Rossby waves. When $T_y > 0$ the direction of propagation is westward, so the response remains local to the boundary. When $T_y < 0$, waves can propagate eastwards and the response is basinwide.

In Appendix D a simple model is used to consider this effect further. For $T_y>0$, the northward transport forced immediately adjacent to the western boundary is out of phase with that in the surface layer. This is due to a bottom velocity comparable with the surface velocity, but in the opposite direction. The surface velocity is not greatly altered from that expected for an

inviscid Kelvin wave but (see Appendix D) the boundary layer structure of the barotropic response is heavily dependent on the viscous scheme used in the model. For $T_y<0$, the transport is in phase with the surface velocity, and the bottom velocity is negligible. The viscous scheme used is less important in this case, since the frictional boundary layer is next to the eastern rather than the western boundary.

The above transport variations were forced on an f-plane. We now consider how they are altered when β effects are taken into account and the topography of Fig 2.16 is truncated. The balance in the interior where there is no topography will be $\beta \psi_x = 0$ which coupled with the constraint on the eastern boundary that ψ should be zero there, implies that ψ should be zero in the interior. Hence, for truncated topography, variations in ψ will be confined to the western boundary region for both signs of T_y .The bottom topography was changed so that for x>400 km the depth of the ocean was a constant 1000 m for all latitudes. Figures 2.17(c) and 2.17(d) show the streamfunctions for the β -plane calculations with this topography. β was taken as 2×10^{-11} m^{-1} s^{-1} , and f was 5×10^{-5} s^{-1} at y=800 km. The transport forced with $T_y>0$ is much reduced in amplitude compared to the f-plane case, though the shape of the response is similar.

For a fetch of 360 km and wind stress of 0.1 N m^{-2} the values of transport generated were low (0.5 Sverdrup). For the Florida Current the fetch is several times that used, so larger transports could result. The efficacy of the process also depends on what changes in topography the Kelvin wave experiences as it travels equatorward, and it is less clear what values should be taken for this. Whether the passage of a Kelvin wave generated to the north of the Florida Straits can induce variations in Florida Straits transport comparable with those

observed can not be answered in this calculation. A more detailed study involving the proper geometry and topography is required.

2.6: Summary and Conclusions:

The motivation behind this chapter is to understand the seasonal variation of a western boundary current in the presence of bottom topography and islands in a wide baroclinic ocean. The seasonal variation of the Florida Current, measured by Niiler and Richardson, has for a long time not been understood, since application of the Sverdrup relationship predicted seasonal variations of far greater magnitude and almost opposite phase to those measured (Niiler and Richardson [1973]). This same relationship, however, has been used successfully to predict the mean flow of the Florida Current (Leetmaa et al [1977]). This suggests that there is a difference between the dynamics of the mean flow and that of the annual cycle.

Anderson and Killworth [1977] investigated the response of a one-dimensional two layer ocean initially at rest to a steady wind forcing imposed at t=0. This was done in order to clarify the corresponding response of the fully three dimensional model of Anderson et al [1979]. It was found that the Sverdrup balance was set up on the timescale of the baroclinic response. When baroclinic Rossby waves emitted from the eastern edge of the wind forcing had fully passed over the bottom topography, the transport rose to the value appropriate for a homogeneous flat-bottomed ocean, i.e. the Sverdrup value. The effect of topography was therefore compensated for by the baroclinic response.

Consider now the response of this model to periodic forcing. For forcing periods much longer than the baroclinic adjustment time of $2\Lambda_1$ (in dimensional units $2\Lambda_1 = 2Lf^2/(\beta g'H_1)$ corresponding to the time taken for a baroclinic Rossby wave to cross the basin), the ocean will be very close to baroclinic equilibrium so that the Sverdrup balance almost holds for the baroclinic mode. If the relevant wind stress variation does not extend to the eastern boundary, then the appropriate adjustment time is that for a baroclinic Rossby wave to travel from the eastern edge of the forcing, not the eastern boundary. This means that the effect of bottom topography will be almost totally compensated for, with all the transport in the upper layer. Conversely at periods short enough that the interior baroclinic response has much lower amplitude than the maximum Sverdrup value for the forcing, the transport is that for a homogeneous ocean and so strongly affected by topography. For periods less than $\Lambda_1/2$ the amplitude of the boundary response was at the barotropic level (about 5% of the value for steady forcing), and the phase roughly zero. At intermediate periods of about $2\Lambda_1$ the amplitude and phase of the response in the boundary current region varied rapidly with period. Because the baroclinic mode is far less affected by the barotropic mode than the barotropic by the baroclinic (due to the δ factor $\delta \ll 1$ in Eq 2.2), this variation can be understood in terms of a growing non-equilibrium baroclinic response forcing the barotropic mode over the topography with comparatively little feedback.

The above results from the one dimensional model suggest that unless forcing adjacent to the western boundary is considered, the seasonal response of the Florida straights will be essentially barotropic, and hence strongly dependent on topography. Integration of the seasonal components of

curl($\underline{\tau}$) along a latitude circle will not measure western boundary transport variations. At annual period, we expect the Mid-Atlantic ridge to weaken the contribution to boundary layer transport resulting from seasonal wind stress changes in the eastern half basin.

The one dimensional model suffers from the obvious limitation that two dimensional topography, wind stress, and geometry cannot be handled, so a two dimensional two layer model was developed. It was first verified that transport variations outside of the tropics were predominantly barotropic at 'short' periods such as the annual. Later it was shown that seasonal transport variations can also be generated by a uniform wind stress over varying topography with a virtually identical streamfunction pattern at higher latitudes to that predicted for a homogeneous ocean. The vertical distribution of the transport in this case was not, however, barotropic. Due to a baroclinic Kelvin wave the upper layer can carry a larger than barotropic proportion of the transport variations. Because the transport generation does not depend on wind stress curl, but on the wind stress itself, this method of transport generation could also potentially explain the phase of the boundary transport variations.

The effect of an island oriented north-south on transport variations forced to the east of the island was investigated in Section 2.4. For a homogeneous ocean, the effect of an island is much the same as the effect of strong bottom topography, and this similarity carries over to the case of a baroclinic ocean at 'short' periods. It was found that for a channel to the west of the island, both with and without topography, the proportion of transport that passed between island and coast was greater for larger north-south scales of forcing. Thus a topographic barrier

such as a chain of islands acts as a spatial filter in a baroclinic ocean at 'short' periods, such that larger north south wavelengths contribute proportionately more to transport variations.

Yet another method of transport generation that could be important near a western boundary is the effect of a baroclinic coastally trapped wave passing over varying topography. This is possible due to the coupling of modes over the topography. For topography with a north-south gradient, a meridional transport is generated. The details of the transport variations generated depend on the sign of the slope. If the slope is appropriate for eastward propagation of topographic Rossby waves, then the streamfunction is affected basinwide. For slope of opposite sign, the response is local, with the details depending on the dissipation scheme used (see Section 2.5). Since this mechanism of transport generation depends on the alongshore wind stress, it could also potentially explain the phase of the boundary transport variations.

Two mechanisms of transport generation other than wind stress curl have been described which could be relevant to understanding the seasonal cycle of the Florida Current. These are:

(1) Transport generation by the magnitude of the wind stress over varying bottom topography.

(2) Transport generation by the passage of a coastally trapped baroclinic signal over varying topography.

The generation of transport variations by Rossby waves has been neglected in the above list since it is a small effect at extratropical latitudes for 'short' periods such as the annual.

The relative importance of the above mechanisms can only be determined for a particular problem such as the Florida Straits transport by use of the real winds in association with the correct bottom topography and geometry.

CHAPTER THREE

Most of this chapter is written up in Anderson and Corry [1985b]*

The Florida Current

3.1: Introduction:

The pioneering work of Niiler and Richardson [1973] showed that the Florida Current had a mean transport of 30 Sverdrups and suggested an annual cycle of 4 Sverdrups. These results were based on a series of experiments each lasting a few weeks but spanning several years. The fact that the measurements were not distributed uniformly over the year, combined with the existence of energetic high frequency fluctuations (Wunsch and Wimbush [1977], Brooks [1979]), made it difficult to define precisely the annual cycle and to distinguish seasonal from interannual variability. Fig 3.1 is a replot of the Niiler and Richardson data aimed at visually maximising the seasonal effect; this includes a maximum in Summer and a minimum in Fall. There is a gap in the data during August, but this is filled on the figure by later data from Brooks [1979]. Recent work by Molinari, Schott, Zantopp and others in the STACS program further supports such a seasonal cycle (See Chapter 1).

The mean transport of 30 Sverdrups is consistent with expectations based on integrating the annual mean wind stress curl across the basin at latitude 31°N (Leetmaa, Niiler and Stommel [1977], Leetmaa and Bunker [1978]). However, integration of the seasonal wind stress curl across latitude 31°N suggests a seasonal variation of the Florida Straits transport of ± 15 Sverdrups with a maximum in Winter. The fact that neither the

* Anderson, D.L.T. and R.A. Corry [1985b] J. Phys. Oceanogr, 15, pp 773 – 786

strength nor phase of the observed seasonal transport is consistent with the Sverdrup relationship suggests that the dynamics governing the mean flow must be different from those governing the seasonal variation.

In Chapter 2 the dynamics of the seasonal variation of western boundary currents was investigated. It was shown that the Sverdrup balance is unlikely to hold at annual period for the North Atlantic. For periods much less than the time taken for the wind-generated baroclinic Rossby waves to pass over bottom topography, the ocean response is primarily that for a homogeneous ocean and thus strongly modified by topography. For periods much longer than this time the Rossby waves compensate for the effect of topography and the non-topographic Sverdrup balance holds. For the Atlantic at 25°N it can take years to decades for compensation by baroclinic Rossby waves to occur, depending on the distance from the western boundary of the wind stress variability. This means that at annual period the Sverdrup balance is not likely to be applicable. At such periods (annual or less), variations in transport can be due to barotropic Rossby waves generated by $\mathrm{curl}_z(\underline{\tau}/H)$ (see Eq B13) where $\underline{\tau}$ is the wind stress and H is the ocean depth. This can be split into two parts, one resulting from the curl of the wind stress and the other from gradients in topography. It is important to note that transport variations can be forced even in the absence of wind stress curl. Since the streamlines follow roughly f/H contours, the Florida Straits transport variations could result from wind forcing to the north-east. In addition to the barotropic mechanism, the work of Chapter 2 showed that a baroclinic Kelvin wave generated further north could induce transport variations as it passes over topography.

In this chapter we wish to model the seasonal cycle of

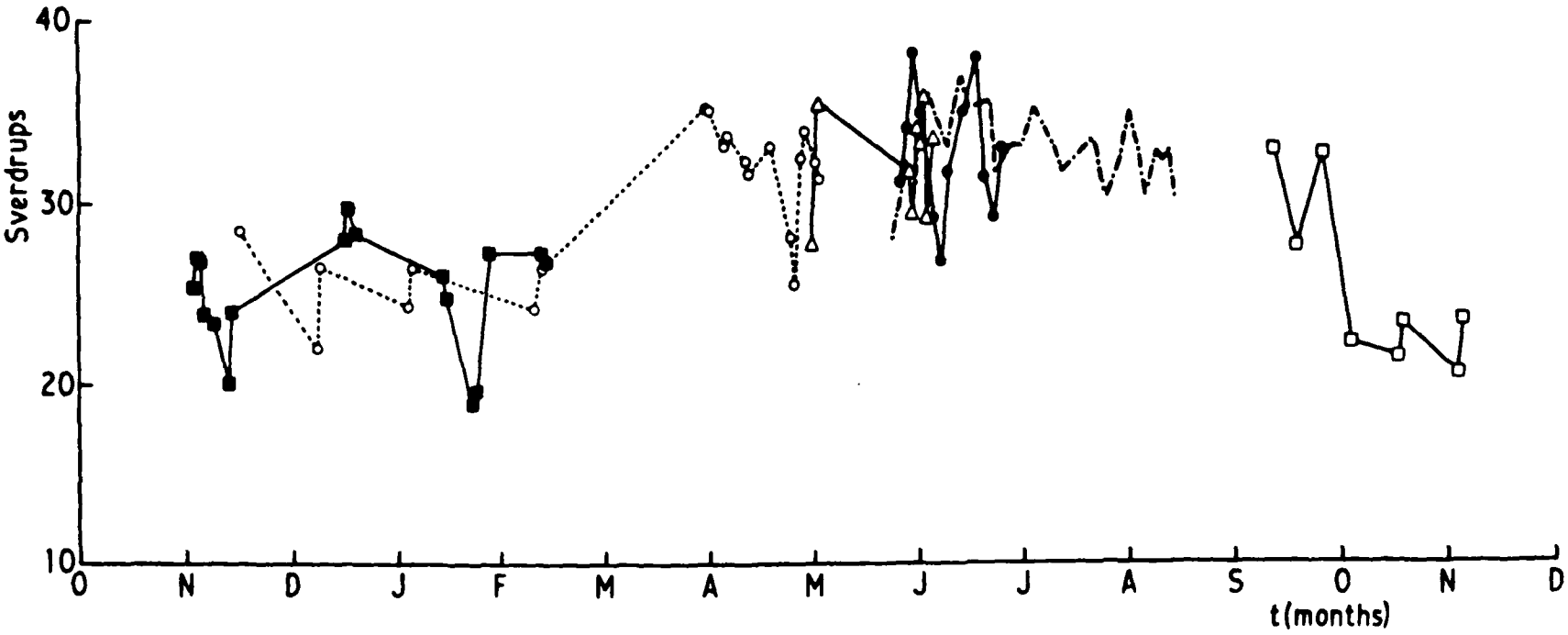

Fig 3.1 A replot of the Niiler and Richardson [1973] data aimed at visually maximising the seasonal effect. Later data from Brooks [1979] are also included on the dot-dash line. The other symbols correspond to data sequences.

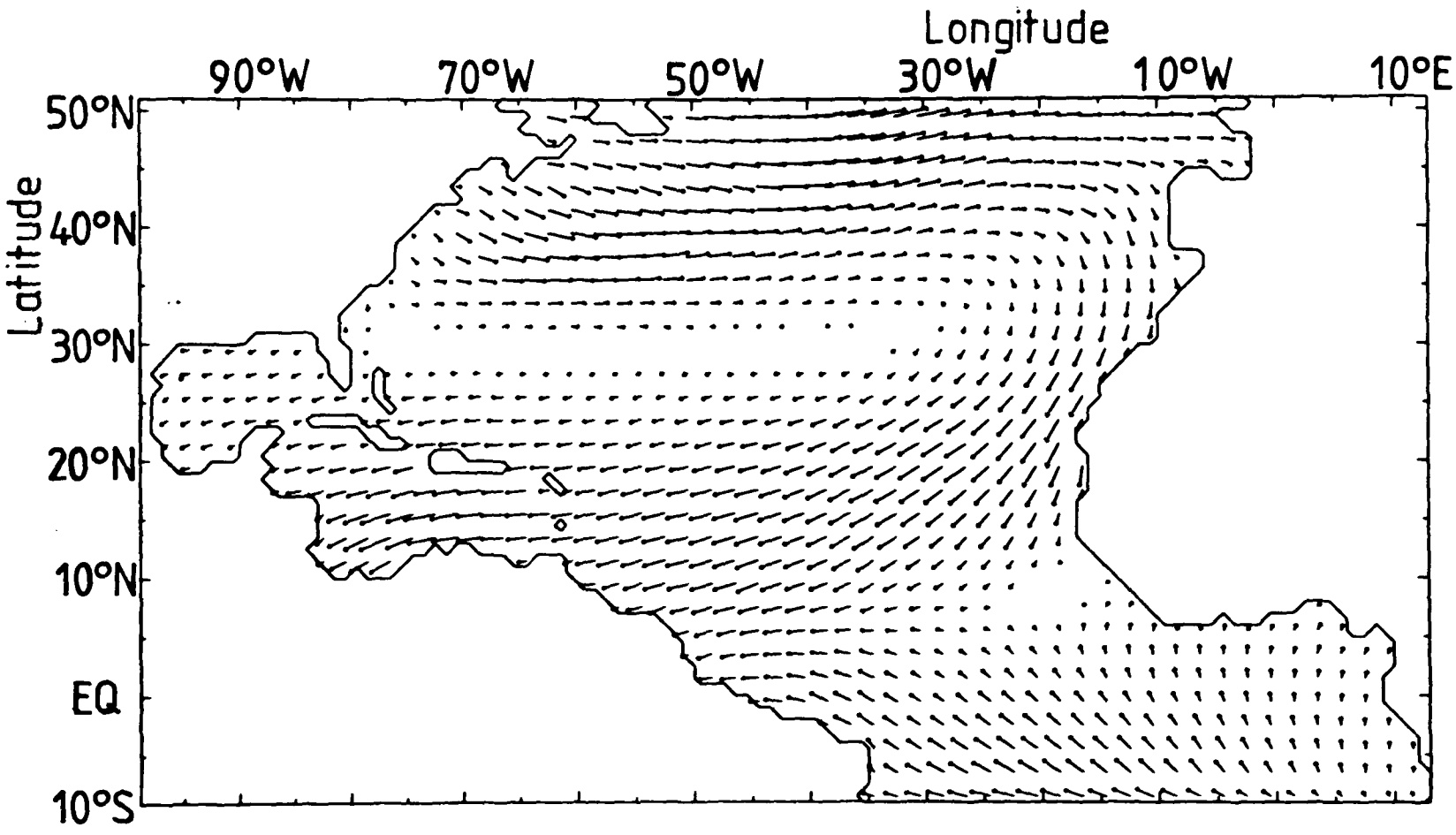

Fig 3.2 The annual mean wind stress. The space between arrowtails is equivalent to .1 N m^{-2}.

transport through the Florida Straits, to find the areas of wind stress which induce the seasonal variation, and to compare the model results with observations. While emphasis is given primarily to the Florida Straits (Section 3.3), some consideration is also given to other regions such as the Antilles Current region, the Caribbean, the Gulf Stream, and an area to the east of the Amazon (Section 3.4).

3.2: The ocean models and the wind stress forcing.

Two models are used. The first is linear and has two layers in the vertical. The model equations and method of solution are the same as described in Appendix B except that the equations are for spherical geometry rather than the β-plane. Two types of friction are included: Laplacian friction with a mixing value of 10^4 $m^2 s^{-1}$ and bottom friction with a damping time of 100 days. Continuous bottom topography can be readily incorporated provided it is confined to the lower layer. In Appendix E the bottom topography actually used and the choice of islands is discussed. Realistic geometry is used as far as possible at a resolution of one degree. The domain extends from 10°S to 50°N. Free slip boundary conditions are used throughout. In addition a single layer barotropic model with or without bottom topography is used to assist in the interpretation of results. The baroclinic model is integrated for five years, but the barotropic model only for shorter times.

The wind stress data were prepared on a one-degree grid by Hellerman from the data compiled by Bunker and Goldsmith [1979], and consist of averages for each month over several years. The annual mean wind stress is shown on Fig 3.2. Since the model to

be used is linear, we can separate the seasonal variations of wind stress from the mean wind stress and consider the effect of each separately. The seasonal wind stresses are the monthly means after the annual mean has been subtracted. The transport values and streamfunction patterns which will be presented are those at the end of each month's integration. There was very little difference between the fourth and fifth years of integration at all latitudes, and virtually no difference in the transport of the Florida Straits between the first and fifth years of integration, confirming a result of Chapter 2, that wind-forced baroclinic Rossby waves have very little effect on the seasonal variations of transport at these or higher latitudes.

Figs 3.3 show the streamfunction throughout the basin during the fifth year of integration of the baroclinic model. For comparison we show on Figs 3.4 the equilibrium streamfunctions for January, April, July and October for the case of a flat-bottomed ocean. In the latter case the western boundary transports are close to the Sverdrup values, and thus reflect the curl of the wind stress to the east.

The models used in this paper are more appropriate for studying variability than the mean state, but for completeness, the results for the mean wind stress will be considered in Section 3.5, after discussing the seasonal variation in Sections 3.3 and 3.4.

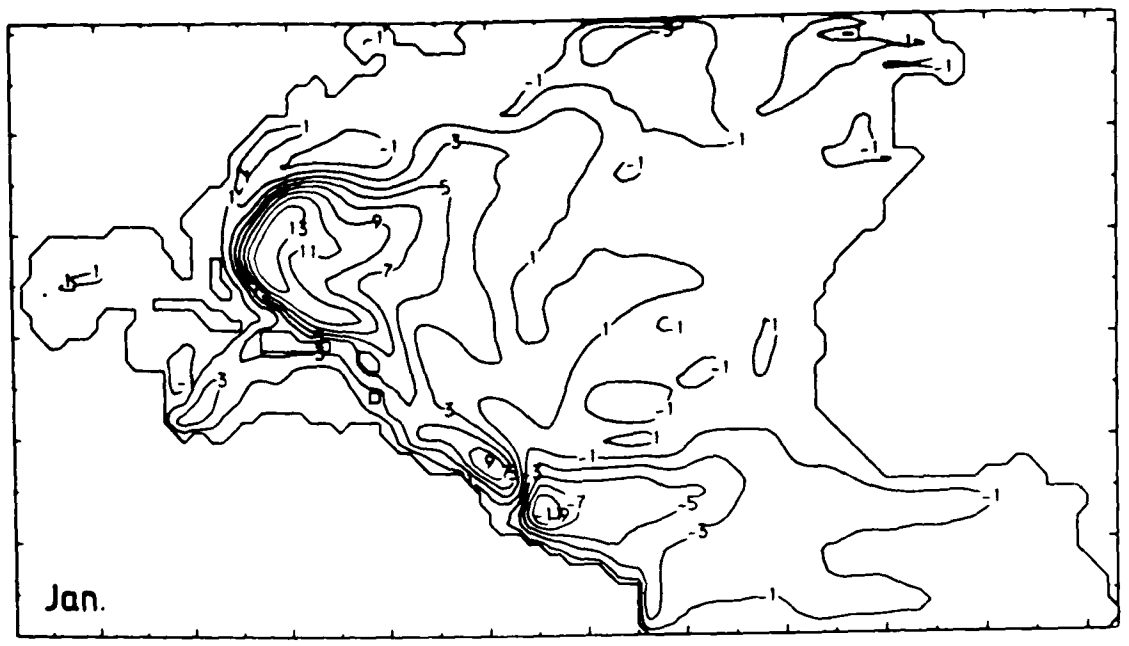

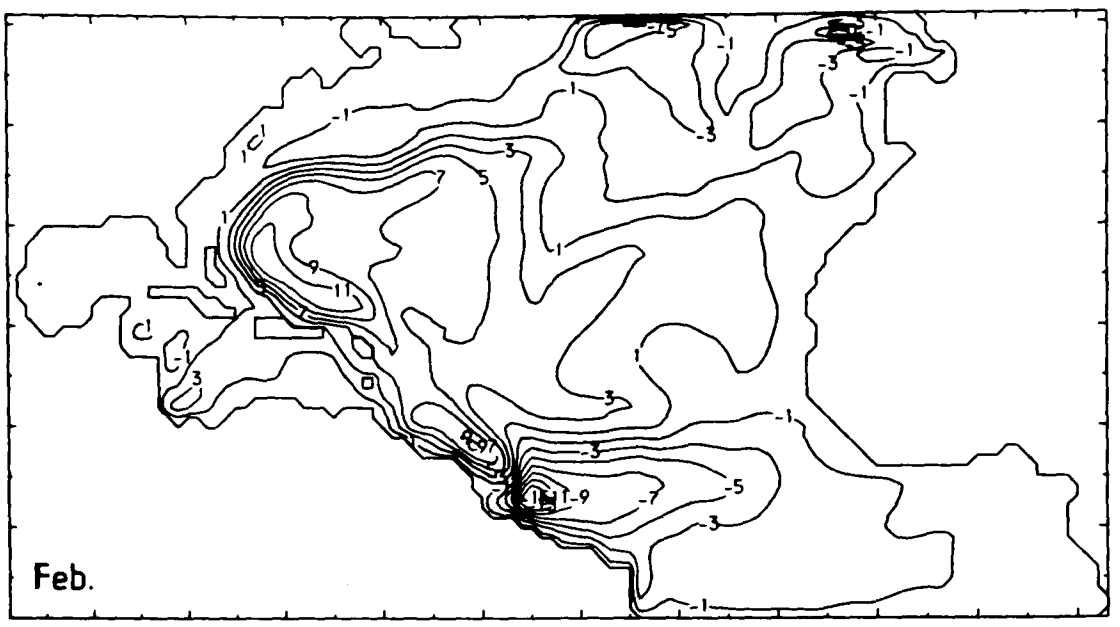

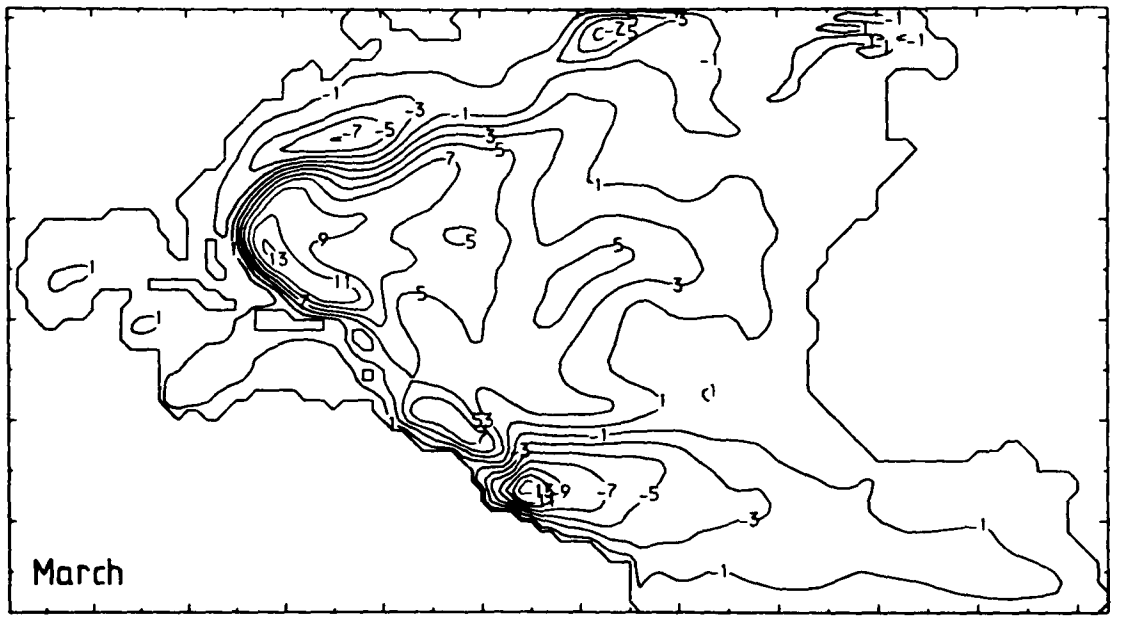

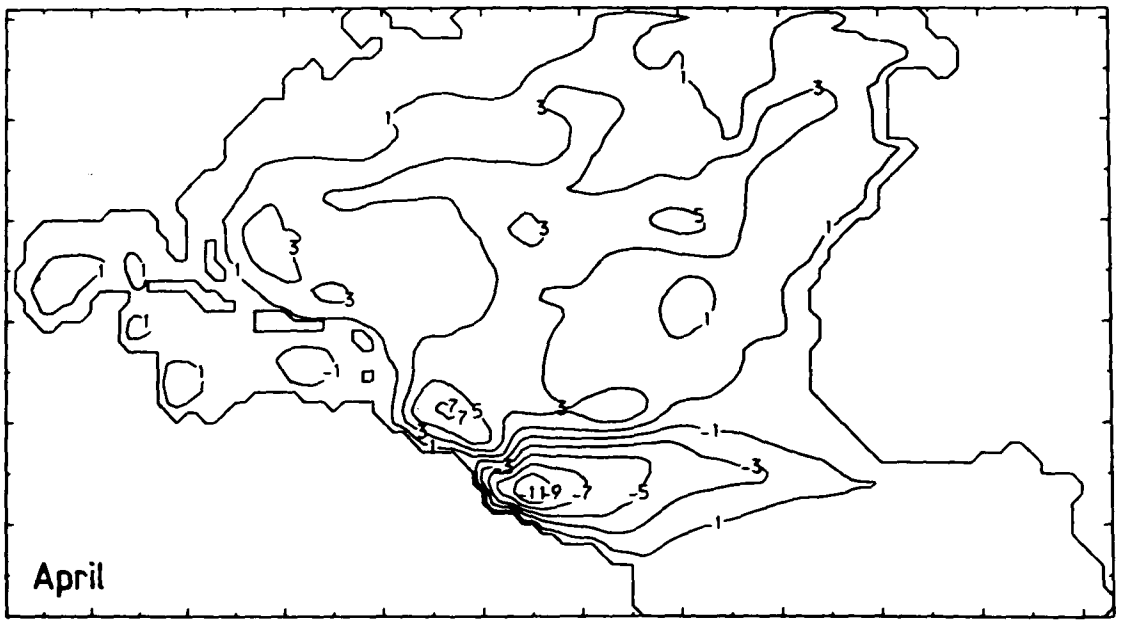

Figs 3.3 The streamfunctions during the fifth year of integration when the seasonal wind stresses for January to December are used. Bottom topography is smoothed as in Appendix E.

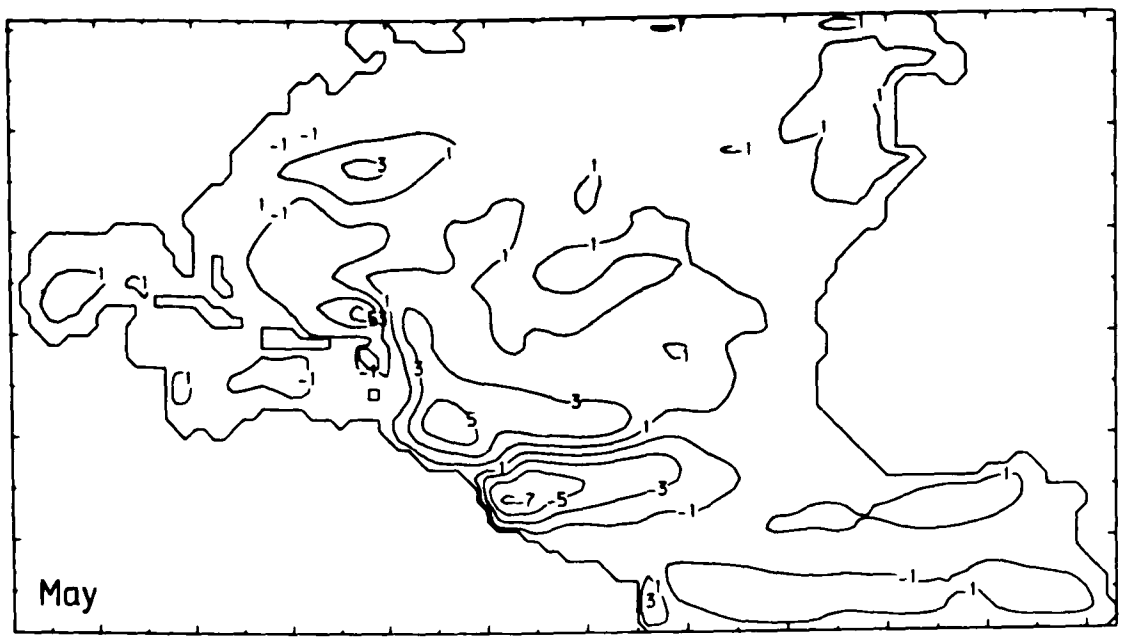
May

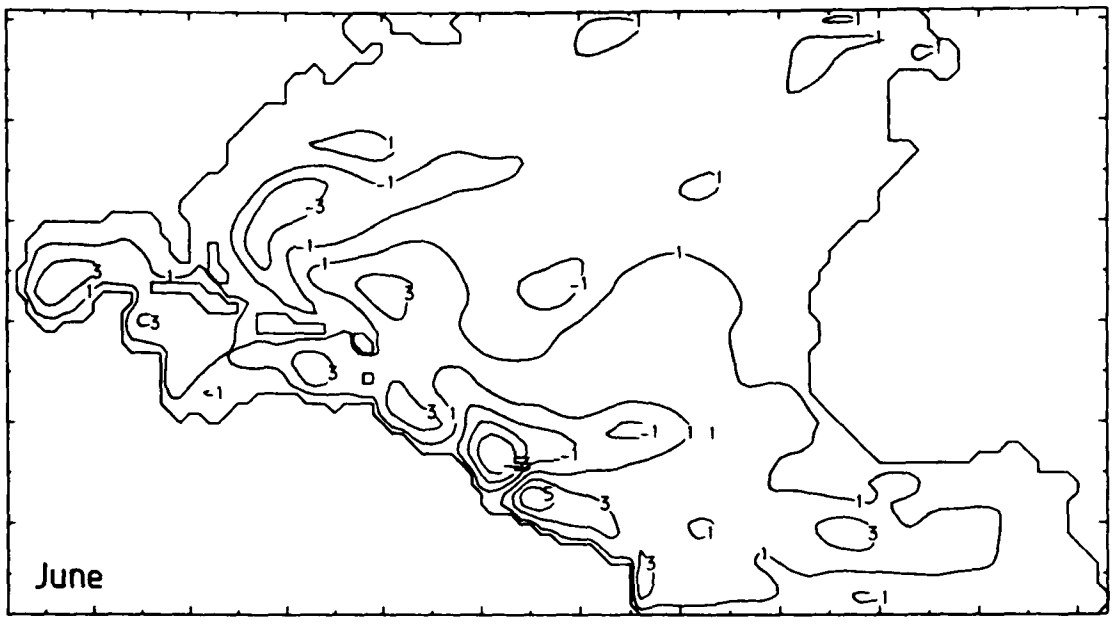
June

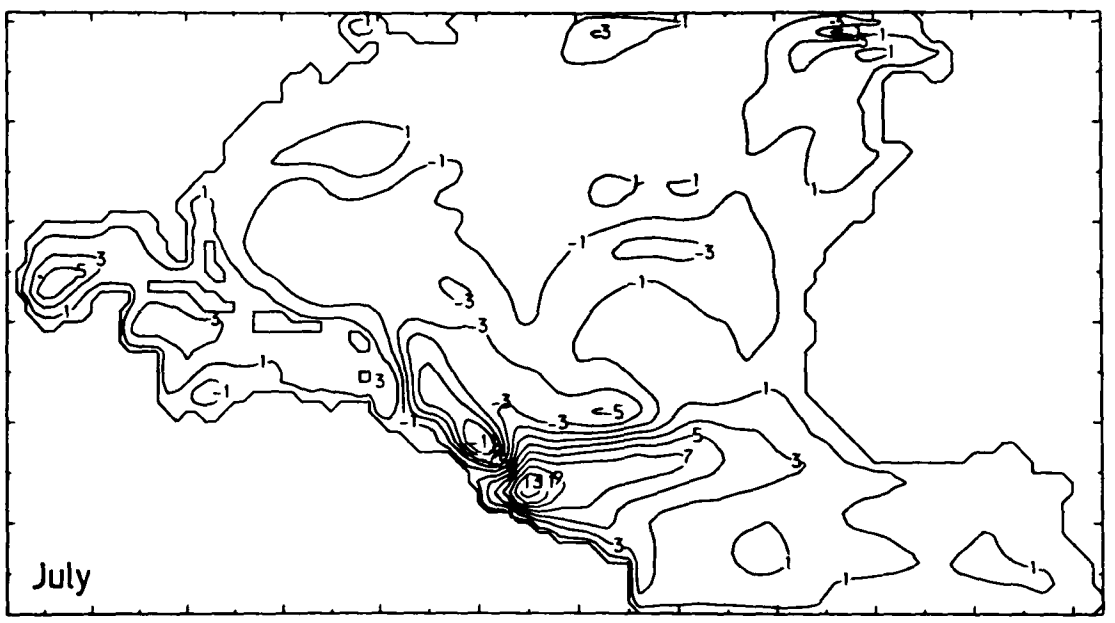
July

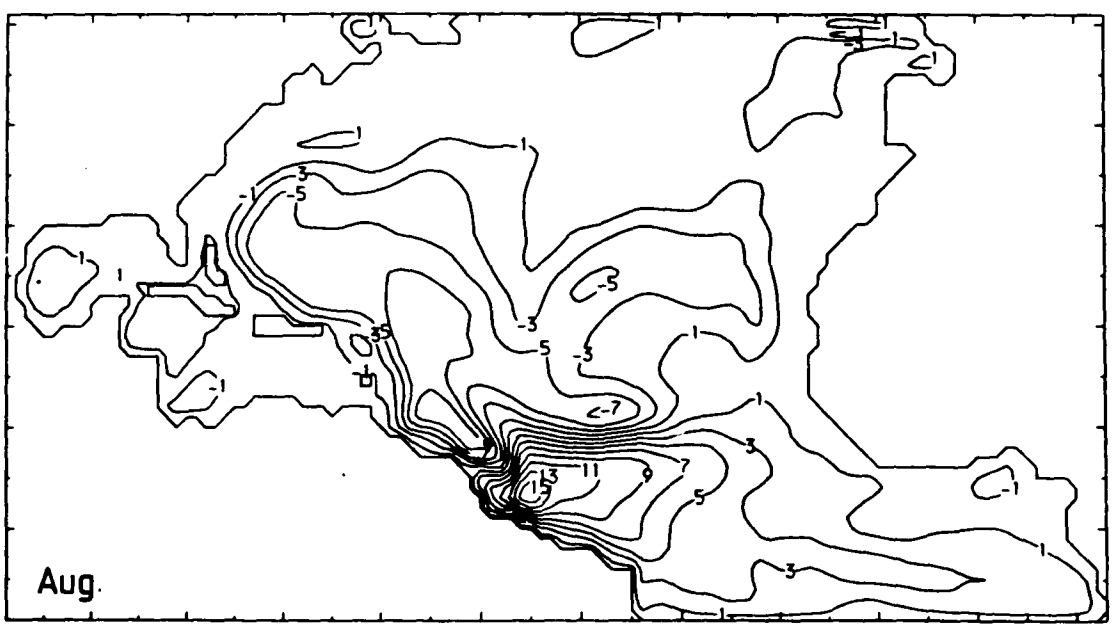
Aug.

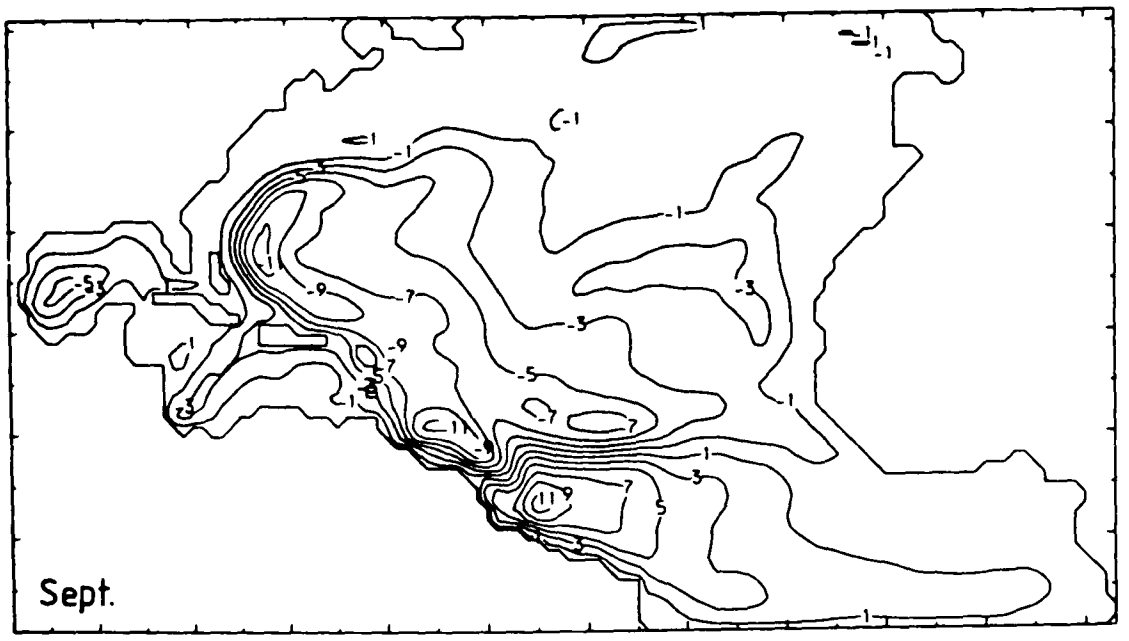
Sept.

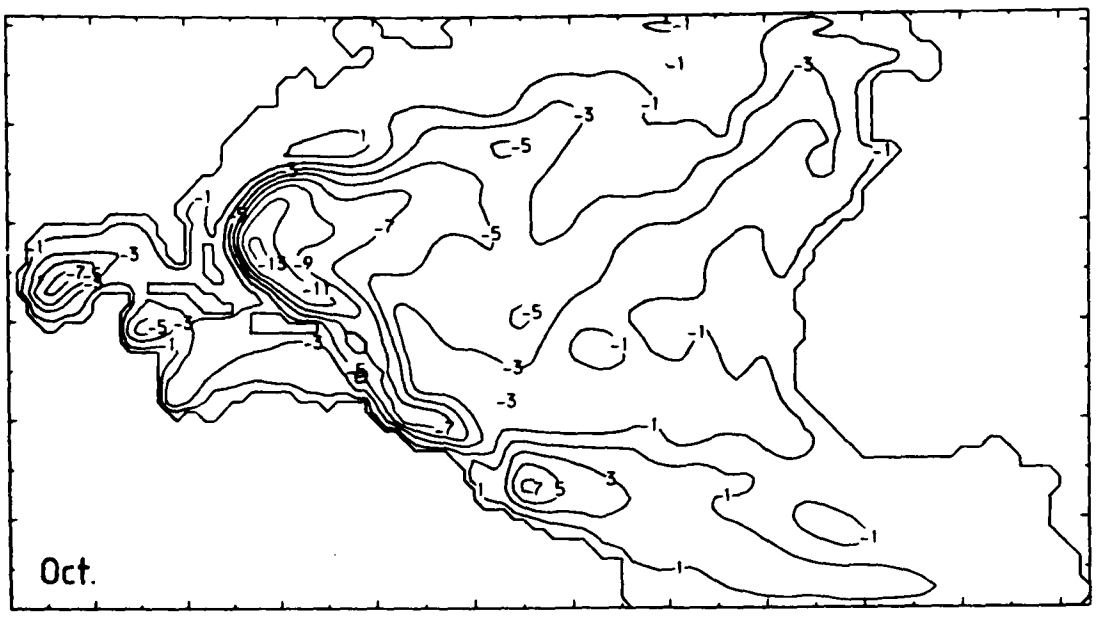
Oct.

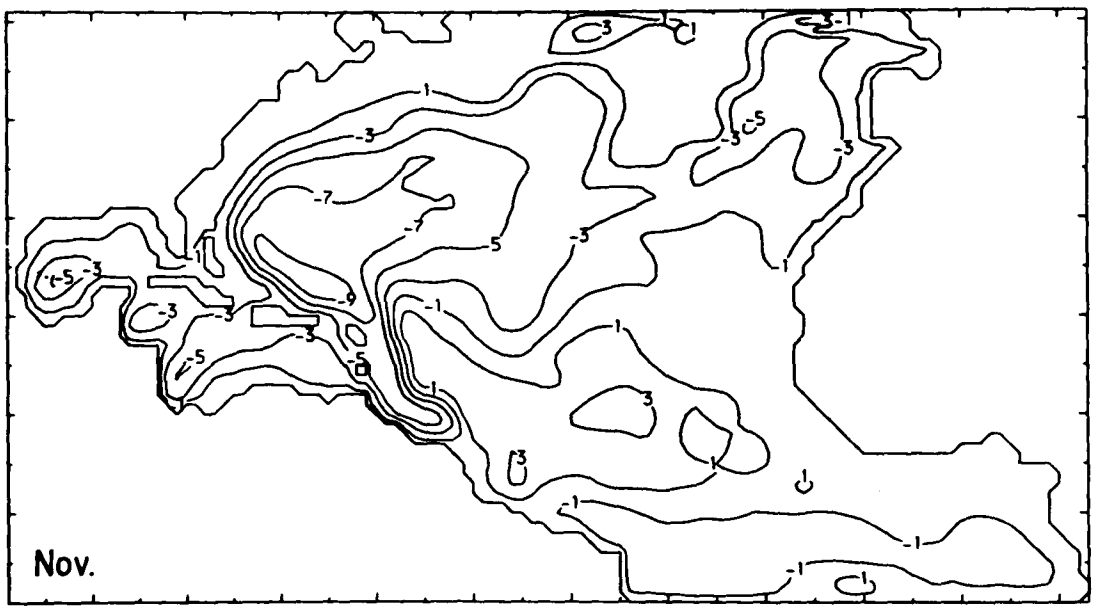
Nov.

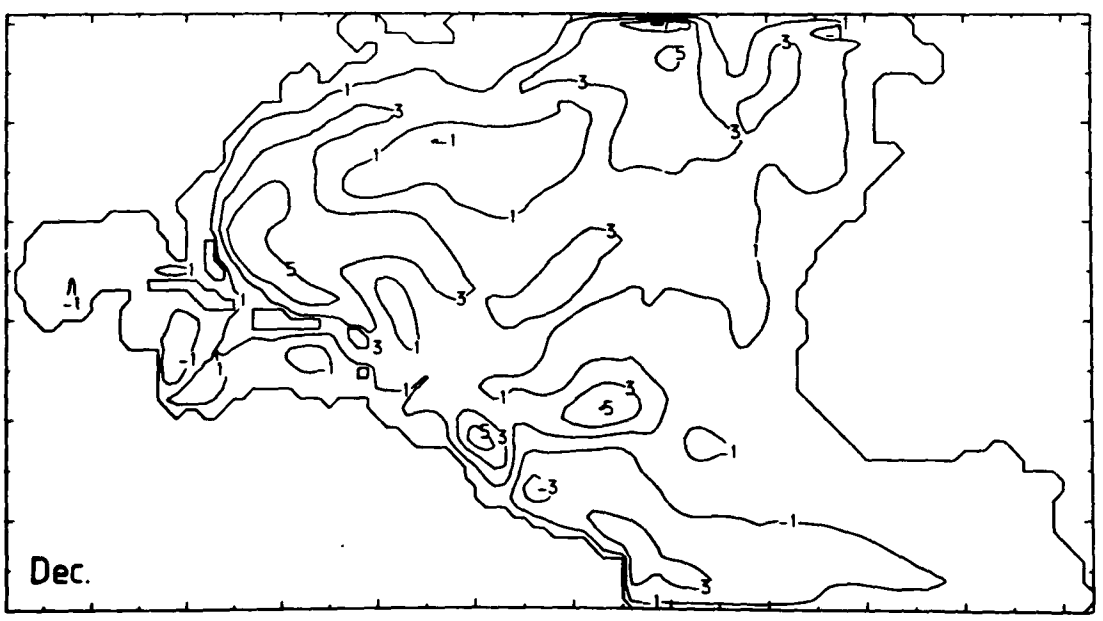
Dec.

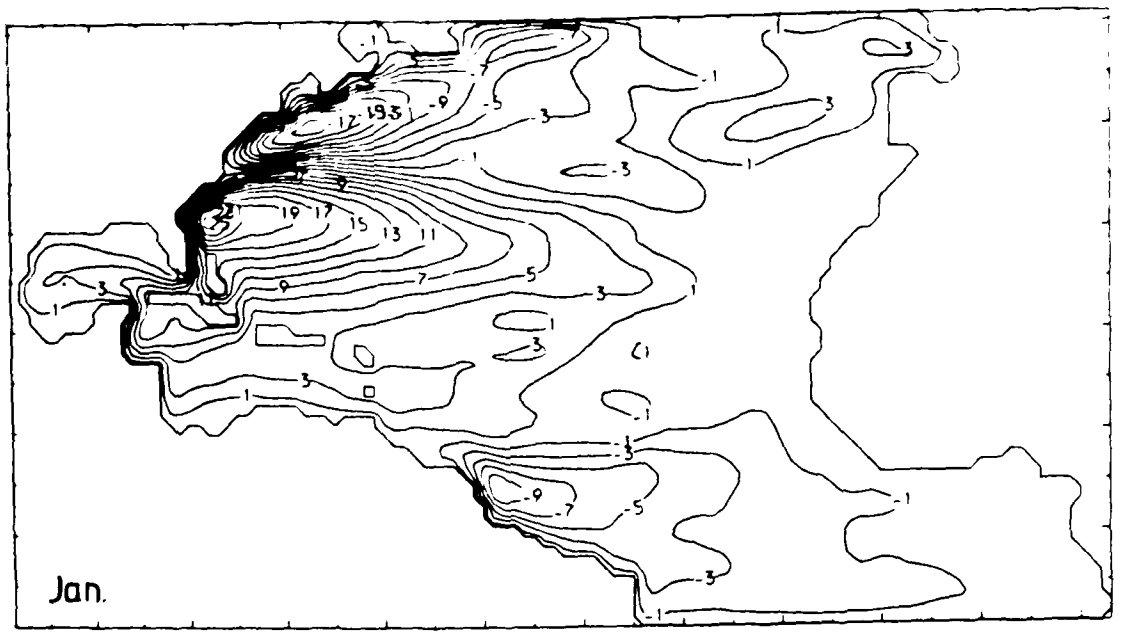

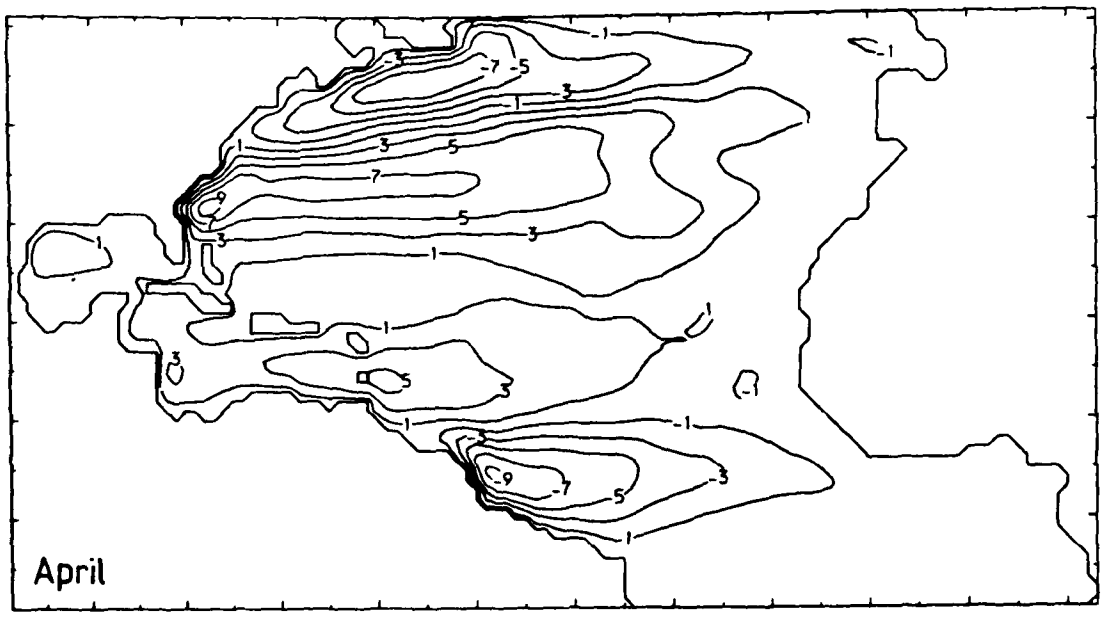

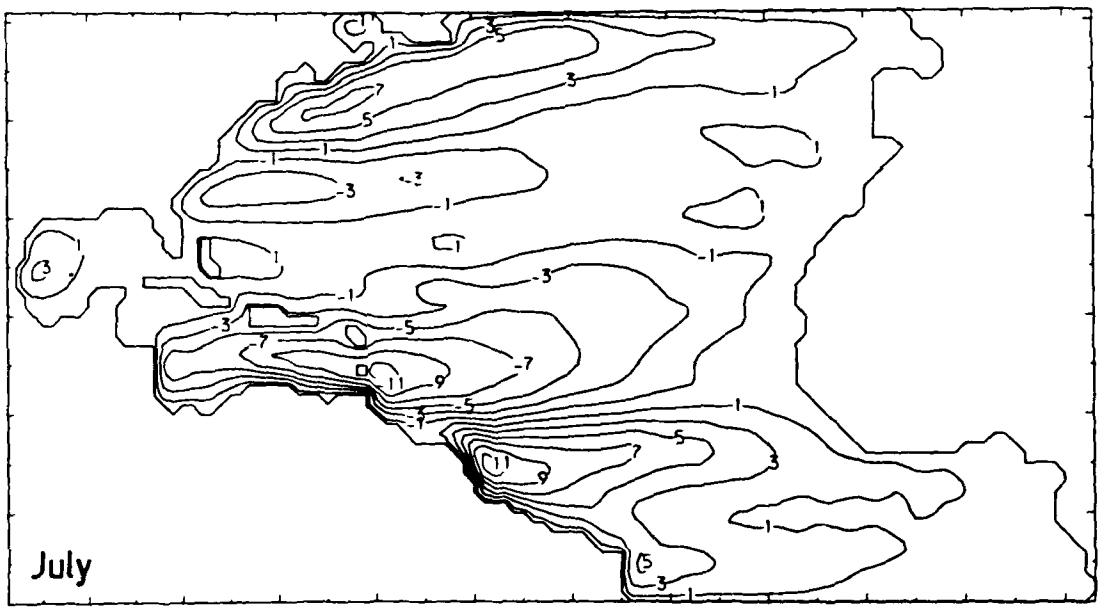

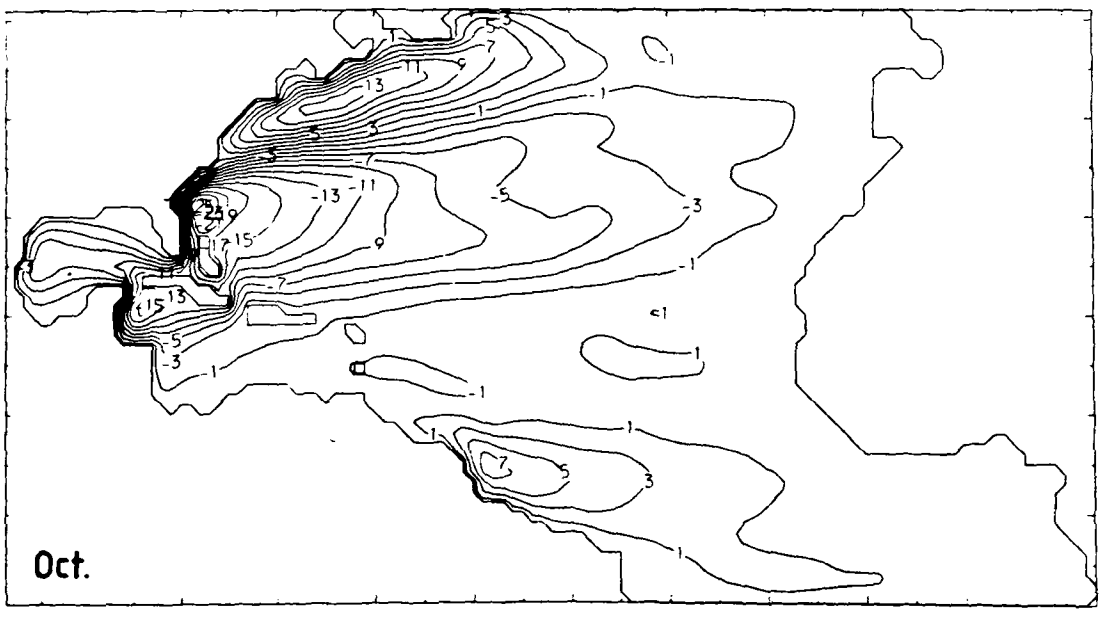

Figs 3.4 The resulting streamfunctions when a flat-bottomed model is integrated with the seasonal wind stresses for January, April, July and October. North of Cape Hatteras we see that there is a gyre which has opposite sign to the gyre east of Florida. This is true of every month except December, which lacks the two gyre structure.

3.3: The seasonal variation of transport through the Florida Straits.

3.3.1 Transport variations in a baroclinic ocean.

Fig 3.5(a) shows the predicted variation of transport through the Florida Straits. The variation in transport is small (a peak to peak variation of 3.5 Sverdrups), with a maximum at the end of July and a pronounced decrease to a minimum at the end of October. These predicted variations appear to agree in phase with the annual cycle of Fig 3.1, though the magnitude is roughly a factor of two too small. For comparison Fig 3.5(b) shows the predicted transports through the model straits in the absence of bottom topography. We see here that the peak to peak variation in transport is greater than thirty Sverdrups, and that the maximum in transport is now in the Winter. The great difference between Fig 3.5(a) and Fig 3.5(b) shows the importance of bottom topography for the Florida Straits transport at annual period. Comparison of Figs 3.3 and Figs 3.4 further emphasises this fact.

We can determine the transport induced by the passage of the baroclinic signal over topography if we subtract the transport variations for a homogeneous ocean from those for the baroclinic ocean. Fig 3.5(c) shows the Florida Straits transport variations for a homogeneous ocean with bottom topography. Since we have shown in Chapter 2 that baroclinic Rossby waves are not important in modulating the seasonal transport at the latitude of the Florida Straits, most of the difference between Figs 3.5(a) and 3.5(c), plotted as Fig 3.5(d), is probably a result of the passage of the baroclinic Kelvin wave as suggested by Anderson [1979]. Though Fig 3.5(d) does not exhibit an outright Summer

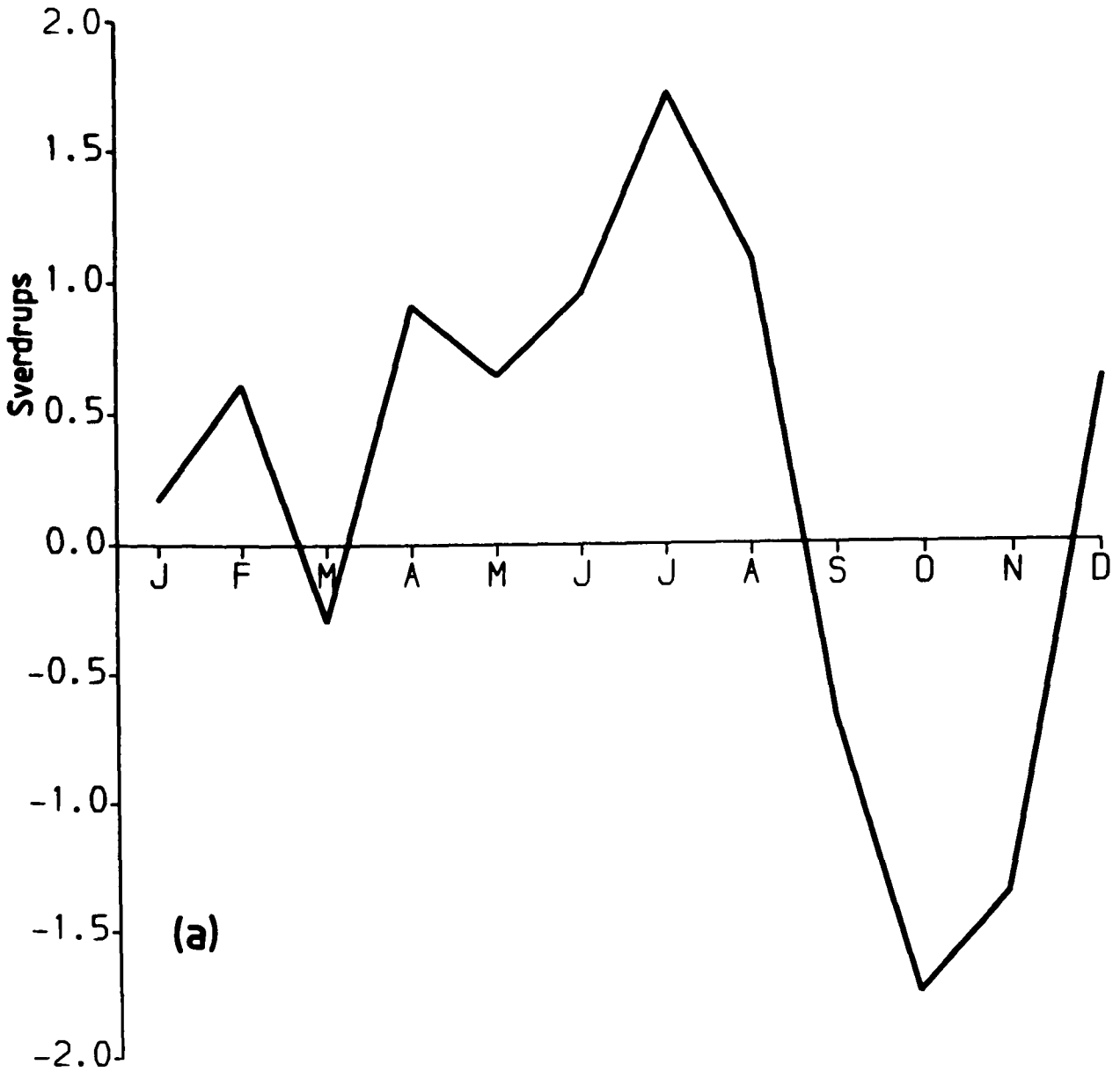

Fig 3.5(a) The transport through the Florida Straits when the baroclinic model with bottom topography is forced by the seasonal wind stresses.

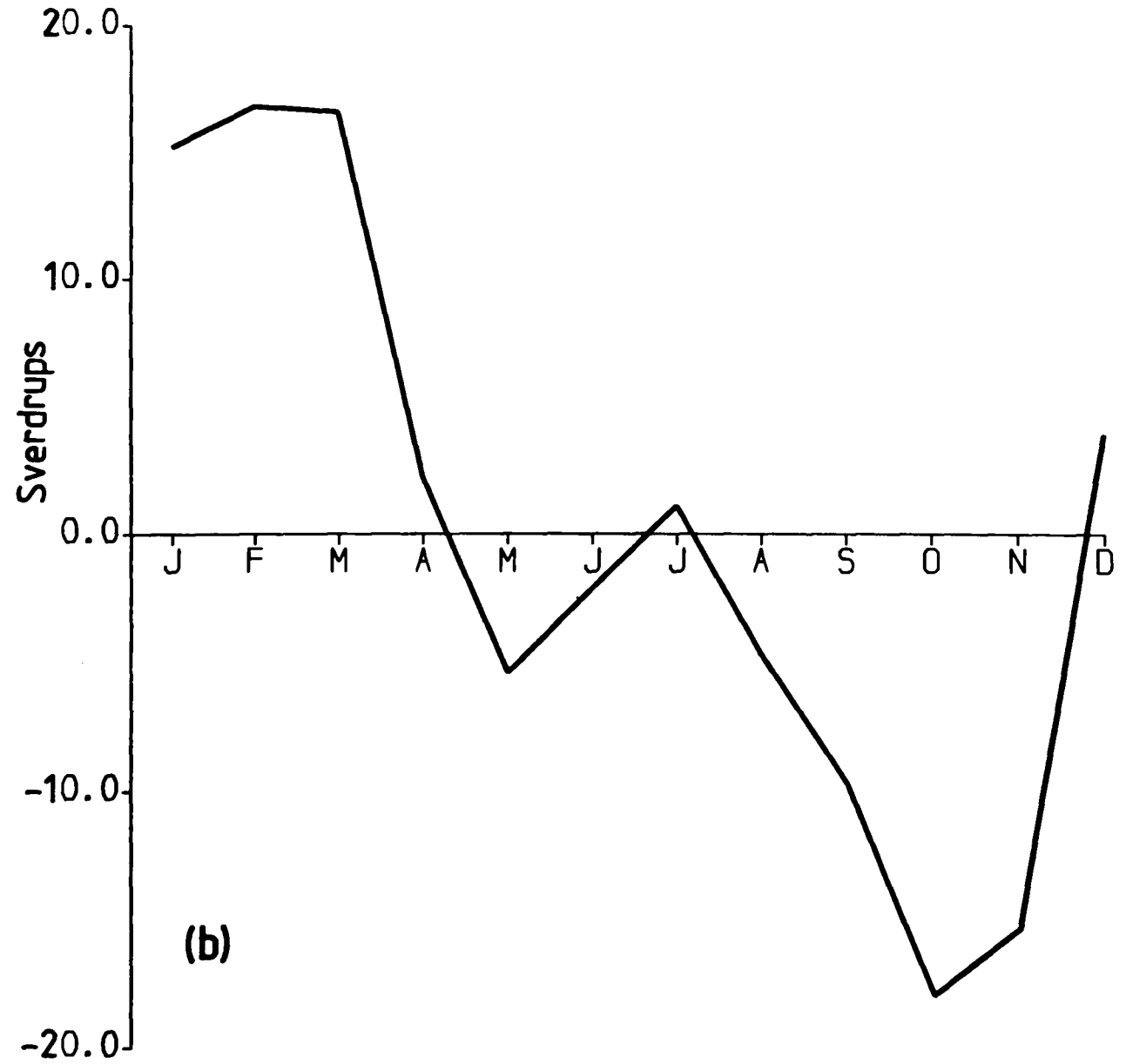

Fig 3.5(b) The transport through the Florida Straits when a flat-bottomed ocean is forced by the seasonal wind stresses. This figure should be compared with Fig 3.5(a).

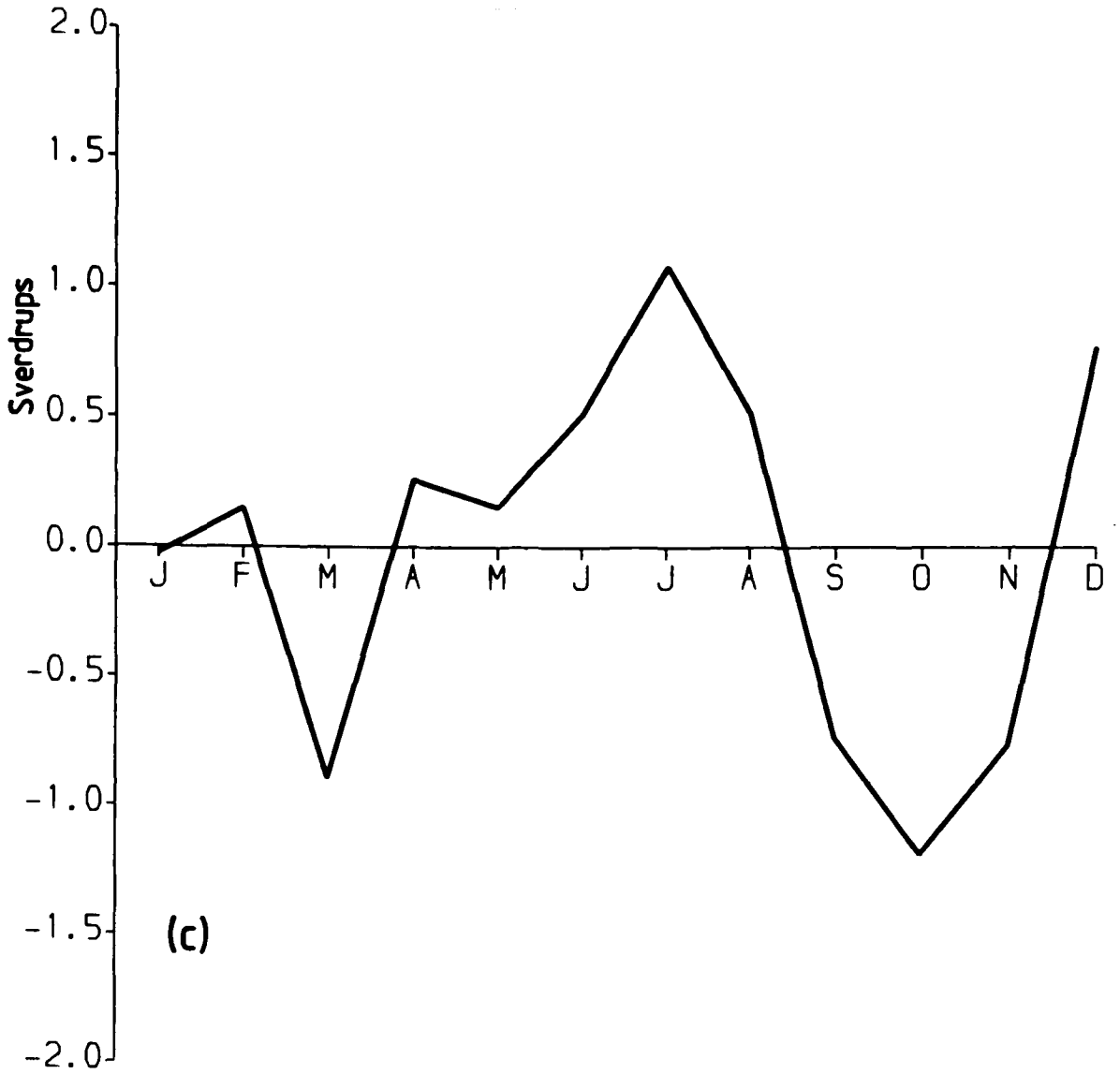

Fig 3.5(c) The transport through the Florida Straits for a homogeneous ocean when forced by the seasonal wind stresses.

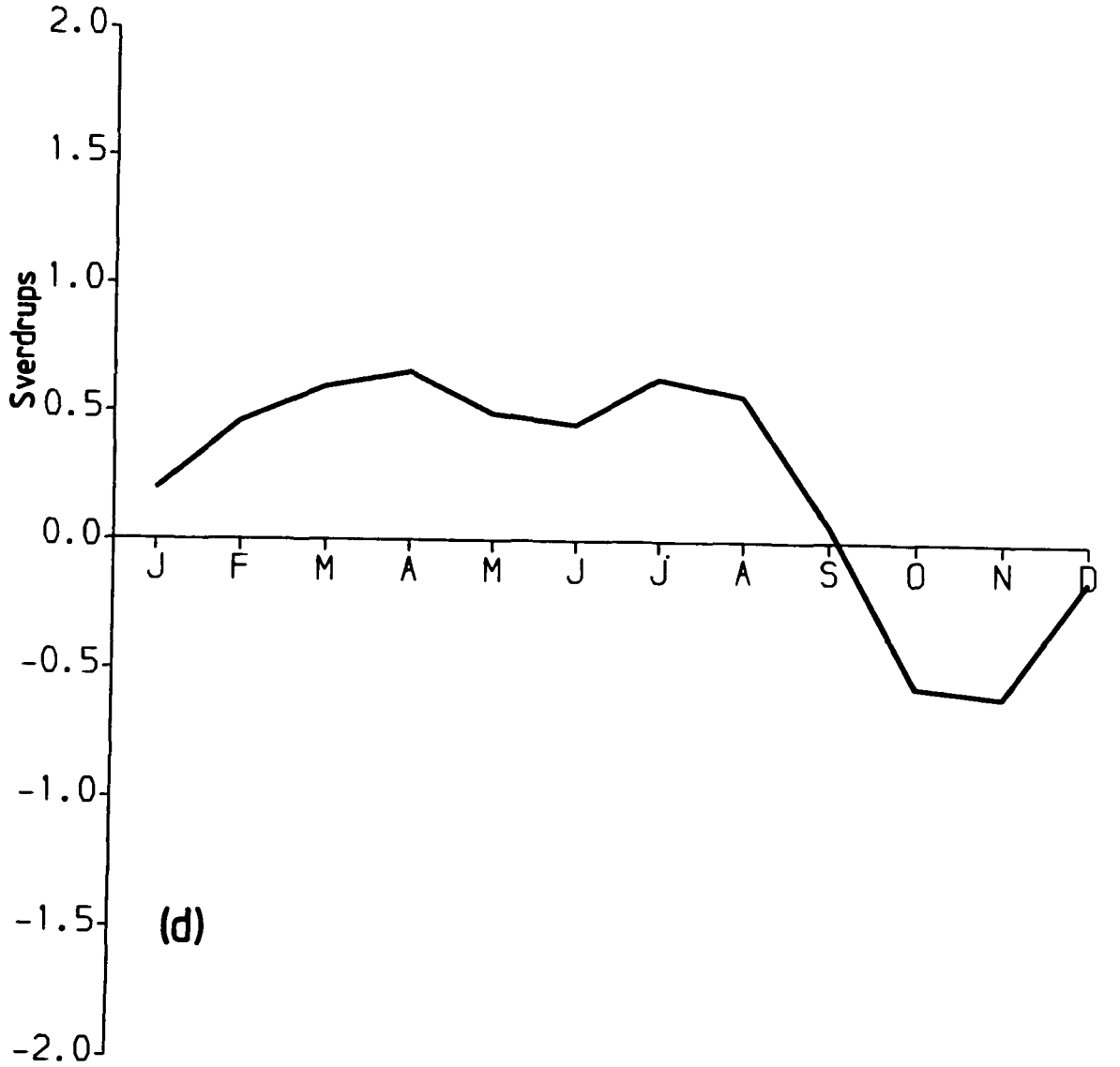

Fig 3.5(d) The contribution to Fig 3.5(a) of baroclinic effects over topography. i.e. the difference between Fig 3.5(a) and Fig 3.5(c).

maximum, baroclinic effects are shown to increase the peak to peak variation between July and October.

Although the mean wind stress has been removed, Fig 3.5(d) shows a mean transport of about a quarter of a Sverdrup. The reasons for this apparent contribution to the mean are discussed in Appendix F. Fig 3.5(c) has very little mean transport. This reflects the fact that the response at the end of each month's integration for the homogeneous model is almost in equilibrium (see Appendix F).

In order to assess the importance of varying geometry on the seasonal cycle of the Florida Straits transport, two further integrations were performed, each for one year. In the first, the passage between Cuba and the island representing the Bahamas was blocked, and in the second the Windward Passage (see Fig 3.8) was blocked. The Florida Straits transport for each of the baroclinic calculations are shown in Fig 3.6(a). There is little difference to Fig 3.5(a), suggesting that neither of these passages is important for the seasonal variation of Florida Straits transport.

3.3.2 The upper layer transport through the Florida Straits

Fig 3.6(b) shows the seasonal variation of northward transport in the upper layer across the Florida Straits. This figure should be compared to Fig 3.5(a). We see that the upper layer transport is comparable to the total transport. This implies a substantial velocity in the upper layer since it is only 100 m thick. In fact, if we multiply the upper layer transport in Sverdrups by five, we obtain the approximate surface velocity (averaged across the Straits) in cm/s.

Anderson [1979a] has modelled the seasonal cycle of the

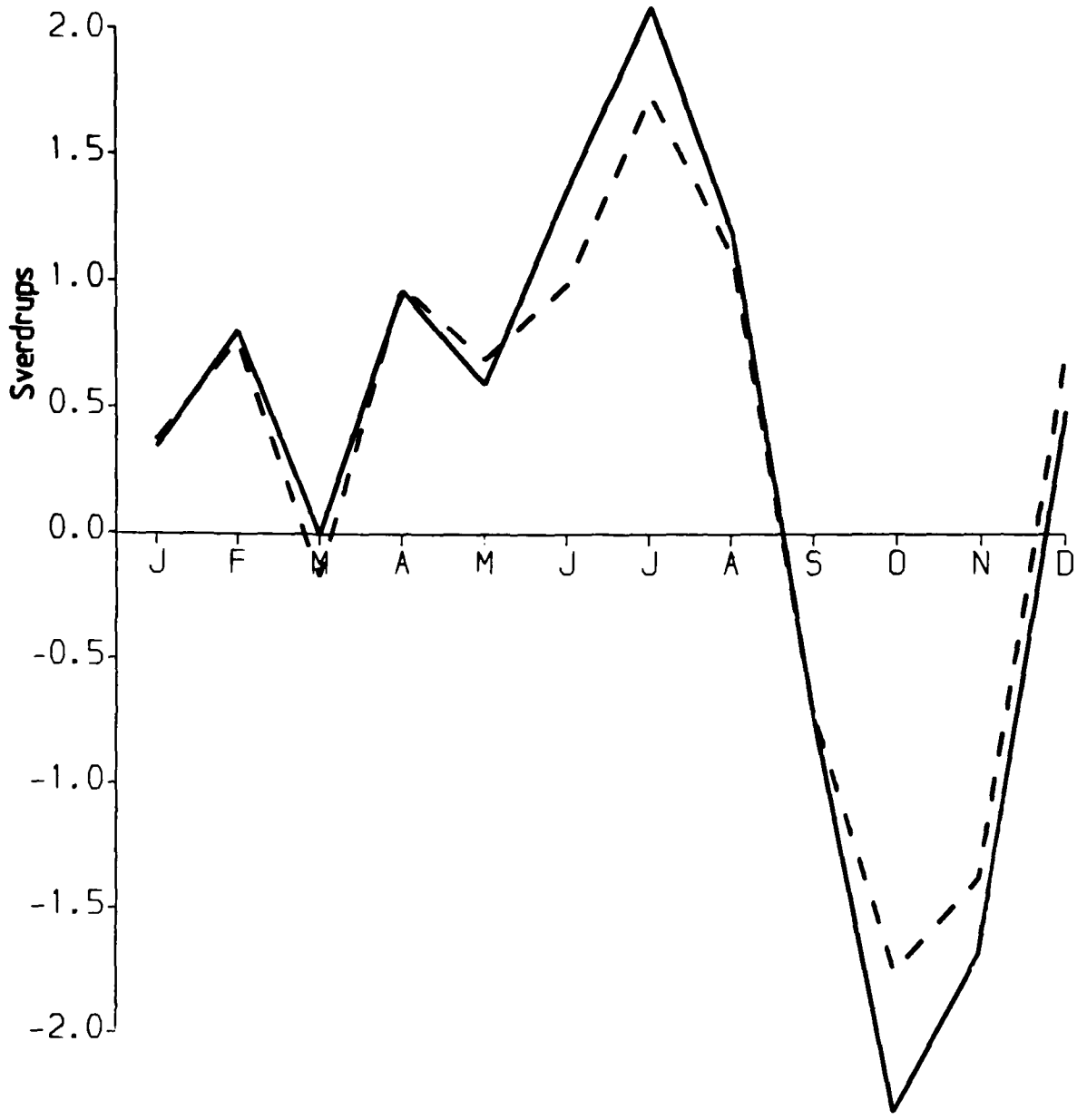

Fig 3.6(a) The transport through the Florida Straits during the first year of integration of the baroclinic model, with the passage between Cuba and the Bahamas blocked (solid line), and with the Windward Passage blocked (dashed line). Compare with Fig 3.5(a).

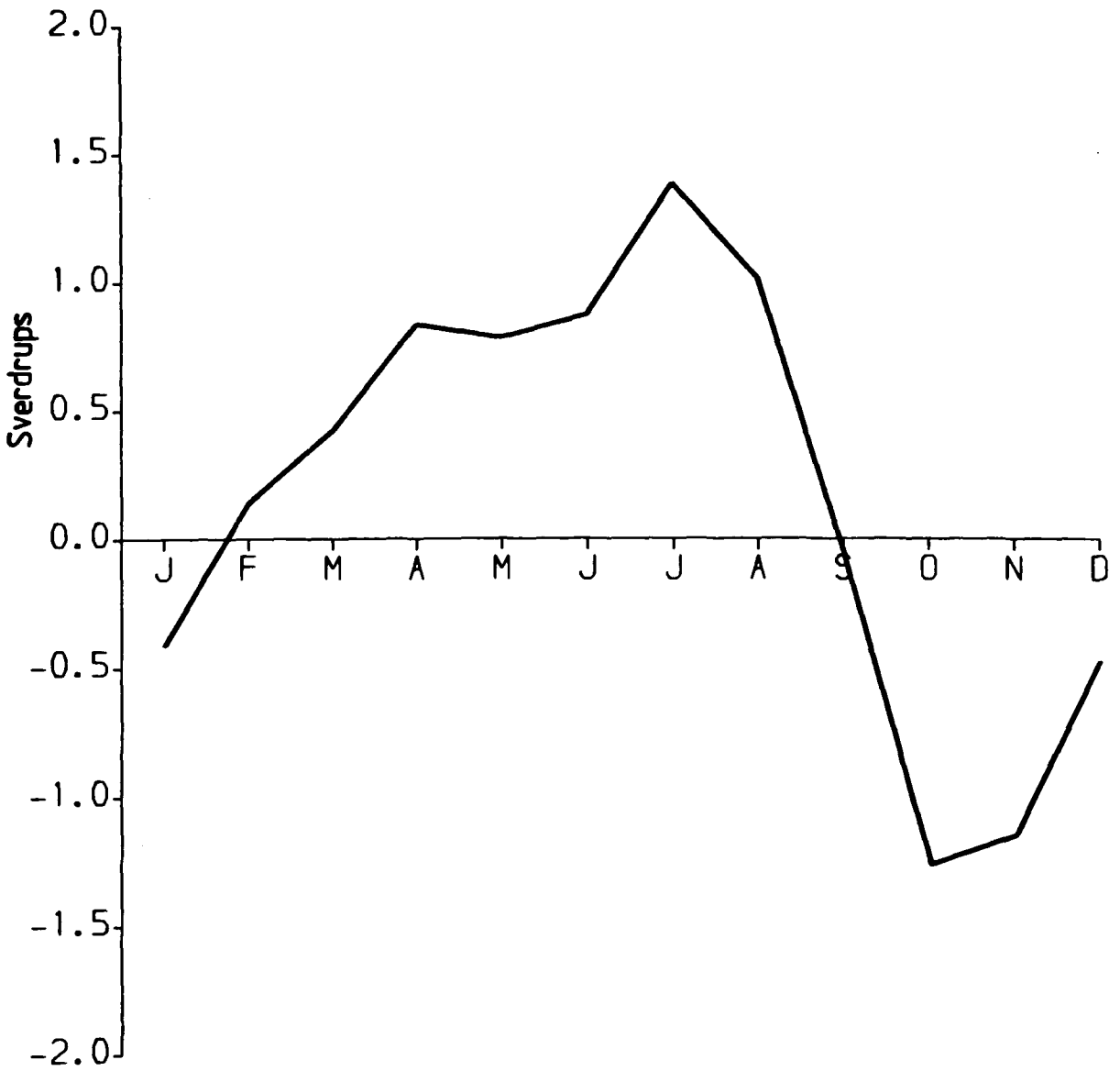

Fig 3.6(b) The upper layer transport through the Florida Straits. The upper layer is 100 m deep

surface currents in the North Atlantic using a multi-level model without bottom topography. Anderson and Killworth [1977] show that for a two layer ocean, the baroclinic mode is not greatly affected by topography, though the barotropic mode can be influenced directly through the topography, and indirectly, through a coupling between the topography and the baroclinic mode. The fact that the baroclinic flow is not strongly affected by topography means that the results of Anderson [1979a] on the seasonal variation of the surface currents are unlikely to be significantly altered by the presence of variable bottom depth, but the transport can be. This thesis concerns itself primarily with the effect on wind-forced transport variations of the baroclinic mode and topography. The seasonal variation of the surface currents of the North Atlantic (forced by the same Bunker winds) is dealt with in Anderson [1979a]. Fig 3.6(b) agrees well in phase with the model variation of Anderson [1979a] and the measured variation of Fuglister [1951], there being a maximum in July and a minimum in October-November for all three curves. The measured variation has about twice the amplitude of the model variation for both models. This could be due to a bias in measurements of drift velocity towards the centre of the current, where the Summer-Winter contrast in surface velocity is about 60 cm/s (Niiler and Richardson [1973]), i.e. much greater than the averaged surface current variation across the Straits. Because the seasonal variation of the currents is forced primarily by the meridional wind stress (Anderson [1979a]), we expect the northward surface current in the Florida Straits to be determined primarily by the Kelvin wave forced along the North American coast, which propagates southward through the Florida Straits (for a meridional wind the Ekman flow will be longitudinal). For the full winds there will also be small contributions due to the

Ekman flow and due to baroclinic Rossby waves.

Anderson [1979a,b] suggested that the seasonal variation of the Florida Current could be forced by the passage of a Kelvin wave over topography. Although the Kelvin wave dramatically intensifies the proportion of transport carried by the upper layer, its effect on transport is not so great (Fig 3.5(d)).

3.3.3 Transport variations in a homogeneous ocean.

We consider here the separate effects of the zonal and meridional components of wind stress for the case of a homogeneous ocean with bottom topography. Fig 3.7(a) shows the transport variation predicted using the zonal wind stress only, while Fig 3.7(b) shows the corresponding plot for the meridional wind stress. The meridional wind stress reduces the size of the December maximum expected from the zonal wind stress, and creates the overall summer maximum of Fig 3.5(c). The pronounced annual cycle of Fig 3.7(b) is in contrast to the large semiannual signal of Fig 3.5(c), which has maxima at the end of July and December, and minima at the end of October and March.

The results of Section 2.2 suggest that because of the strong topographic effect of the Mid-Atlantic ridge on transport variations, only the wind stress in the western half basin is likely to be important in forcing seasonal variation in Florida Straits transport. The importance of winds to the west is further enhanced by the fact that most of the seasonal wind change occurs there. To determine the relative importance of different regions for the seasonal variation of the Florida Current we consider two forcing regions marked A and B on Fig 3.8. This is not done in the case of the baroclinic model because the wind stress itself is needed to force the baroclinic

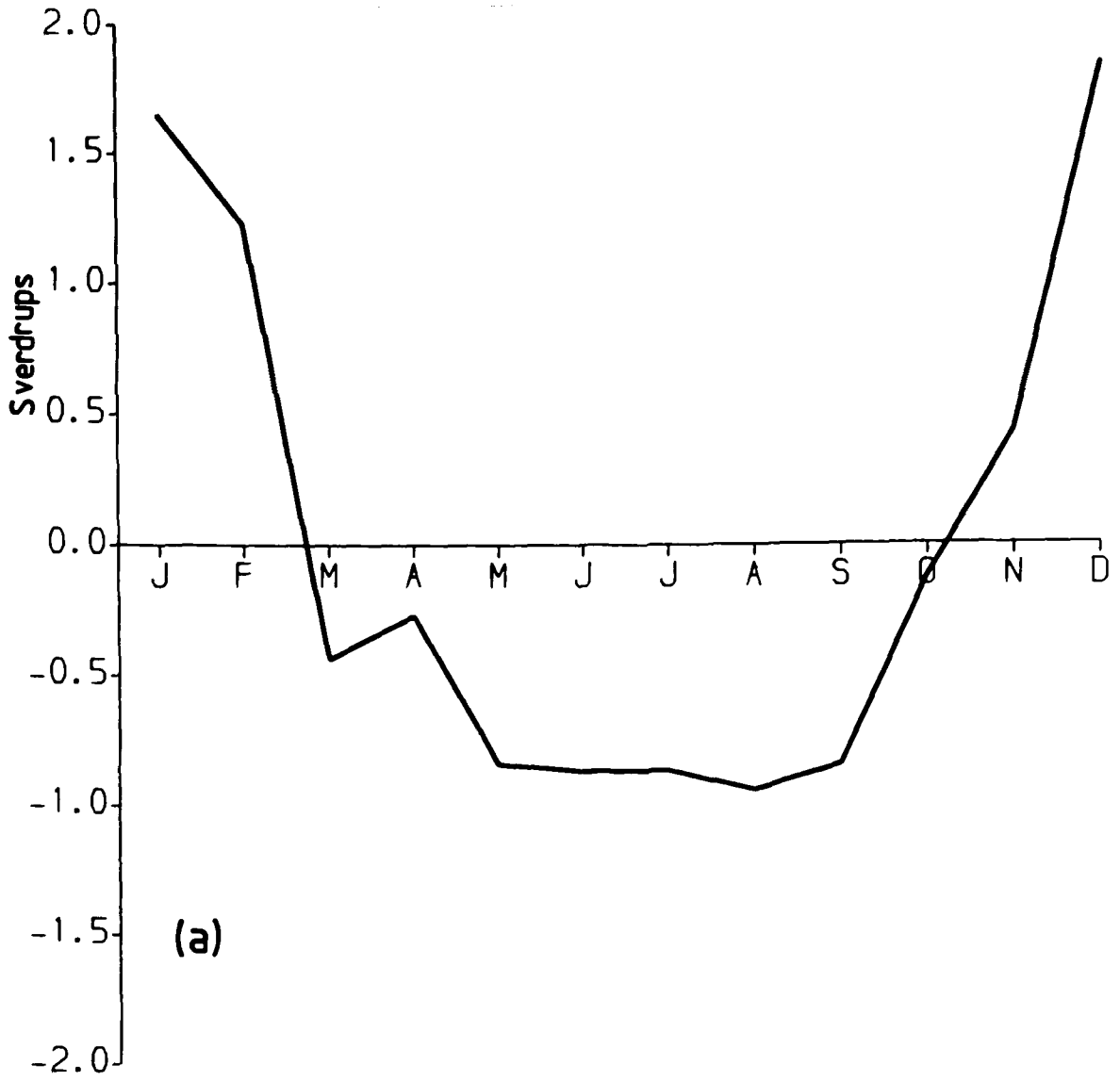

Fig 3.7(a) The transport variation through the Florida Straits when a homogeneous ocean with topography is forced by the zonal component of the seasonal wind stresses.

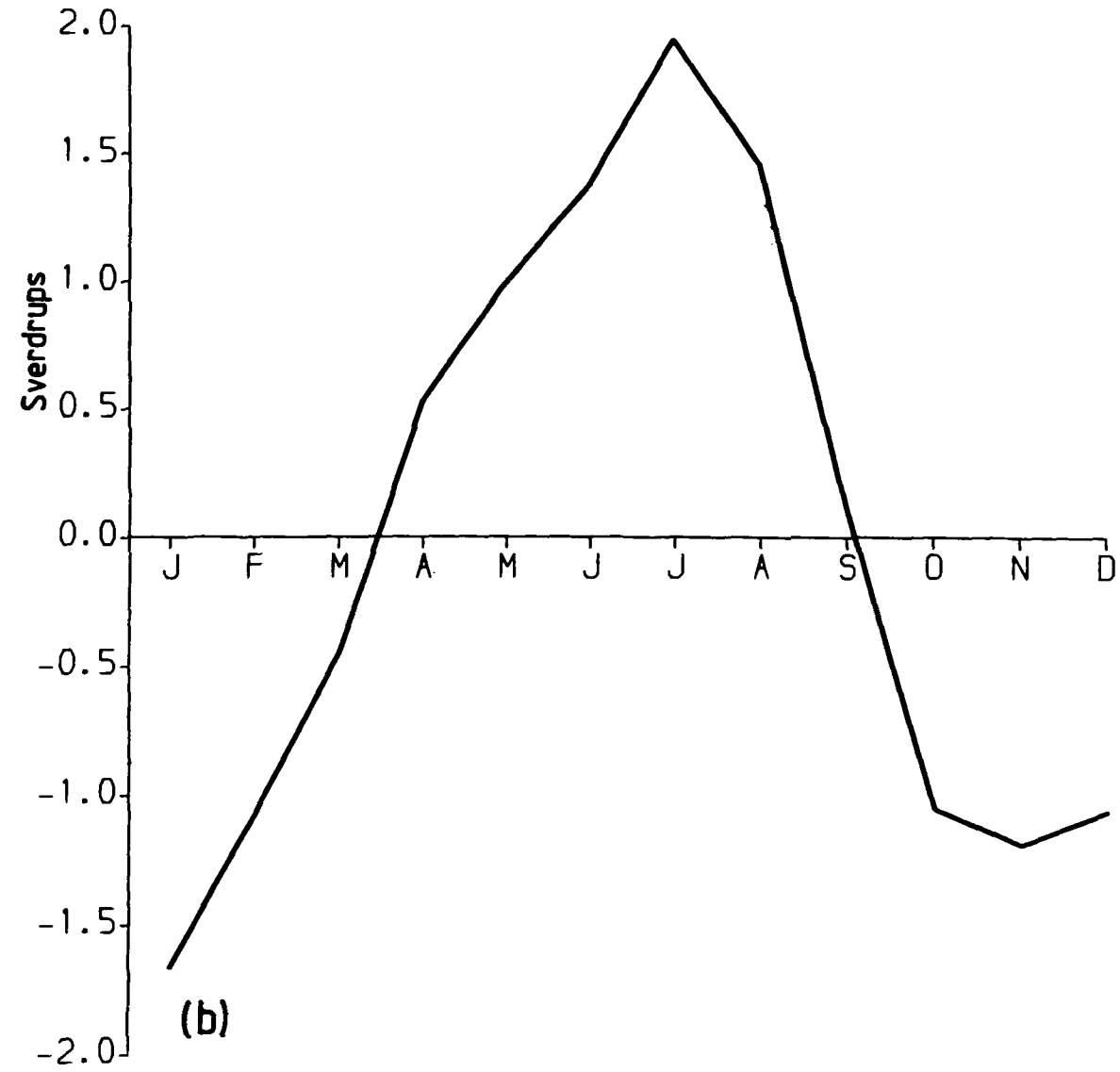

Fig 3.7(b) As for Fig 3.7(a), but for the meridional wind stress.

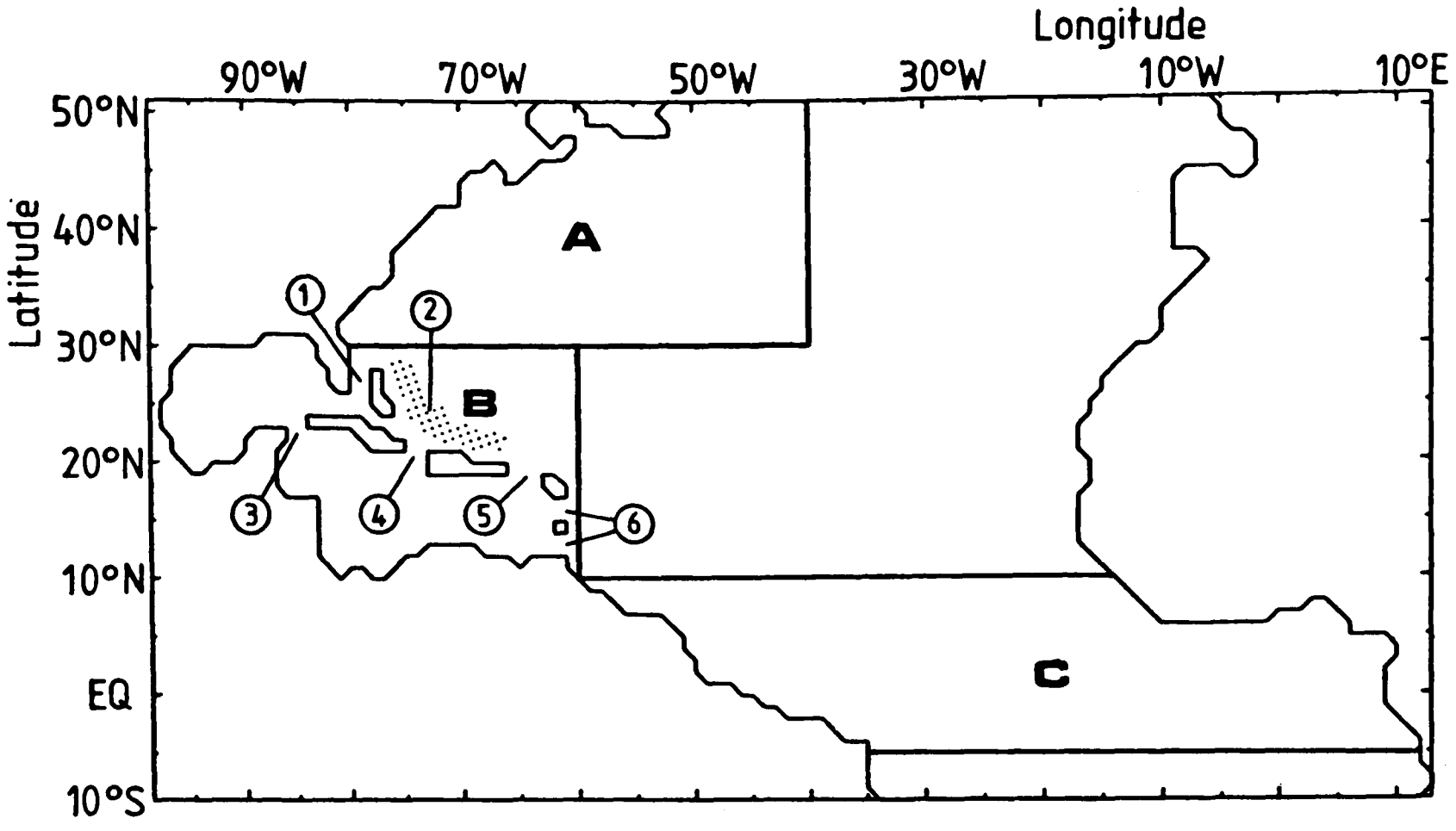

Fig 3.8 Areas A, B and C referred to in the text are shown, together with (1) The Florida Straits; (2) The Antilles Current area (shaded); (3) The Yucatan Straits; (4) The Windward Passage; (5) The Anegada passage; (6) The passages of the Lesser Antilles.

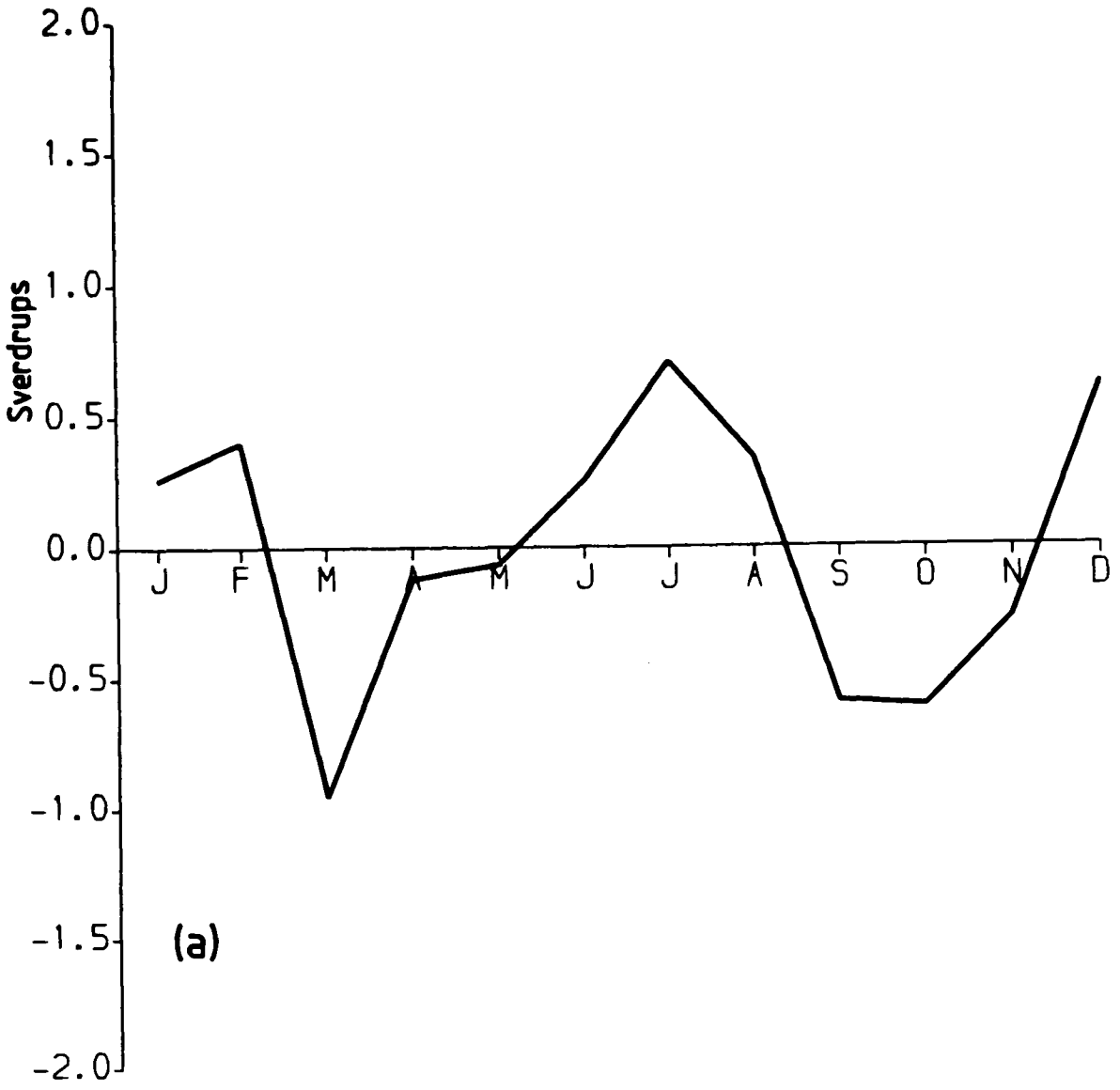

Fig 3.9(a) The contribution of the wind stress over area A to the seasonal variation of the Florida Straits transport in a homogeneous ocean. All the features of Fig 3.5(c) are reproduced, with most of the amplitude.

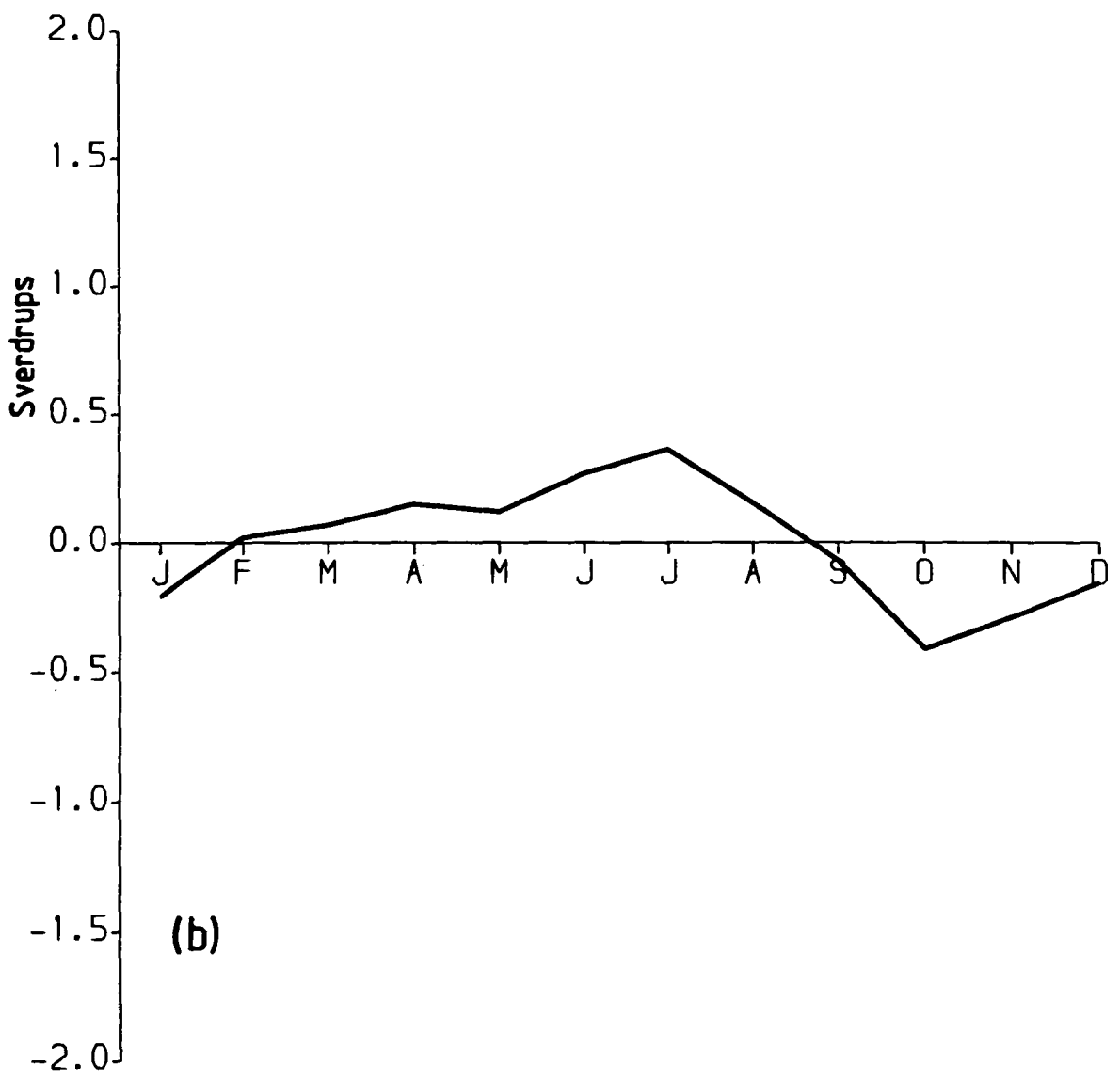

Fig 3.9(b) The contribution of the wind stress over area B to the seasonal variation of the Florida Straits transport in a homogeneous ocean. The variation is less than that of Fig 3.9(a), though still significant.

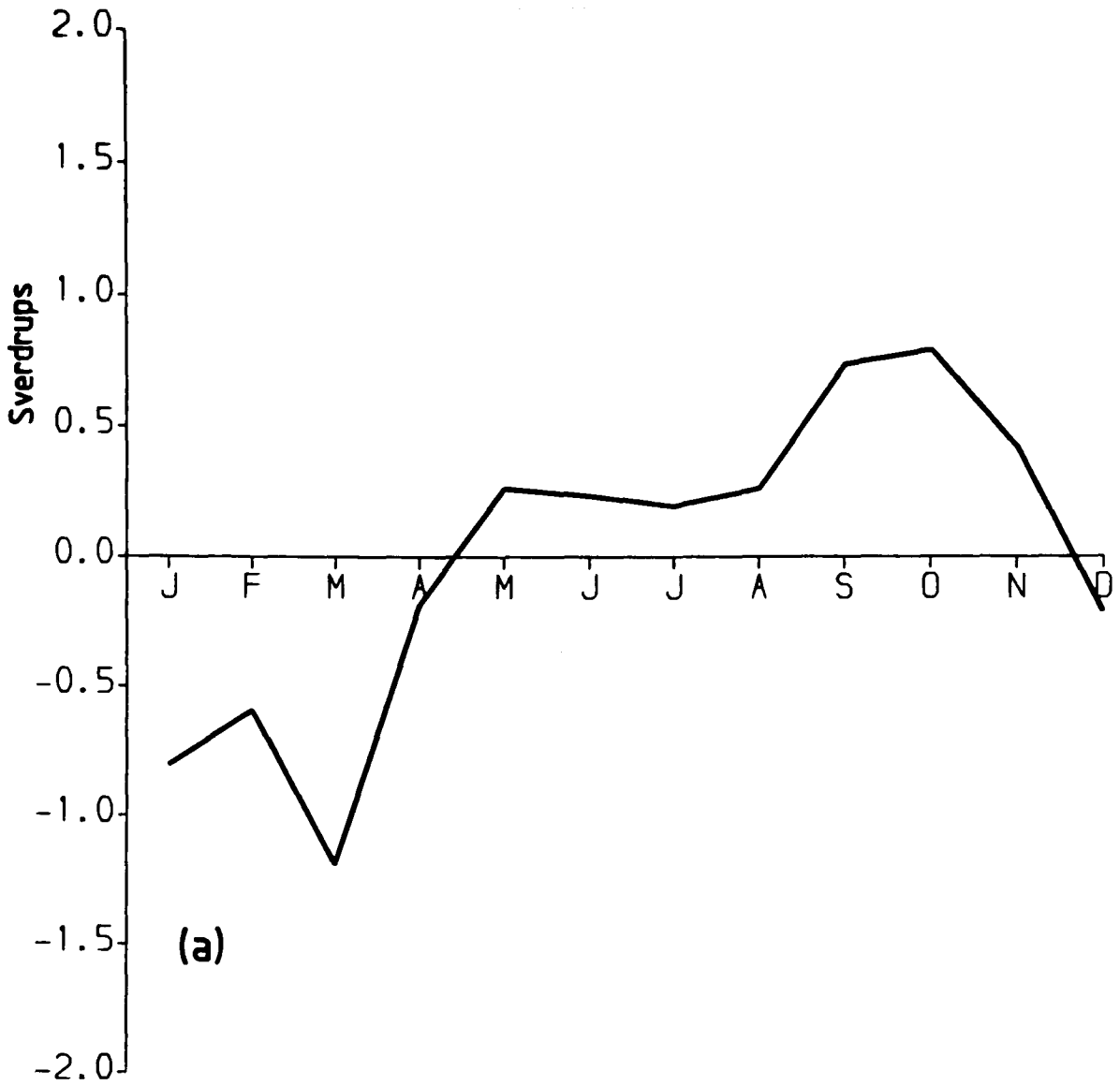

Fig 3.10(a) The contribution to fig 3.9(a) due to the curl of the wind stress.

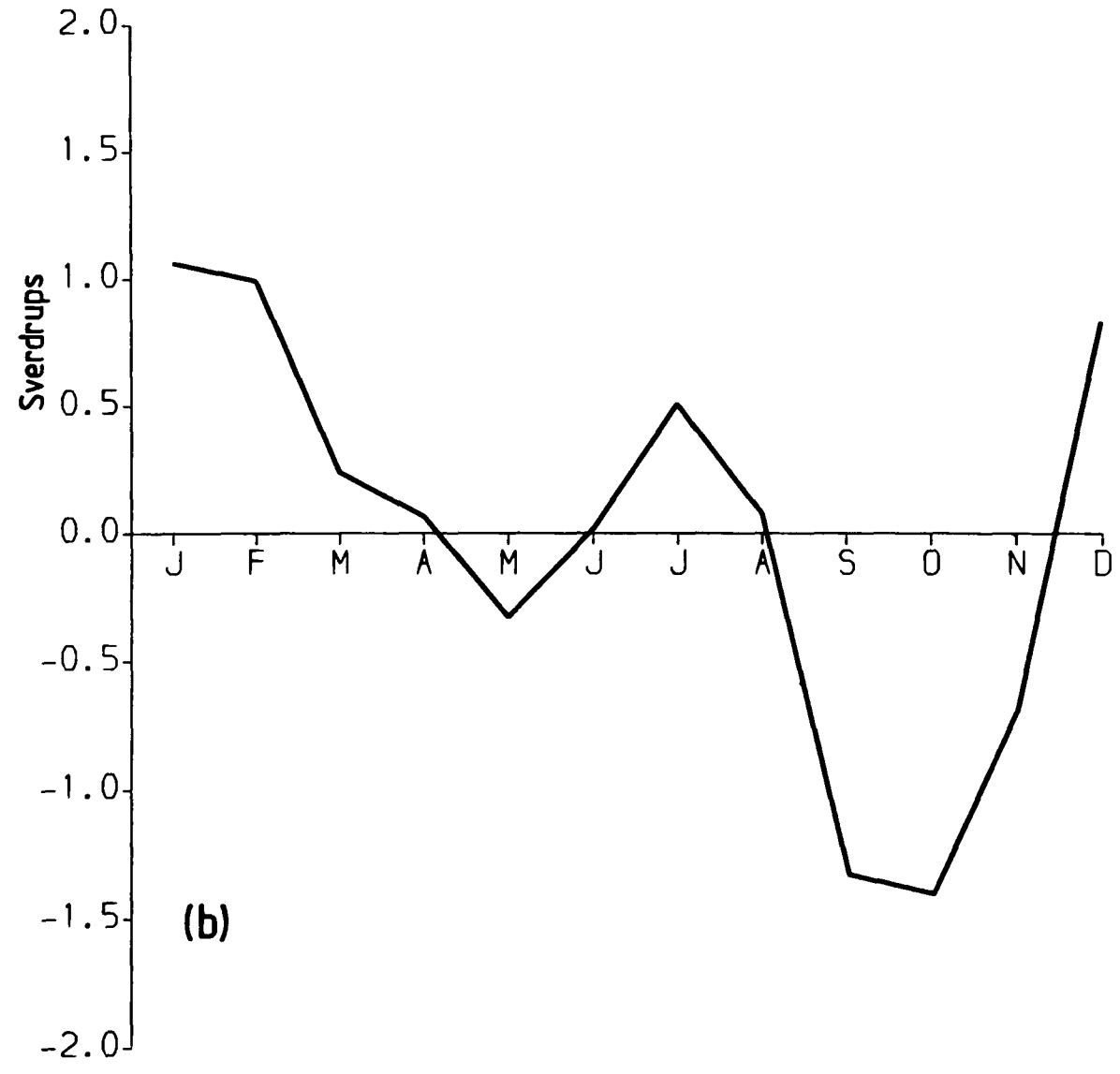

Fig 3.10(b) The contribution to Fig 3.9(a) due to gradients in topography associated with the wind stress.

mode, and restructuring the region of wind stress introduces spurious effects at the edges of the regions. The barotropic model, however, is driven by $curl_z(\underline{\tau}/H)$ and it is this which is split up into regions A and B rather than the wind stress.

The contributions to Florida Straits transport forced by the two areas are shown in Figs 3.9(a) and 3.9(b). The contribution from areas other than A and B (not shown) was negligible during the Summer, and less than 0.2 Sverdrups at other times of the year. Region A to the north of the Bahamas and to the west of the Mid-Atlantic ridge, accounts for a large part of the variation in transport of the Florida Current. While the forcing of region B results in a smaller Florida Straits transport than that of region A, it is none the less in good phase agreement with the observed transport (Fig 3.1). It is possible to speculate that processes not contained in this model could act to enhance the Florida Straits response to Caribbean forcing.

The total transport variation is forced by $curl_z(\underline{\tau}/H)$. This can be split into a part depending on the curl of the wind stress, and another depending on gradients of topography. Fig 3.10(a) shows the contribution due to the curl of the wind stress for area A, while Fig 3.10(b) shows the contribution associated with gradients in topography. From these figures we see that the Winter contributions (which are indeed larger than the Summer contributions) roughly cancel, whereas the subsidiary Summer maximum of Fig 3.10(b) is augmented by Fig 3.10(a). Fig 3.5(b) and Fig 3.10(a) are both curl generated transports but show very different behaviour. The reason for this is that due to topography they are sampling different areas of ocean. In the case of Fig 3.5(b), the transport is a measure of the curl to the east, whereas in the case of Fig 3.10(a) the transport variations result from curl changes to the north-east. These curl-forced

variations in the north-western Atlantic are deflected south-westward by topography to affect transport variations in the Florida Current. Examination of Figs 3.4 shows that north of Cape Hatteras the curl drives a cyclonic circulation in Winter with anticyclonic circulation during the Fall. The deflection southward of the streamlines by topography gives rise to the Winter minimum and Fall maximum of Fig 3.10(a).

The splitting of the wind forcing into two contributions, as above, cannot be done in the presence of islands because the streamfunction equation B13 is not used to solve for the island value of the streamfunction. Instead, a line integral of B12 is taken around the island, as explained in Appendix B. This explains why only area A was looked at above, rather than using the total area.

3.4: Seasonal variation of transport in other parts of the North Atlantic.

In this section we consider transport variation in areas of the North Atlantic other than the Florida Current. Regrettably there are as yet no measurements of total transport in these areas with which to compare the model results. Instead transport measurements are usually based on hydrographic data, with an assumed level of no motion. Since the seasonal variation of transport in our model is mainly barotropic, this will not in general be well represented in geostrophic transport calculations, so no comparison with observations is attempted in this section.

The interested reader may, however, wish to consult the studies of Gunn and Watts [1982]; Olson, Schott, Zantopp and

Leaman [1984], and Worthington [1977], where some estimates of seasonal variations in the Antilles Current and Gulf Stream are given.

One question of particular interest is whether or not there is an Antilles Current flowing to the east of the Antilles and Bahamas island arc (see Fig 3.8). The model seasonal variations of Fig 3.3 almost represent total transport in this region since there is little mean transport (see Fig 3.14). Between December and March there is a northwestward transport of the order of ten Sverdrups, from April to July there is little transport and during the Fall the transport is predicted to be southeastward. The seasonal variability of the Antilles Current is a strong feature of this model since it is due to the blocking effect of topography in the Florida Straits (see Section 2.4). Schott (private communication), however, is of the opinion that measurements reported by Olson et al [1984] are not consistent with model results. These measurements show a southeastward transport to the east of the Bahamas during April, but not during the Fall. It is therefore of considerable interest to know whether or not such variability really exists.

The model variation of transport through the Windward Passage is shown on Fig 3.11. During late Summer and early Fall water flows into the Caribbean whereas during late Fall and Winter the flow is out of the Caribbean.

Fig 3.12 shows the model seasonal transport variation of the Gulf Stream between Bermuda and the North American coast. There is a Winter maximum with a minimum in October-November. This is in marked contrast to the phase of the Florida Current variation with its Summer maximum.

On Fig 3.13 we show the variation of transport through passages of the Caribbean (shown on Fig 3.8). The solid line

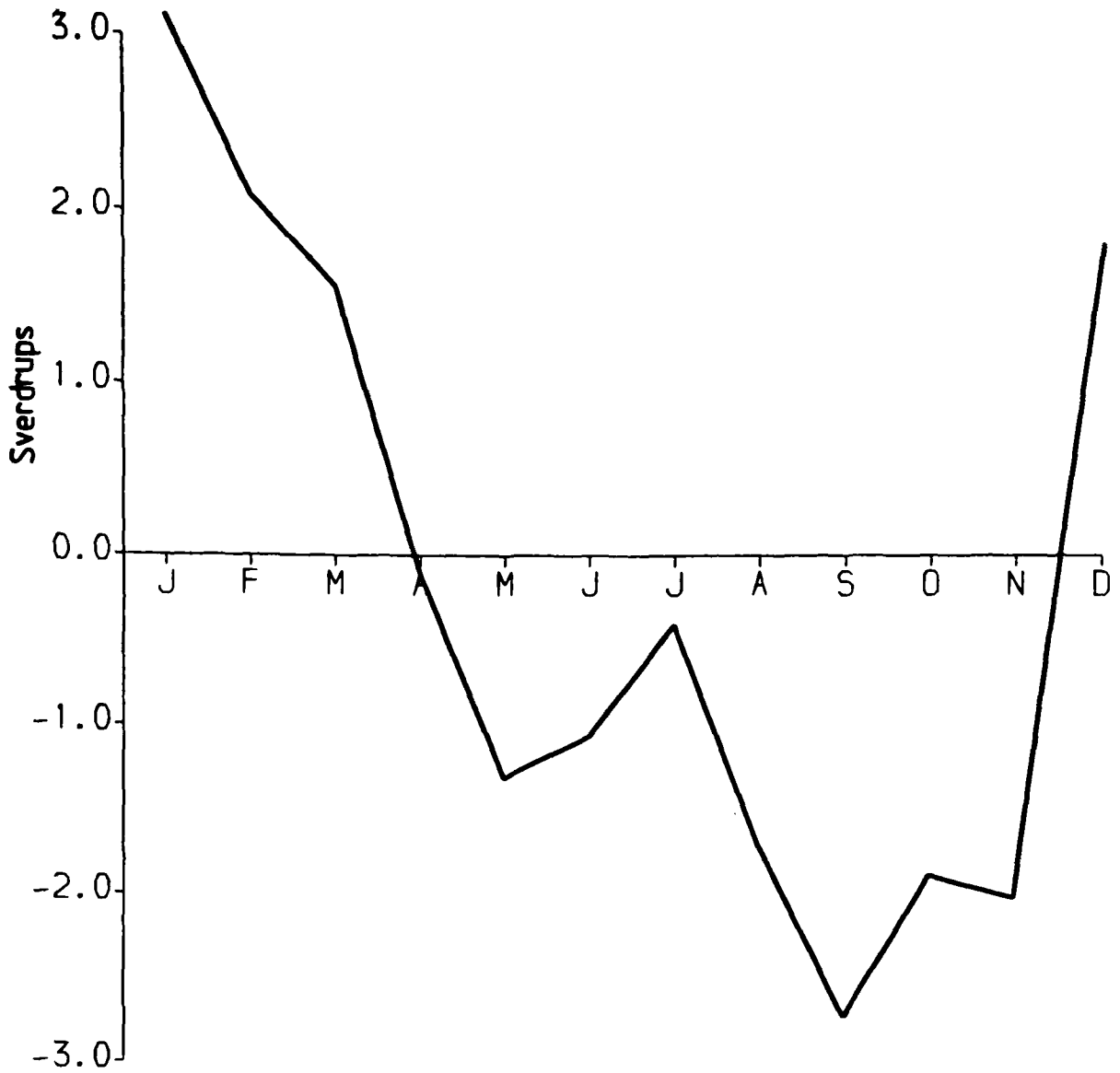

Fig 3.11 The northward transport through the Windward Passage for the baroclinic model forced by the seasonal wind stresses.

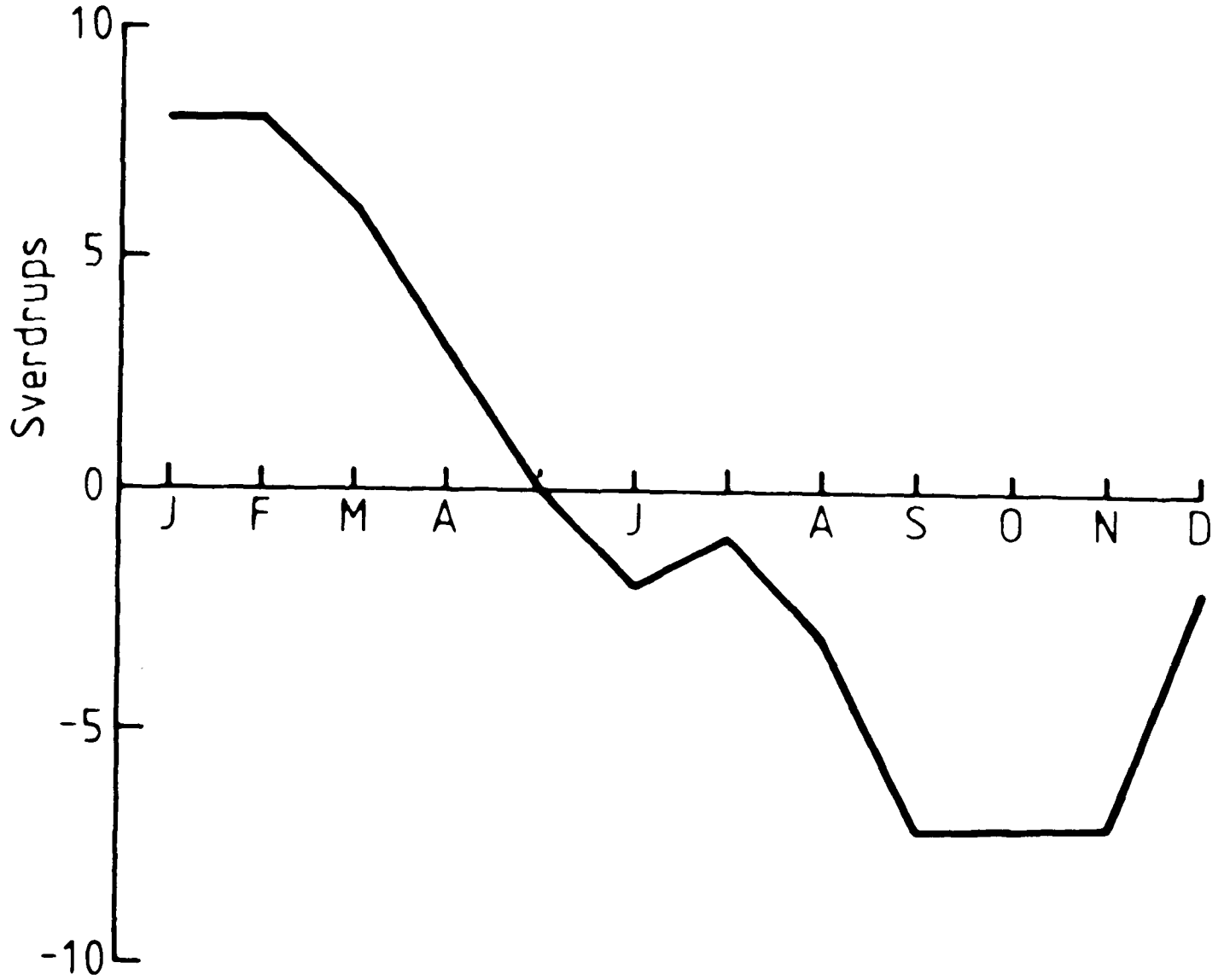

Fig 3.12 The model seasonal variation of transport between Bermuda and the North American coast.

shows the seasonal variation of transport eastward through the Lesser Antilles. During the Winter there is an increased westward flow, balanced by a flow out of the Caribbean through the other three passages. During the late Summer and Fall the situation is reversed, with a large reduction in the westward flow through the Lesser Antilles balanced again by flow inward through the other three passages. During the Spring and Summer the situation is more complex, and the flow out through the Yucatan straits has a maximum. It is worth noting that it is only the flow out through the Yucatan straits (almost equal to the flow through the Florida Straits) that exhibits the Summer maximum expected from the data of Niiler and Richardson [1973].

From Fig E1 we see that the Venezuela and Cayman basins are separated by the Jamaica ridge. This explains the deflection of streamlines toward the Windward passage seen on some of Figs 3.3, whereby streamlines from the east are deflected north-eastward when they encounter the South American coast at 12°N 80°W. This topographic deflection of the seasonal variations is expected since they are primarily barotropic.

On Figs 3.3 we can see an intense feature off the mouth of the Amazon. It has a predicted seasonal variation greater than that of the Antilles Current farther north. To its northwest is a similar feature which varies in antiphase, and to its northeast is a zonal current which changes direction during the year. If we force with the seasonal winds over area C of Fig 3.8, which includes the tropical belt from 5°S to 10°N, then the southern feature is well reproduced each month, in most cases without the northern feature. It was found that both the northern and southern features were forced by the curl of the wind stress, rather than by the effect of wind stress over varying topography. The northern feature is forced by winds to the north of area C,

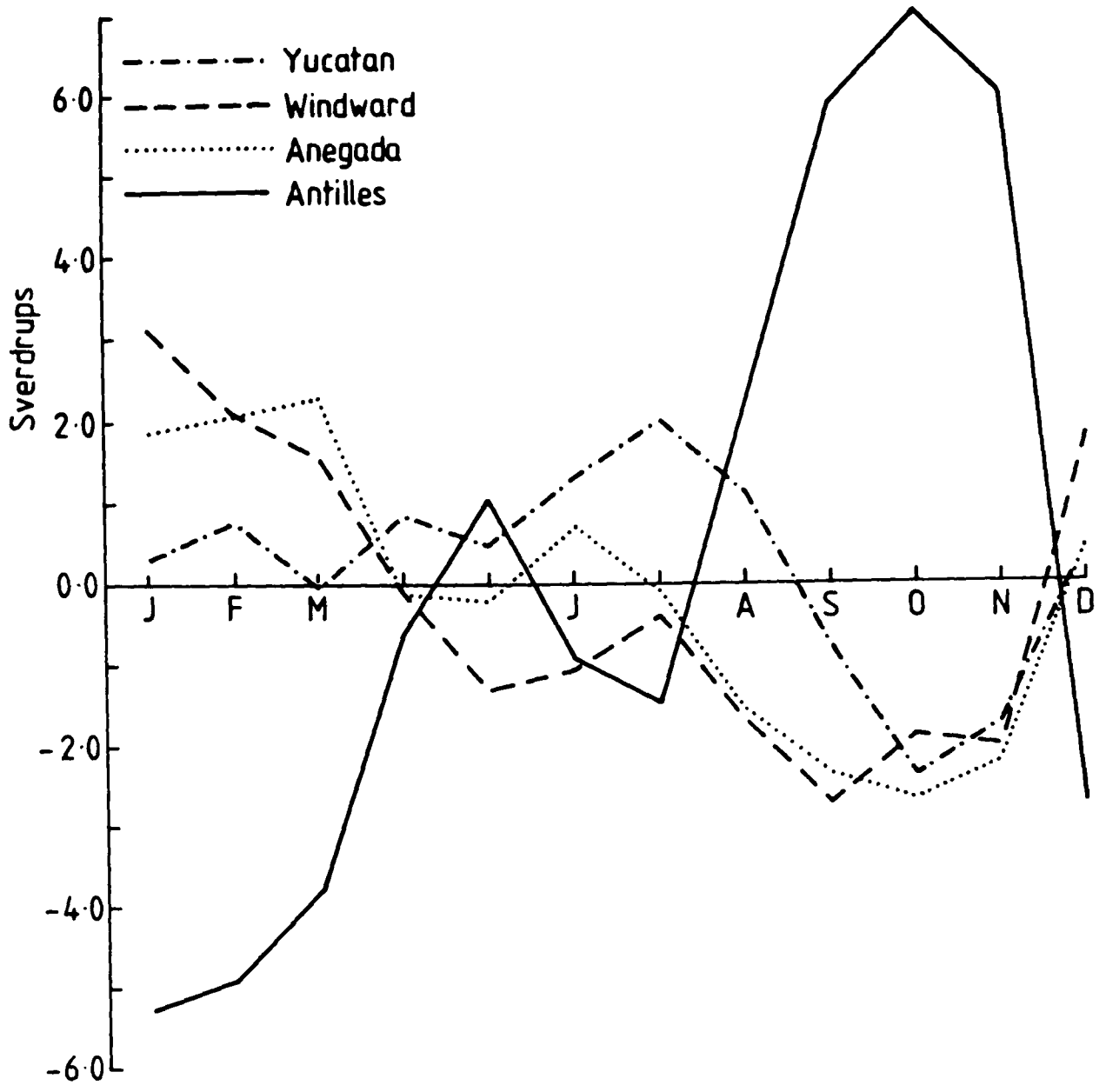

Fig 3.13 The flow out of the Caribbean through the Lesser Antilles, together with the flow out of the Caribbean through the Yucatan Straits, the Windward Passage, and the Anegada Passage, as calculated from the baroclinic model. See also Fig 3.8.

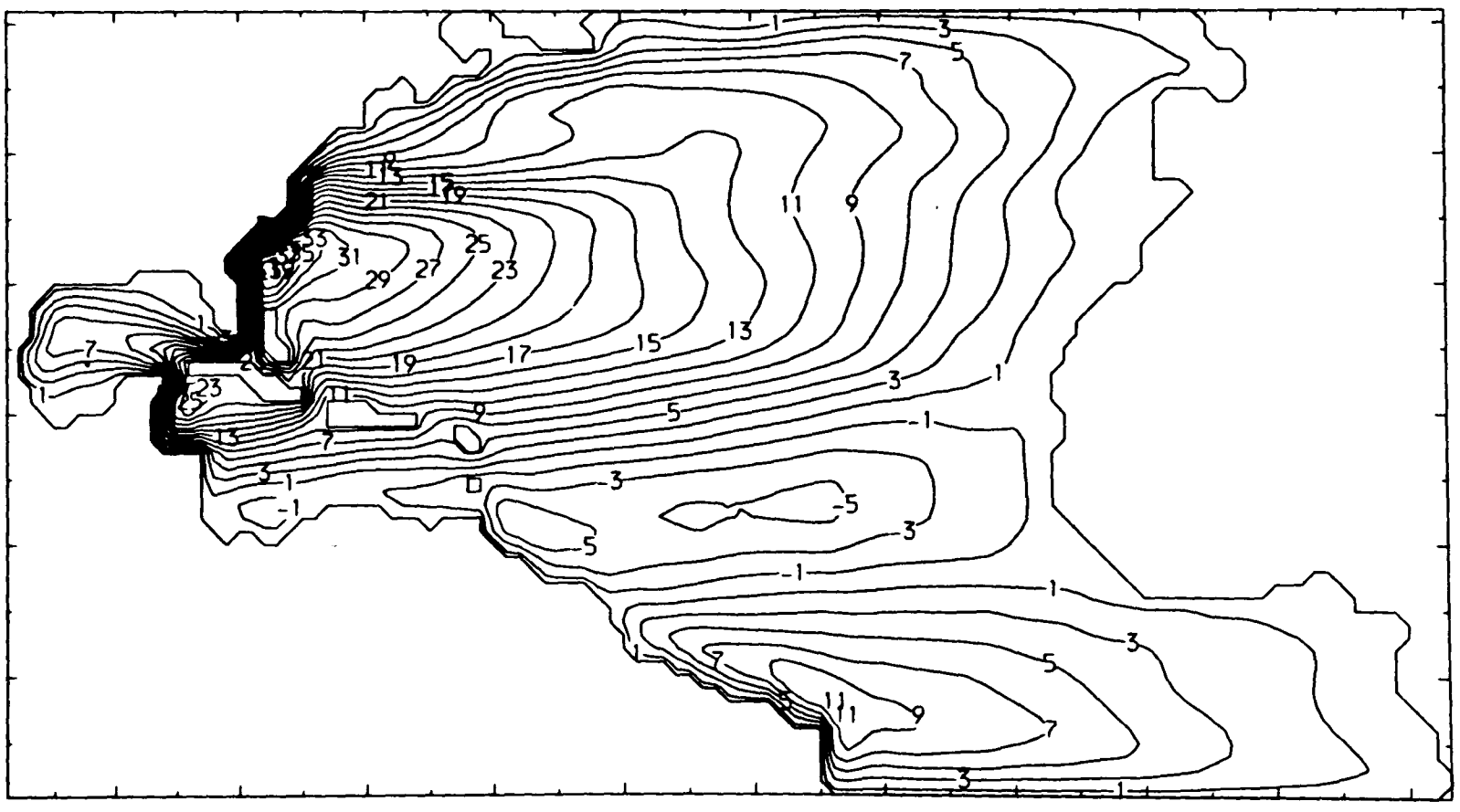

Fig 3.14 A plot of the streamfunction forced by the wind stress of Fig 3.2 in a flat bottomed ocean. All the islands of Appendix E are used in this calculation.

with the resulting transport variations deflected southward by topography to enter this area.

3.5: The mean flow:

3.5.1 Introduction

Anderson and Killworth [1977] show that for a switched-on wind stress the initial effect of bottom topography in reducing the boundary current transport can be compensated for by the passage over the topography of baroclinic Rossby waves. For the baroclinic model used in this study and for time independent forcing, the transport with bottom topography becomes the same as that for a homogeneous ocean with a flat bottom. Since it is quicker to integrate the barotropic equations, the mean streamfunction was obtained by this means.

3.5.2 Comparison of the model with data

The model transport through the Florida Straits is 30.5 Sverdrups (Fig 3.14), which is in close agreement with the value measured by Niiler and Richardson [1973]. Leetmaa, Niiler and Stommel [1977] show that this value is consistent with the integral of the wind stress curl across the basin at the latitude of the Florida Straits. A consequence of this result is that the Antilles current, to the east of the Bahamas, has no mean northward transport. This conclusion is supported by Gunn and Watts [1982]. Fig 3.14 also indicates little mean transport by the Antilles Current.

To the north, the transport of the model Gulf Stream

increases downstream to about 40 Sverdrups. This maximum transport is much less than that observed, which can reach 120 Sverdrups. The disparity between observed and predicted transport indicates the importance to the mean circulation of processes not included in this model, such as eddy driven mean flows (Holland and Rhines [1980]).

To the south, the model shows substantial transport through the passages of the Northern Caribbean (see Fig 3.8). In particular most of the transport through the Yucatan Straits (22.5 Sverdrups) is contributed by the flow through the Windward passage (12.5 Sverdrups). This is at variance with several authors. For instance Morrison and Nowlin [1982] suggest that almost all the transport through the Yucatan Straits flows from the eastern Caribbean rather than through the Windward passage. On the other hand Roemmich [1982] suggests that while the bulk of the transport through the Yucatan Straits comes from the eastern Caribbean, a substantial part (7 Sverdrups) enters via the Windward passage. Gunn and Watts [1982] have also measured a substantial geostrophic transport through the Windward passage of 15 ± 5 Sverdrups during the Summer of 1972, though it is not clear that this is a reliable measure of the mean transport.

The model shows a mean transport through the Yucatan Straits that is less than the mean transport through the Florida Straits. The highest figure for geostrophic transport through the Yucatan Straits in the literature appears to be 27 Sverdrups during October 1970 (Hansen and Molinari [1979]). This is three Sverdrups lower than the mean flow through the Florida Straits, so it is possible that several Sverdrups do flow westward through passages in the Bahamas to the south of Miami, though probably not as much as the 8 Sverdrups shown on Fig 3.14.

In the model Gulf of Mexico a western boundary current of

about seven Sverdrups is evident. This compares well with the estimate of Blaha and Sturges [1981] of 8 Sverdrups.

3.6: Summary and Conclusion.

The seasonal variation of the Florida current, measured by Niiler and Richardson [1973], has not previously been understood because application of the Sverdrup relationship predicted seasonal variations of far greater magnitude and almost opposite phase to those measured. The same relationship has, however, been successfully used to predict the mean flow of the Florida Current (Leetmaa, Niiler and Stommel [1977]). This suggests that there is a difference between the dynamics of the mean flow and that of the annual cycle.

In Chapter 2 the dynamics of the seasonal variation of western boundary currents was investigated. It was shown that the non-topographic Sverdrup balance is unlikely to hold at annual period for the North Atlantic. For periods much less than the time taken for the wind generated baroclinic Rossby waves to pass over bottom topography, the ocean response is primarily that for a homogeneous ocean and thus strongly modified by topography. For periods much longer than this time, the baroclinic Rossby waves compensate for the effect of topography and the non-topographic Sverdrup balance holds. For the Atlantic at 25°N it can take years to decades for compensation by baroclinic Rossby waves to occur, depending on the distance of the wind stress variability from the western boundary, so at annual period the non-topographic Sverdrup balance is not likely to be applicable.

In Section 3.3 we investigate the seasonal variation of the

transport through the Florida Straits. The total transport variation in the baroclinic calculation was found to be small (± 2 Sverdrups) and to agree in phase with observations, although the data show a larger amplitude of ± 4 Sverdrups. Part of the seasonal variation results from baroclinic activity over topography. A Kelvin wave generated by winds to the north of the Florida Straits generates transport variations as it passes south over varying bottom topography. As expected the effect of baroclinic Rossby waves at the latitude of the Florida Straits was found to be small relative to the effect of the coastal Kelvin wave. The part of the transport variability which would be forced in a homogeneous ocean can be split into two independent contributions due to the zonal and meridional wind stress. It is the meridional component of wind stress which forces the Summer maximum. In contrast, the mean transport is forced primarily by the zonal wind stress curl.

To determine the relative importance of different regions for the seasonal variation of the Florida Straits transport we considered two forcing regions marked A and B (Fig 3.8) in the homogeneous model. Region A, to the north of the Bahamas and to the west of the Mid-Atlantic ridge, accounts for a large part of the variation in transport of the Florida Current, since transport streamlines from this region are deflected south-west to affect the Florida Current. The variability due to winds over region A can further be split into a part depending on the curl of the wind stress and a part depending on the wind stress over gradients in topography. It was found that in Winter the curl forced variations contributed a minimum in northward transport which roughly cancelled a maximum in the variations forced by wind stress over topographic gradients, and that during the Summer both processes added to give the Summer maximum. The

October minimum is due to the variations forced by topographic gradients.

Although the primary motivation of this thesis is to explain the seasonal cycle of transport variations in the Florida Straits, other parts of the North Atlantic are considered in Section 3.4. Observations of transport in these regions are scarce, and it is not possible to adequately compare model results with observations. In the Antilles region, the model results suggest that if the Antilles Current exists, it is seasonal in nature, with a northwestward transport of about ten Sverdrups during the Winter, and a southeastward transport of about ten Sverdrups during the Fall. However, more recently Olson, Schott, Zantopp and Leaman [1984] have questioned the existence of a seasonal Antilles Current. The seasonal variation of the Antilles Current is a robust feature of our model. At annual period, only a small part of the seasonal transport passes through the Florida Straits. Instead, most of the transport is to the east of the Bahamas as a result of topographic blocking in the Caribbean and Florida Straits region. It is therefore of particular interest to determine if the seasonal variation in transport suggested by Figs 3.3 in the Antilles region really occurs.

CHAPTER FOUR

Comparison between models

4.1: Introduction

In Chapter Three a two layer model was used with realistic bottom topography and seasonally varying winds to predict the seasonal variation of the Florida Current. Much of the variation was found to be barotropic, i.e. a large proportion of the variation of Fig 3.5(a) could be accounted for by a simple one layer model (Fig 3.5(c)). In this chapter we compare the streamfunction patterns at the end of each month's integration for the simple one layer model with the corresponding streamfunction produced by the Semtner model (Semtner [1974]).

4.2: The one layer calculations

These are the same as the calculations which produced Fig 3.5(c) in Chapter Three. The one layer model was forced with the seasonal winds one month at a time for one year. As is shown in Appendix F, the streamfunction at the end of each month's integration is approximately in equilibrium with the forcing, so only one year of integration is needed to give satisfactory streamfunction patterns. The streamfunction patterns at the end of each month are shown in Figs 4.1. They are very similar to Figs 3.3, which show the streamfunction for the two layer model. This confirms the primarily barotropic nature of the seasonal response over the North Atlantic. Though away from the

boundaries there will be surface intensification due to the Ekman drift, this has only a small effect on the streamfunction (see Section 2.3.4).

4.3: The Semtner model calculations

The Semtner model is fully described in the Semtner Report (Semtner [1974]). It is a level model in which topography can be incorporated. The equations of motion and the heat and salt equations using spherical coordinates are solved. The resolution of the model was one degree, in common with the one layer model. Twelve levels in the vertical were used with depths (at the bottom of each level) of: 50 m, 400 m, 900 m, 1300 m, 1700 m, 2100 m, 2500 m, 3000 m, 3500 m, 4000 m, 4750 m, and 5500 m respectively. The first level is used to resolve the Ekman drift, the bottom of the second level is at the minimum depth of the ocean in the application of Chapter 3 (see Appendix E). The bottom of the third level is the approximate depth of the Florida Straits between Florida and the Bahamas, and is of course an important parameter since it limits the transport variations through the Straits. The vertical resolution was chosen to decrease with depth because it is the shallow topography that blocks transport variations, and it is important to resolve this as well as possible. The number of levels at each point was found by fitting to the smoothed topography of Appendix E, i.e. the bottom level has the level depth nearest to the depth of the smoothed topography.

The model ocean was made homogeneous, so that a comparison could be made with the one layer model. This was done by making the temperature and salinity uniform throughout the ocean. There

will be a small increase of density with depth due to the effect of pressure. This slight stability is desirable to avoid repeated convective adjustment within the model due to gravitational instability. Baroclinic effects will be negligible.

The relaxation scheme used was successive-over-relaxation, with immediate updating of the streamfunction. The value of the over-relaxation parameter used was 1.8. This achieved convergence typically within 20 iterations for a two-hour timestep. It was found that this method of relaxation did not work (the model 'blew up') if the semi-implicit treatment of the Coriolis term (an option within the model) was used with complicated topography. The semi-implicit treatment supposedly allows a longer timestep, since barotropic Rossby waves and inertial waves are filtered. In any case, we do not wish to filter the barotropic Rossby waves, so the semi-implicit treatment was not used. A forward timestep was also taken every one hundred leap-frog timesteps to avoid 'splitting' of results at alternate timesteps. This is similar to the procedure used in the one-layer model (see Appendix B).

The islands of the one layer model were changed slightly for use in the Semtner model. In particular the island representing the Bahamas had its two southern grid points (out of four) changed from level zero (land) to level one (50 m depth). This allowed the island to be used. There has to be a minimum gap of two grid points between one land mass and another in the Semtner model. There were other minor changes to the grid in the Newfoundland area, and in the western Gulf of Mexico.

The model was forced with the same seasonal winds (multiplied by one tenth) as were used to force the one layer model. This was done one month at a time for one year. The

streamfunction patterns at the end of each month of integration are also shown on Figs 4.1 for comparison with the one-layer model. The upper diagram on each page is from the Semtner model, and the lower diagram is from the one layer model. There are twelve pages in all (one for each month). The response of the Semtner model has been multiplied by ten. This process of multiplying the forcing of the Semtner model by one tenth, and then multiplying the response by ten is done to ensure that non-linear effects are absolutely negligible. We are therefore assessing the differences between a level formulation with no-slip boundary conditions and an Arakawa B-grid, and a layer formulation with free-slip boundary conditions and an Arakawa C-grid. The different grids are known to affect the propagation of baroclinic Kelvin waves (Hsieh, Davey and Wajsowicz [1983]), but the barotropic response ought to be reproduced well in each case. The response of both models is linear for practical purposes. The horizontal eddy viscosity was the same for both models (10^4 m^2/sec), as was the resolution (one degree). There is also a vertical eddy viscosity of 10^{-3} m^2/sec in the Semtner model together with an eddy diffusivity (for the heat and salt equations) of 10^3 m^2/sec. The one layer model also includes a small bottom friction not present in the Semtner model. These latter differences between the models should result in only minor differences between the streamfunction patterns. The major differences away from boundaries should be due to the differences between a layer and level formulation in the way they handle topography. In the layer formulation, depth can take any value, whereas in the level formulation it can take only discrete values.

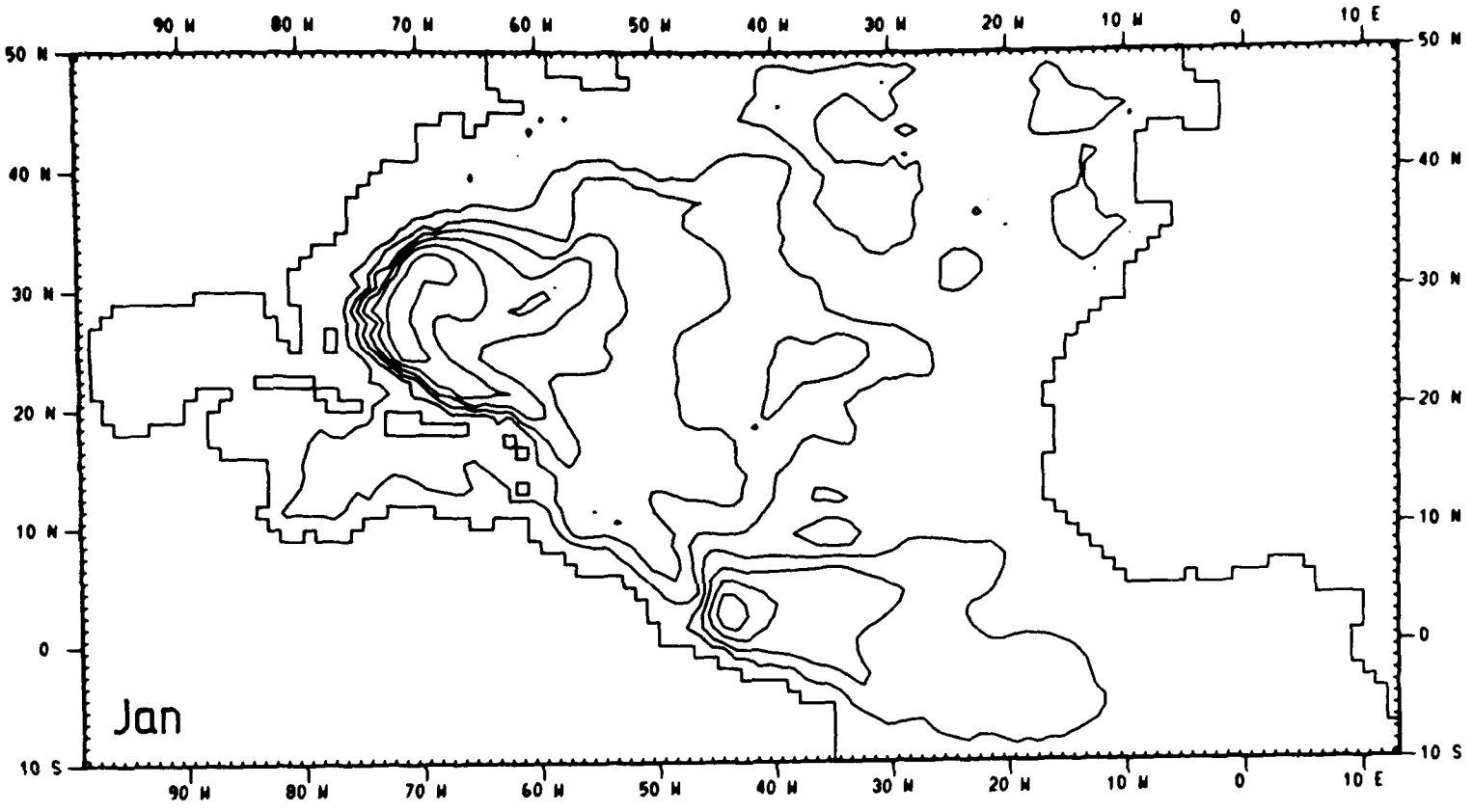

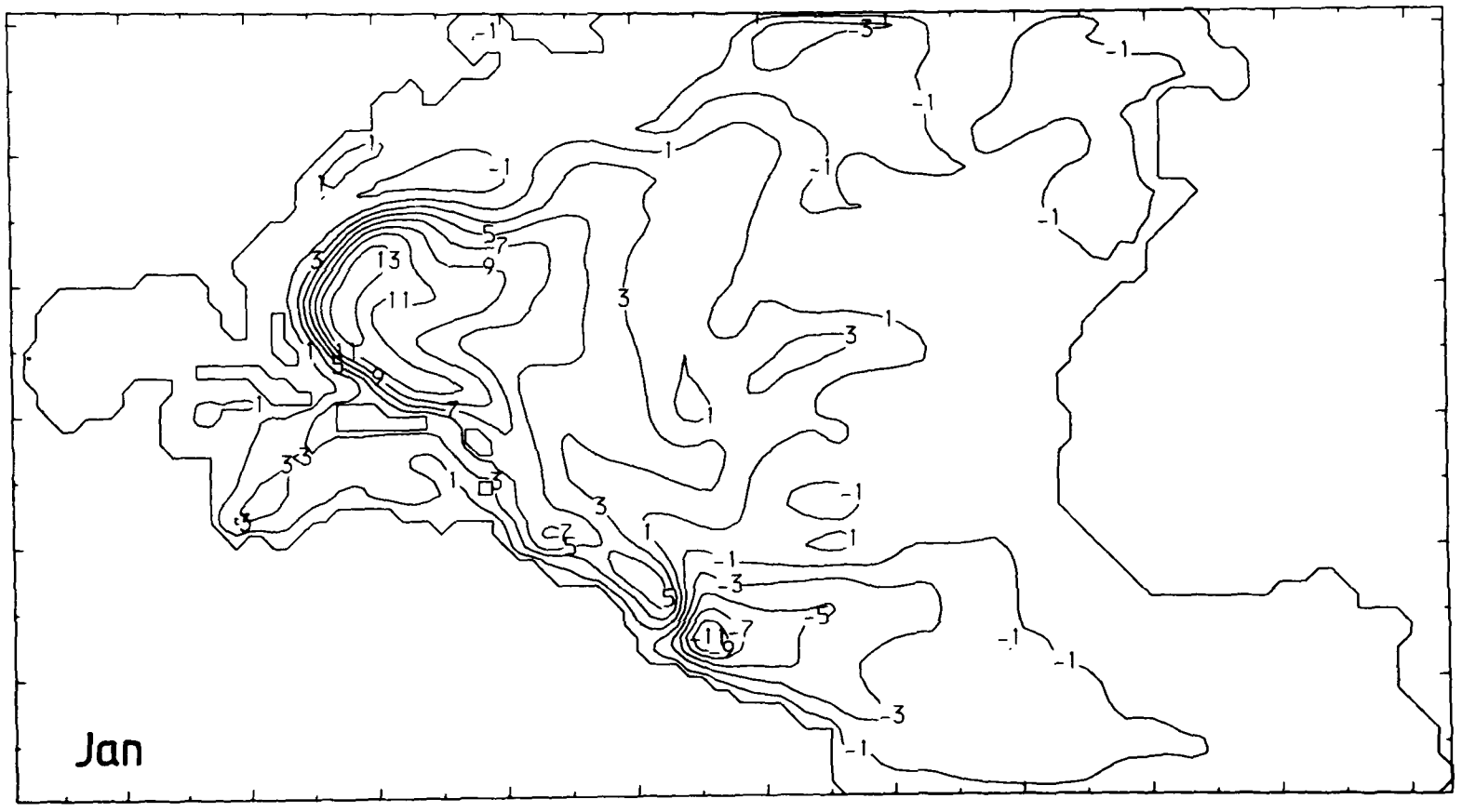

Fig 4.1 A comparison between the one layer model and the Semtner model. The upper diagram on each page is from the Semtner model, and the lower diagram is from the one layer model. The streamfunctions are at the end of each month's integration.

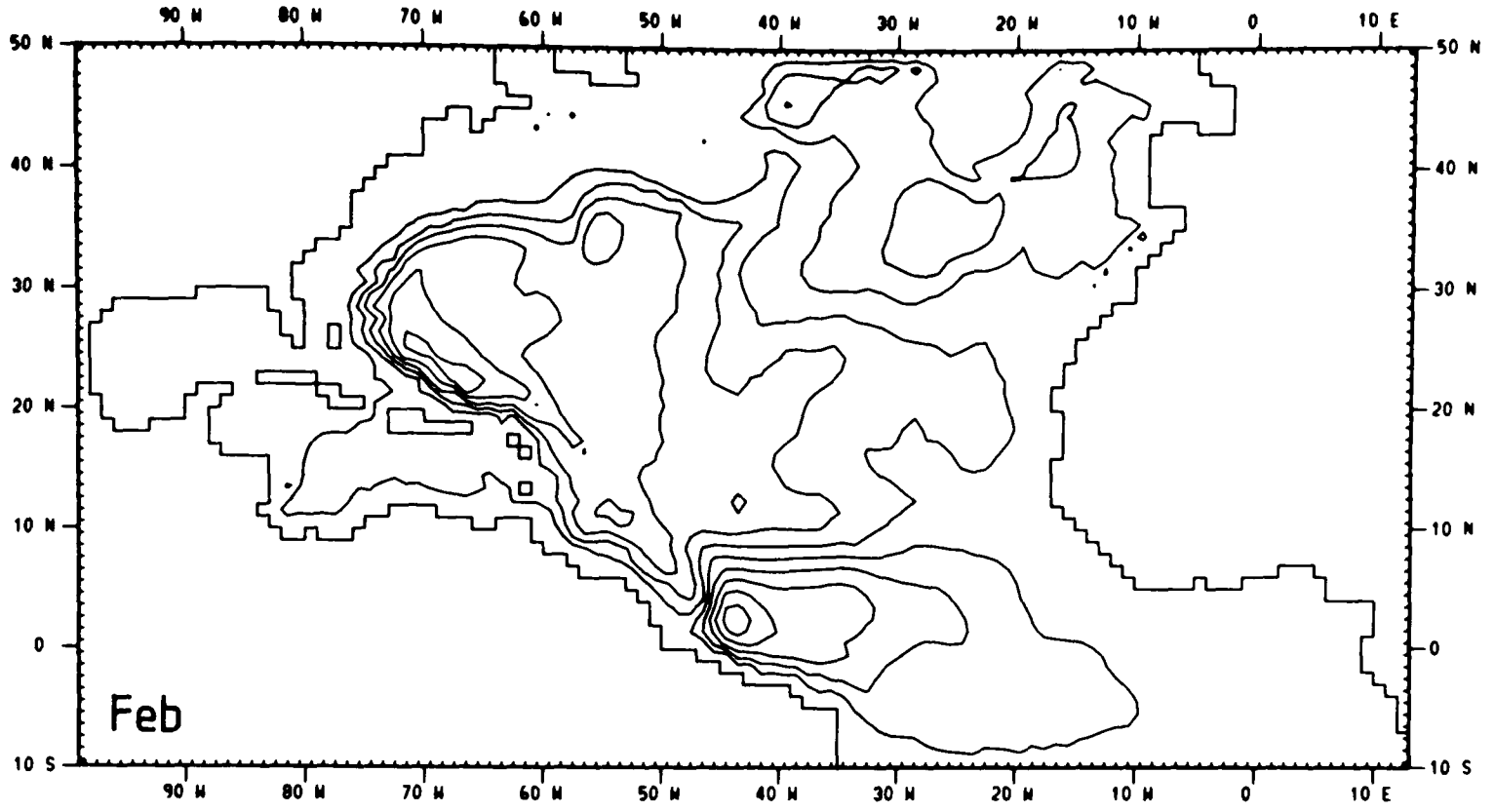
90 W
80 W
70 W
60 W
50 W
40 W
30 W
20 W
10 W
0
10 E
50 N
40 N
30 N
20 N
10 N
0
10 S
Feb

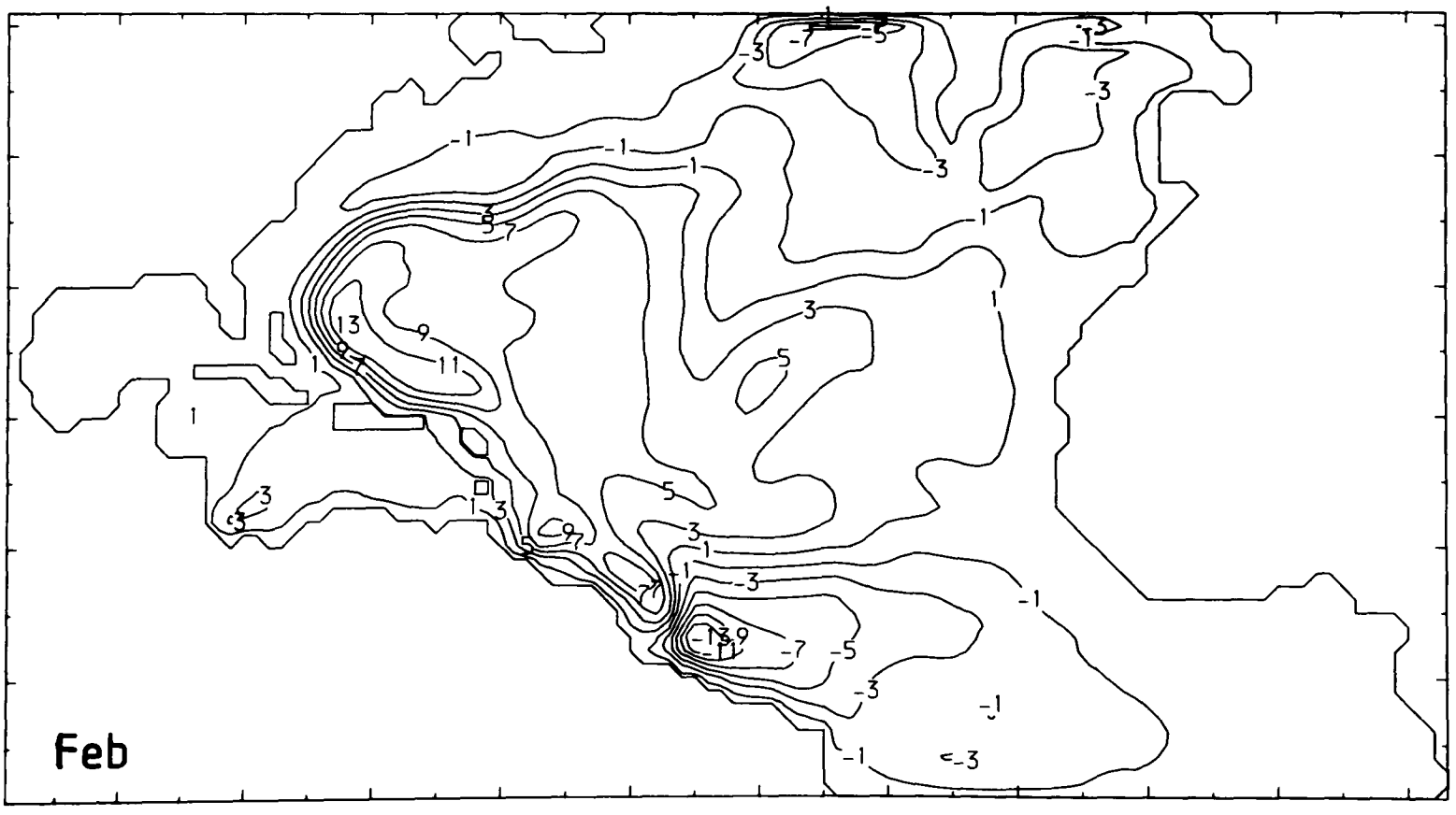
Feb

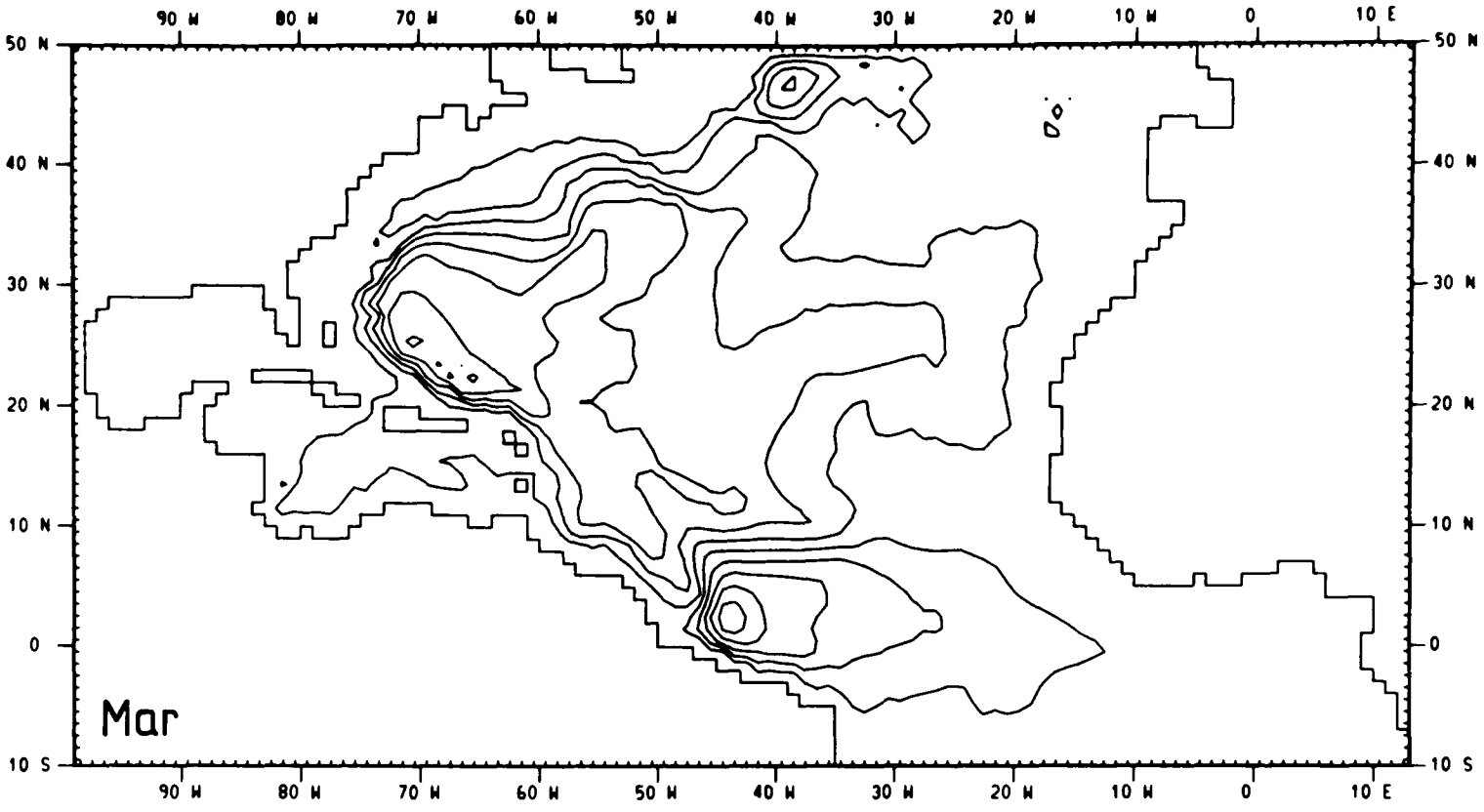
90 W
80 W
70 W
60 W
50 W
40 W
30 W
20 W
10 W
0
10 E
50 N
40 N
30 N
20 N
10 N
0
10 S
Mar

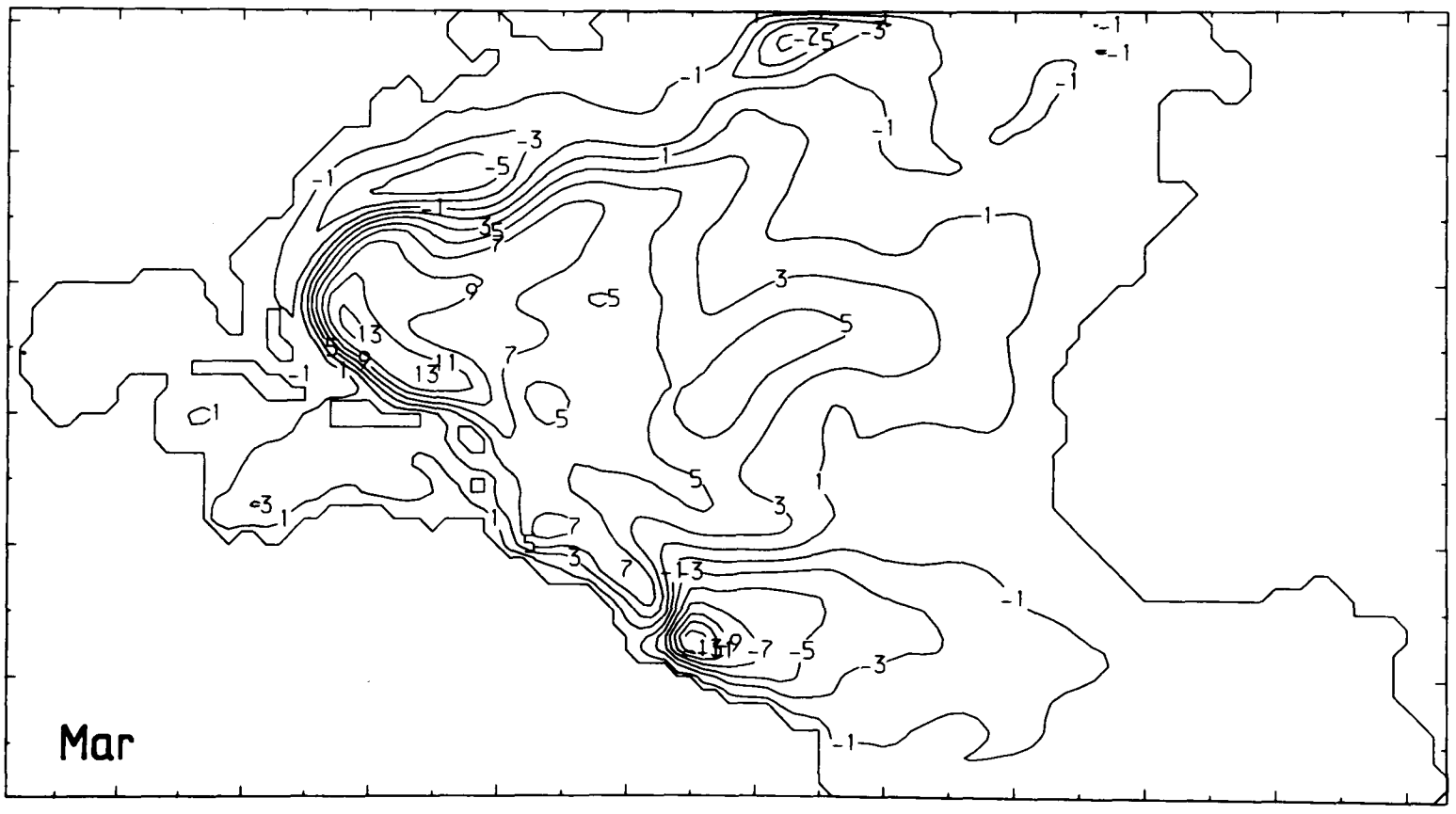
Mar

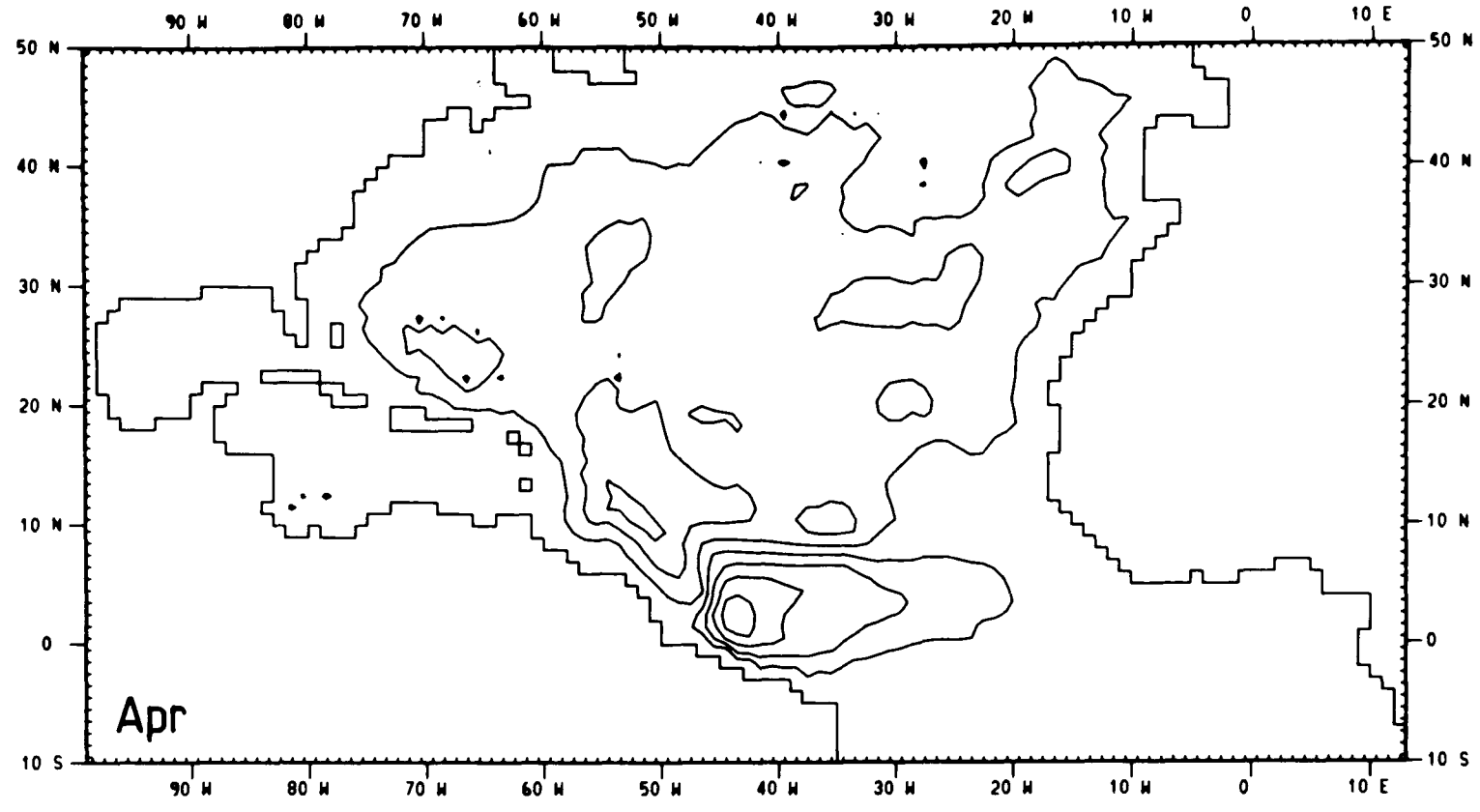
90 W
80 W
70 W
60 W
50 W
40 W
30 W
20 W
10 W
0
10 E
50 N
40 N
30 N
20 N
10 N
0
10 S
Apr

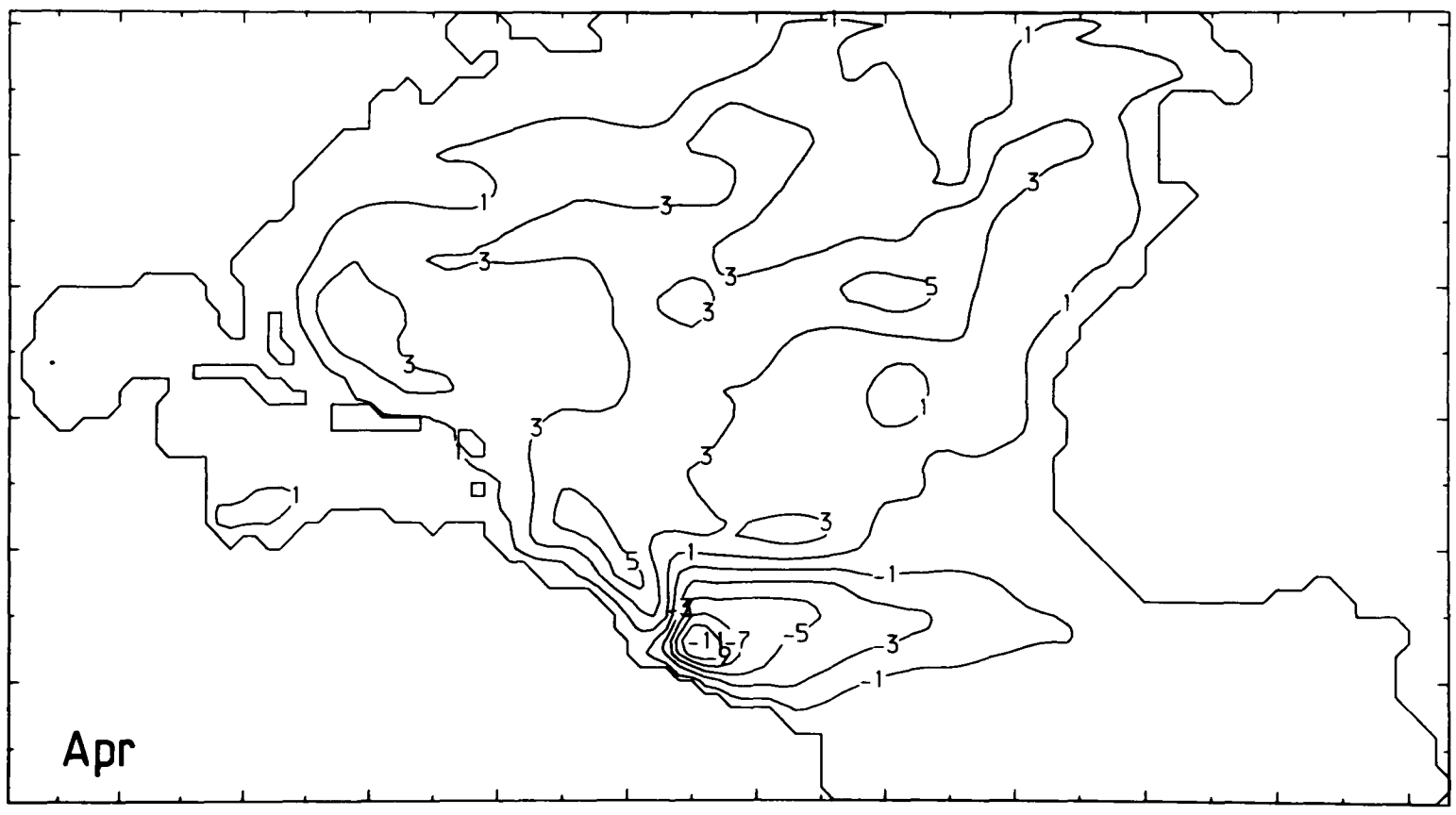
Apr

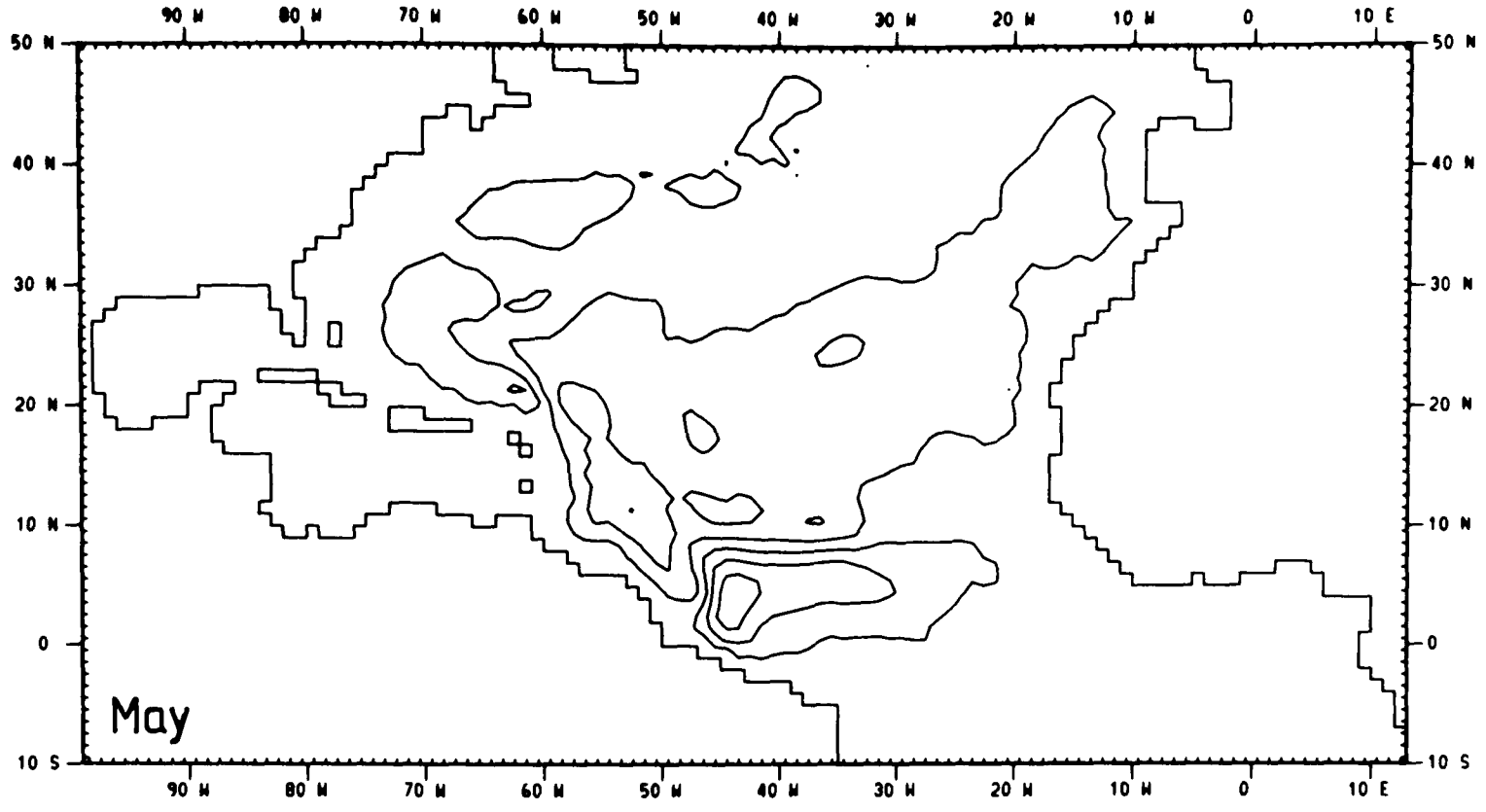
90 W
80 W
70 W
60 W
50 W
40 W
30 W
20 W
10 W
0
10 E
50 N
40 N
30 N
20 N
10 N
0
10 S
May

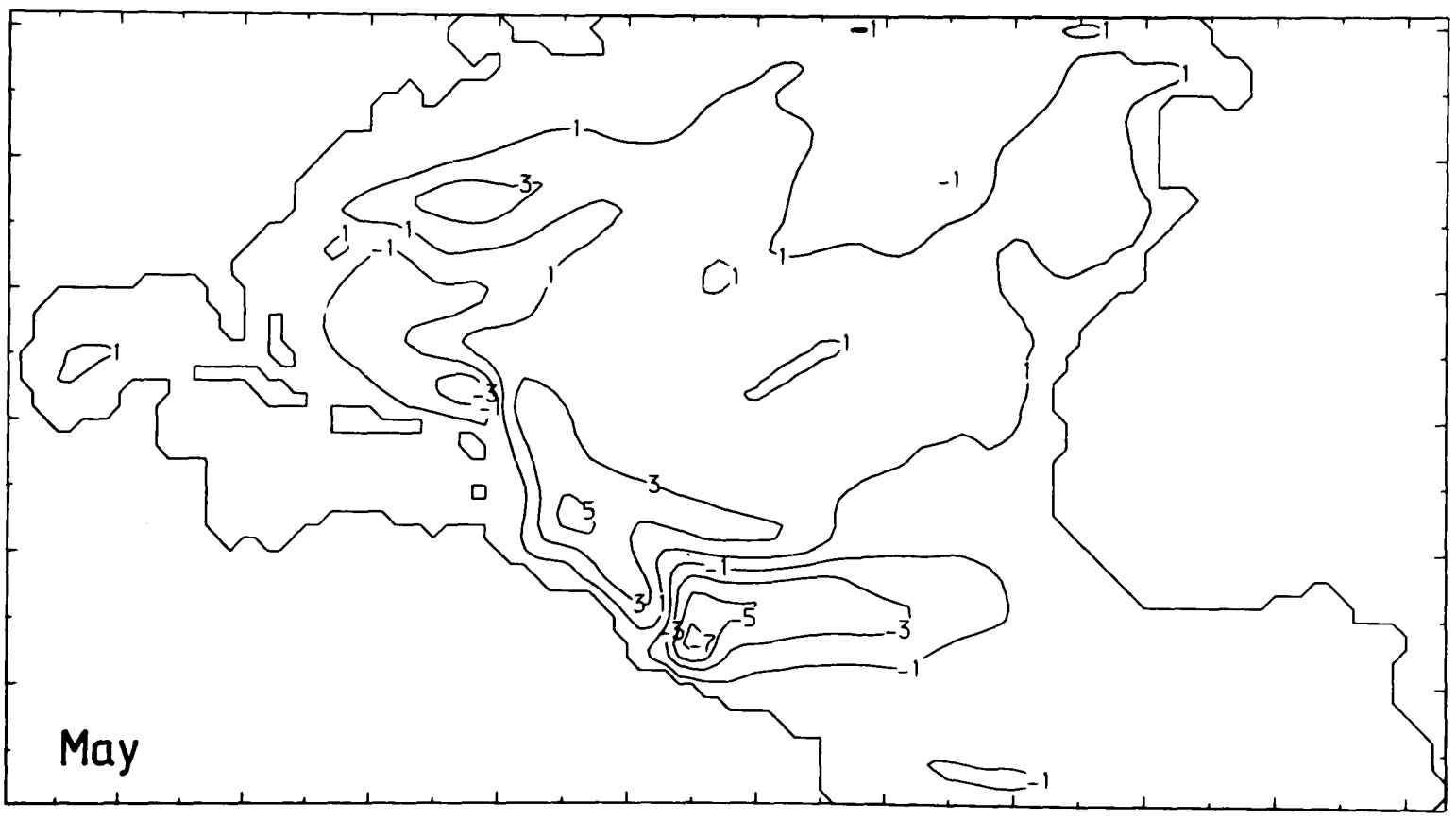
May

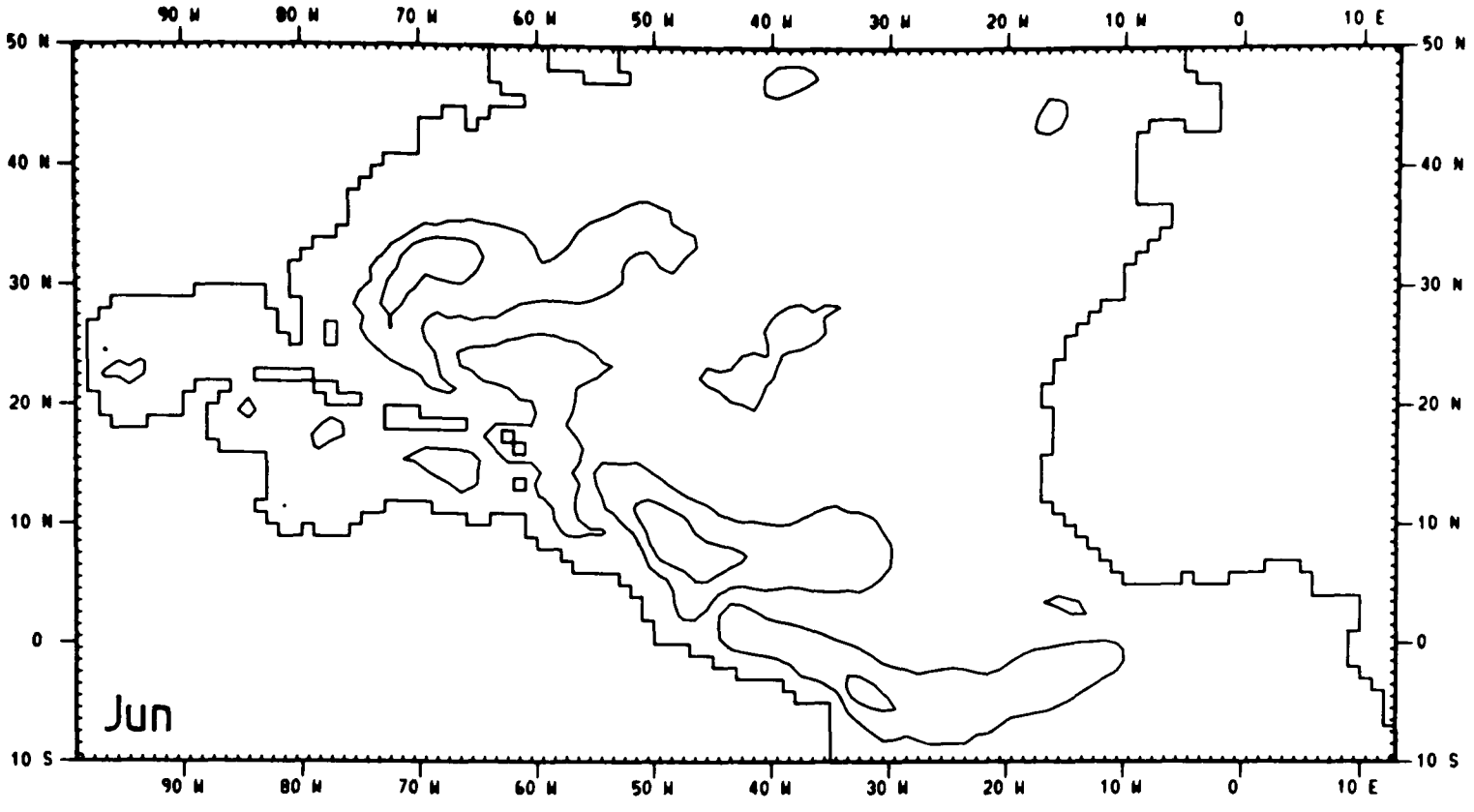
90 W
80 W
70 W
60 W
50 W
40 W
30 W
20 W
10 W
0
10 E
50 N
40 N
30 N
20 N
10 N
0
10 S
Jun

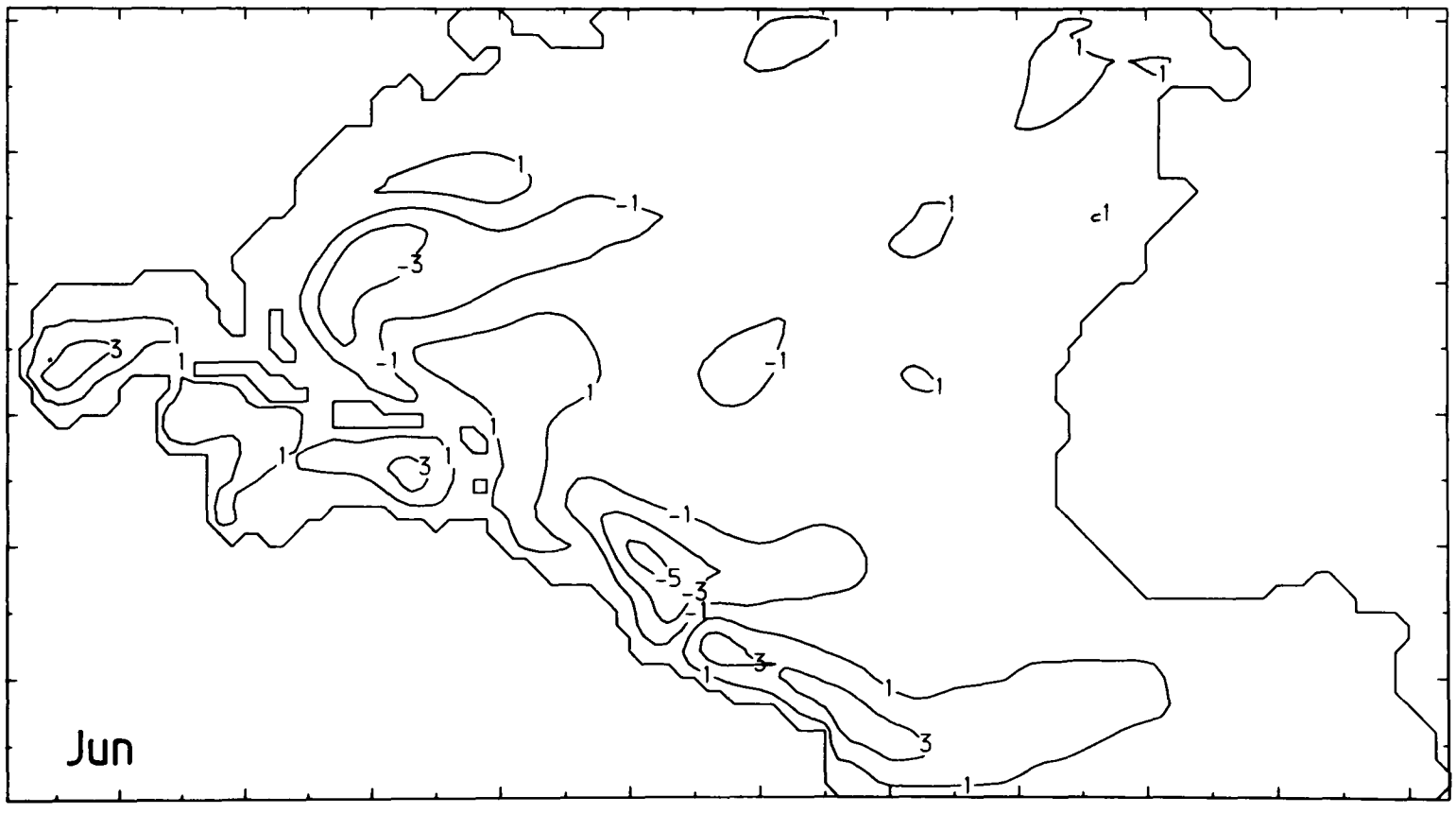
Jun

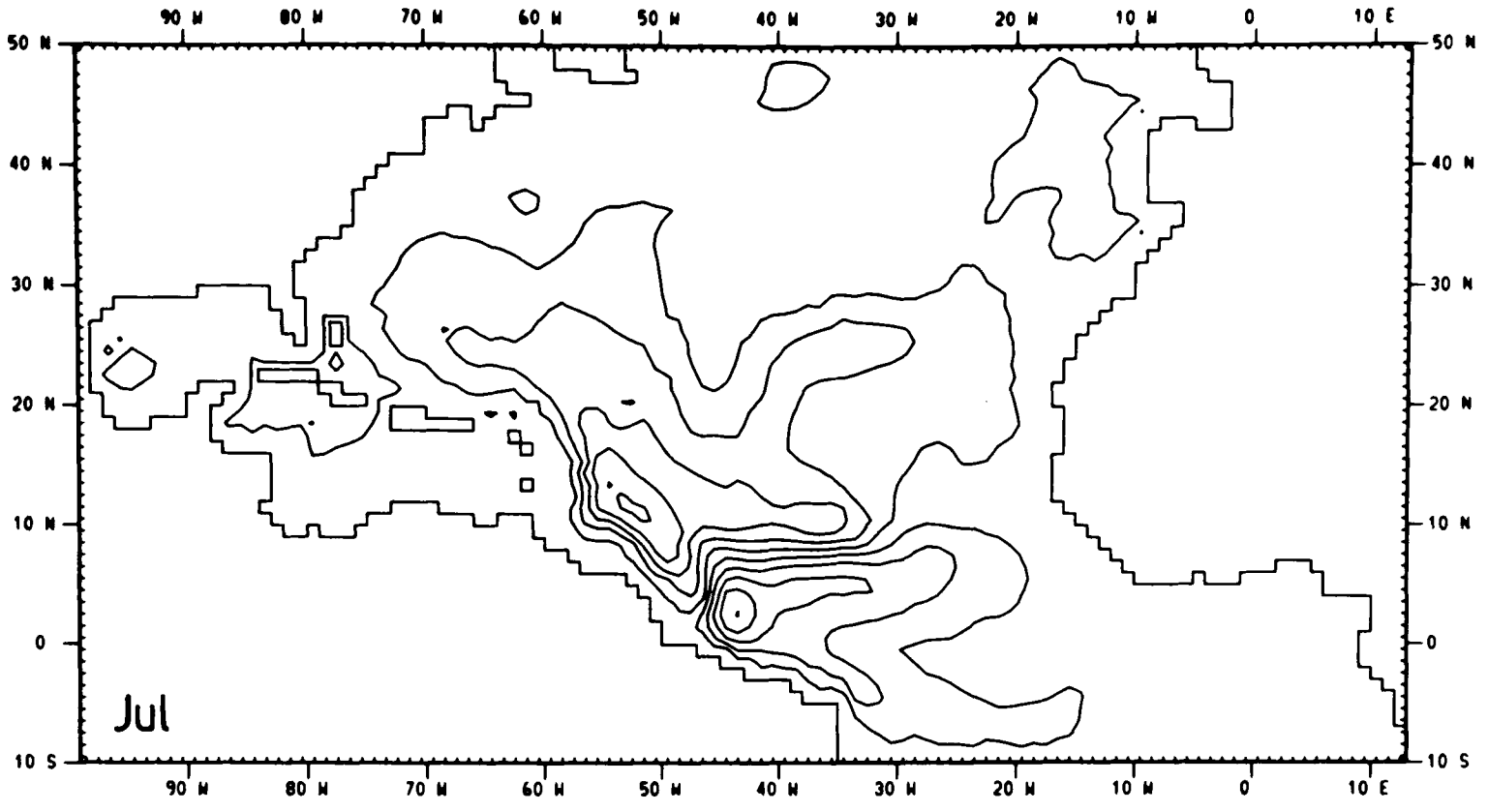
90 W
80 W
70 W
60 W
50 W
40 W
30 W
20 W
10 W
0
10 E
50 N
40 N
30 N
20 N
10 N
0
10 S
Jul

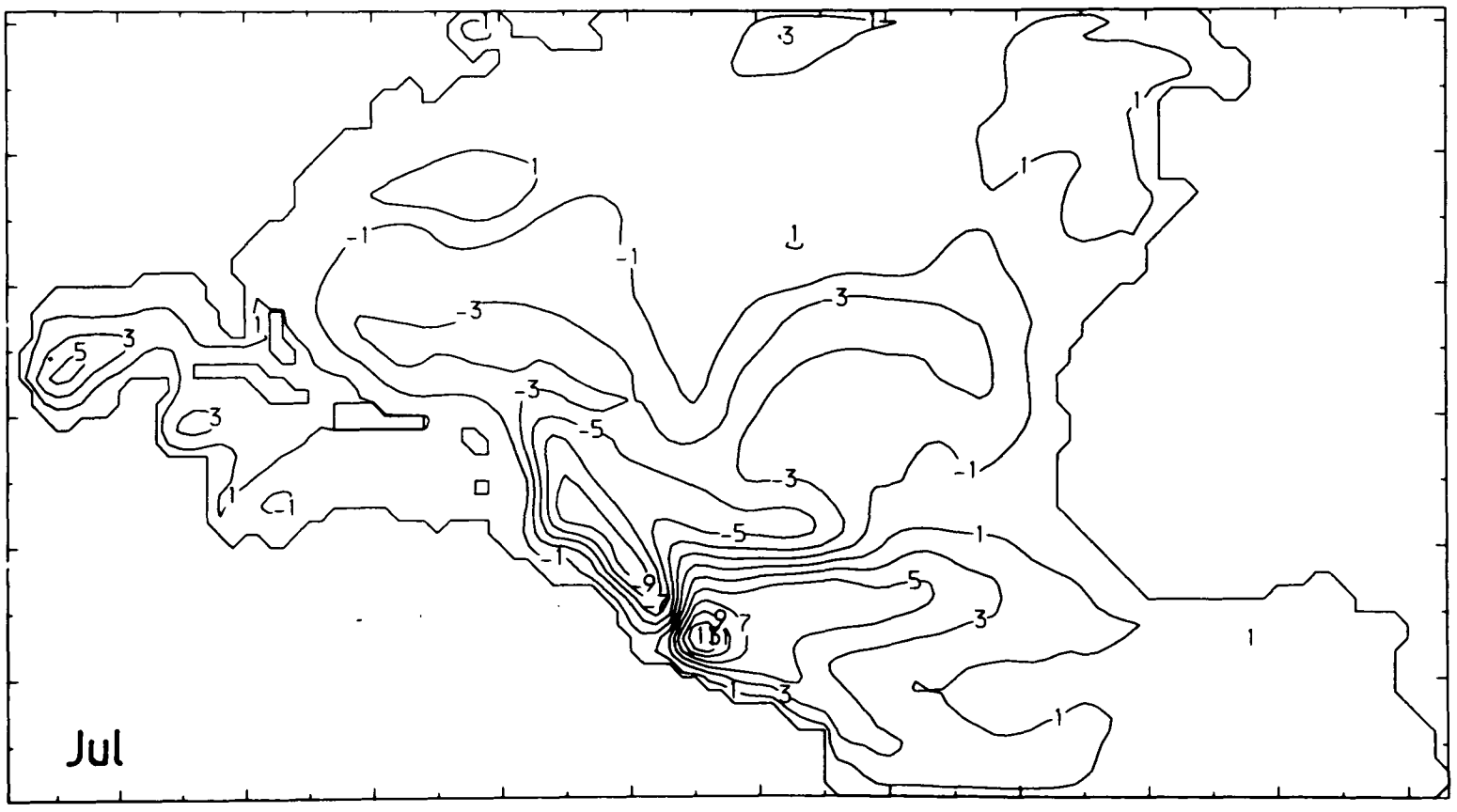
Jul

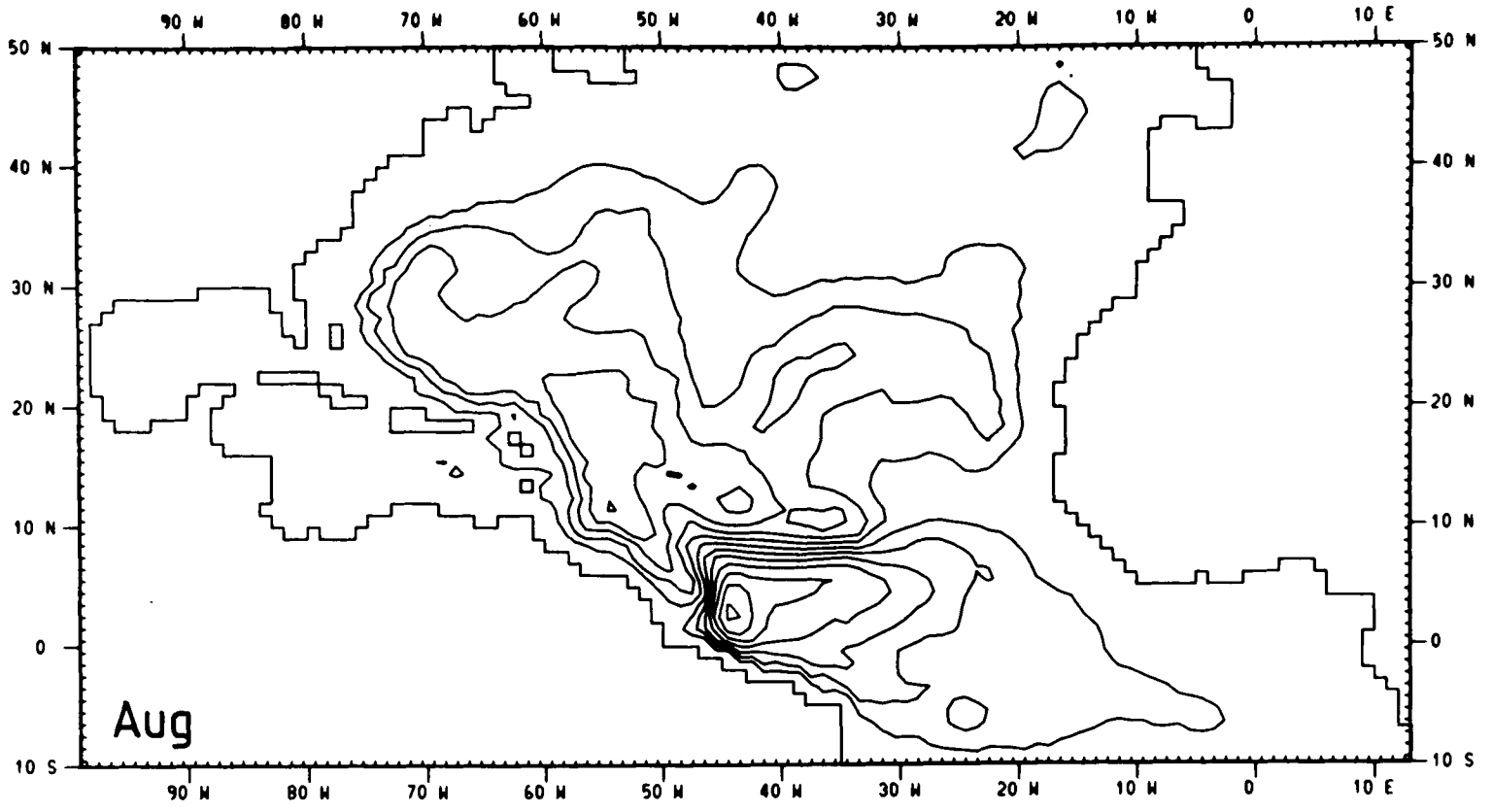
90 W
80 W
70 W
60 W
50 W
40 W
30 W
20 W
10 W
0
10 E
50 N
40 N
30 N
20 N
10 N
0
10 S
Aug

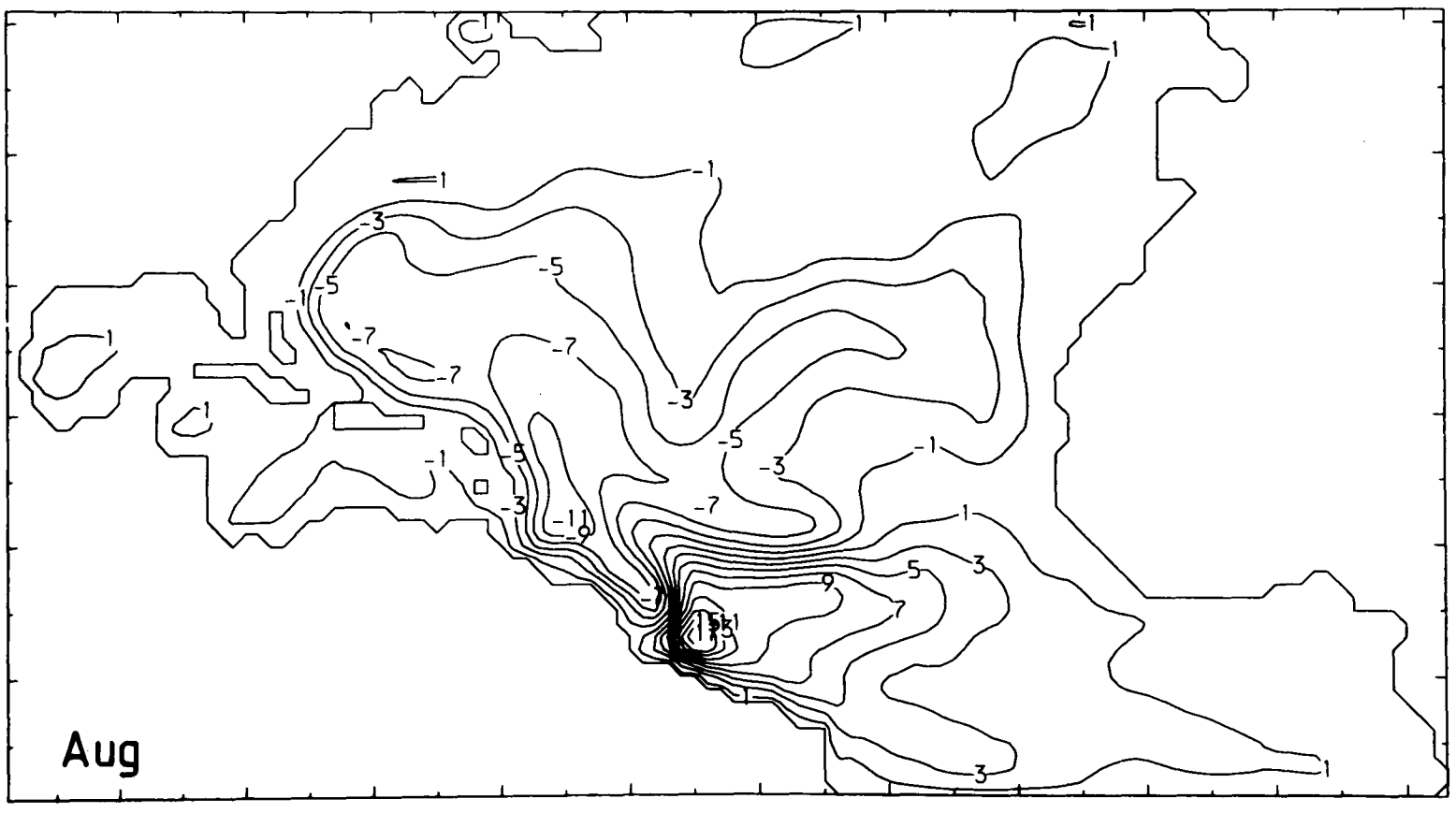
Aug

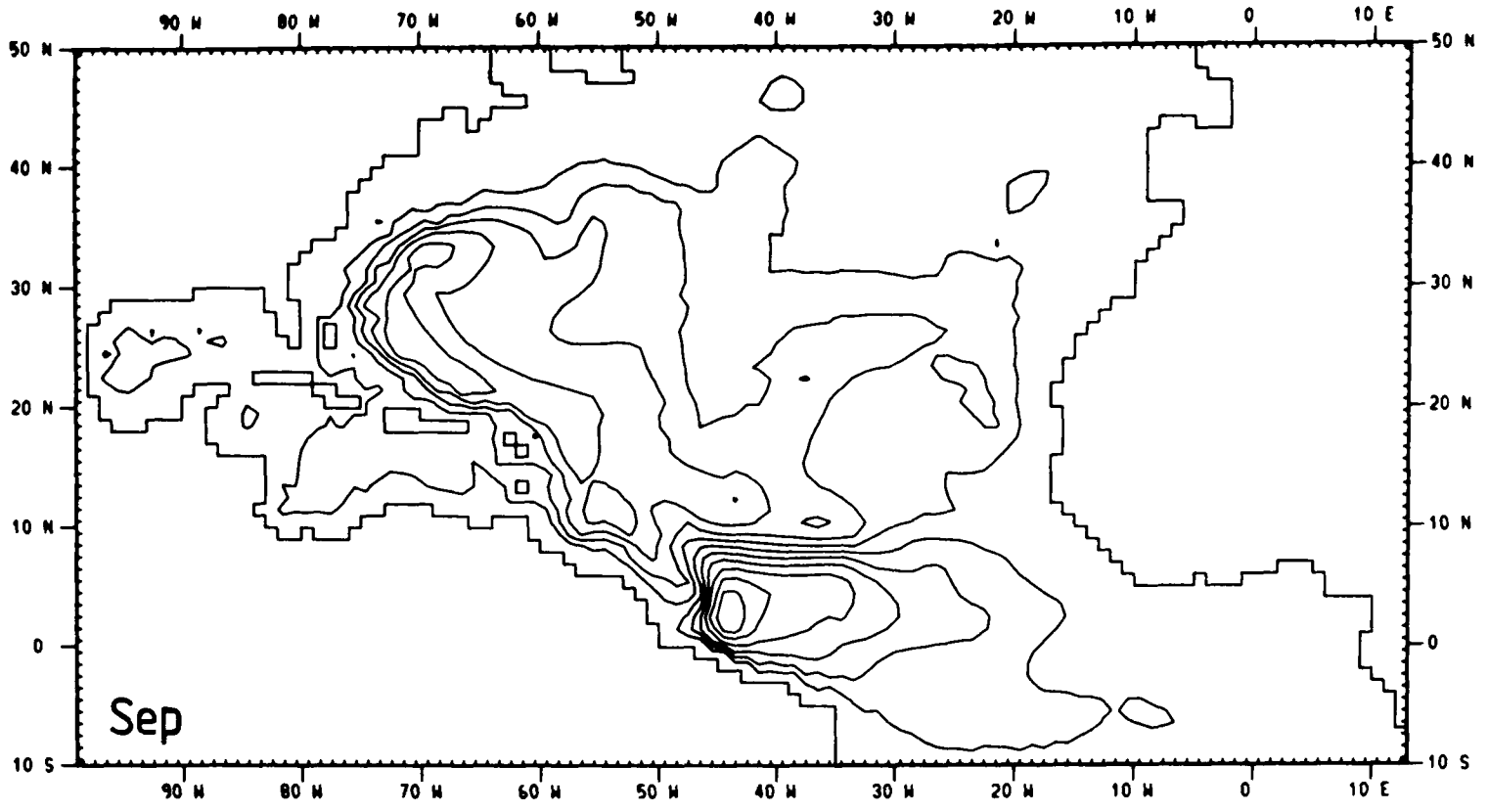
90 W
80 W
70 W
60 W
50 W
40 W
30 W
20 W
10 W
0
10 E
50 N
40 N
30 N
20 N
10 N
0
10 S
Sep

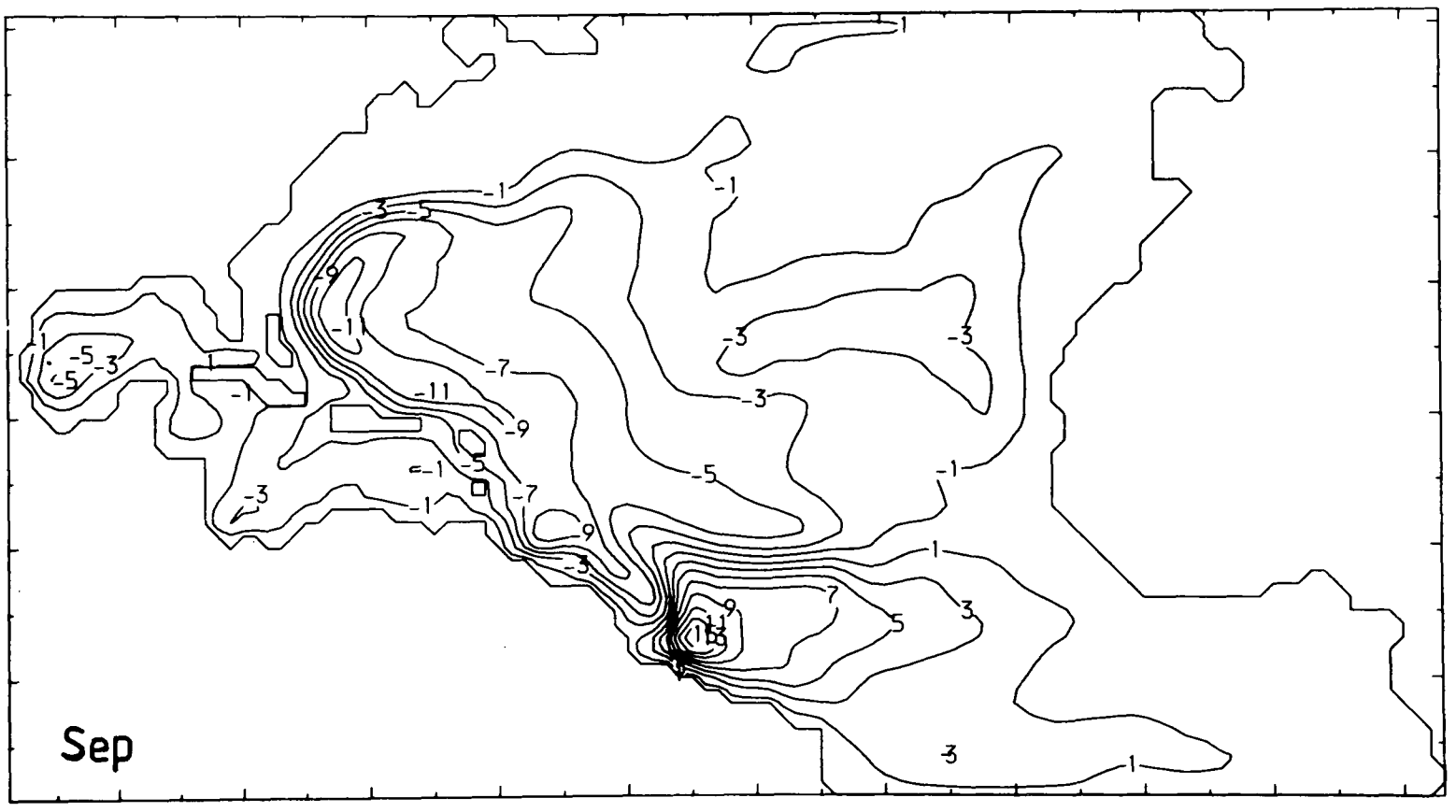
Sep

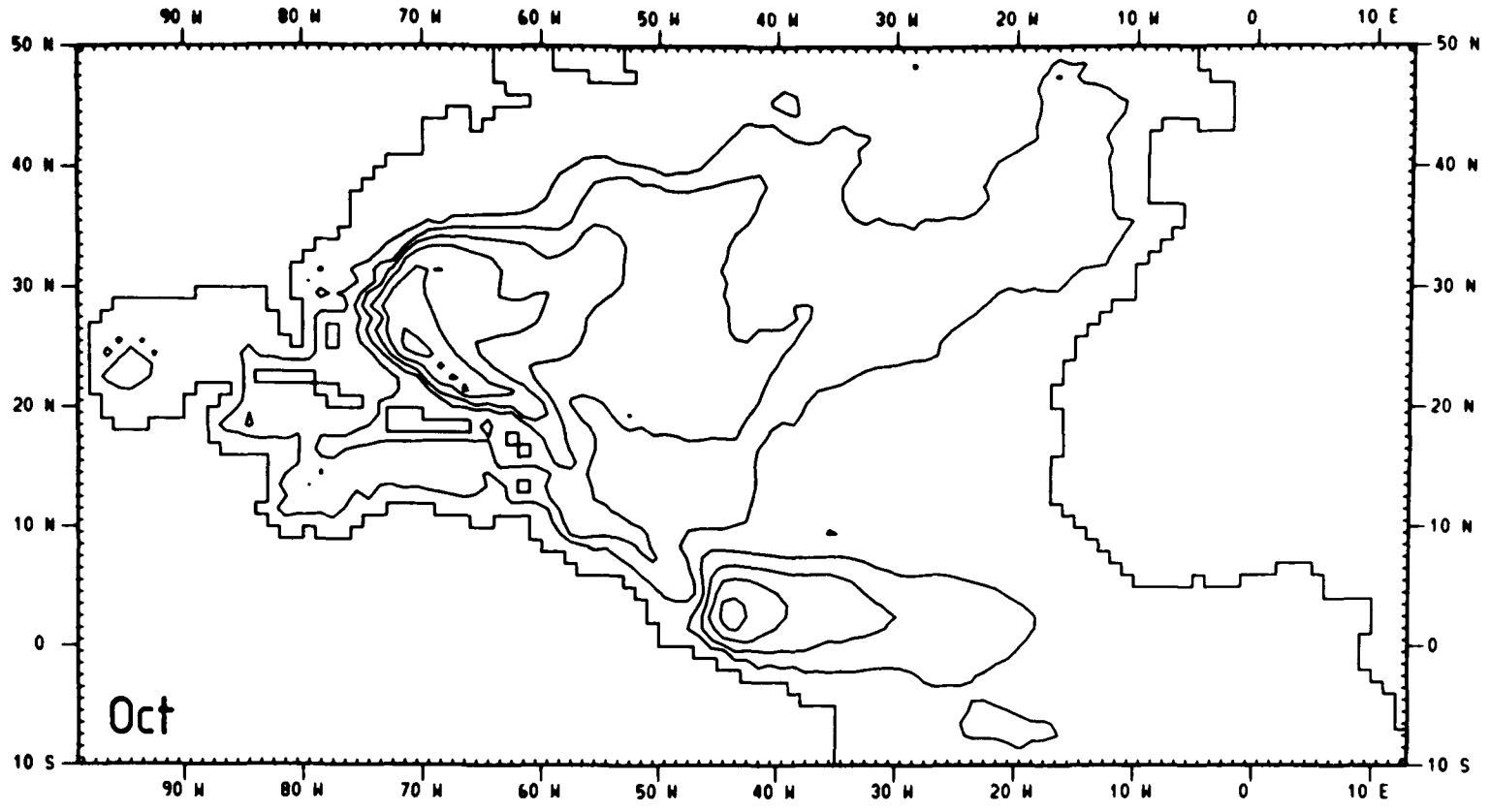
90 W
80 W
70 W
60 W
50 W
40 W
30 W
20 W
10 W
0
10 E
50 N
40 N
30 N
20 N
10 N
0
10 S
Oct

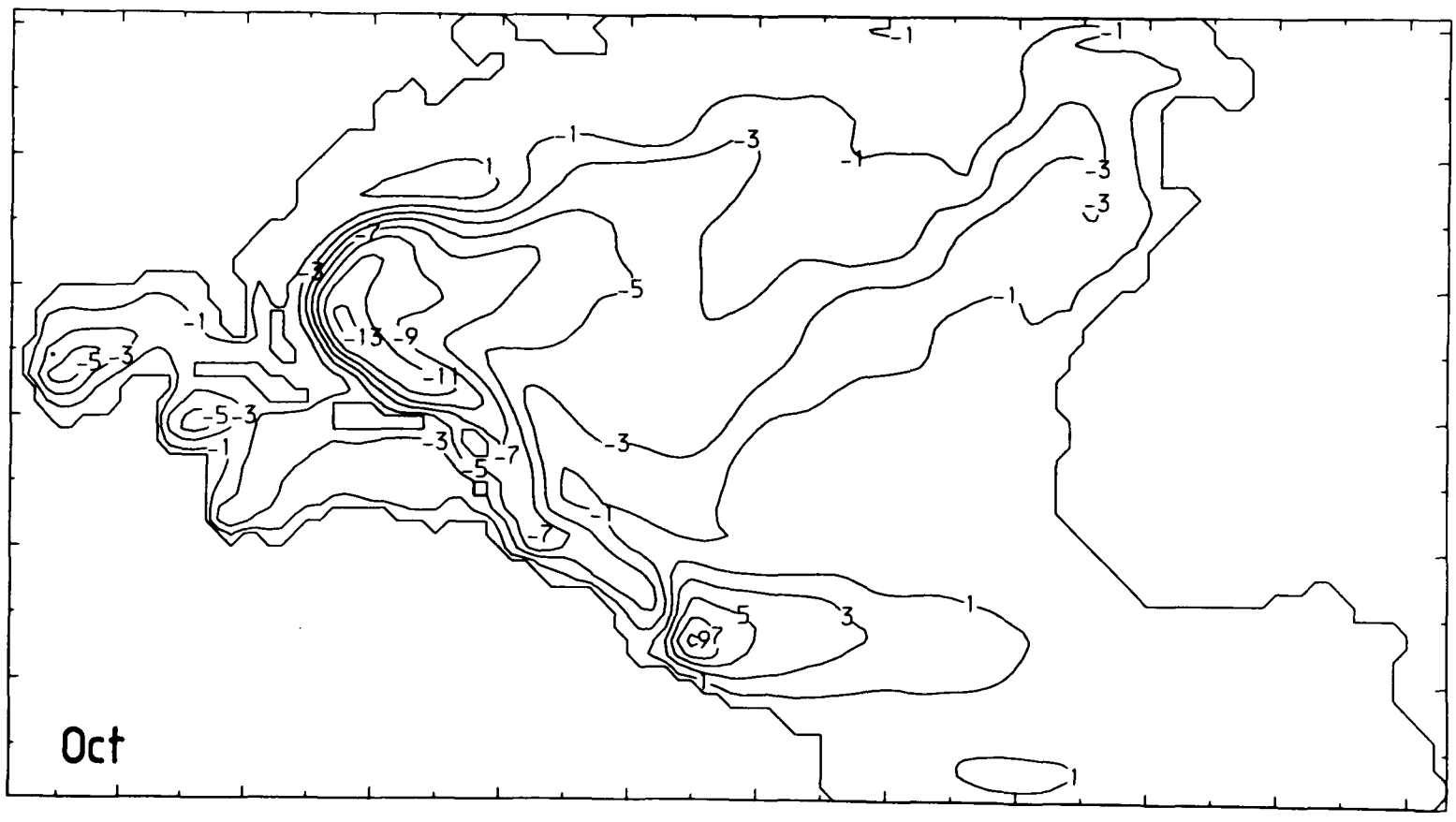
-1
-1
-1
-3
-1
-3
-3
-7
-3
-5
-1
-13
-9
-11
-5
-3
-5
-3
-1
-3
-7
-5
-7
-1
-1
5
3
1
97
1
Oct

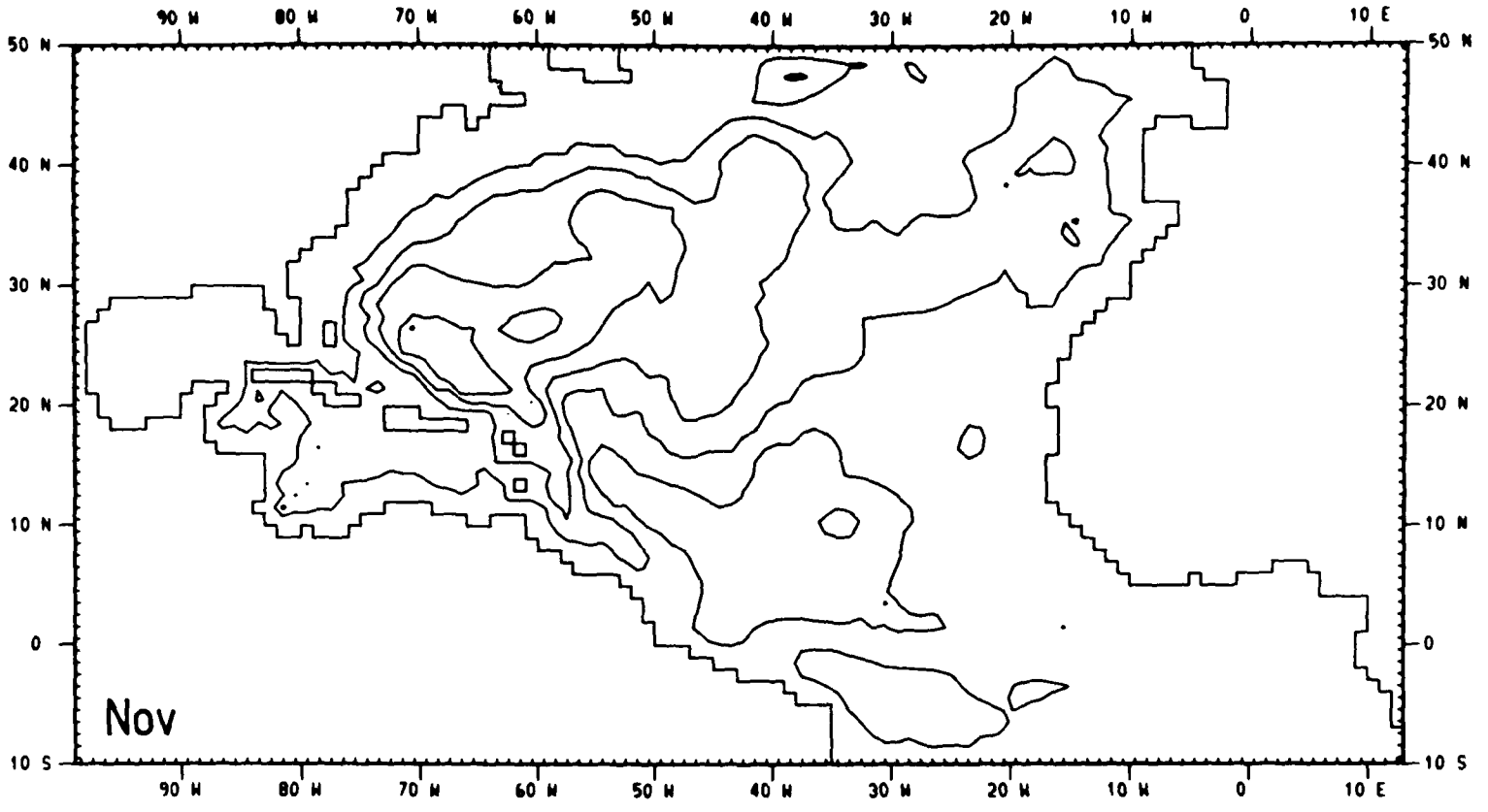
90 W
80 W
70 W
60 W
50 W
40 W
30 W
20 W
10 W
0
10 E
50 N
40 N
30 N
20 N
10 N
0
10 S
Nov

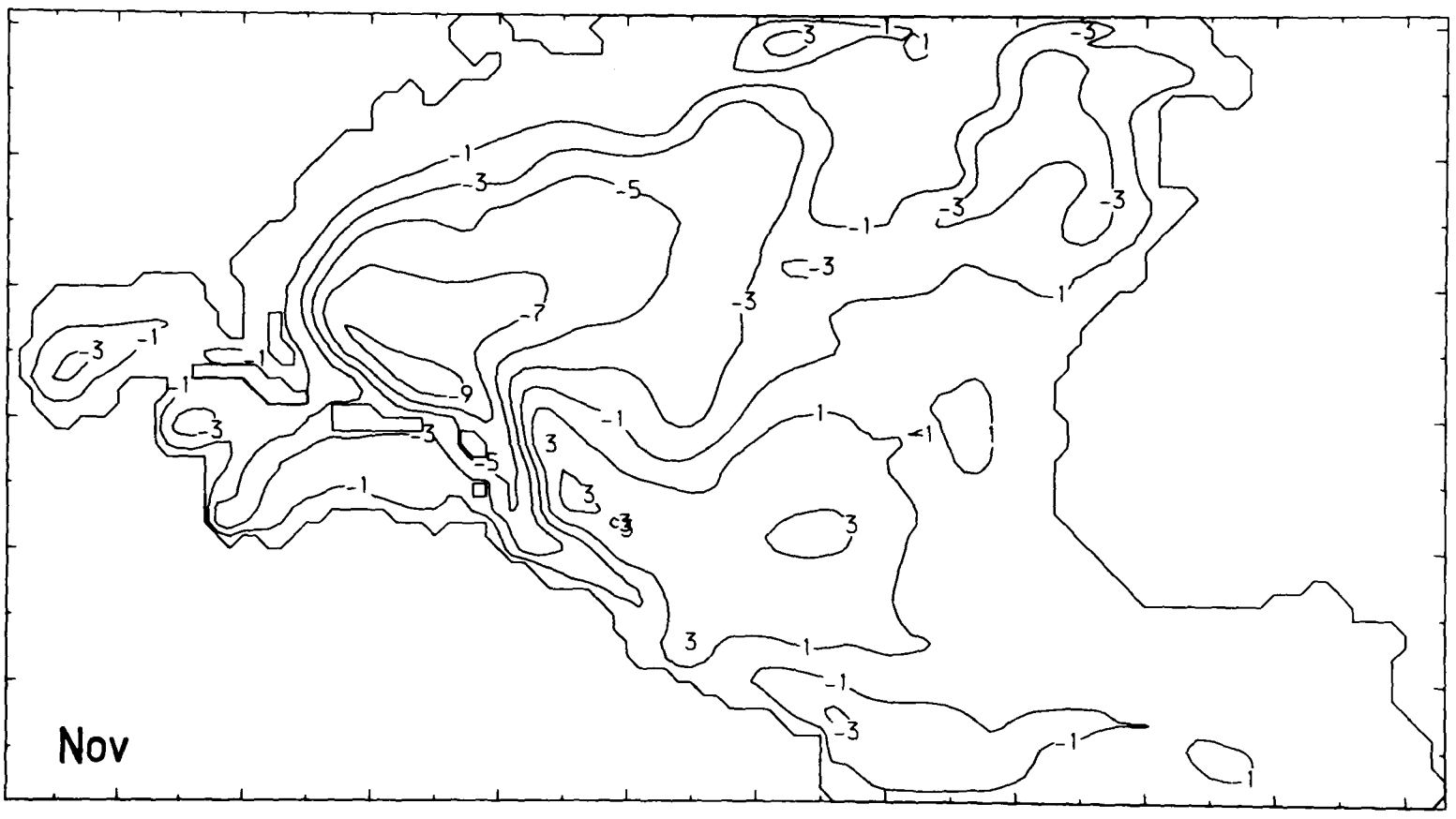
Nov

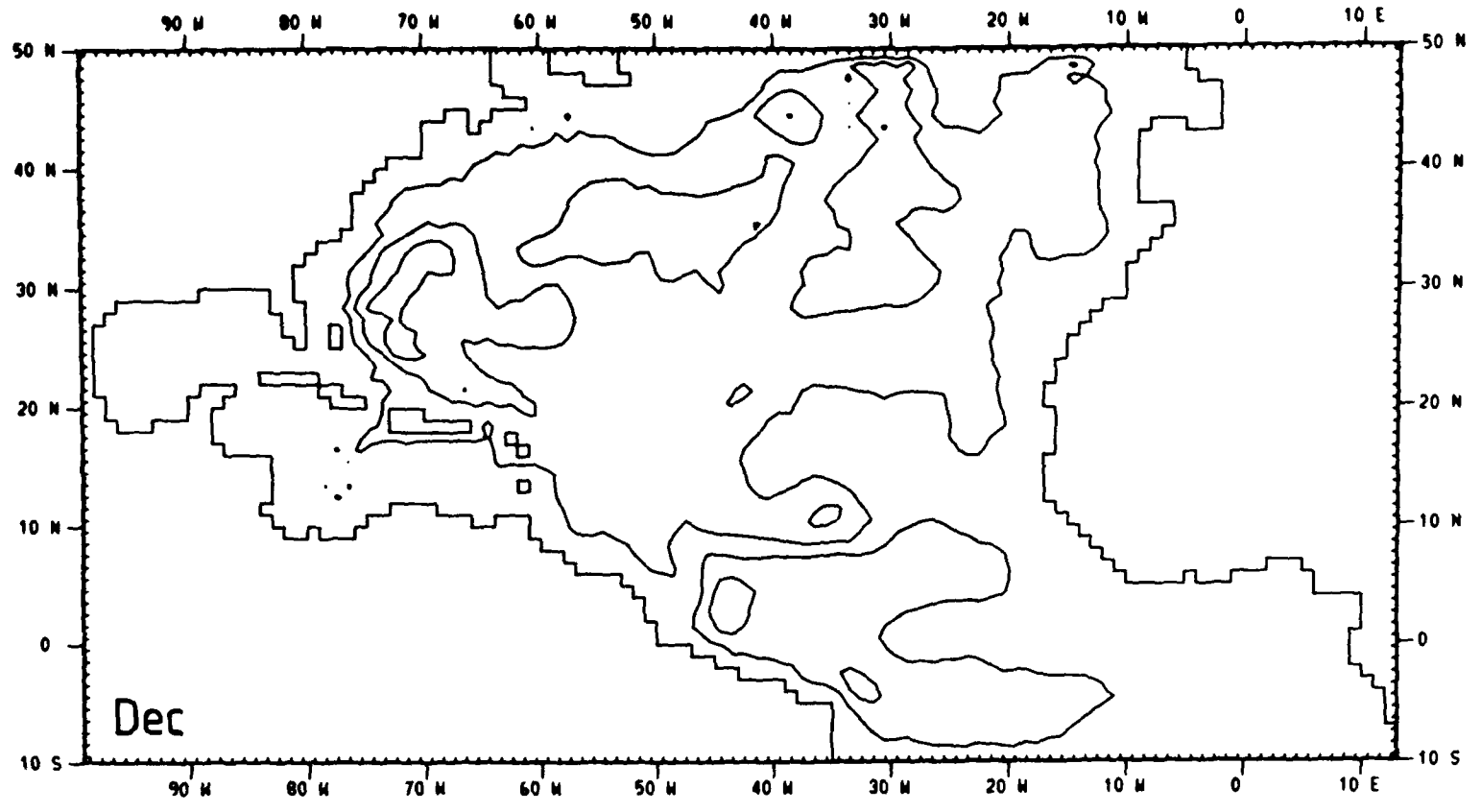
90 W
80 W
70 W
60 W
50 W
40 W
30 W
20 W
10 W
0
10 E
50 N
40 N
30 N
20 N
10 N
0
10 S
Dec

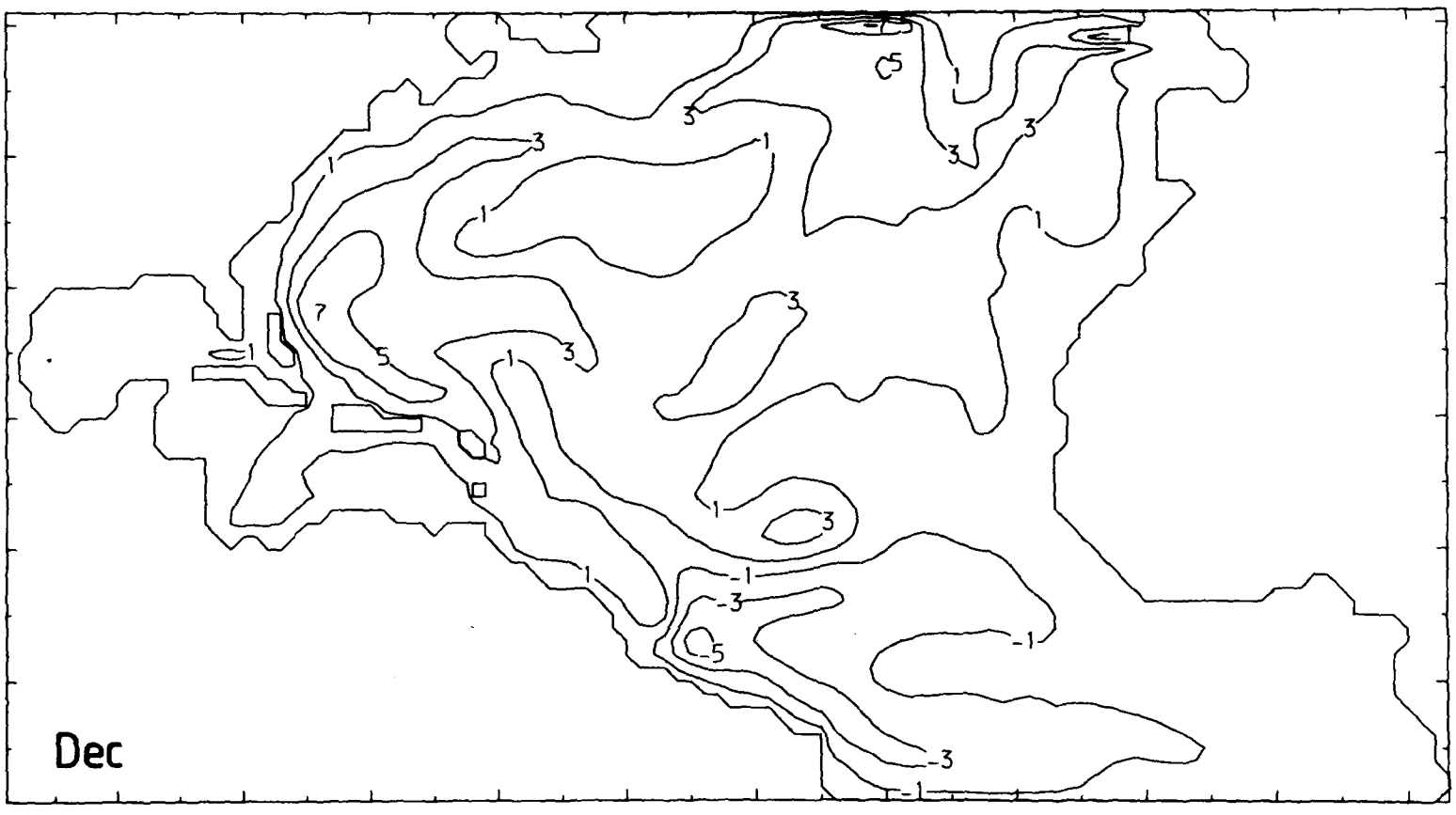
Dec

4.4: A comparison of the models

In the Antilles region and the western equatorial Atlantic (the two major regions of transport variation) the model results are very similar. This should be stressed. However, the amplitude of the variation is consistently slightly lower for the Semtner model. To find the amplitude, simply count the contours, which are two Sverdrups apart. The zero contour is not plotted; rather the 1 Sverdrup and -1 Sverdrup contours are plotted. The agreement between the models is sufficiently good that the sign of the streamfunction in the major features is the same. Thus for instance in January, the transport in the Antilles Current in the Semtner model is 11 Sverdrups, whereas it is 13 Sverdrups for the one layer model.

The fact that the Semtner model appears to have a slightly lower transport variation than the one layer model is rather surprising at first sight, since the one layer model has a small bottom friction in addition to the eddy viscosity common to both models, so away from boundaries we might expect a higher transport in the Semtner model.

The fact that the models are not in perfect equilibrium at the end of each month does not explain the consistently lower values of variation in the Semtner model for both the Antilles region and the western equatorial Atlantic, though basin modes may play some part in the discrepancy.

The discrepancy must be due to the difference in formulation of the models, i.e. the differences between a level and a layer formulation. In the layer formulation, depth can take any value, whereas in the level formulation it can take only discrete values. This is bound to have some effect, because the gradients

in depth (associated with wind stress) affect the forcing of the streamfunction (see Eq B13), and the f/H contours also determine the direction of flow.

In the Caribbean and the Gulf of Mexico the variation of the Semtner model is also lower than the variation of the one layer model, although the sign of the variation is the same. In the Caribbean we expect the no-slip boundary conditions between the islands of the Lesser Antilles to reduce the inflow of water. This is certainly the case. The deflection of streamlines towards the Windward Passage in the Caribbean which initially had an east-west orientation is also a feature reproduced by both models. This is expected because of the barotropic nature of the response (see Section 3.4).

4.5: The Florida Current

Fig 4.2 compares the model predictions of the homogeneous Semtner model and the one layer model for the Florida Current. Apart from the large drop in transport in March which is evident for the one layer model, the two models agree well, despite the no-slip boundary condition of the Semtner model, which one would expect to reduce the amplitude of the flow through the narrow Straits. Both models predict a Summer maximum (at the end of July), and a minimum at the end of October. Indeed the drop in transport between July and October is greater for the Semtner model than for the one layer model. This is in contrast to the variation in other regions, where the Semtner model has a lower amplitude. This may be partly explained by the fact that the minimum depth of the Florida Straits is 800 m for the one layer model, whereas it is 900 m for the level model. The smaller

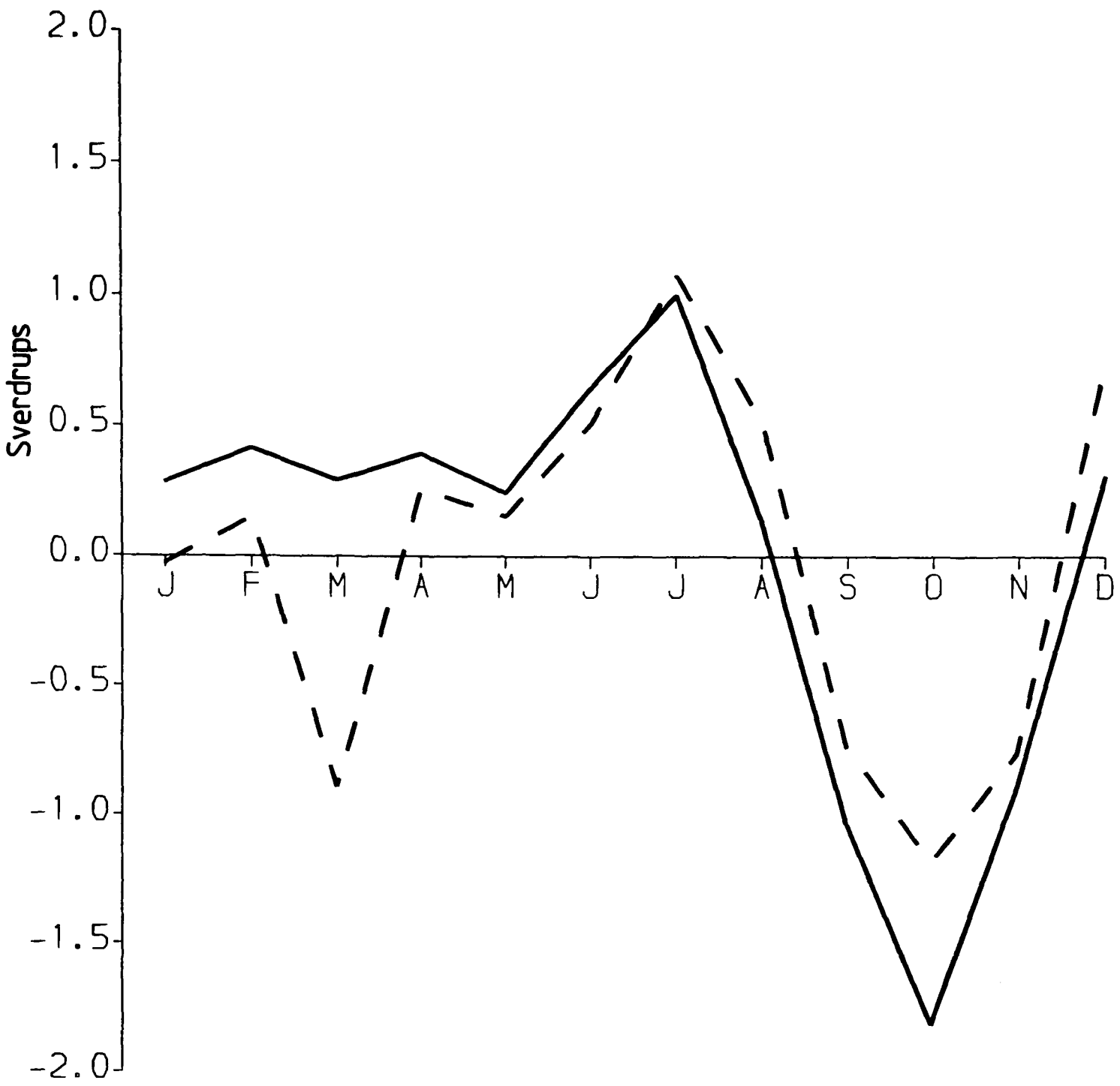

Fig 4.2 The predicted transport variation through the Florida Straits for one year of integration for the Semtner model (solid line) and the one layer model (dashed line).

minimum depth for the one layer model may make the variation smaller in amplitude than the corresponding variation of the Semtner model. However, it should be pointed out that the greatest difference between the two models is in March, not in October. In March, the magnitude of the flow through the Straits for the one layer model is actually greater than the magnitude for the Semtner model. This shows that factors other than the minimum depth of the Florida Straits are important in accounting for differences between the models in this area.

4.6: Summary and Conclusion

We have compared model results from two different homogeneous models of the North Atlantic. One of the models is the simple one layer model of Chapter 3, whereas the other model is the complex and computer-time-consuming model of Semtner [1974]. Both were forced with the seasonal winds of Chapter 3 for one year. The streamfunctions at the end of each month's integration were compared. It was found that the model results were very similar, especially in the Antilles region and the western equatorial Atlantic. This again suggests that transport variations forced by winds east of the Bahamas are blocked by the topography in the Florida Straits and pushed into the Antilles region. This is an important result, with implications for the seasonal variation of the Antilles Current.

The response in the Florida Straits of the Semtner model follows the response of the one layer model, confirming the transport maximum at the end of July and the transport minimum at the end of October. We therefore have two models, one a layer model and the other a level model, agreeing that there ought to

be a Summer maximum in the transport through the Florida Straits, in agreement with the data of Niiler and Richardson [1973]. This has been achieved using the most basic of oceans, i.e. a homogeneous ocean, but with bottom topography. It is the effect of bottom topography that reduces the amplitude of transport variations expected from Sverdrup theory to a realistic level, and changes the expected phase of the variations from a maximum in Winter to a maximum in early Summer. This change of phase is explained more fully in Chapter 3, where baroclinic effects are also included.

A consequence of the results of this Chapter is that if one is interested in the streamfunction only, then the one layer model should be used in preference to a complicated level model because of the saving in computer time. Baroclinic effects are not negligible in the annual variation, as was shown in Chapter 3, but they do appear to be smaller than the barotropic contribution. For a first order estimate of the transport variation in the Florida Straits, realistic winds should be used over the one layer model. This will be done in the next Chapter using ATOLL winds for the period 1981-1984. This will give results which can be compared with the measurements of the STACS program from 1982-1984, and with the climatological variation predicted by use of the Bunker winds.

CHAPTER FIVE

ATOLL Predictions

5.1: Introduction

In this Chapter we force the one layer model of Chapter 3 with ATOLL winds. The ATOLL wind field is analysed every twelve hours (i.e. midnight and midday), and, using a formula developed by Wu [1980], we convert the wind field to wind stress with which to force the ocean model. In common with the previous chapters, we have used monthly means of the ATOLL wind stress to force the ocean model one month at a time. The streamfunction at the end of each month's integration will be in approximate equilibrium with the forcing, and will give an idea of how the streamfunction varies through the year. It would have been possible to force the ocean one day, or indeed twelve hours at a time, but a disadvantage of this approach is that the streamfunction is never in equilibrium, thus complicating the analysis. Also, integrating day by day doubles the amount of computer time used. Sometimes, several datasets are missing in any given month, and, although a meaningful monthly average can still be taken, there would be problems with the day at a time approach.

5.2: The ATOLL winds

The ATOLL (Analysis of the Tropical Oceanic Lower Layer) winds are described by Wise and Simpson [1971]. They are produced by the National Hurricane Centre in Miami, Florida. A

brief description of the data, taken from Wise and Simpson [1971], follows.

> The ATOLL chart is a depiction of boundary layer wind flow. A melange of wind data is analysed to obtain streamlines and isotachs of the ATOLL wind field. The following types of data are incorporated into the analysis: surface winds from ships at sea, 2000-foot PIBAL (pilot balloon) and rawinsonde winds, flight level winds from weather reconnaissance aircraft flying at levels below 5000 feet, satellite winds obtained from cloud displacement in movie loops, and low-level cloud directions reported by land stations.
>
> In the past, analysis of the wind field has been accomplished by manually drawing streamlines and isotachs. However, an objective analysis program has been developed which automates the windfield analysis. In this program, scalar values of the U (west) and V (south) components of the wind are analysed independently and then combined to give an analysis of the resultant vector wind field. The program uses a series of data scans to modify 'guess' values at grid locations over the chart area. Grid points are uniformly spaced at approximately 90 nautical mile intervals. When this program is used operationally, the first guess field will consist of twelve-hour prognostic values north of 35°N and a combination of values from the previous analysis and climatology south of 25°N. Values from both of these fields will be meshed in the band between 25°N and 35°N.
>
> In each data scan all wind reports within a specified elliptical area centred on each grid point are examined. The reported value at each data point is compared with the

value for that location obtained by interpolation from the 'guess' field. The difference for each data point within the ellipse is multiplied by an elliptical weighting factor and the products are averaged to compute a 'correction' to the 'guess' value at the central grid point. When all 'guess' values in the grid have been thus 'corrected', the next scan is commenced, using a smaller elliptical area. The first scan uses 1260-mile by 2520-mile ellipses. The fourth and final scan uses 360-mile by 720-mile ellipses. The major axis of the ellipses are oriented along the 'guess' wind direction at the central grid point, so that data in the upstream and downstream areas are given more weight than those on either side. When final U and V values have been assigned to each grid point in this analysis, they are used to compute the resultant vector wind speed at each point.

The data that was used in this application covered the area between 123.5°W and 5°W from the equator to 45.4°N. The latitudinal spacing was 1.5 degrees at the equator, and varied approximately as the cosine of latitude. The longitudinal spacing was a constant 1.5 degrees. The model, however, covers the area between 99°W and 13°E from 10°S to 50°N, so the model ocean is not entirely covered by ATOLL winds. The most important area of wind stress missed out is probably the part of area A (see Fig 3.8) between 45°N and 50°N. Winds to the south of the equator or to the east of the Mid-Atlantic ridge are of relatively little relevance to the variation of the Florida Current (see Section 3.3.3)

The grid spacing in the model is one degree, so the wind stress is calculated on the ATOLL grid, and then linearly interpolated onto the model grid. The wind stress is calculated

using the following formula from Wu [1980]:

$$\underline{\tau} = \rho C_D |U| \underline{U}$$

$$C_D = (0.8 + 0.065 |U|) \times 10^{-3}$$

where the wind stress is in units of N/m^2 and the wind speed is in m/s.

The monthly mean ATOLL wind stress does not cover the entire model ocean, so it is treated in the same way as the wind forcing over areas A and B was treated in Section 3.3.3. There, $curl_z(\underline{\tau}/H)$ was split up into areas rather than $\underline{\tau}$. This avoids spurious curl forcing at the edges of the areas. In the same way, spurious effects are avoided at the edge of the ATOLL forcing.

5.3: The predicted variation of the Florida Current from 1981 to 1984

Figs 5.1 show the predicted variation of the transport through the Florida Straits at the end of each month for the years 1981-1984 when the homogeneous model is forced by the ATOLL winds. It should be noted that the mean wind stress is still present in these calculations. If the mean transport were to be properly included, we would need a baroclinic model which was run for several decades. The mean transport would be entirely in the upper layer and instead of a contribution of a couple of Sverdrups, which is present in the homogeneous model, there would be a contribution of about thirty Sverdrups through the Florida Straits. This compensation of the effect of topography by baroclinic Rossby waves would also be a factor at periods longer

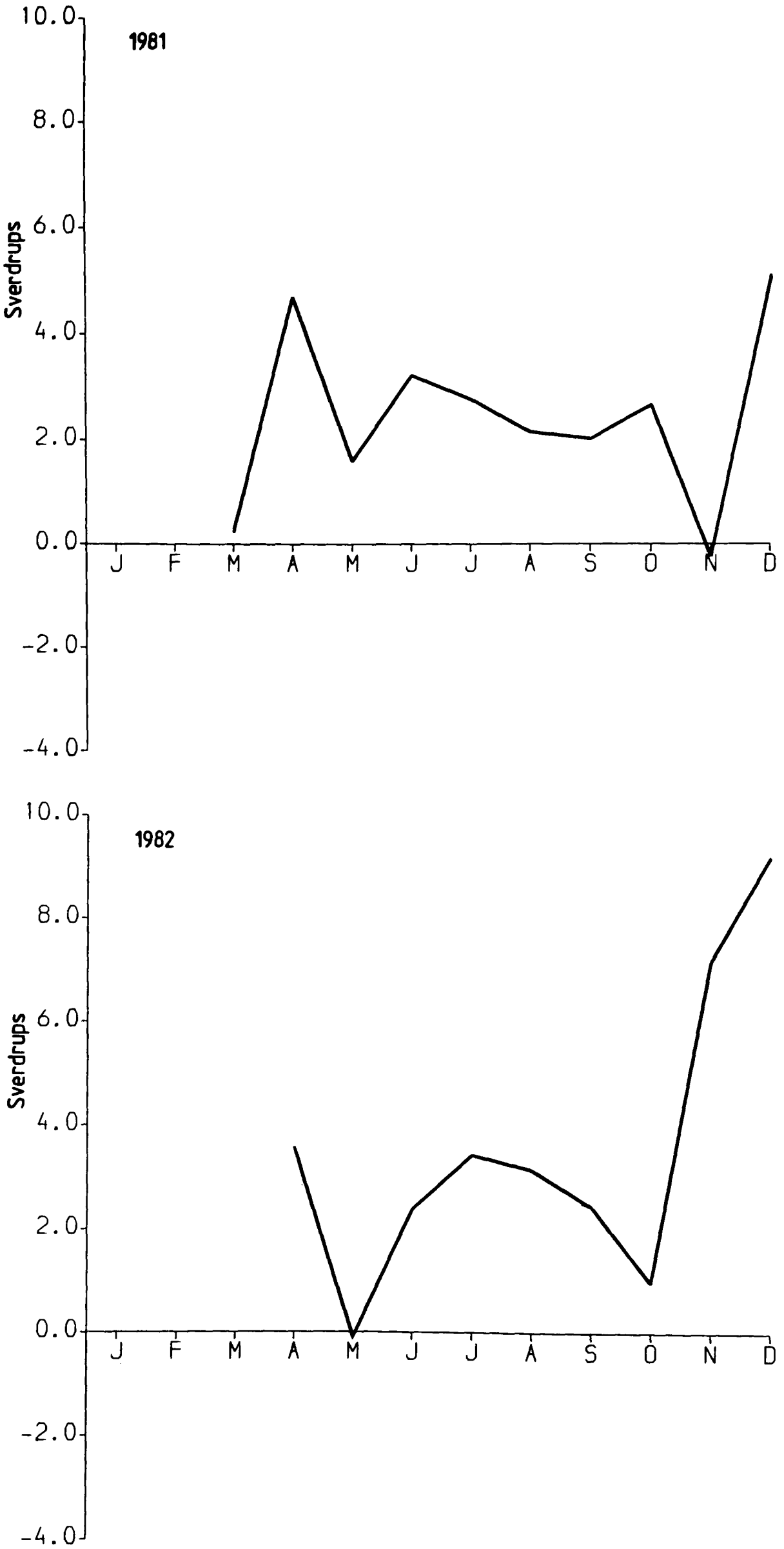

Fig 5.1 The transport through the Florida Straits when the one layer model is forced by ATOLL winds for the years 1981 to 1984. The transport values are at the end of each month's integration.

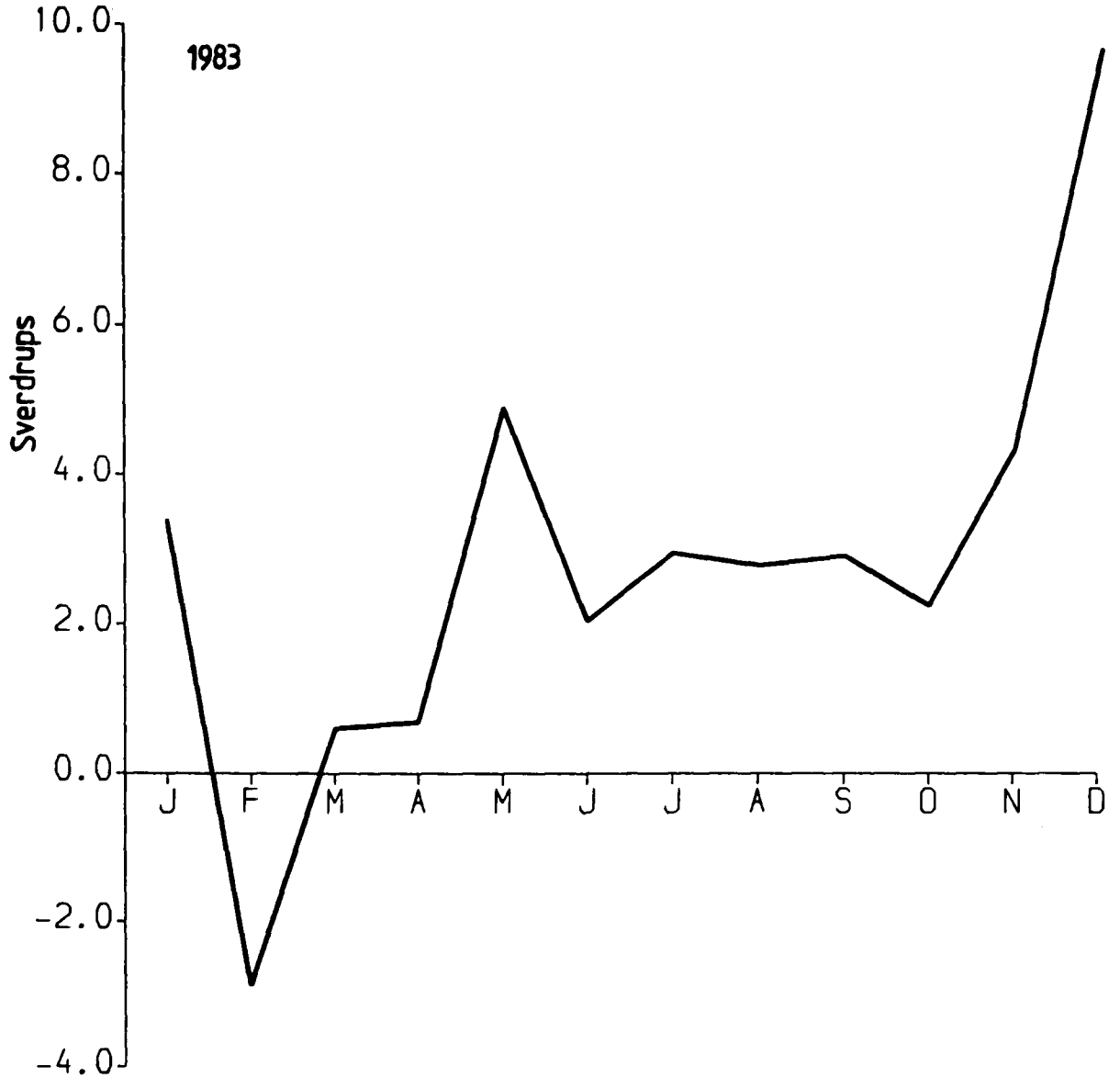
1983
Sverdrups
10.0
8.0
6.0
4.0
2.0
0.0
-2.0
-4.0
J
F
M
A
M
J
J
A
S
O
N
D

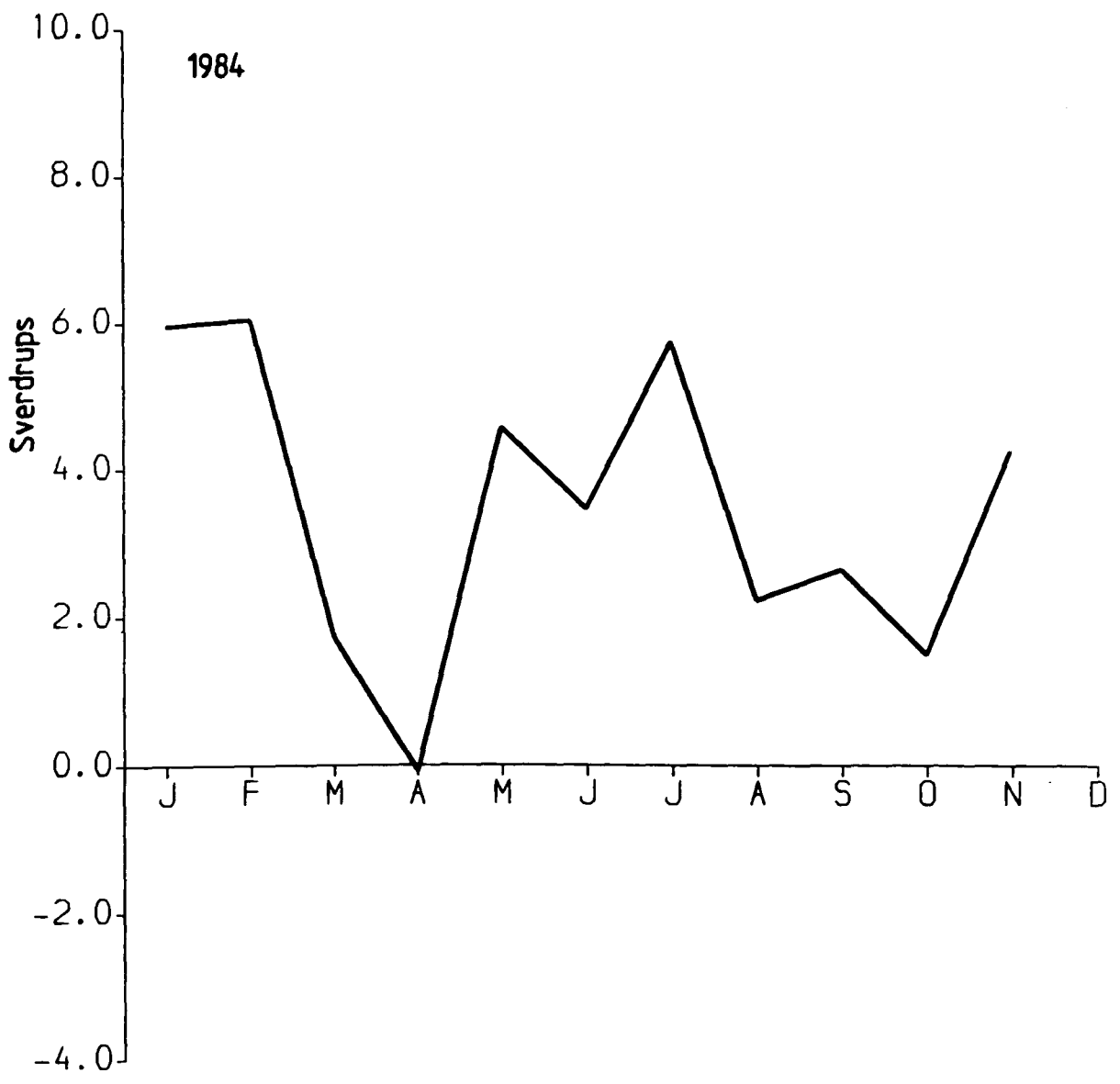
1984
Sverdrups
10.0
8.0
6.0
4.0
2.0
0.0
-2.0
-4.0
J
F
M
A
M
J
J
A
S
O
N
D

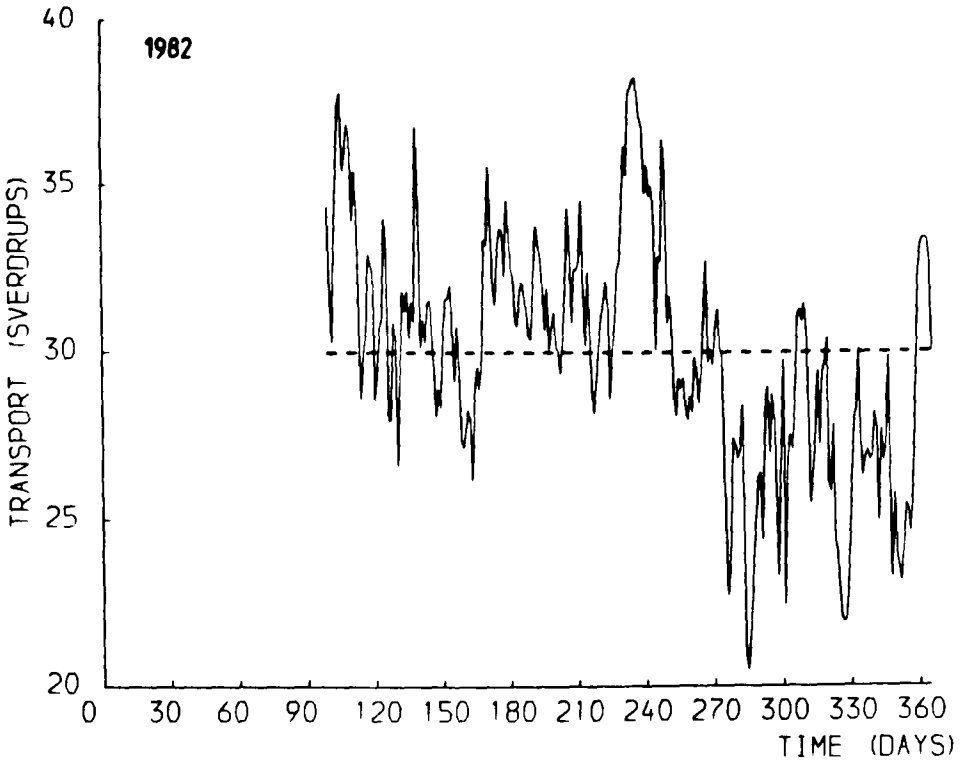

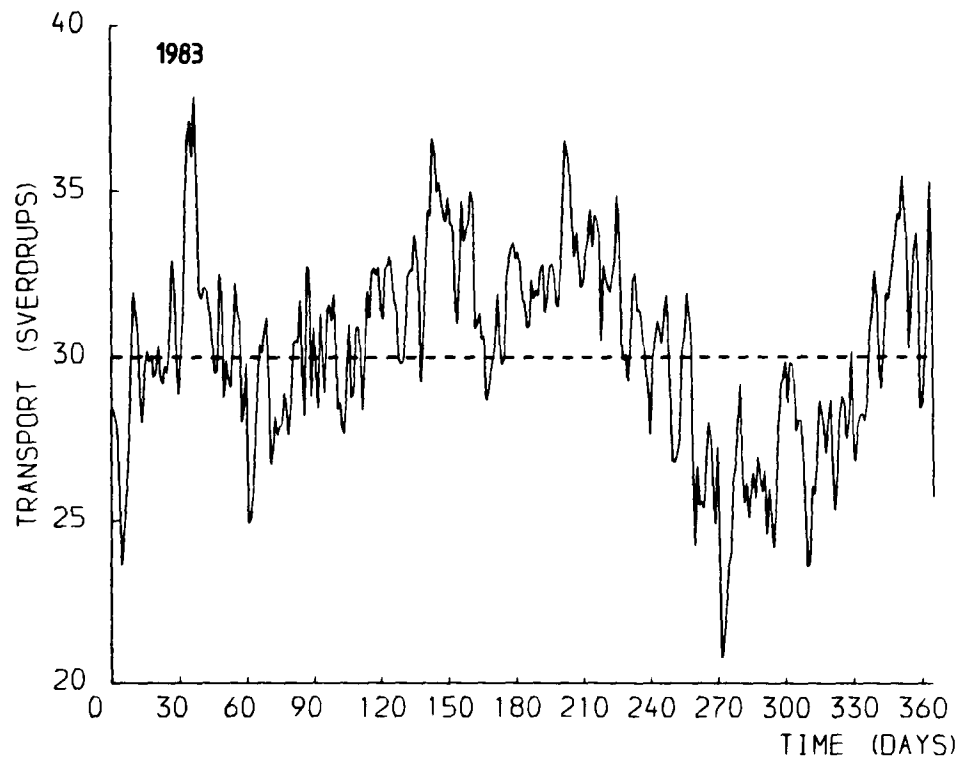

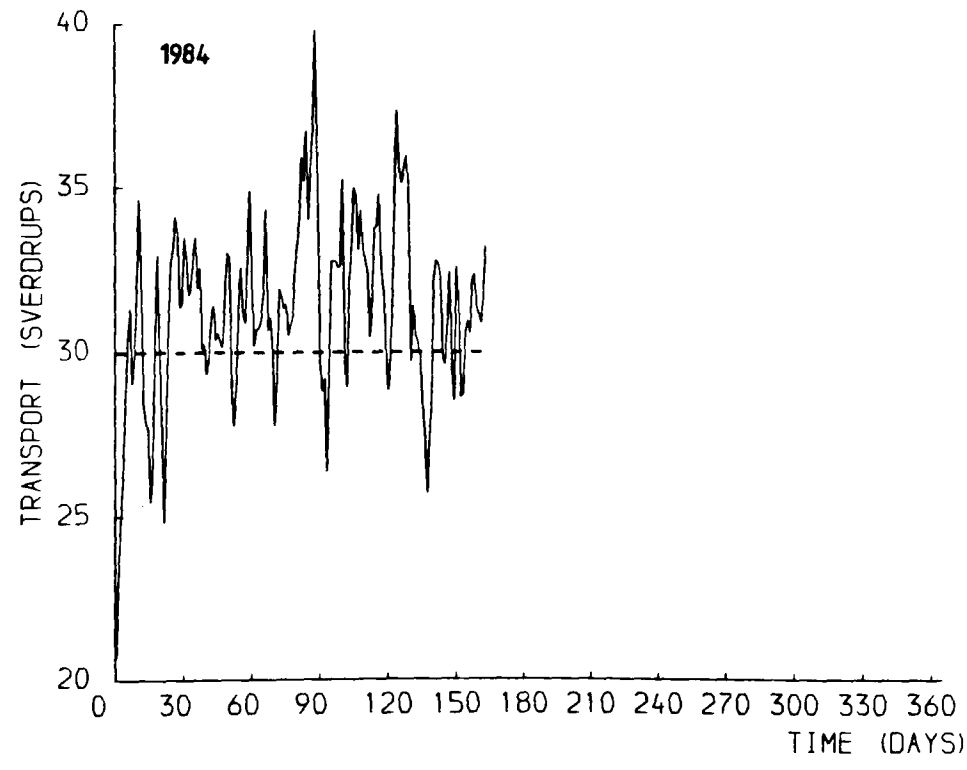

Fig 5.2 The STACS transport time series. The data represents moored current meter transports, except during the winter of 1982/1983 when cable transports are used.

than a few years. The mean wind stress (averaged over several decades), interannual variability and monthly variations of wind stress are all included in the monthly means of ATOLL wind stress. The response to each component of wind stress forcing is more or less baroclinic depending on the period of the component (see Section 2.2), and will therefore be represented well by a homogeneous ocean to a greater or lesser extent. The monthly variations should be represented well by the homogeneous ocean, and we shall look at these, ignoring the mean transport and the interannual variations.

We observe immediately from Figs 5.1 two important results of this investigation. Firstly, the variation is of much larger amplitude than the variation of Fig 3.5(c) (the 'Bunker' variation), and secondly not one of the years 1981-1984 is predicted to have an overall Summer maximum.

The larger amplitude of the ATOLL variations compared to the Bunker variation can be explained by the averaging of several years of monthly data for the Bunker datasets. The averaging process may give some meaning to an 'average' year, but the variations of wind stress within this average year may be of lower amplitude than would be the case in any one year of data.

We come now to the question of the Summer maximum. In two of the years, i.e. 1982 and 1984, there are signs of the Bunker variation, with a subsidiary maximum at the end of July and a subsidiary minimum at the end of October. In both of these years, however, the overall maximum is in the Winter. In 1981, 1982 and 1983 the overall maximum is at the end of December, and in 1981 and 1983 there is no sign of a Summer maximum, subsidiary or not. The concept of an annual cycle that is repeated year after year is therefore not supported by these results. The most repeated feature of the four years is a Winter maximum, in

contradiction with the results of Niiler and Richardson [1973], which show a Summer maximum.

The data of Niiler and Richardson [1973] span the years 1964-1971, and are not necessarily comparable with the years 1981-1984. However, the measurements of the STACS program provide a time series of transport through the Florida Straits which is directly comparable with the model predictions of this Chapter. This transport time series is reproduced on Fig 5.2, and covers the period April 1982 to May 1984. This figure includes recent data which has not been published, and represents an amalgamation of current meter and cable transports. Further details about the measurement of the time series can be found in Chapter One.

The transport time series starts with a drop between April and May 1982, which appears to be reproduced by the model. The data then show a large rise towards a peak near the end of August, whereas the model shows a smaller rise to a peak near the end of July. The data then exhibit a large drop between August and October of greater than ten Sverdrups. The model results also show a much smaller drop between the end of July and the end of October. During November and December the data exhibit several minima, with the transport generally remaining below the mean of thirty Sverdrups. However, the model predicts a pronounced rise in transport to the end of December, more pronounced than the predicted drop between the end of July and the end of October. This must rate as a major disagreement with reality. The data definitely exhibit a Summer maximum and a Fall minimum during 1982, whereas the model, forced by the ATOLL winds, predicts a maximum at the end of December, with a minimum at the end of May. The rise towards the end of December is not just a quirk of that month, but is present in the November

prediction as well.

During 1983 the data again show a Fall minimum, which is not reproduced in the slightest by the ATOLL prediction, and broad May and July maxima. There is a narrow peak at the beginning of February which would not show up as an overall maximum if a monthly running mean were applied to the data. For this year the data do show a rise in transport in December, but it does not lead to an overall maximum, as in the ATOLL prediction.

During 1984 the ATOLL prediction is of a maximum in January and February, followed by a pronounced fall in transport to the end of April. This is not reproduced at all by the STACS data.

The STACS data so far appear to support the measurements of Niiler and Richardson [1973] in that Summer maxima have been measured. The data for 1982 and 1983 also show a minimum in transport during the Fall, preceded by a pronounced drop in transport from the Summer maximum. These features are reproduced by the Bunker variation of Fig 3.5(a), albeit at much reduced amplitude. The Bunker variation is meant to represent a 'typical' year. Although the ATOLL predictions do not support the concept of a repeated annual cycle, the STACS measurements and the Niiler and Richardson data to a large extent do. The main features of the measured annual cycle (the Summer maximum followed by a pronounced drop to a Fall minimum) are those of the Bunker variation. From a comparison of model results and measurements, there is a case for believing that the Bunker winds represent a typical annual cycle, and that the variation of Florida Current transport predicted from these winds also represents a typical year. This is not the case for the ATOLL winds, and the next Section investigates possible reasons for this discrepancy.

5.4: Model results

5.4.1 The relative importance of the zonal and meridional components of the ATOLL wind stress.

In Section 3.3.3 it was shown that the meridional component of the Bunker wind stress was the cause of the overall Summer maximum (see Fig 3.7(b)), though the zonal component produced a variation of about equal magnitude. Here, we investigate the relative importance of these components for the ATOLL winds.

Figs 5.3 show the contribution due to the zonal component of wind stress during the years 1981-1984, and Figs 5.4 show the corresponding variation due to the meridional component. Together, the curves add up to Figs 5.1. We see that the zonal component gives a variation that is sometimes more than three times the variation due to the meridional component. A major difference, then, between the ATOLL and Bunker wind stresses is the reduced importance of the meridional wind stress. This could be crucial to the prediction of a Summer maximum because of the importance of the meridional wind stress for the Bunker variation. If we double the amplitude of the predicted variation due to the zonal component of the Bunker wind stress (see Fig 3.7(a)), then we would undoubtedly obtain a Winter maximum. Since the phase of the variation in Figs 5.3 roughly follows that of Fig 3.7(a) (with large transports at the beginning and the end of each year), and Figs 5.4 do not always even show a Summer maximum, we expect and obtain Winter maxima.

It is concluded that the meridional wind stress, which plays a crucial part in the Bunker Summer maximum, is of much reduced importance in the ATOLL predictions. This could account for the

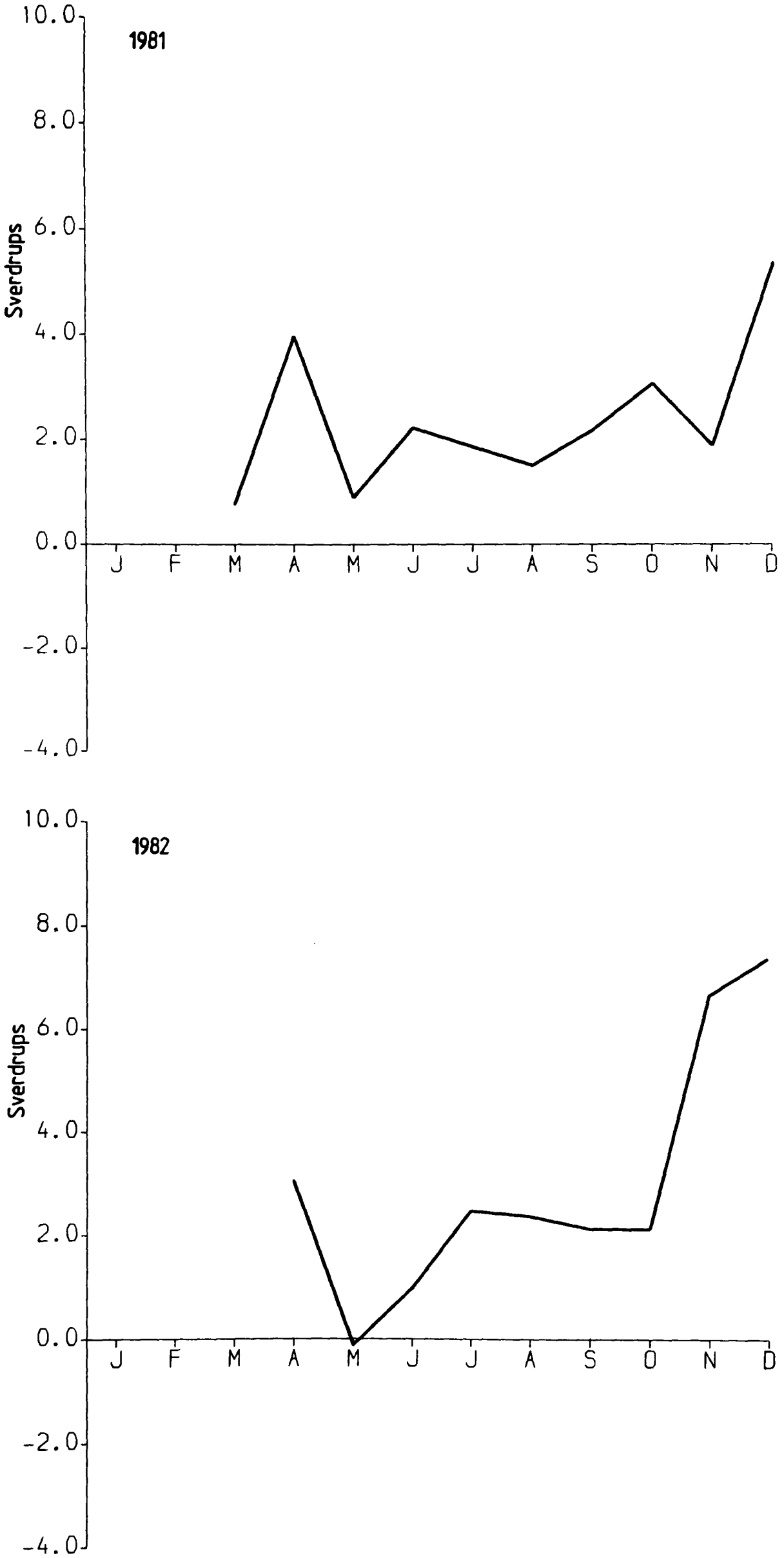

Fig 5.3 The transport through the Florida Straits when the one layer model is forced by the zonal component of the ATOLL winds for the years 1981-1984.

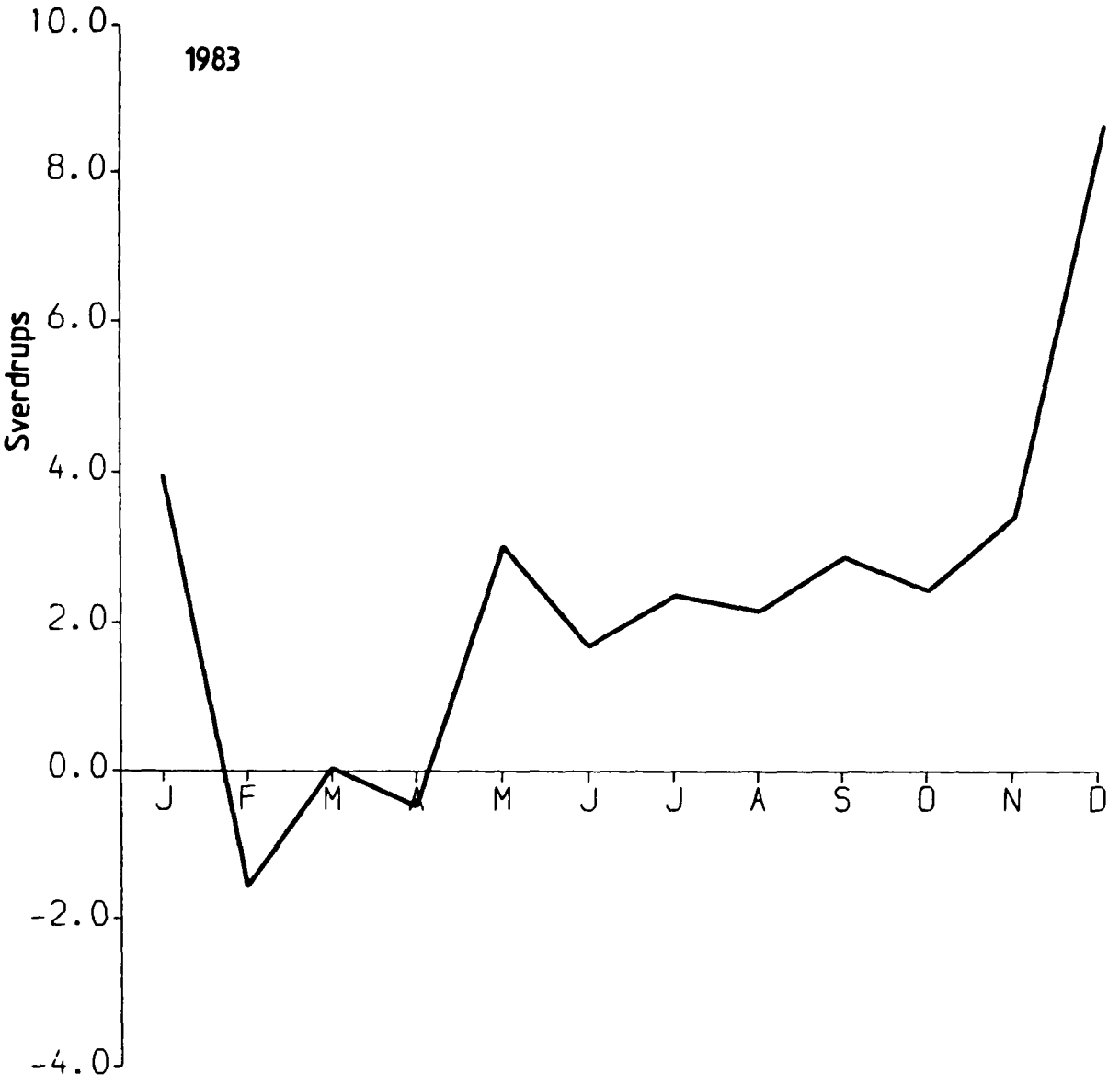
1983
Sverdrups
10.0
8.0
6.0
4.0
2.0
0.0
-2.0
-4.0
J
F
M
A
M
J
J
A
S
O
N
D

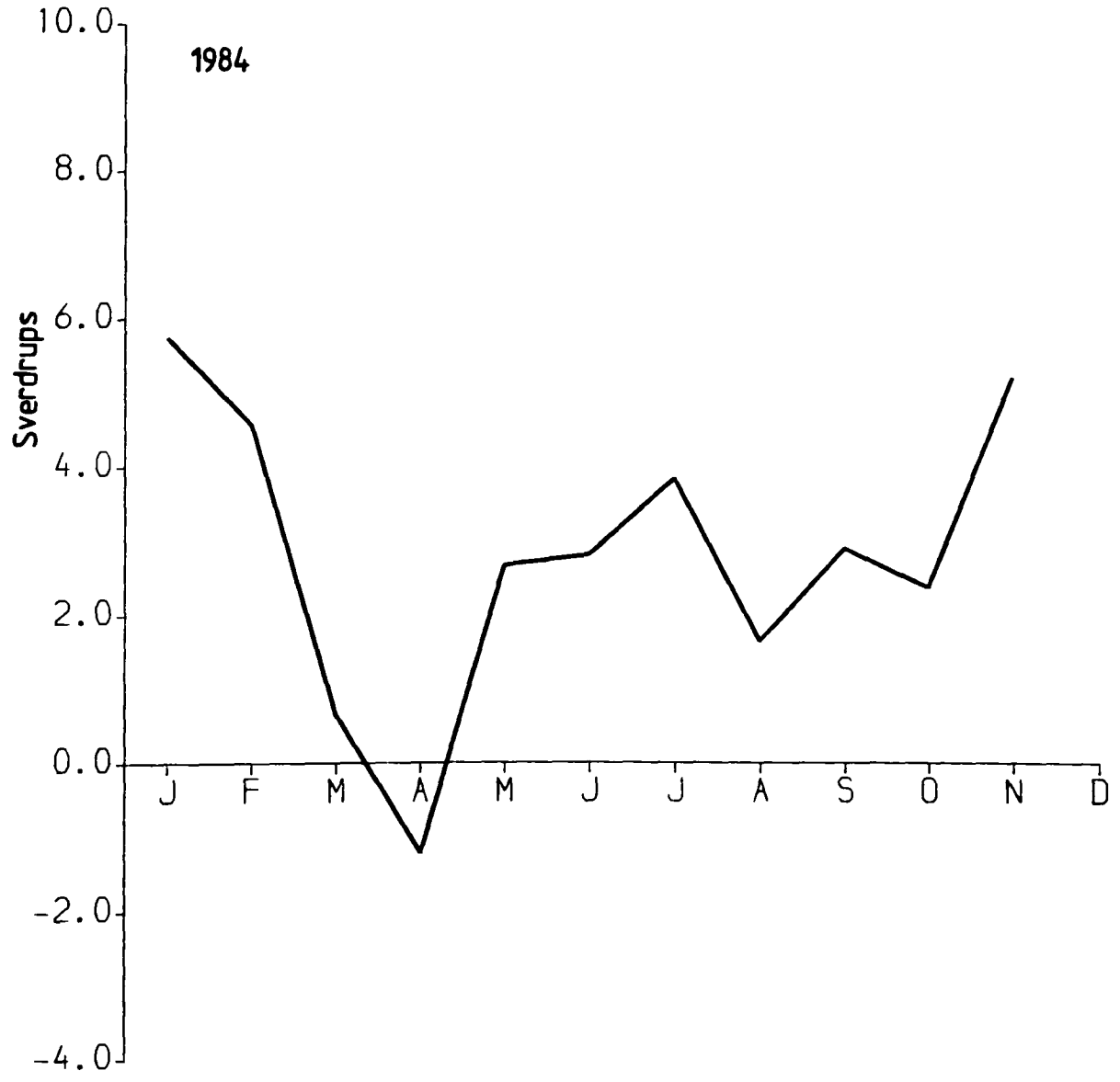
1984
Sverdrups
10.0
8.0
6.0
4.0
2.0
0.0
-2.0
-4.0
J
F
M
A
M
J
J
A
S
O
N
D

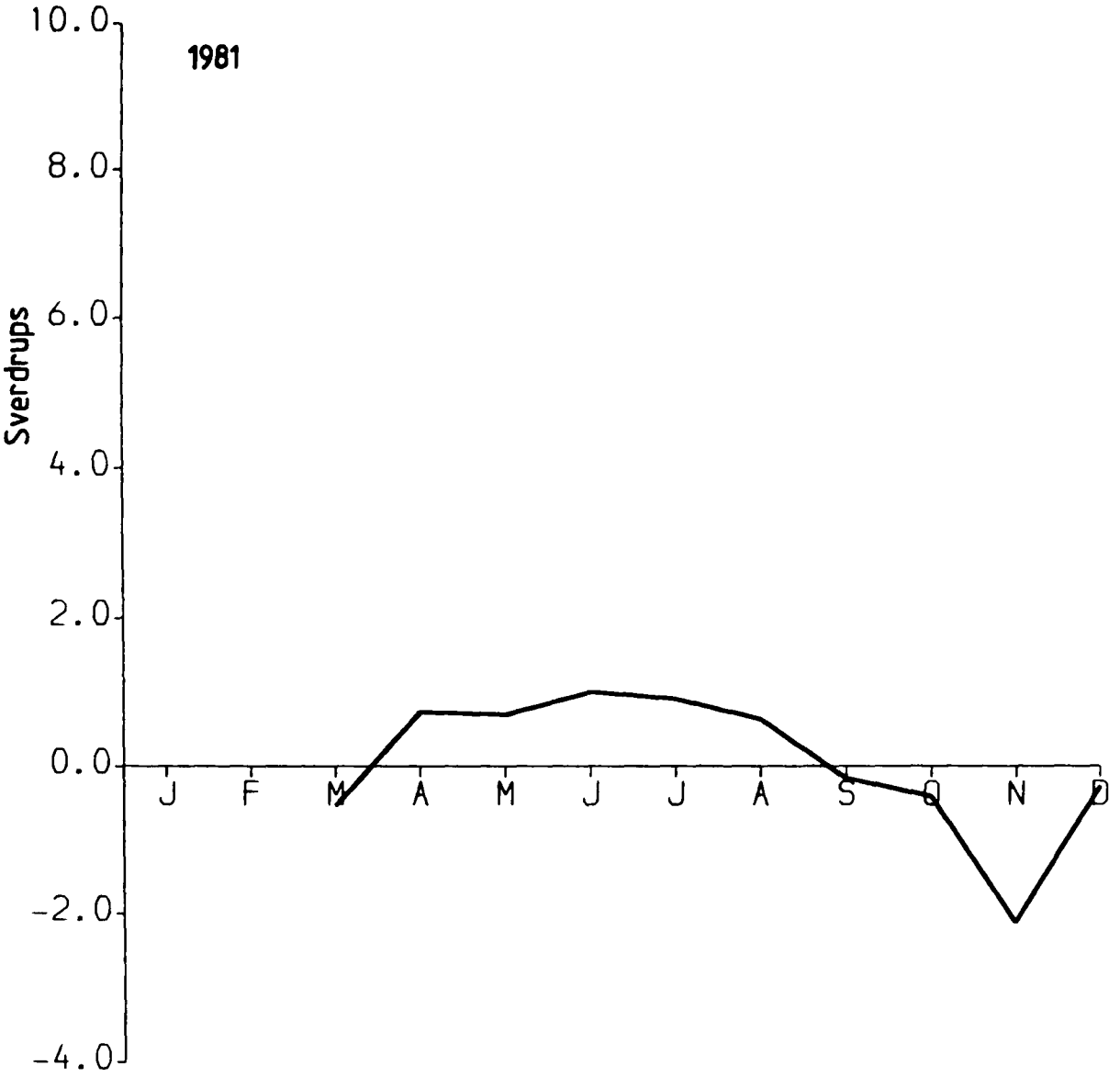

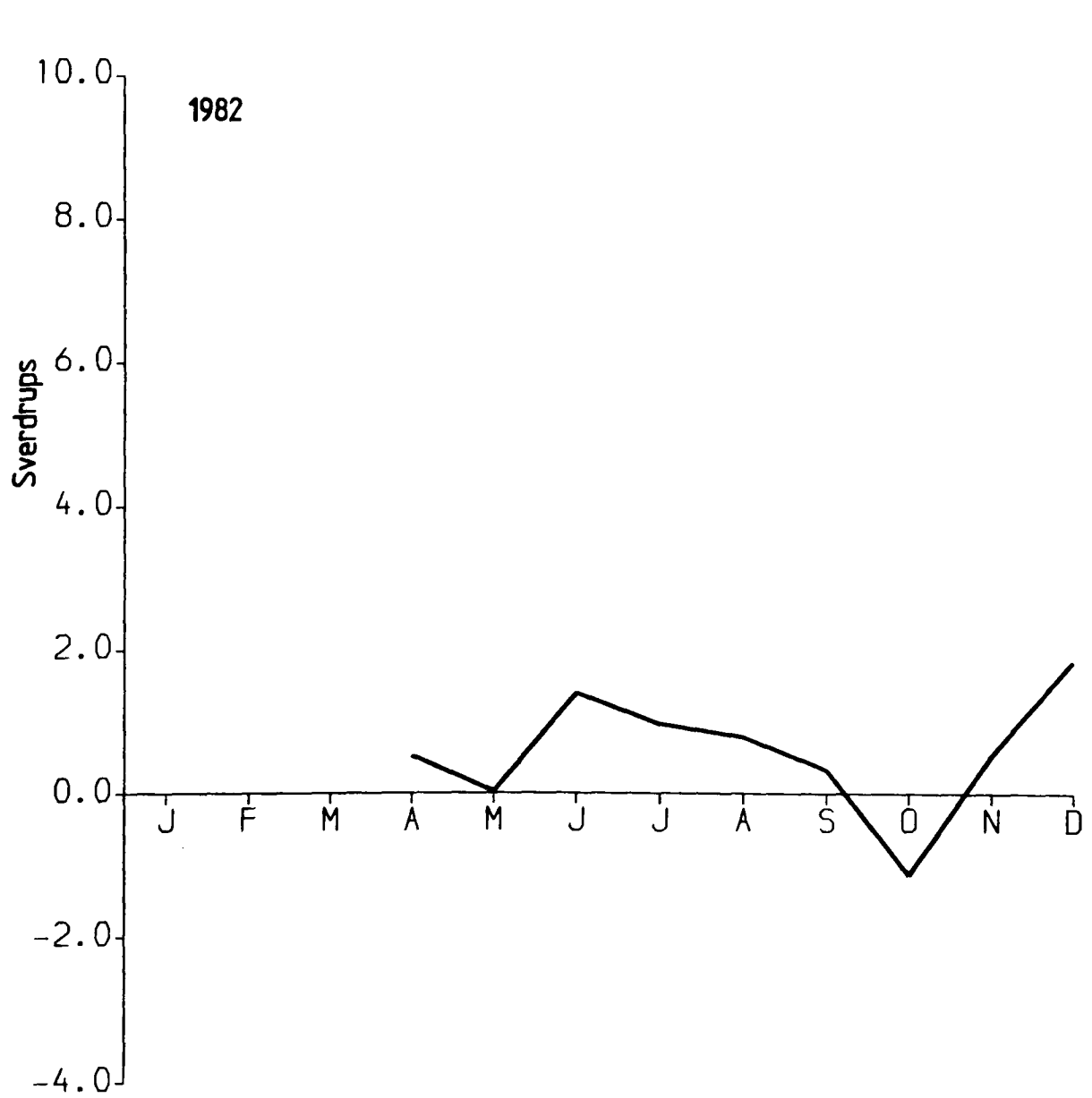

Fig 5.4 The transport through the Florida Straits when the one layer model is forced by the meridional component of the ATOLL winds for the years 1981-1984.

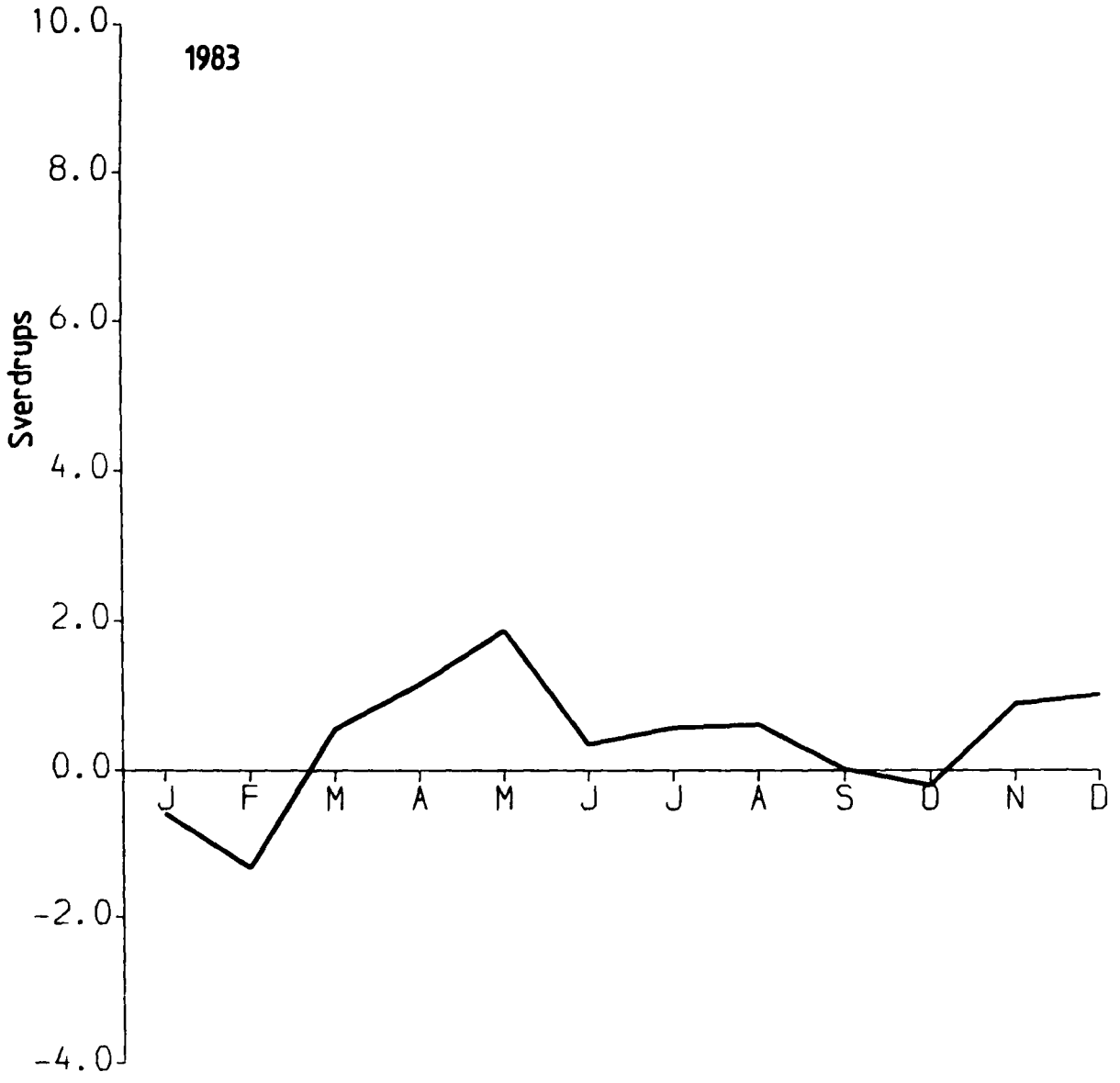
1983
Sverdrups
10.0
8.0
6.0
4.0
2.0
0.0
-2.0
-4.0
J
F
M
A
M
J
J
A
S
O
N
D

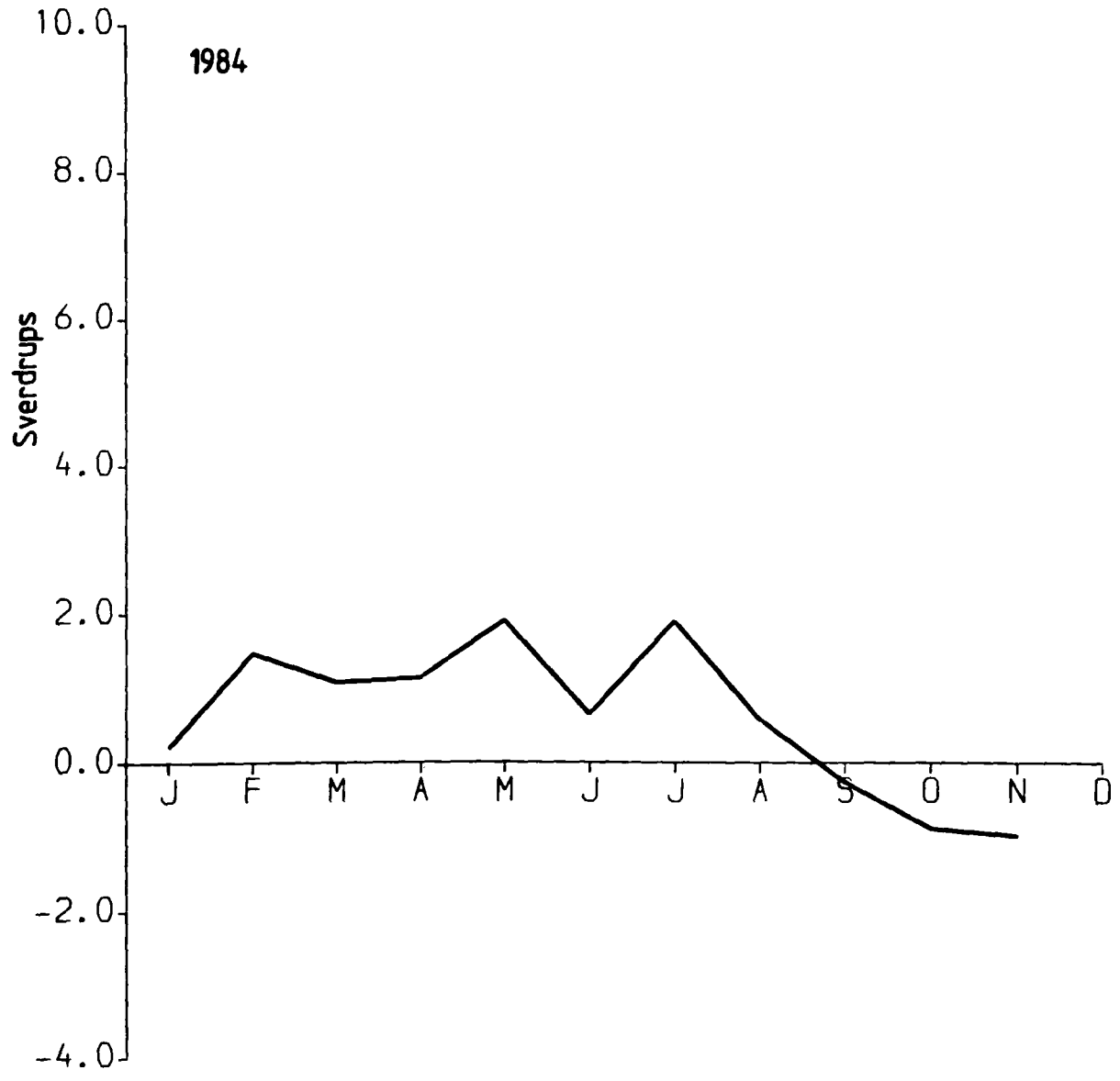
1984
Sverdrups
10.0
8.0
6.0
4.0
2.0
0.0
-2.0
-4.0
J
F
M
A
M
J
J
A
S
O
N
D

lack of a predicted Summer maximum.

5.4.2 The relative importance of wind stress curl forcing and forcing associated with gradients in bottom topography.

In Section 3.3.3 we forced areas A and B (see Fig 3.8) with the Bunker wind stresses to find the relative importance of each area for the Florida Straits transport variation. It was found that area A, to the west of the Mid-Atlantic ridge and to the north of the Florida Straits, contributed a larger proportion of the transport variation than any comparable area. The forcing in this area was then split up into two parts, one depending on the curl of the wind stress, and the other on gradients in bottom topography. It was found that, though the signal from each part was strong in the Winter, the Winter contributions roughly cancelled, giving an overall Summer maximum. The two contributions were comparable in magnitude. Here, we look again at area A (though in this case the ATOLL wind stress only reaches to 45°N), and assess the relative importance of the two parts of the forcing for the ATOLL wind stresses.

Figs 5.5 show the contribution to the Florida Current transport variation of the forcing in area A for the years 1981-1984. Comparison with Figs 5.1 confirms a result of Chapter 3, that this area is the most important for transport variations through the Florida Straits. Figs 5.6 show the contribution due to the curl of the wind stress in this area, and Figs 5.7 show the contribution associated with gradients in topography. Together, Figs 5.6 and Figs 5.7 add to give Figs 5.5. We see that, except during the Winter months, the part of the variation associated with gradients in topography dominates the contribution due to the wind stress curl. Immediately to the

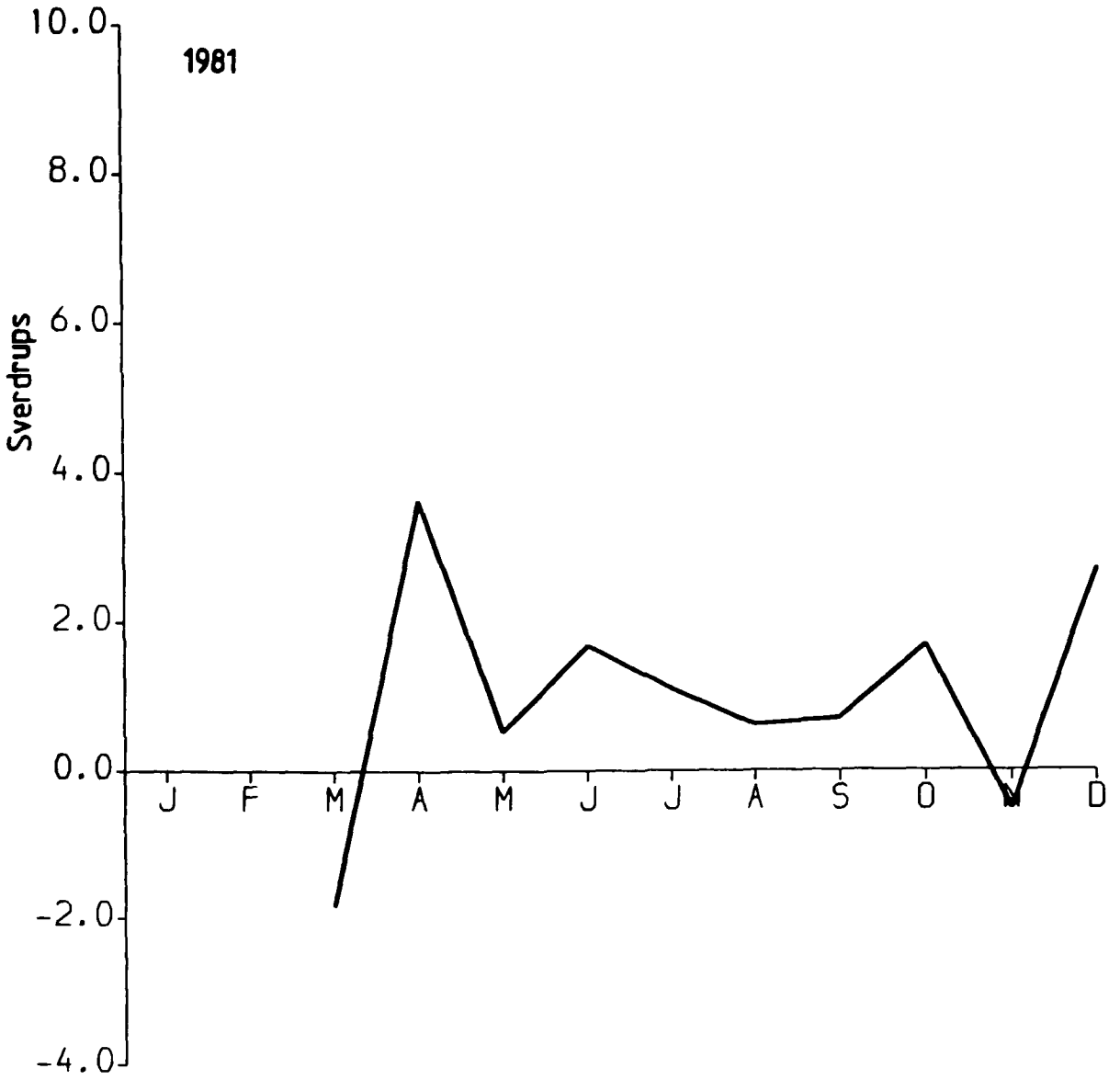

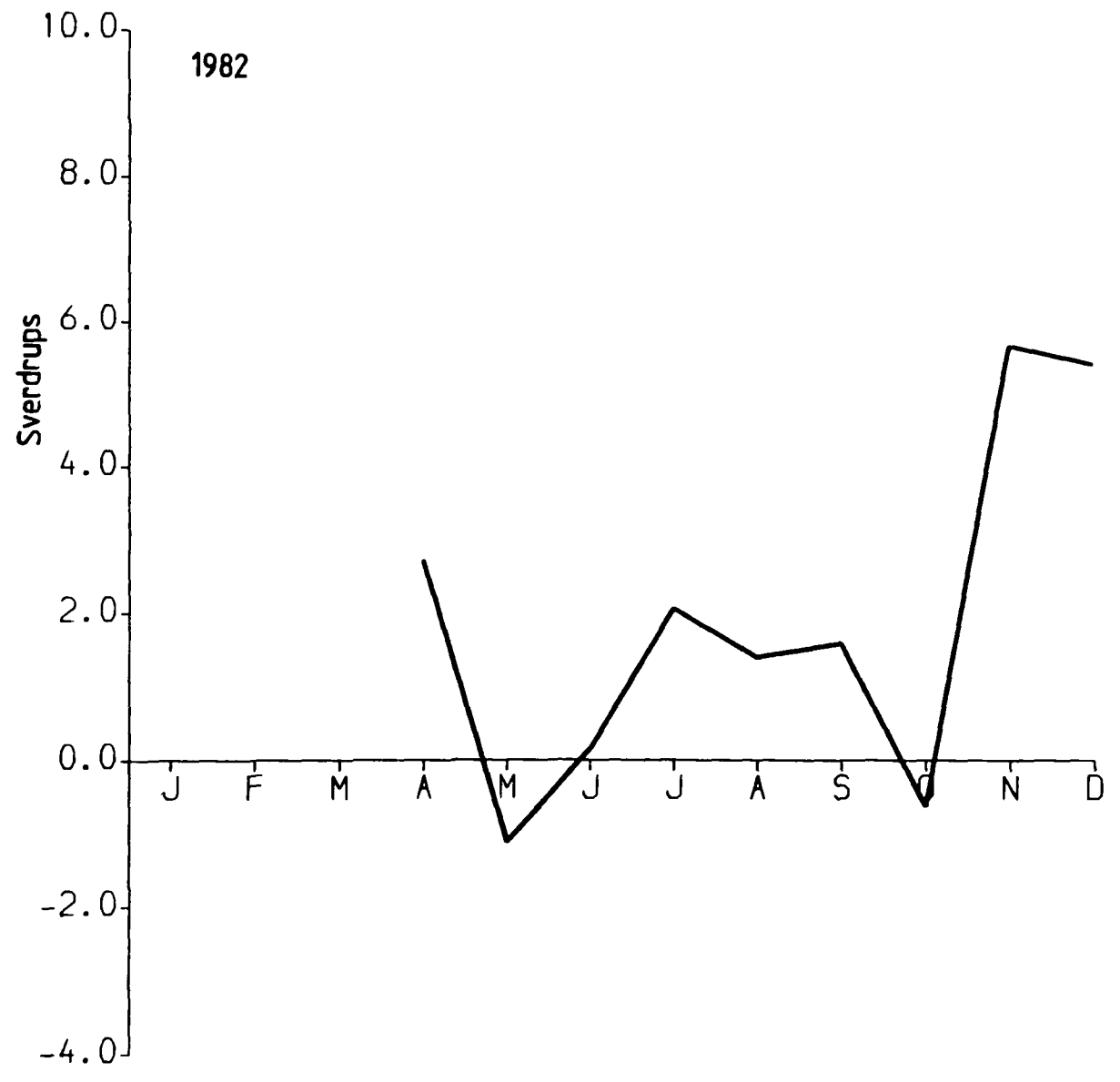

Fig 5.5 The transport through the Florida Straits when the one layer model is forced by the ATOLL winds over area A for the years 1981-1984. Comparison with Fig 5.1 shows the importance of this area.

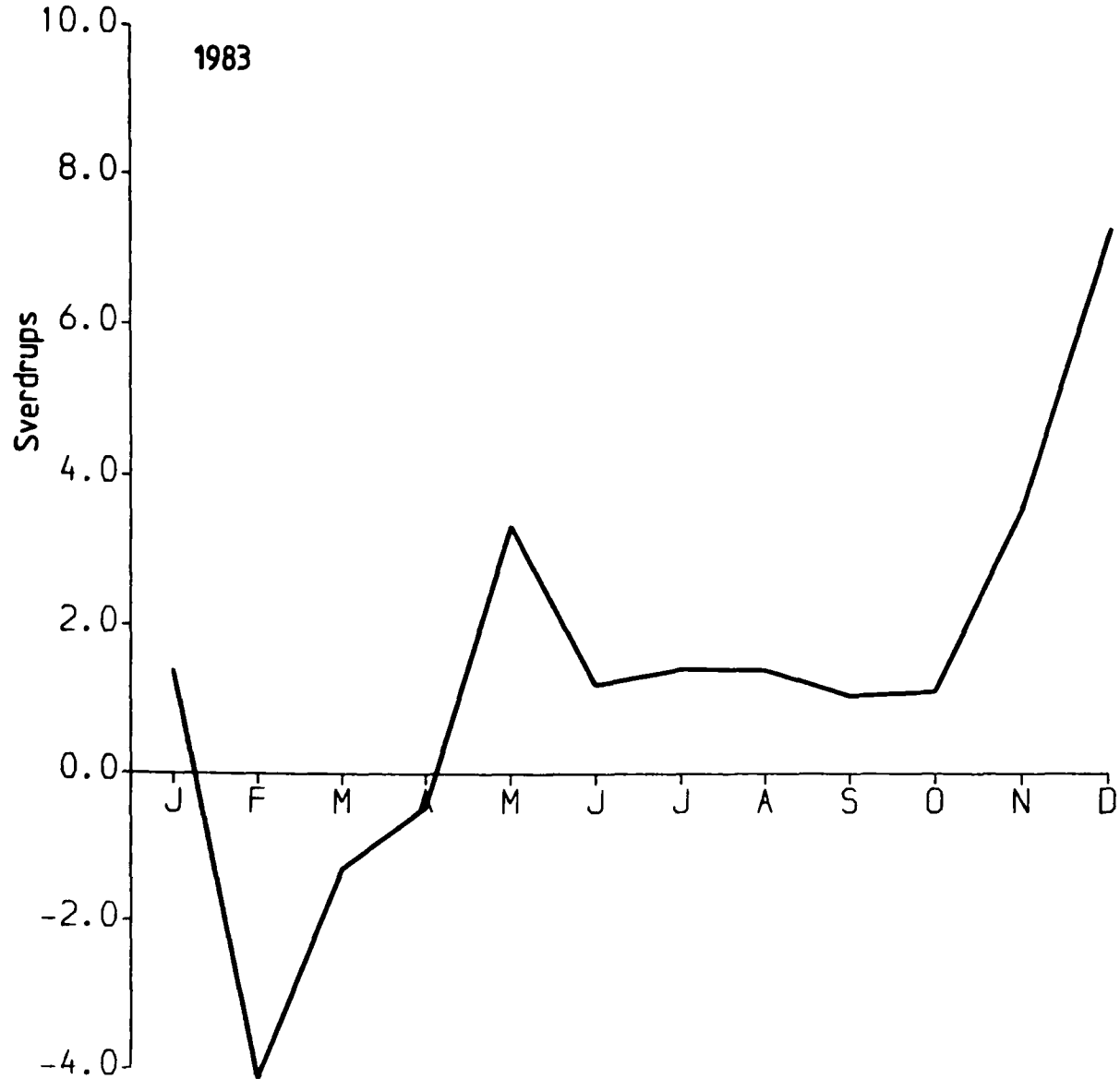
1983
Sverdrups
10.0
8.0
6.0
4.0
2.0
0.0
-2.0
-4.0
J
F
M
A
M
J
J
A
S
O
N
D

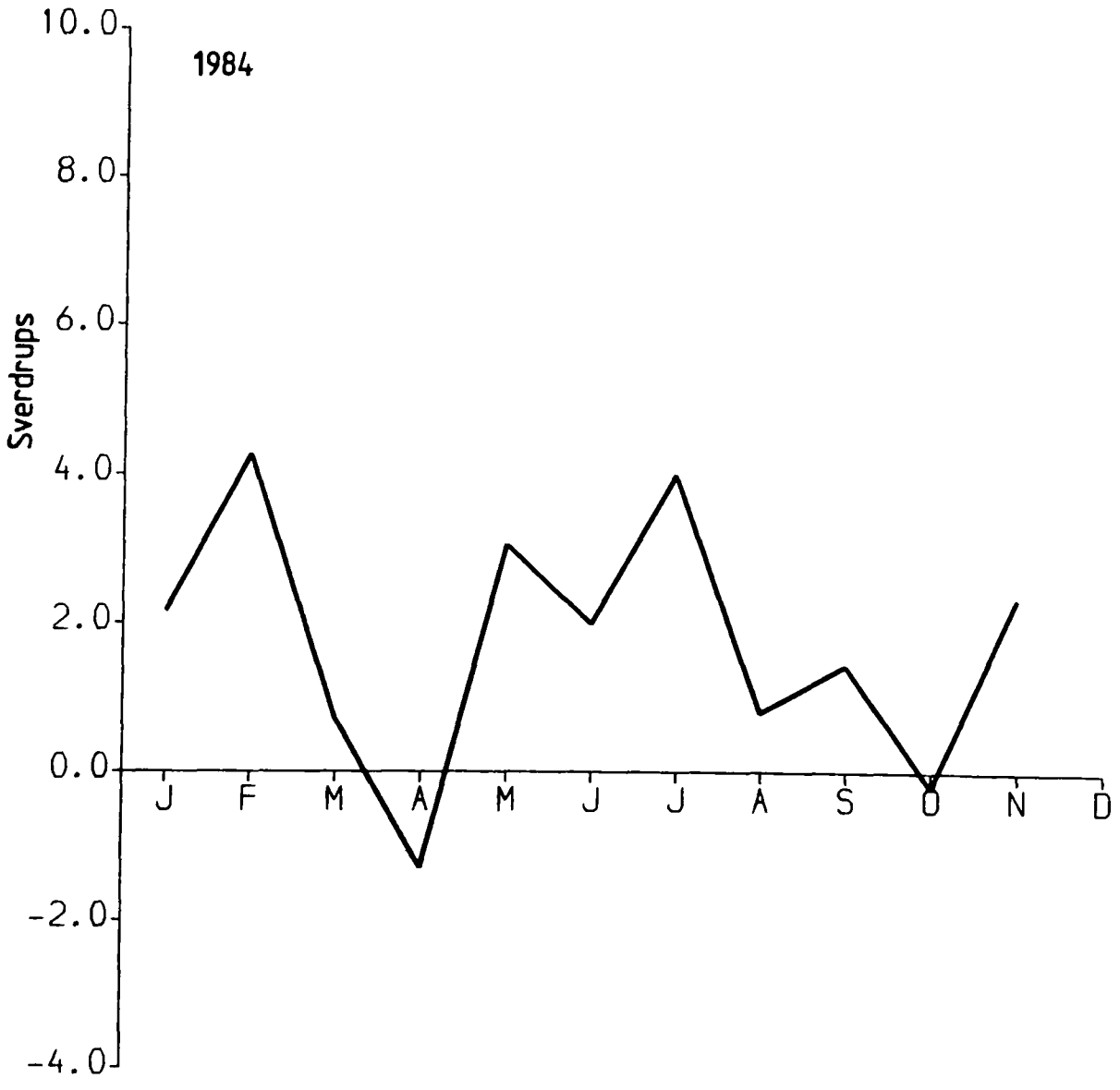
1984
Sverdrups
10.0
8.0
6.0
4.0
2.0
0.0
-2.0
-4.0
J
F
M
A
M
J
J
A
S
O
N
D

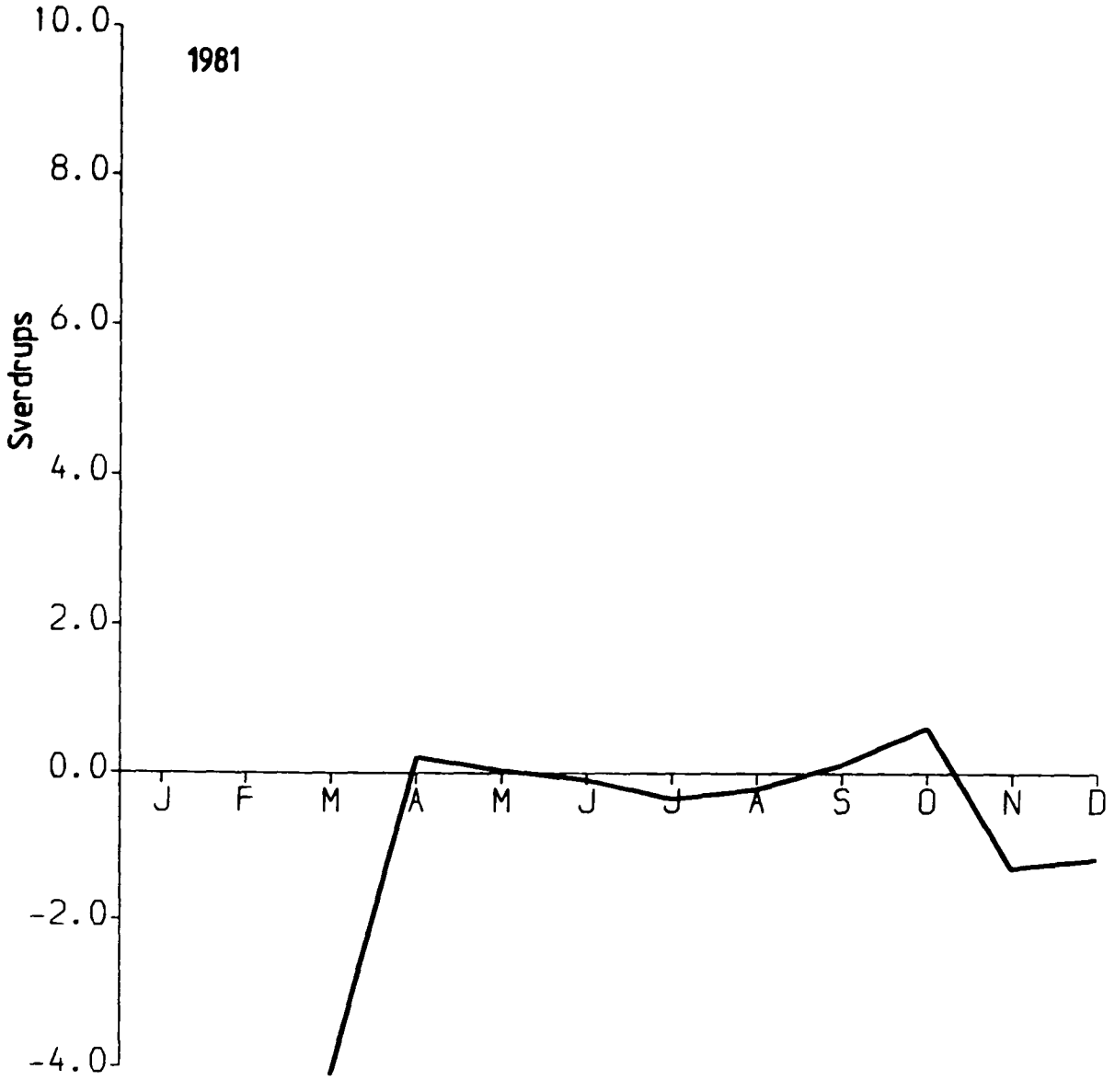

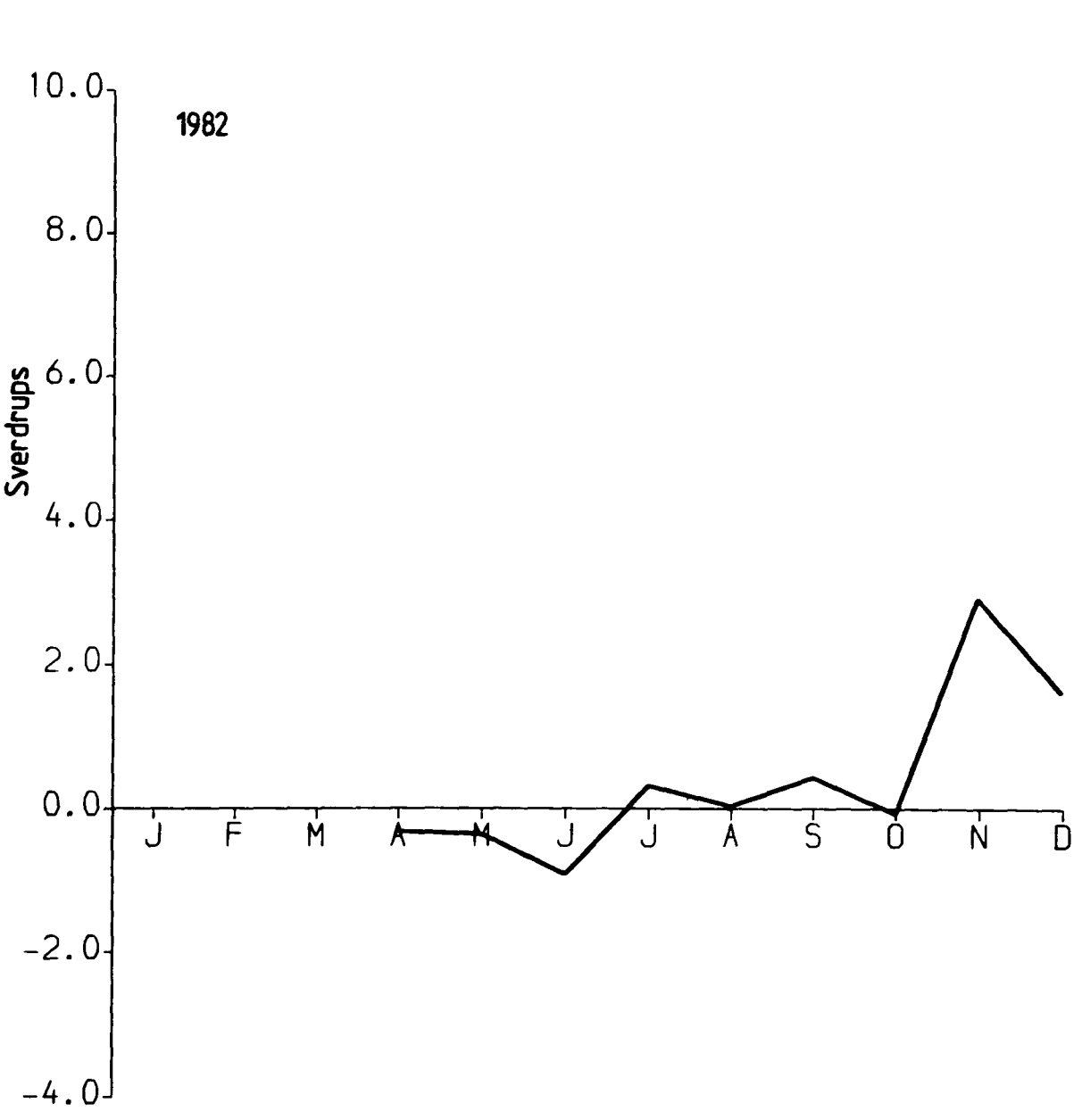

Fig 5.6 The contribution to the Florida Current transport variation due to the curl of the wind stress in area A for the years 1981-1984. Fig 5.6 and Fig 5.7 add to give Fig 5.5.

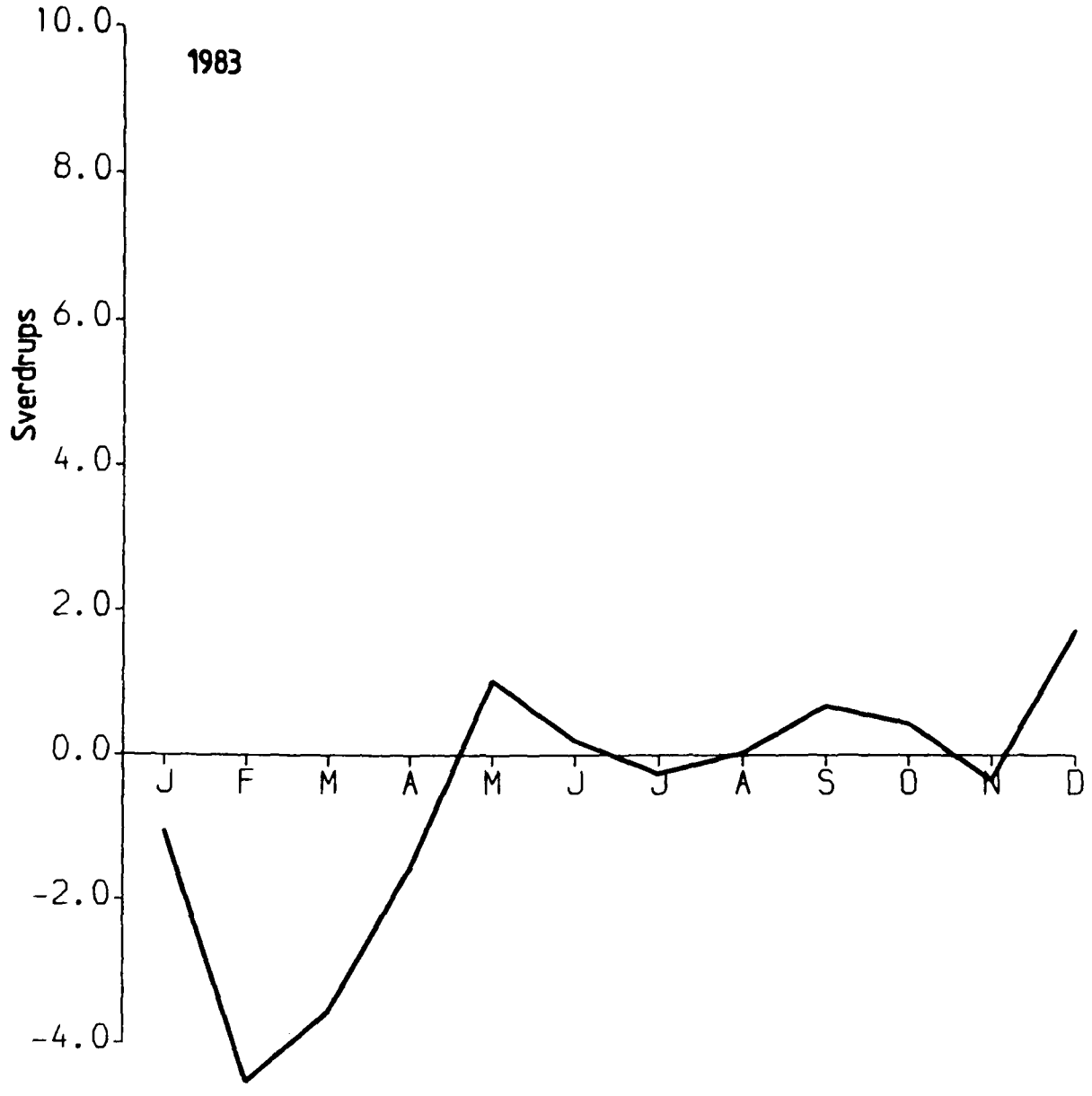
1983
Sverdrups
10.0
8.0
6.0
4.0
2.0
0.0
-2.0
-4.0
J
F
M
A
M
J
J
A
S
O
N
D

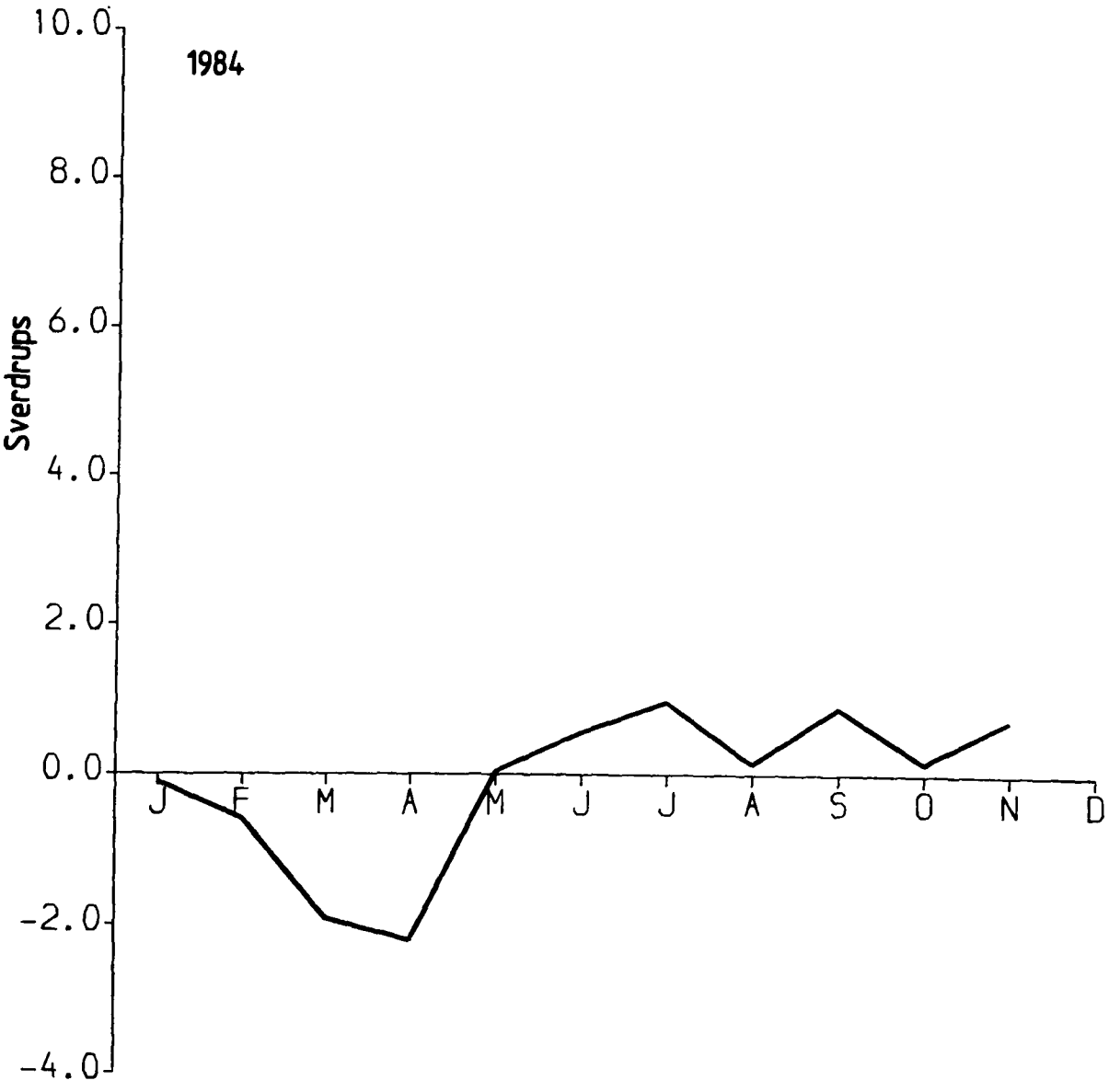
1984
Sverdrups
10.0
8.0
6.0
4.0
2.0
0.0
-2.0
-4.0
J
F
M
A
M
J
J
A
S
O
N
D

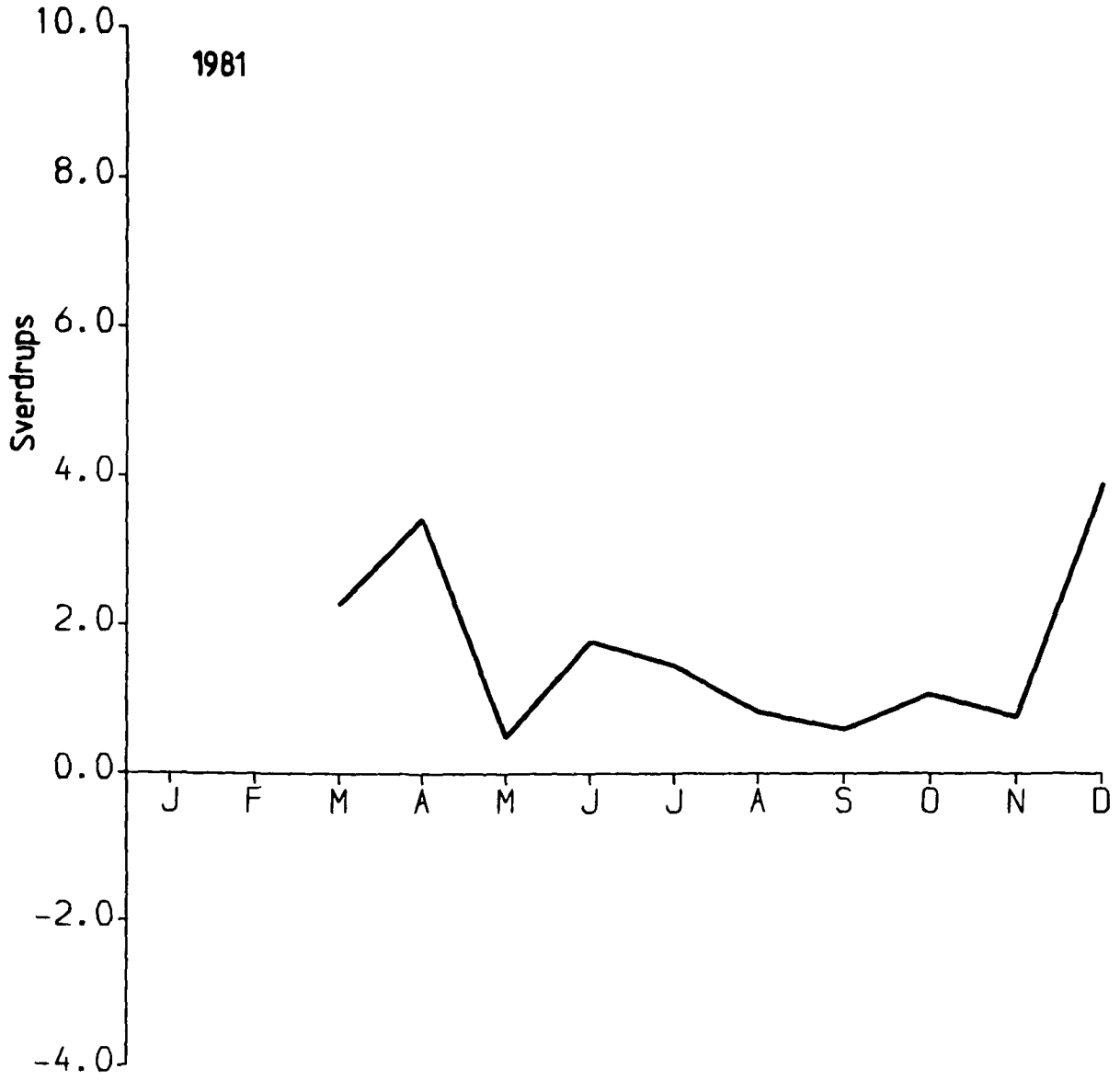

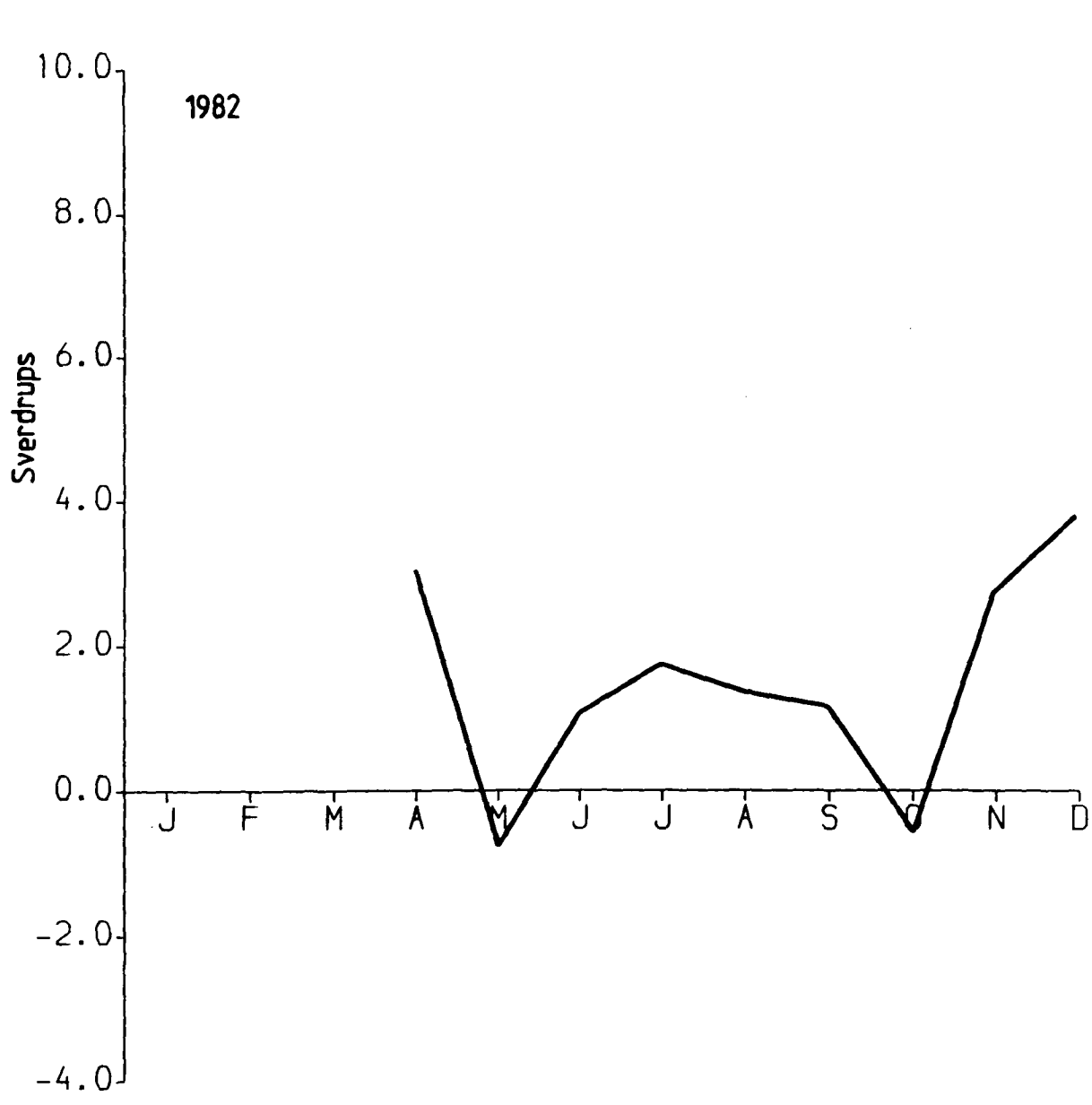

Fig 5.7 The contribution to the Florida Current transport variation due to the wind stress associated with gradients in bottom topography in area A for the years 1981-1984.

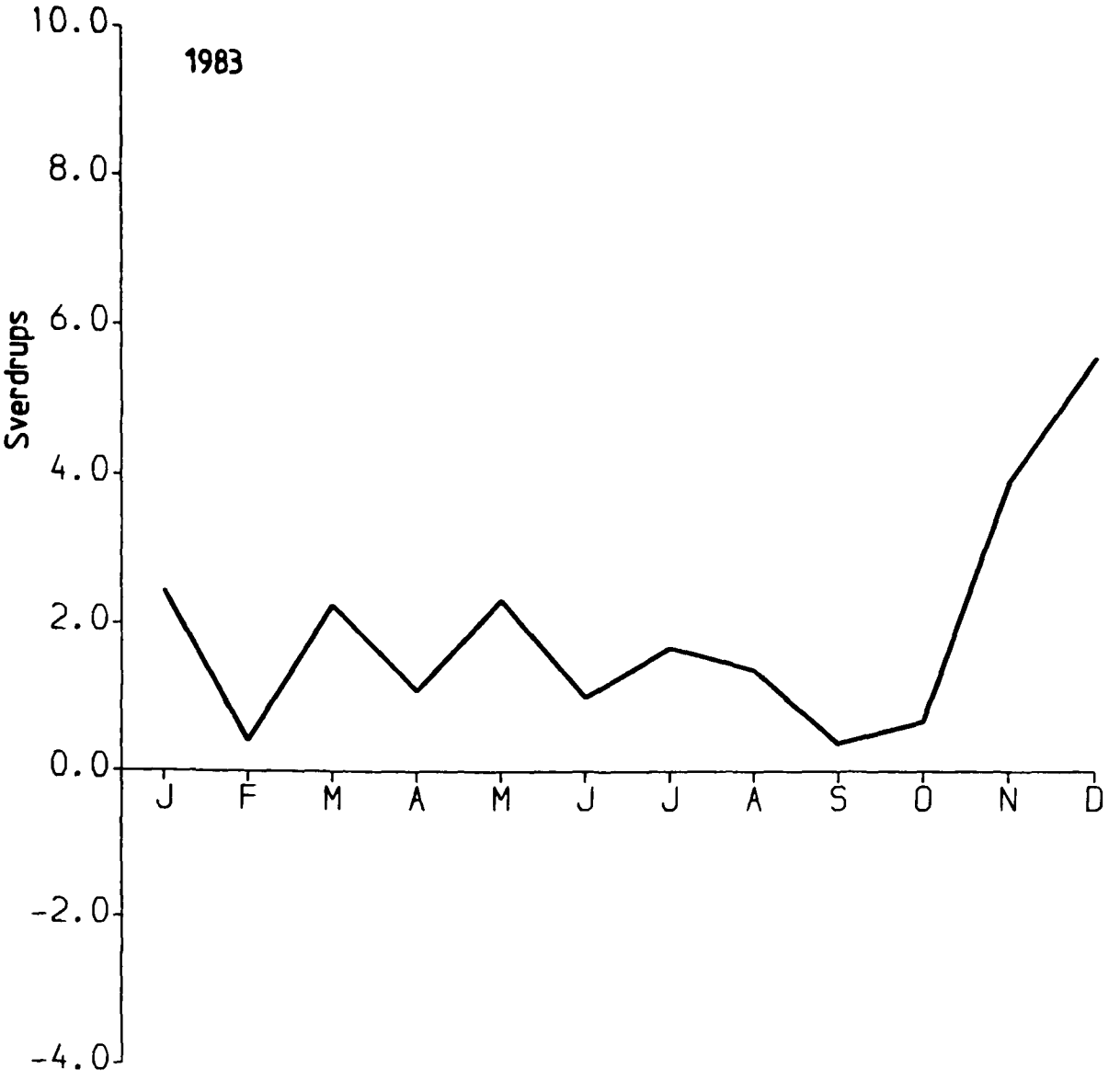
1983
Sverdrups
10.0
8.0
6.0
4.0
2.0
0.0
-2.0
-4.0
J
F
M
A
M
J
J
A
S
O
N
D

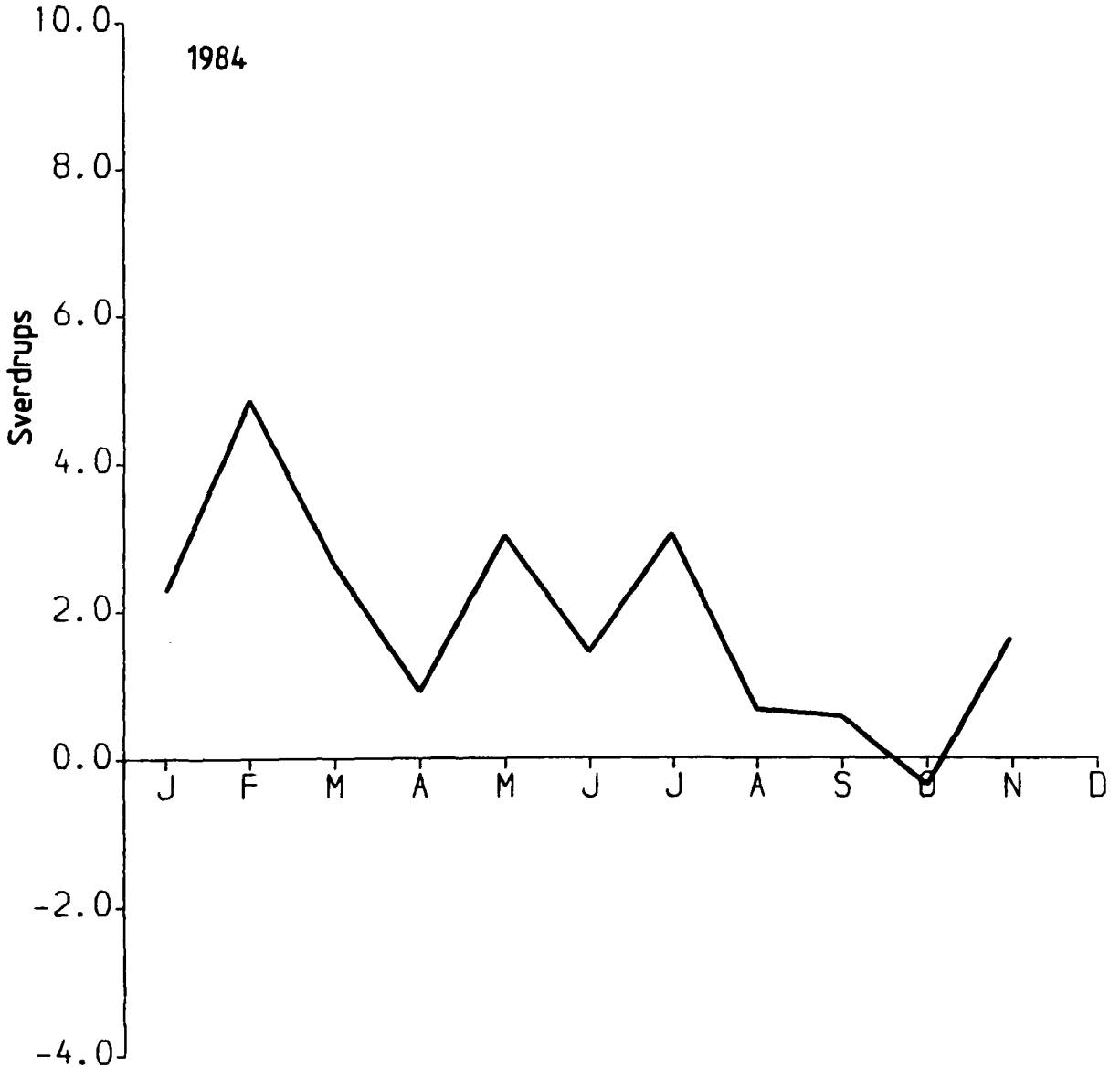
1984
Sverdrups
10.0
8.0
6.0
4.0
2.0
0.0
-2.0
-4.0
J
F
M
A
M
J
J
A
S
O
N
D

east, perusal of streamfunction plots shows that this situation is reversed, as one would expect, since gradients of topography are small away from the coast.

Since the meridional component of ATOLL wind stress contributes less to the variation than the zonal component (see previous Section), and the contribution associated with gradients in bottom topography is dominant for most of the year, it follows that a large part of the variation is forced by the zonal component of wind stress over gradients in topography. This is despite the fact that the transport through the Florida Straits is more sensitive to the meridional component over gradients in topography (a uniform eastward wind stress of 0.1 N m^{-2} gives a northward transport of 1.3 Sverdrups through the Straits, whereas a northward wind stress of 0.1 N m^{-2} gives 2.8 Sverdrups). These figures again suggest the importance of a correct meridional wind stress.

The minimum at the end of October for the Bunker variation is shown in Section 3.3.3 to be due to the wind stress associated with gradients in bottom topography (see Fig 3.10). This minimum involves both the zonal and meridional components of wind stress (Fig 3.7). However, we see from Figs 5.7 that for the ATOLL winds there is no sign of a pronounced minimum at the end of October due to this part of the forcing, except perhaps during 1984. Considering that the mechanism involving gradients in bottom topography appears to be dominant at this time of year for the ATOLL data, this must also be considered a significant difference between the ATOLL and Bunker data which accounts for the lack of a predicted October minimum in the years 1981-1984. A minimum during the Fall appears to be a feature supported by the recent STACS data (Fig 5.2), the historical tidal data (Fig 1.9), and surface current data (Fuglister [1951]), though

neither of the latter two are reliable measures of the total transport.

The Sverdrup transport through the Florida Straits for the Bunker winds is shown on Fig 3.5(b). The maximum transport occurs at the beginning of the year, and is naturally forced by winds to the east. The curl-forced transport of Fig 3.10(a), however, has a minimum at the beginning of the year. This was explained in terms of the deflection of streamlines by topography, so that winds to the north-east became important rather than winds directly east. The same effect appears to occur with the ATOLL data, since for 1983 and 1984 there is a minimum in curl-forced transport at the beginning of the year (Fig 5.6), whereas the Sverdrup transport for 1983 (Fig 5.8) has a maximum in February. The 1983 winds are discussed further in the next Section.

5.4.3 The mean ATOLL wind stress and variability about the mean for 1983

In Chapter 3 we looked at the streamfunction pattern for a flat-bottomed ocean produced by the mean Bunker wind stress (Fig 3.13), and the variability of the Sverdrup transport through the Florida Straits about the mean (Fig 3.5(b)). Here we do the same flat-bottom calculations for the 1983 annual mean ATOLL wind stress, and the 1983 monthly means. This is not done to assess the importance of interannual or seasonal fluctuations in the Florida Current, since it takes years to decades for compensation of the effect of bottom topography by baroclinic Rossby waves to occur. Rather, the Sverdrup transport is seen as a simple diagnostic which enables an assessment of how 'reasonable' the ATOLL winds are.

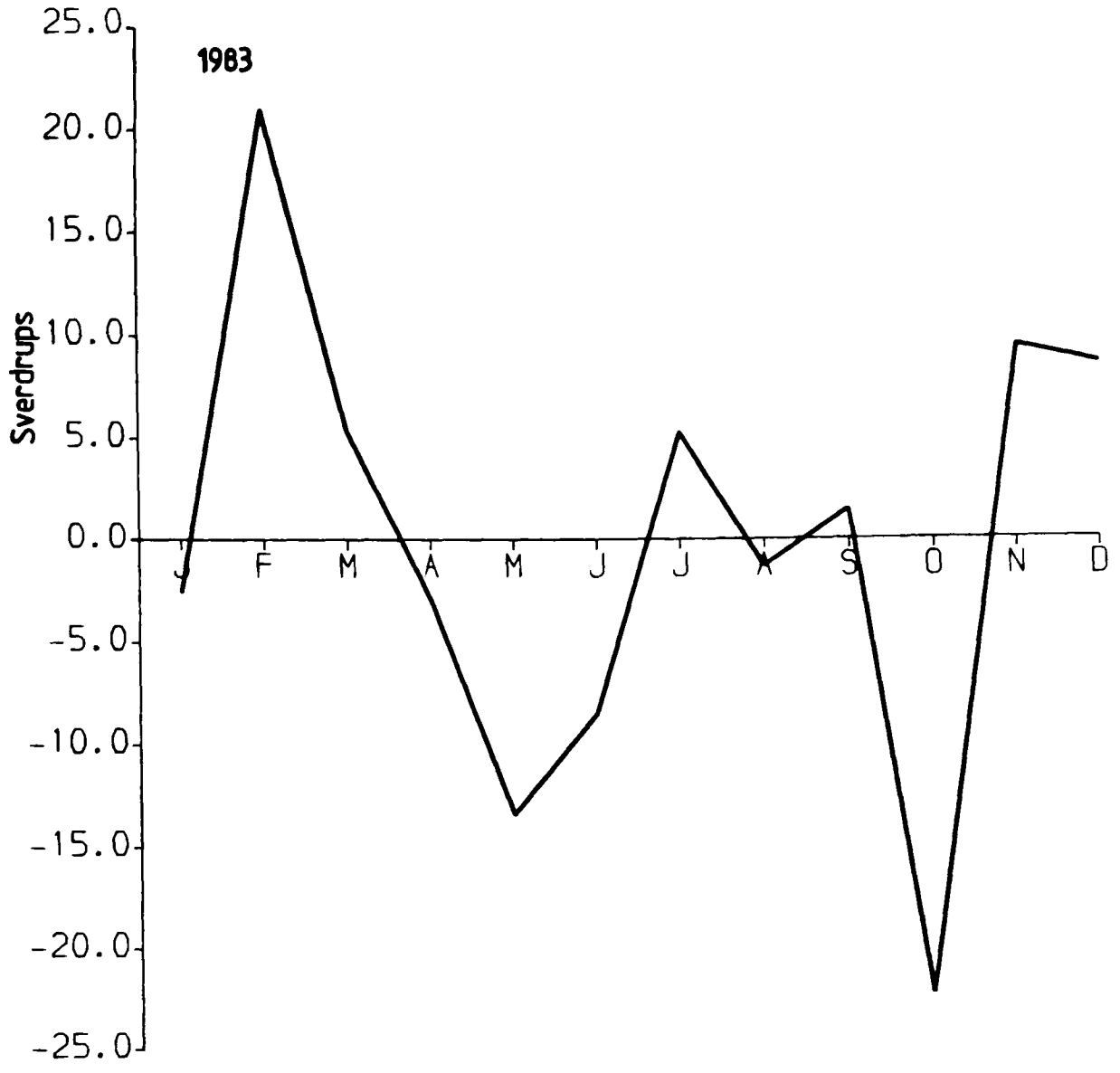

Fig 5.8 The Sverdrup transport through the Florida Straits for each month of 1983 using the ATOLL monthly means.

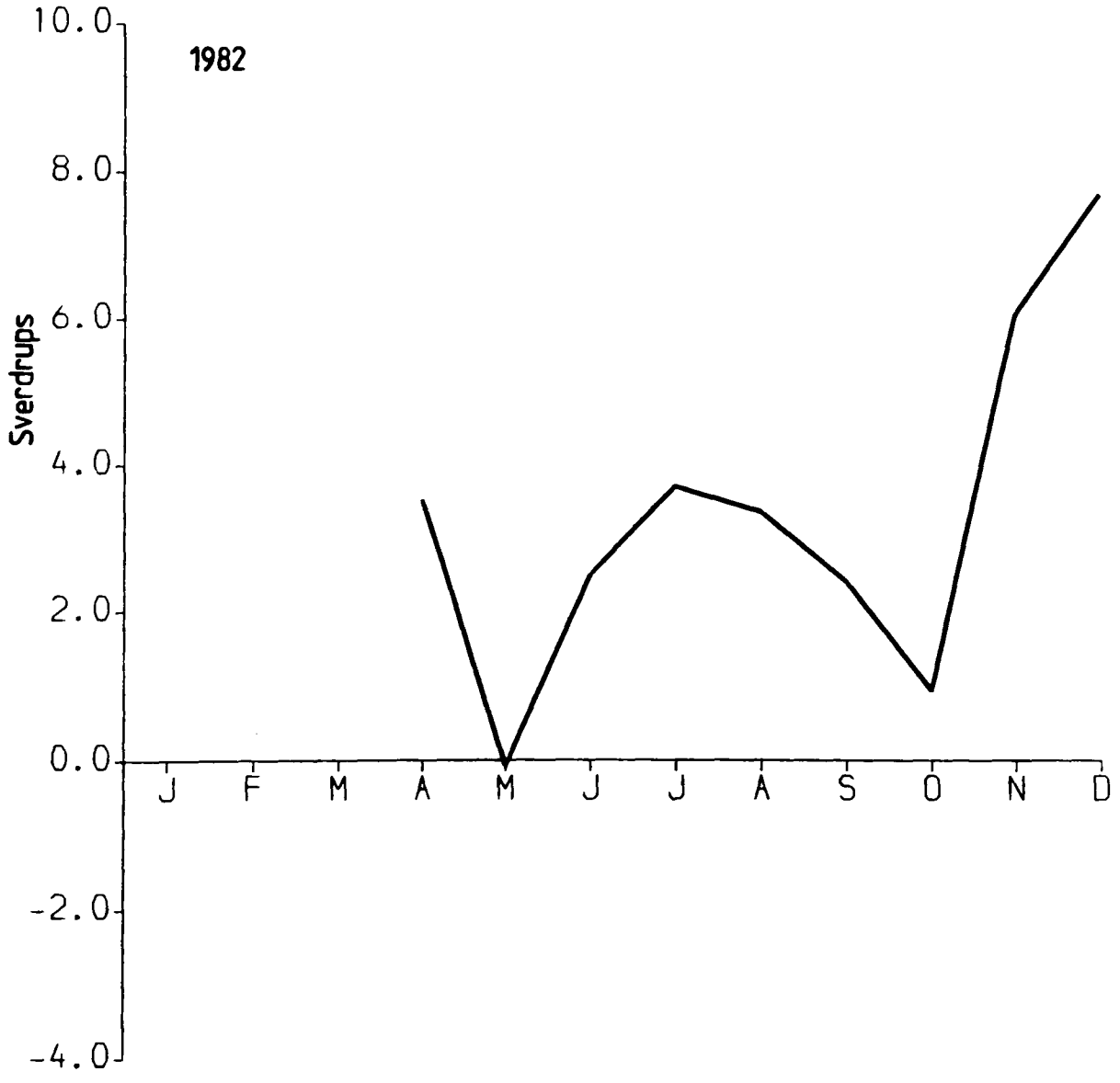

Fig 5.10 The variation of transport through the Florida Straits during 1982 using a constant drag coefficient in the wind stress formula. This Figure should be compared with the 1982 curve of Fig 5.1.

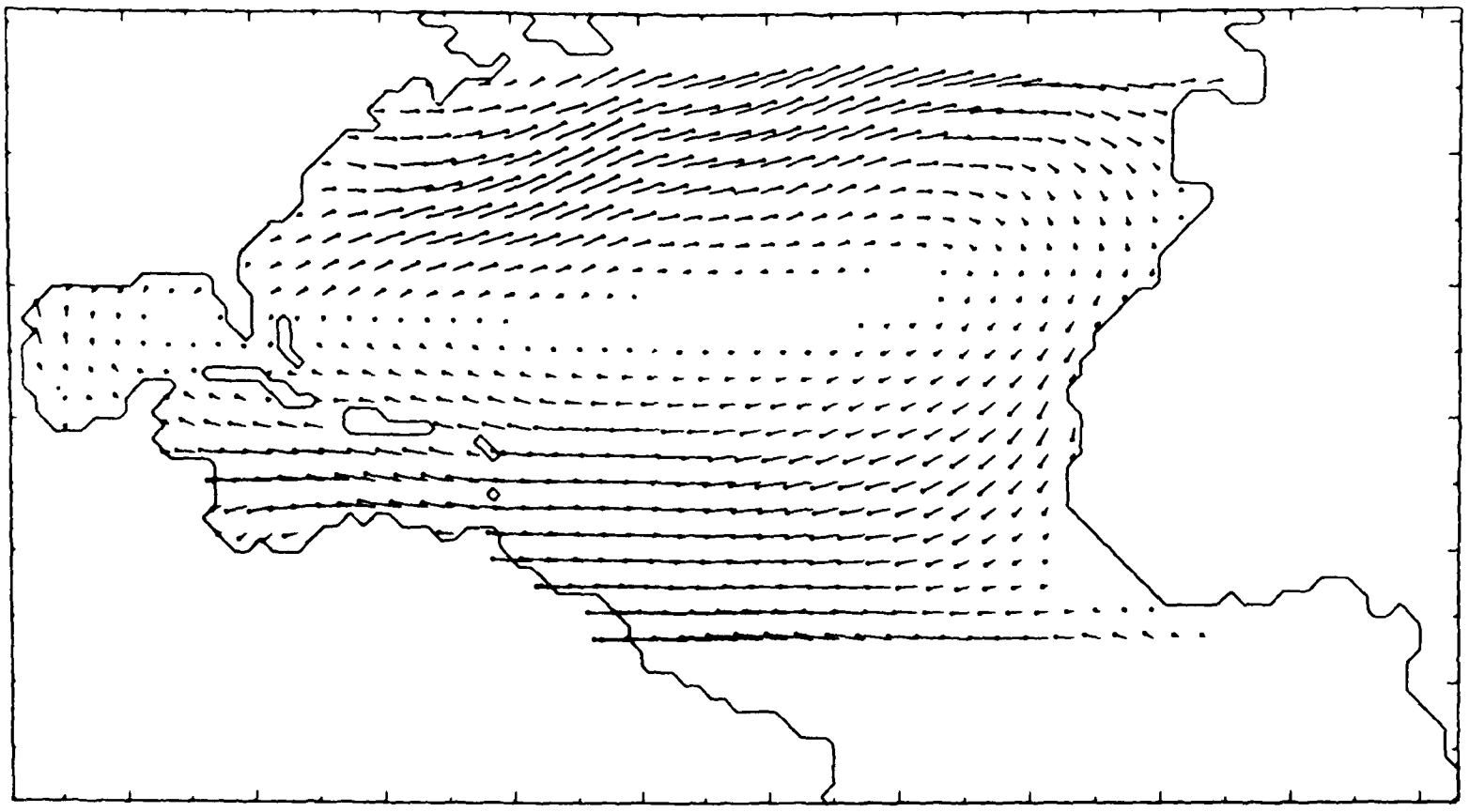

Fig 5.9(a) The 1983 annual mean ATOLL wind stress. The spacing between arrowtails corresponds to 0.1 N m^{-2}.

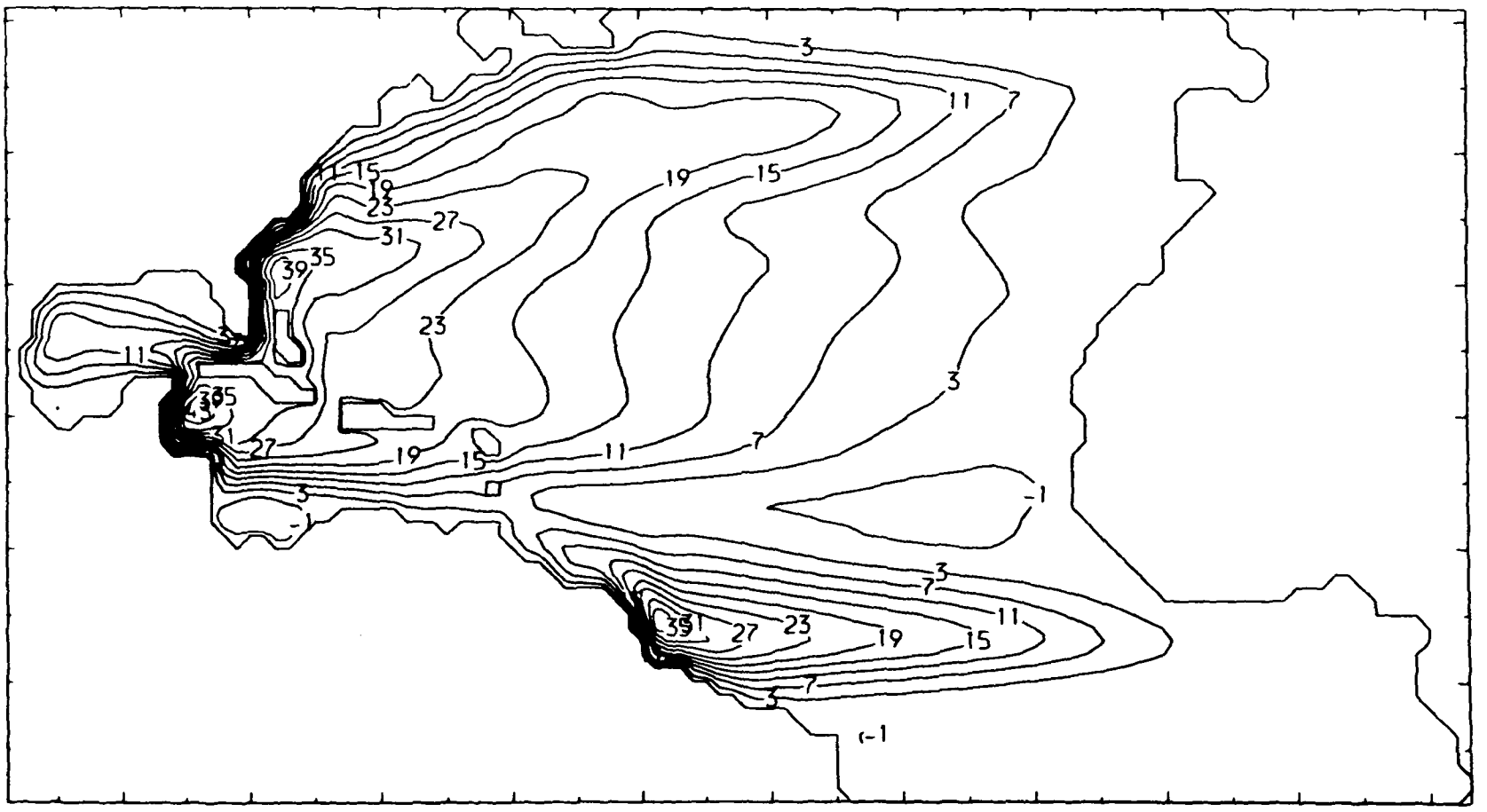

Fig 5.9(b) The equilibrium transport forced by the wind stress of Fig 5.9(a) over a flat-bottomed ocean. The contours are marked in Sverdrups.

Fig 5.9(a) shows the 1983 mean ATOLL wind stress. Comparison with Fig 3.2 shows that the ATOLL wind stresses have larger values than the Bunker equivalents, particularly in the equatorial and North Atlantic. This can result in larger transports. Fig 5.9(b) shows the flat-bottom equilibrium transport corresponding to the wind stress of Fig 5.9(a). The transport through the Florida Straits is 36 Sverdrups, which is in reasonable agreement with the Bunker value of 30.5 Sverdrups (Section 3.5). In the Florida Straits region, the ATOLL Sverdrup transport appears to be 'reasonable', i.e. little different to the Bunker calculation. This is not the case near the equator, where a substantial North Brazilian Coastal Current (NBCC) is predicted. The 1983 ATOLL annual mean wind stress reaches over 0.3 N m^{-2} near the equator. These values are much larger than the corresponding Bunker values of wind stress, which are typically 0.1 N m^{-2}.

Fig 5.8 shows the variation in Sverdrup transport through the Florida Straits for 1983. The mean transport for the year has been subtracted. This Figure should be compared with Fig 3.5(b). We see that the ATOLL variation has a maximum in February and a minimum in October, with intermediate values during the Spring and Summer. This agrees fairly well in phase with the variation of Fig 3.5(b). However, the variation is somewhat greater in magnitude, and the ATOLL values in January and November appear anomalous.

In conclusion, for the Florida Straits the ATOLL winds and the Bunker winds give similar results, both in the seasonal variation of Sverdrup transport and in the annual mean transport, though for both the ATOLL results are about 20% greater in magnitude. Near the equator, however, the ATOLL annual mean winds give rise to a much larger wind stress and associated curl

than the Bunker equivalent.

5.4.4 A simpler drag coefficient

The drag coefficient used in the above calculations varied with wind speed in such a way that higher wind speeds have a greater drag coefficient. This could over-emphasise the importance of large winds, in particular during the Winter months. To investigate this effect monthly averages of ATOLL wind stress were calculated for 1982 in the same way as before, but using $C_D = 1.5 \times 10^{-3}$, a constant. The two drag coefficients are equal at a wind speed of about 10 m/s. Fig 5.10 shows the variation during 1982 using the modified monthly mean wind stresses over the one layer model with topography. This figure should be compared with the 1982 curve of Fig 5.1. It is seen that the curves are very similar, and although the December maximum is slightly reduced in magnitude, it still remains a pronounced maximum, in disagreement with the STACS data. It is concluded that the Winter maxima evident in Figs 5.1 are not due to over-emphasis of the strong winds.

5.5: Summary and Conclusion

In this Chapter the one layer model of Chapter 3 has been forced with monthly mean wind stresses derived from ATOLL winds. These predictions of transport through the Florida Straits have been compared with recent STACS data. The comparison showed that the ATOLL predictions were not satisfactory. In particular, Summer maxima and Fall minima were measured, whereas use of the ATOLL data predicted December maxima. Use of the Bunker winds,

however, reproduces the phase of STACS measurements, though the predicted amplitude is lower. The lower amplitude can be partially explained by the averaging of several years of data to give the Bunker monthly means. It was concluded that to a large extent the annual cycle is repeated year after year, and that the Bunker variation is a reasonable prediction of this annual variation. This has been found not to be the case when ATOLL winds are used. The meridional component of the wind, which is crucial for the Bunker Summer maximum, is markedly less important than the zonal wind in the ATOLL data. This could explain the lack of predicted Summer maxima.

For the ATOLL winds it was found that the contribution to Florida Current transport variations due to the wind stress curl was usually less important than the contribution associated with gradients in bottom topography. For the Bunker winds the two contributions were of about equal importance. These model results show that the wind stress associated with topographic gradients is an important generator of transport variations. The topography is also critical in the way it deflects curl forced transport variations. For both reasons, it would be desirable to model regions near coasts (where topography changes rapidly) with greater resolution of the topography.

CHAPTER SIX

Summary and Further work

6.1: Summary and Conclusions

The motivation behind the work of this thesis has been to investigate the physics of the seasonal variation of western boundary currents, in particular the Florida Current. Although the Sverdrup relationship accounts for the mean flow through the Florida Straits (Leetmaa, Niiler and Stommel [1977]), it does not account for the seasonal variation (Niiler and Richardson [1973]). This suggests a difference between the dynamics of the mean flow and the seasonal variation.

Chapter 2 is devoted to an explanation of these differences in dynamics. The linear response of a simple one dimensional two layer model to a periodic wind stress curl in the presence of bottom topography was first investigated. For periods much less than the time taken for the wind generated baroclinic Rossby waves to pass over the topography (i.e. 'short' periods), the ocean response is primarily that for a homogeneous ocean and is thus strongly modified by topography. For periods much longer than this time (i.e. 'long' periods), the Rossby waves compensate for the effect of topography and the non-topographic Sverdrup balance holds. For the Atlantic at 25°N, the long period limit is of the order of years to decades, depending on the location of the wind stress variability. Thus at annual period the non-topographic Sverdrup balance is not applicable. By consideration of a simple model a difference in dynamics

between the seasonal variation and the mean flow has already been explained. However, there are additional effects at seasonal timescales which cannot be investigated using the one-dimensional model. A two-dimensional model was used for further work.

The effect of a baroclinic Kelvin wave passing over varying bottom topography is one of the effects not included in the one-dimensional model. Although the wave is baroclinic, the coupling of modes over topography allows transport to be generated. This effect is independent of the Sverdrup relation, and is potentially important at seasonal time scales. The other important effect is associated with the fact that the seasonal variations in transport are primarily barotropic. This means that a uniform wind stress (with no curl) over varying bottom topography can generate transport variations. This again is an effect independent of the Sverdrup relation. The relative importance of these (and other) effects for the seasonal variation of the Florida Current can only be determined by using the appropriate geography and bottom topography in a model of the North Atlantic. This has been done in Chapter 3.

The measurements of Niiler and Richardson [1973] showed a Summer maximum in the annual cycle, with an amplitude of about four Sverdrups. This contrasts with the seasonal variation of the Sverdrup transport at the Florida Straits which has a Winter maximum, and an amplitude about four times greater. The prediction of Florida Straits transport variations using Bunker monthly winds over a two layer model with the correct topography is given in Chapter 3. A Summer maximum (at the end of July) is predicted, together with a Fall minimum (at the end of October). These features agree in phase with the Niiler and Richardson [1973] transport data and the recent STACS measurements. Although the amplitude of the model prediction is only about two

Sverdrups, this model prediction still represents a real advance on Sverdrup theory. Other aspects of the Florida Straits transport variation and the transport variation of other areas of the North Atlantic are discussed in Chapter 3.

In Chapter 4 the Semtner model (Semtner [1974]) and a one layer model are forced with the Bunker seasonal winds, and streamfunctions are compared. Both models are of a homogeneous ocean, but one is a layer model, and the other is a level model. It was found that the results from the two models were generally in agreement, both for the Florida Current and other parts of the North Atlantic. This inspires greater confidence in the results from the one layer model. Also, the one layer model ought to be used in an application where we are interested in results from a homogeneous ocean, because of the saving in computer time.

In Chapter 5 we force the one layer model with ATOLL winds for the years 1981-1984, and compare the results with the STACS measurements between April 1982 and May 1984. In contrast to the annual cycle forced by the Bunker winds, which is in general agreement with the STACS measurements, the ATOLL predictions are not satisfactory. In particular December maxima are predicted, whereas Summer maxima and Fall minima are measured. It was concluded from further calculations that the meridional component of wind, which is crucial to the overall Bunker Summer maximum, is markedly less important than the zonal component for the ATOLL winds, and that this could lead to a lack of predicted Summer maxima.

6.2: Further work at shorter timescales

Given that the ATOLL winds are calculated at twelve hour

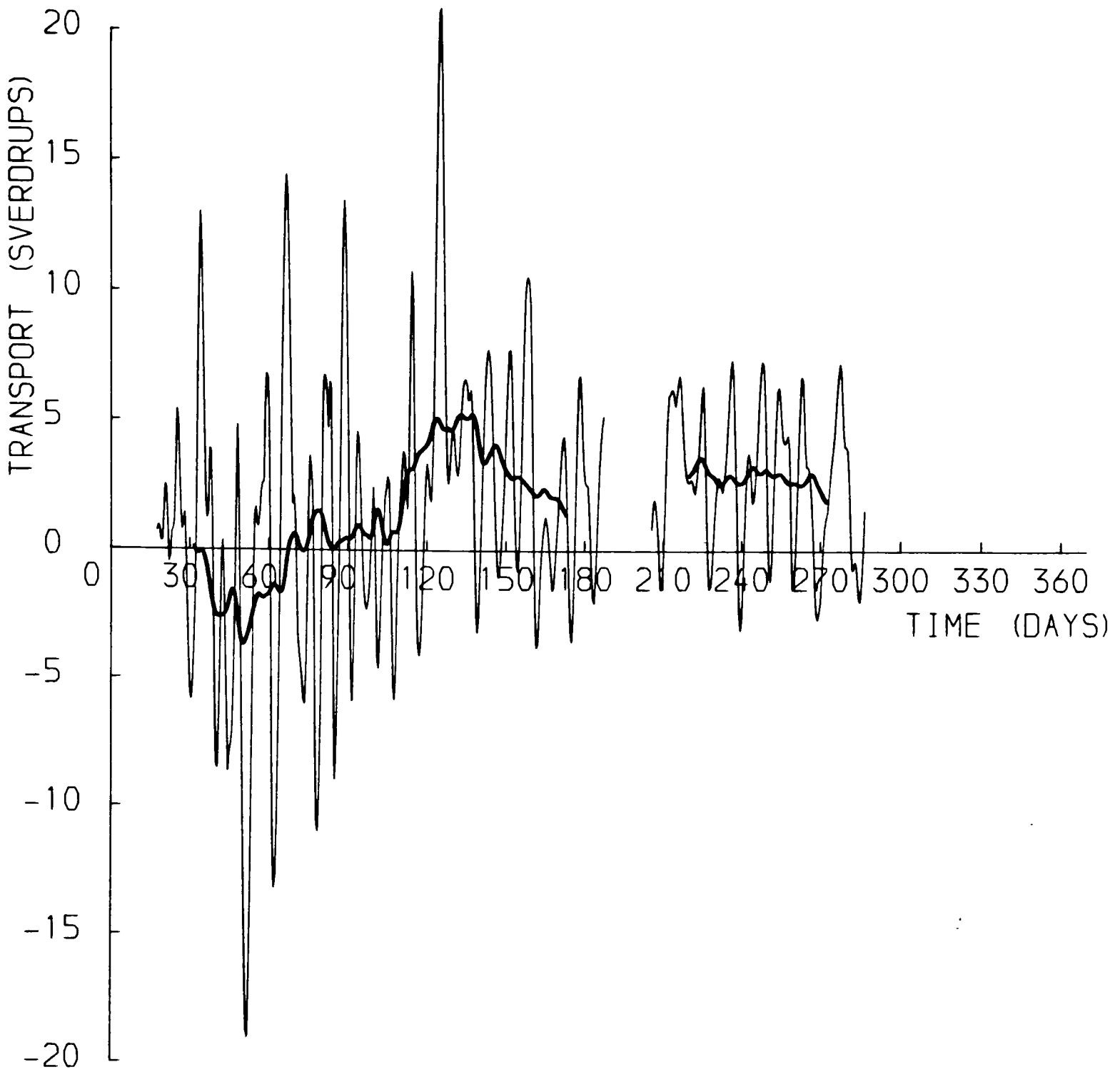

Fig 6.1 The transport variation when the one layer model is forced by ATOLL winds at daily timescales. A 28 day running mean has been drawn through the transport values. Time is in days through 1983.

intervals, an obvious extension of the work done so far would be to force the one layer model at daily timescales. The results of a preliminary calculation are shown on Fig 6.1. The calculation is started at rest on Jan 18 1983 and again on July 25 1983. A 28 day running mean has been drawn through the predictions. The friction and other model parameters were the same as in Chapters 3 and 5.

Comparison of the running mean with the 1983 curve of Fig 5.1 shows that the process of taking monthly means of the wind stress, and forcing the model ocean one month at a time gives rise to a variation that is similar to the monthly running mean. Another more interesting result is that the predicted short time scale variations are too great in amplitude, as a comparison with Fig 5.2 shows. The topography appears to be less effective at blocking transport variations at these short periods. The generation of continental shelf waves (Adams and Buchwald [1969]) could play a part at these high frequencies, together with the transmission and decay of barotropic topographic Rossby waves incident on the continental shelf (Kroll and Niiler [1976]). The importance of bottom topography in both these processes suggests that a model with better resolution would be appropriate. However, it is not clear how one would differentiate between the two effects with generalised wind and topography. Although the framework of a homogeneous ocean is about as simple as it could be, the analysis of results in terms of known physics is not a simple task.

Appendix A

The solution of the equations of the one dimensional model:

The model equations are given in Section 2.2, and the method by which the equations are obtained is further explained in Anderson and Killworth [1977]. The equations are:

(A1) $$(\bar{u}_{xx} - \Lambda_0 \bar{u})_t + \bar{u}_x + \frac{\Lambda_1 T}{1-T}\hat{u}_t - \frac{i T_x}{\varepsilon(1-T)}(\bar{u} - \hat{u}) = 1$$

(A2) $$(\hat{u}_{xx} - \Lambda_1 \hat{u})_t + \hat{u}_x - \frac{i\delta T_x}{\varepsilon(1-T)}(\hat{u} - \bar{u}) = 1$$

The meaning of the symbols is given in Section 2.2.

To solve this pair of coupled equations for the baroclinic velocity $\hat{u}$ and the barotropic velocity $\bar{u}$ as a function of time we use the leap-frog time stepping procedure. We solve A2 first for the baroclinic velocity because the $\hat{u}_t$ term in A1 can only be evaluated once this has been done. There is no corresponding $\bar{u}_t$ term in A2. If we denote the progression of time by the integer J and the dimension x by the integer I, where x and t are split into equal intervals DX and DT, then:

(A3) $$(R(I,J+1)-R(I,J-1))/(2DT) = K(I,J)$$

where R is $\hat{u}_{xx} - \Lambda_1 \hat{u}$ and K is a forcing depending on $\bar{u}$ and $\hat{u}$ at time J. This can be rewritten as the matrix equation

(A4) $$\underline{A}\ \underline{z} = \underline{k}$$

where z is a column vector containing the elements z_i, which correspond to the baroclinic velocities at time J+1 at each I which are to be solved for. If we use the finite difference approximation for R

(A5) $$R(I,J)=(\hat{u}(I+1,J) + \hat{u}(I-1,J) - 2\hat{u}(I,J))/DX^2 - \Lambda_1 \hat{u}(I,J)$$

then $\underline{A}$ is a tridiagonal matrix of the form:

$$\underline{A} = \begin{bmatrix} b_1 & c_1 & & 0 \\ a_2 & & \ddots & \\ & \ddots & & c_{n-1} \\ 0 & & a_n & b_n \end{bmatrix}$$

and $\underline{k}$ is another column vector.

The vector $\underline{z}$ can be solved for directly by the following simple algorithm. Defining:

$$w_1 = c_1/b_1 \quad ; \quad w_i = c_i/(b_i - a_i w_{i-1}) \qquad 2 < i < n-1$$

$$g_1 = k_1/b_1 \quad ; \quad g_i = (k_i - a_i g_{i-1})/(b_i - a_i w_{i-1}) \qquad 2 < i < n$$

the components z_i of the solution vector $\underline{z}$ are then given recursively by:

$$z_n = g_n \quad ; \quad z_i = g_i - w_i z_{i+1} \qquad 1 < i < n-1$$

With the calculation of the quantities w_i and g_i, the above procedure is equivalent to the reduction by Gaussian elimination of the matrix equation A4 to a new matrix equation, after the forward course of Gaussian elimination

$$\underline{W}\ \underline{z} = \underline{g}$$

where W and g take the form:

$$\underline{W} = \begin{bmatrix} 1 & w_1 & & 0 \\ & 1 & \ddots & \\ & & \ddots & w_{n-1} \\ 0 & & & 1 \end{bmatrix} \qquad \underline{g} = \begin{bmatrix} g_1 \\ g_2 \\ \vdots \\ g_n \end{bmatrix}$$

The new matrix is upper triangular with unit diagonal entries. The recursive solution for $\underline{z}$ is just the backward substitution for $\underline{z}$.

The above method for the solution of $\hat{u}$ is explicit. The solution of $\bar{u}$ is similar, but implicit. This means that $\bar{u}(I,J)$ is taken as the mean of $\bar{u}(I,J+1)$ and $\bar{u}(I,J-1)$. A similar mean is used for $\hat{u}(I,J)$, since $\hat{u}(I,J+1)$ has already been calculated. Thus there is a term in $\bar{u}(I,J+1)$ on the right hand side of A3, where now R is $\bar{u}_{xx} - \Lambda_0 \bar{u}$. This is taken over to the left hand side, and the appropriate matrix equation is solved in the same

way (The matrix $\underline{A}$ is still tridiagonal).

Appendix B

The equations of the two layer model:

Consider a layer of fluid density ρ_1 and mean depth H_1, overlaying a denser fluid of density ρ_2 and depth H_2, with topography of variable depth T, as shown in Fig B1. The pressure in each of the layers is given by:

$$P = P_0 + \rho_1 g(\eta_1 - Z) \qquad \text{[Layer 1]}$$

$$P = P_0 + \rho_1 g(H + \eta_1 - \eta_2) + \rho_2 g(\eta_2 - H_1 - Z) \qquad \text{[Layer 2]}$$

The linearised momentum and continuity equations for each layer are therefore:

$$(B1) \qquad U_{1t} - fV_1 = -g\eta_{1x} + X/(\rho_1 H_1) + D\nabla^2 U_1$$

$$(B2) \qquad V_{1t} + fU_1 = -g\eta_{1y} + Y/(\rho_1 H_1) + D\nabla^2 V_1$$

$$(B3) \qquad \eta_{1t} - \eta_{2t} + H_1(U_{1x} + V_{1y}) = 0$$

$$(B4) \qquad U_{2t} - fV_2 = -g\eta_{1x} - g'\eta_{2x} - BU_2 + D\nabla^2 U_2$$

$$(B5) \qquad V_{2t} + fU_2 = -g\eta_{1y} - g'\eta_{2y} - BV_2 + D\nabla^2 V_2$$

$$(B6) \qquad \eta_{2t} + ([H_2 - T]U_2)_x + ([H_2 - T]V_2)_y = 0$$

Where $g' = g(\rho_2 - \rho_1)/\rho_1$, the Boussinesq approximation has been made, P_0 is assumed constant, and it is assumed that the wind

stress decreases linearly down to the interface between the layers. D and B are coefficients of diffusion and bottom friction respectively. For the calculations of Section 2.3, $D=10^4\ m^2\ s^{-1}$, $B=4\times 10^{-8}\ s^{-1}$, $g'=0.03\ m\ s^{-2}$, $H_1=100\ m$, and $H_2=3900\ m$.

If we add B3 and B6 and make the rigid lid approximation (equivalent to setting $\eta_{1t}=0$) we obtain:

$$(B7)\qquad (H_1 U_1+[H_2-T]U_2)_x+(H_1 V_1+[H_2-T]V_2)_y=0$$

This allows the introduction of a streamfunction ψ such that:

$$(B8)\qquad -\psi_y = H_1 U_1+[H_2-T]U_2 = H\bar{U}$$

$$(B9)\qquad \psi_x = H_1 V_1+[H_2-T]V_2 = H\bar{V}$$

Where $\bar{U}$ and $\bar{V}$ are 'barotropic velocities'. Multiplying B4 by $[H_2-T]/H$, and B1 by H_1/H and adding we obtain:

$$(B10)\qquad \bar{U}_t-f\bar{V} = -g\eta_{1x}+X/\rho_1 H\ -g'\eta_{2x}\ [H_2-T]/H\ +F^x$$

Where $H=H_1+H_2-T$ and F^x is a friction term. Similarly we obtain:

$$(B11)\qquad \bar{V}_t+f\bar{U} = -g\eta_{1y}+Y/\rho_1 H\ -g'\eta_{2y}\ [H_2-T]/H\ +F^y$$

Equations B10 and B11 can be combined and written in vector form:

$$(B12)\quad [\bar{u}_t-f\bar{v}]\,\underset{\sim}{i}+[\bar{v}_t+f\bar{u}]\,\underset{\sim}{j}=-g\underset{\sim}{\nabla}\eta_1+\frac{\underset{\sim}{\tau}}{\rho_1 H}-g'\underset{\sim}{\nabla}\eta_2[H_2-T]/H+\underset{\sim}{F}$$

Operating with $curl_z$ on this equation gives:

$$(B13)\quad \left|\frac{\Psi_{xt}}{H}\right|_x + \left|\frac{\Psi_{yt}}{H}\right|_y = curl_z\left[f\frac{\nabla\Psi}{H} + \frac{g'\nabla\eta_2 H_1}{H} + \frac{\tau}{\rho_1 H} + F\right]$$

This is the equation used to determine the mass transport stream function Ψ. The baroclinic equations can be obtained by subtracting B4 from B1, and B5 from B2 respectively to give:

$$(B14)\quad \hat{U}_t - f\hat{V} = g'\eta_{2x} + X/\rho_1 H_1 + BU_2 + D\nabla^2\hat{U}$$

$$(B15)\quad \hat{V}_t + f\hat{U} = g'\eta_{2y} + Y/\rho_1 H_1 + BV_2 + D\nabla^2\hat{V}$$

where $\hat{U} = U_1 - U_2$ and $\hat{V} = V_1 - V_2$.

The interface displacement η_2 is obtained from B3 (since $\eta_{1t} = 0$). The velocities U_1 and V_1 required in this equation can be obtained from the streamfunction Ψ and the baroclinic velocities since:

$$U_1 = \hat{U} - (\Psi_y + H_1\hat{U})/H$$

$$V_1 = \hat{V} - (\Psi_x - H_1\hat{V})/H$$

The model consists of solving B13 for the streamfunction Ψ by an iterative method, and then B14, B15, and B3 by a leapfrog time stepping procedure for the baroclinic velocities and the interface displacement. The relaxation method used to solve B13 was successive over-relaxation (S.O.R.) with the optimum over-relaxation parameter in the absence of topography, i.e.:

$$\frac{2}{1+\sqrt{1-0.5\times[\cos(\pi/M)+\cos(\pi/N)]^2}}$$

where M and N are the number of grid spacings in the x and y

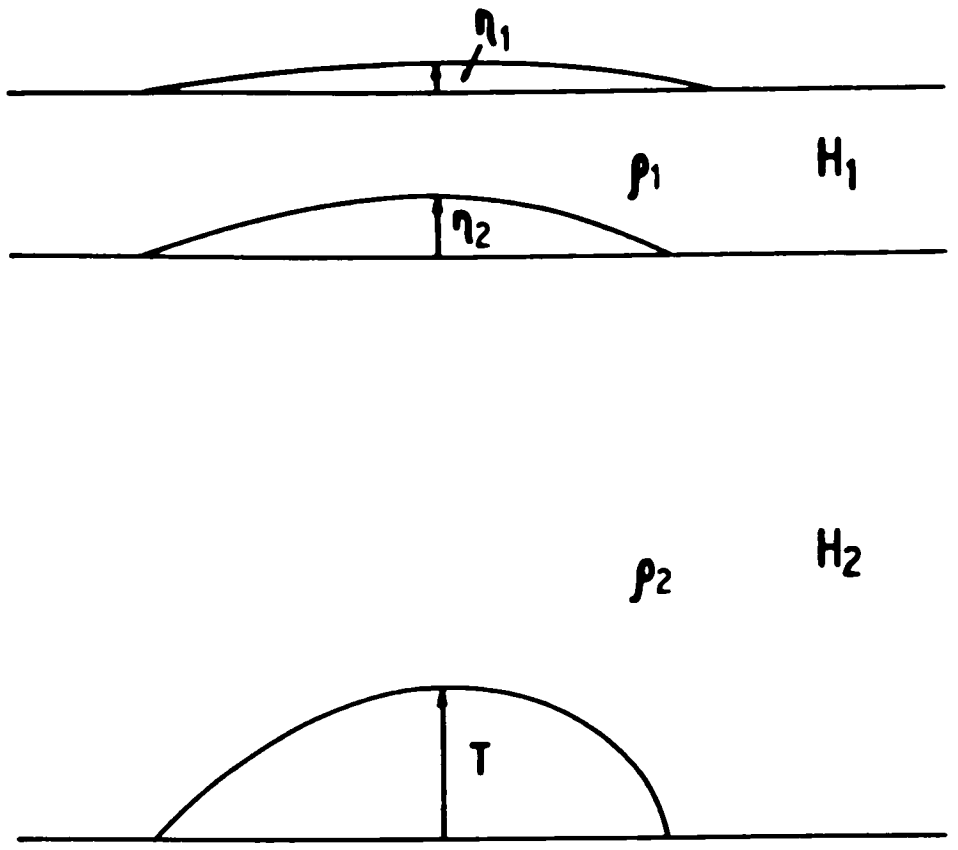

Fig B1 The meaning of various variables in Appendix B.

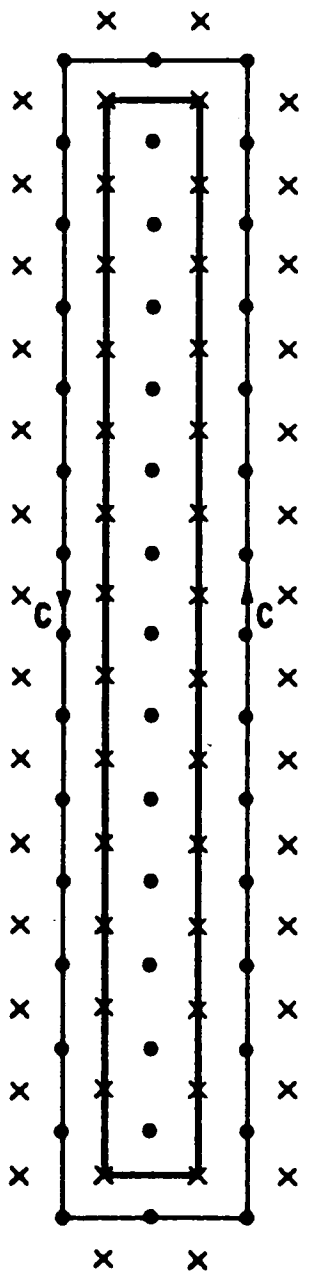

Fig B2 This helps to show how the value of Ψ on the island is solved for.

directions respectively.

The leapfrog timestepping procedure used introduces an unstable solution. This part of the solution can be removed by taking a forward timestep occasionally. In fact, the values of the model variables at timesteps K and K+1 are averaged first (thus losing half a timestep) before the forward timestep is taken. This process was imposed every 300 timesteps.

Boundary conditions and the treatment of the island:

The boundary conditions were free slip on both coast and island. The grid used was grid C of Arakawa and Lamb [1977]. The streamfunction takes the value zero on the coast, and is spatially invariant, but time dependent, on the island. To find the time change of ψ on the island, we take a line integral of B12 around the island. This gives:

$$(B16)\quad \oint_C \left[-\frac{\psi_{yt}}{H}\underline{i} + \frac{\psi_{xt}}{H}\underline{j} \right] . d\underline{s} = \oint_C \left[\frac{f\nabla\psi}{H} + \frac{g' H_1 \nabla \eta_2}{H} + \frac{\tau}{\rho_1 H} + \underline{F}_u \right] . d\underline{s}$$

The island and the path of the line integral are shown on Fig B2. We can see from Fig B2 how the line integral is worked out, given that the values of ψ are evaluated on the crosses and that the integrand on the right hand side is worked out between the crosses. The island can be thought of as a 'large' grid point, with its own value of ψ, and B16 can be solved simultaneously with B13 by S.O.R. to obtain the field for ψ.

The Kelvin wave damper:

In Sections 2.3 and 2.5 a highly effective Kelvin wave

damper was used. A linear damping term was introduced into equations B14, B15 and B3 with a decay time of 10^5 secs (just over one day) for the baroclinic velocities $\hat{u}$, $\hat{v}$ and the interface displacement η_2. This scheme was imposed adjacent to the coastline where the Kelvin wave was to be eliminated. The interface displacement and the baroclinic velocities simply decay to zero, matching the negligible baroclinic activity just to the interior. This scheme is not appropriate where the baroclinic activity just away from the boundary is expected to be high, for instance near the equator where we have equatorial rather than mid-latitude Rossby waves. This scheme is more effective than a simple increase of the lateral viscosity next to the coastline.

Appendix C

Beta-dispersion of low frequency Rossby waves:

Schopf, Anderson and Smith [1981] investigated the dispersion of low frequency Rossby waves on a β-plane. Some of their (corrected) results will be presented here.

The WKB technique is used to give the ray paths. It is valid provided that the scale of the spatial variations is large compared with the wavelength of the waves. This is true for the waves discussed here, since the scale of the variation in f is global but the scale of the waves is only a few degrees.

At any locality the waves are assumed to be approximately sinusoidal:

$$v=\mathrm{Re}\{A(x,y,t)\exp[i\,\phi\,(x,y,t)]\}$$

where the wave amplitude A varies slowly in space and time in comparison with variations in the phase ϕ. The total wavenumbers k, l and frequency w are defined as derivatives of the phase:

$$k=\partial\phi/\partial x \quad ; \quad l=\partial\phi/\partial y \quad ; \quad w=-\partial\phi/\partial t$$

and k, l and w obey the dispersion relation

$$(C1) \qquad w=\Omega(x,y,t;k,l)=-\beta\,k/(k^2+l^2+\beta^2y^2/c^2)$$

where c is the velocity associated with the particular baroclinic mode. Mathematically, the dispersion relation can be interpreted

as a non-linear first-order differential equation for the phase of the waves. The group-velocity or ray paths

$$(C2) \qquad dx/dt = \partial w/\partial k$$

$$(C3) \qquad dy/dt = \partial w/\partial l$$

are the bi-characteristics along which the partial differential equation C1 can be replaced by ordinary differential equations for w, k, l:

$$(C4) \qquad dk/dt = -\partial \Omega /\partial x$$

$$(C5) \qquad dl/dt = -\partial \Omega /\partial y$$

$$(C6) \qquad dw/dt = \partial \Omega /\partial t$$

Physically, the ray paths are important because the wave action is carried along the rays.

Here the propagating medium is time-independent and does not vary in the east-west direction. This has the consequence that along a ray the frequency w and the east-west wavenumber k are both conserved. For the dispersion relation C1, C2-C6 become:

$$(C7) \qquad dx/dt = w/k + 2w^2/\beta$$

$$(C8) \qquad dy/dt = (2w^2/\beta k)l$$

$$(C9) \qquad dl/dt = -(2w^2 \beta /kc^2)y$$

The solution of C7 is linear in t, and the solutions of the

coupled equations C8 and C9 are sinusoidal. If:

$$\Theta = -2w^2 t/kc \tag{C10}$$

$$y_T^2 = (c^2/\beta^2)(-\beta k/w - k^2) \tag{C11}$$

$$= y_o^2 + l_o^2 c^2/\beta^2 \tag{C12}$$

where the subscript 0 refers to the initial values of y and l, and the Rossby waves are generated from a plane eastern boundary aligned along x=0, then:

$$x = x_o - \frac{c}{2\omega}(1 - 4\omega^2 y_T^2/c^2)^{\frac{1}{2}}\Theta \tag{C13}$$

$$y = y_T \cos(\Theta_o - \Theta) \tag{C14}$$

$$l = -\beta y_T/c \sin(\Theta_o - \Theta) \tag{C15}$$

$$\Theta_o = \begin{cases} -\cos(y_o/y_T) & \text{if } l_o > 0 \\ \cos(y_o/y_T) & \text{if } l_o < 0 \end{cases} \tag{C16}$$

where y_T is the maximum latitude to which Rossby wave energy along this particular ray may penetrate. The ray path shape depends on only y_T and Θ . x_o and Θ_o fix the phase of the sinusoidal ray path in relation to the coast.

In two of the diagrams of Section 2.3, lines are drawn north of which Rossby wave activity is expected to be low. The lines drawn represent the caustics where adjacent rays cross. The equation of the caustic is calculated for $l_o=0$ in Schopf, Anderson and Smith [1981]. For $l_o \neq 0$, a simple computer program was constructed which used equations C13 to C16, and calculated

the crossing points of adjacent rays. This program was checked against the analytic formula appropriate when $l = 0$ and found to be satisfactory.

For forcing B of Section 2.3, $l_0 = 0$ and the line drawn reflects this. For forcing A, there will be large amounts of energy at $l_0 = \pm 2\pi/(4\times10^6)$ m^{-1}, because of the sinusoidal nature of the forcing in the northern half of the basin. The lines drawn represent the caustics appropriate to $l_0 = -2\pi/(4\times10^6)$ m^{-1}, since this caustic is farther north of the other.

Appendix D

A simple model of the transport forced by a baroclinic Kelvin wave over topography.

The equation governing the streamfunction is B13 written here as D1:

$$(D1)\quad \left(\frac{\Psi_{xt}}{H}\right)_x + \left(\frac{\Psi_{yt}}{H}\right)_y = curl_z\left[\frac{f\nabla\Psi}{H} + \frac{g' H_1 \nabla\eta_2}{H} + \frac{\underline{\tau}}{\rho_1 H} + \underline{F}\right]$$

The term involving η_2 represents the forcing of the barotropic mode by the baroclinic. Simple scale analysis shows that at annual period and for reasonable slopes, the time dependent terms are small, so that only the problem of steady state forcing need be considered. For an f-plane (D1) can be simplified farther in the region where the wind stress is zero to:

$$(D2)\quad f T_x \psi_y - f T_y \psi_x + g' H_1 (T_x \eta_{2y} - T_y \eta_{2x}) + H^2 curl_z(\underline{F}) = 0$$

If the topography varies with latitude only then D2 becomes:

$$(D3)\quad f T_y \psi_x - H^2 curl_z(\underline{F}) = -g' H_1 T_y \eta_{2x}$$

If the north-south scale of the response is much greater than the zonal scale, and η_2 is as given by Eq 2.8 then D3 can be approximated by D4:

$$(D4)\quad \psi_{xxxx} - \lambda \psi_x = \mu e^{-x/a}$$

Since $\underline{F} \simeq -\frac{\rho}{H}\nabla^2\psi_y \underline{i} + \frac{D}{H}\nabla^2\psi_x \underline{j}$

where $\lambda = fT_y/HD$; $\mu = -(g' H_1)^{\frac{1}{2}} T_y f \eta_o / HD$

By analogy with the Munk solution we anticipate a western frictional boundary layer if $T_y > 0$ and an eastern frictional boundary layer if $T_y < 0$. A particular integral of D4 is:

$$\psi = A\, e^{-x/a} \quad \text{where} \quad A = \mu a^4/(1+\lambda a^3)$$

while the appropriate complementary function, chosen to give $\psi = \psi_{xx} = 0$ on eastern and western boundaries is:

(D5)

$$\psi = B + C\, e^{-x/a} + E\, e^{-\nu x/2} \mathrm{COS}(\sqrt{3}\,\nu\, x/2) + F\, e^{-\nu x/2} \mathrm{SIN}(\sqrt{3}\,\nu\, x/2)$$

where $\nu = \lambda^{\frac{1}{3}}$

If we solve for B,C,E,F we find that for negative slopes ($T_y < 0$), E & F are negligible in comparison to B & C, and for positive slopes ($T_y > 0$), B & C are negligible in comparison to E & F. Approximate values of the coefficients in these cases are:

$$B=C=0 \quad ; \quad E=-A \quad ; \quad F=A(1+2/\nu^2 a^2)/\sqrt{3} \qquad (T_y > 0)$$

$$E=F=0 \quad ; \quad B=-A(1-1/\nu^2 a^2) \quad ; \quad C=-A/\nu^2 a^2 \quad (T_y < 0)$$

The solutions of the above equation expected for the parameter values used (H was taken as 1000 m) are shown in Figs D1 and D2 for the cases of negative and positive slope respectively. Also shown is the streamfunction in Figs 2.17(a),(b) at y=800 km (i.e.

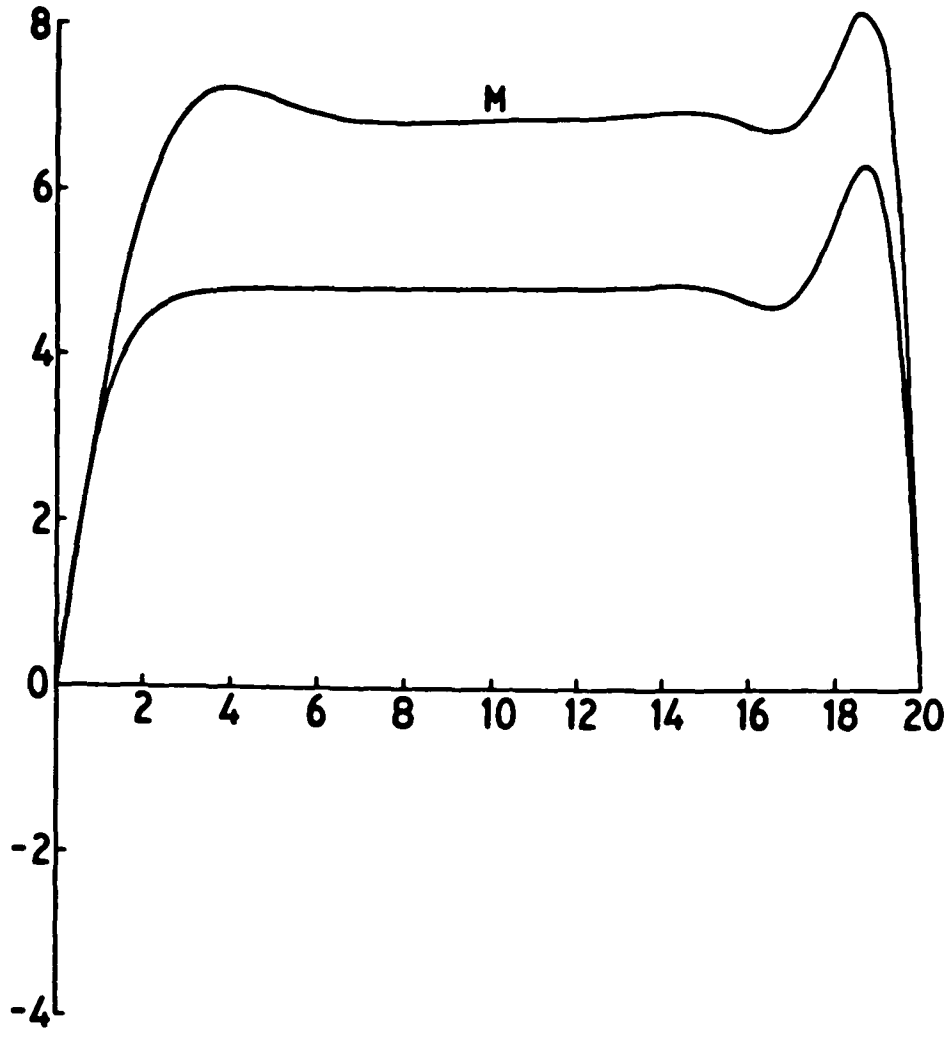

Fig D1 The streamfunction (in units of one tenth of a Sverdrup) plotted vs longitude (in units of 100 km). This diagram is for the case of negative slope, where topographic Rossby waves travel eastward. The curve marked M is from the more complex model. The other curve is evaluated assuming Eq (D4).

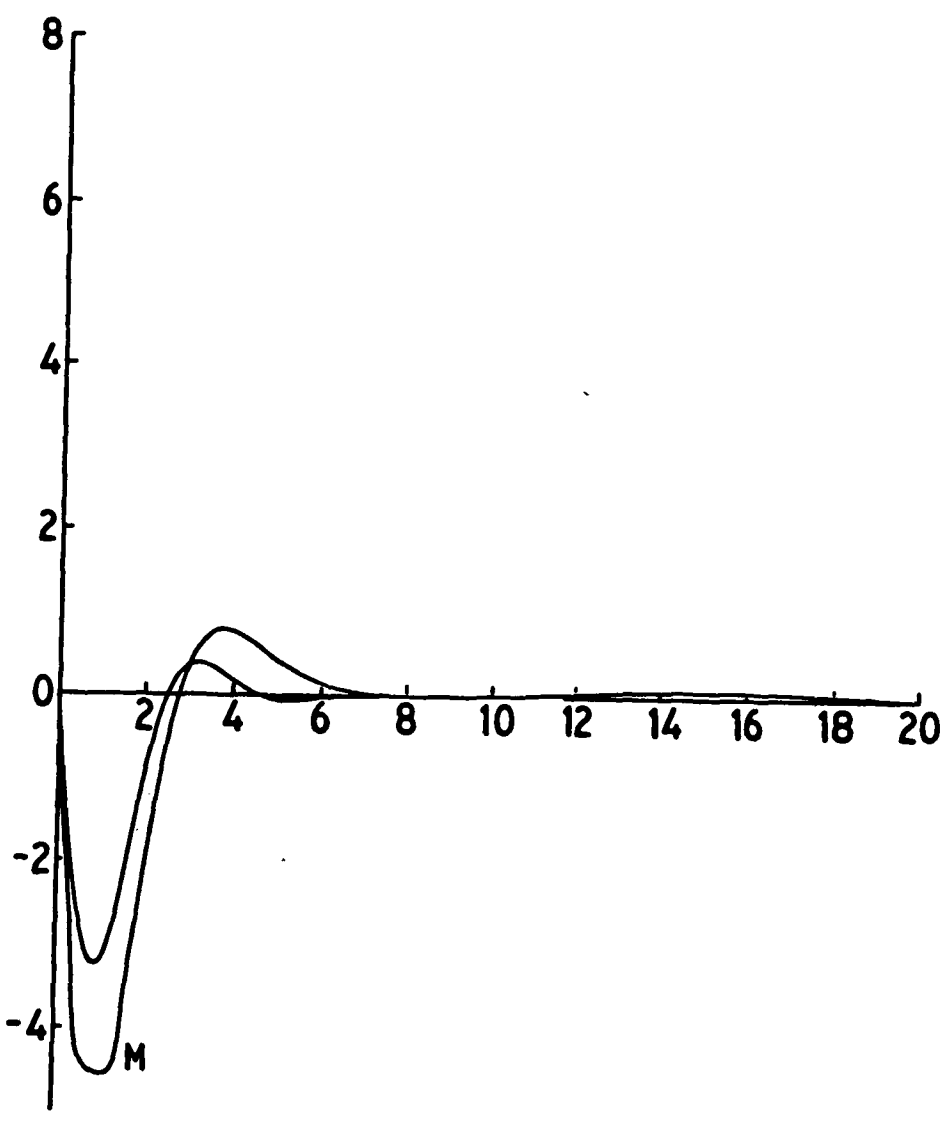

Fig D2 The corresponding curves for positive slope (see Fig D1). The streamfunction is localised near to the western boundary. The curve marked M is from the more complex model.

at the intermediate depth H=1000 m. See Fig 2.16). These curves are marked M. In both cases there is good agreement between the simple model of the appendix and the more complex integration of Section 2.5. Departures are expected due to the y variation in the problem, and deviations of the coastally trapped baroclinic signal from the exponential form of Eq 2.8. These latter will be due to both friction and feedback from the barotropic mode.

Appendix E

The smoothing of the bottom topography.

The bottom topography was obtained from a file containing world surface topography on a 1° grid. The coastline used was derived from this, and the Mediterranean Sea, the Pacific Ocean, and any lakes were removed. The basin (defined with respect to the grid for the streamfunction) extends from 10°S to 50°N, and from 99°W to 13°E. The five islands were to a certain extent manufactured. In particular the Bahamas were represented by a single island, Puerto Rico was joined to the Dominican Republic, thus eliminating the Mona Passage, and the the two small eastern islands are intended to represent the Lesser Antilles.

In order to obtain reasonable results from the numerical model, it was necessary to smooth the bottom topography. The way in which this is done is important, because it is the topography which substantially reduces the amplitude of the variation of the Florida Current, and the forcing of the streamfunction (and thus the phase of the transport variations) depends on the gradients of both topography and wind stress.

To start with, it was decided to fix the topography of the Florida Straits, and allow the rest of the ocean bottom to relax into a smoother field. A very simple Laplacian smoother was used, such that the increment in depth, ΔH, was:

$$\Delta H = \delta \ (HE + HW + HN + HS - 4 \times H)$$

where HE, HW, HN and HS are respectively the most up to date depths to the east, west, north and south of the current grid

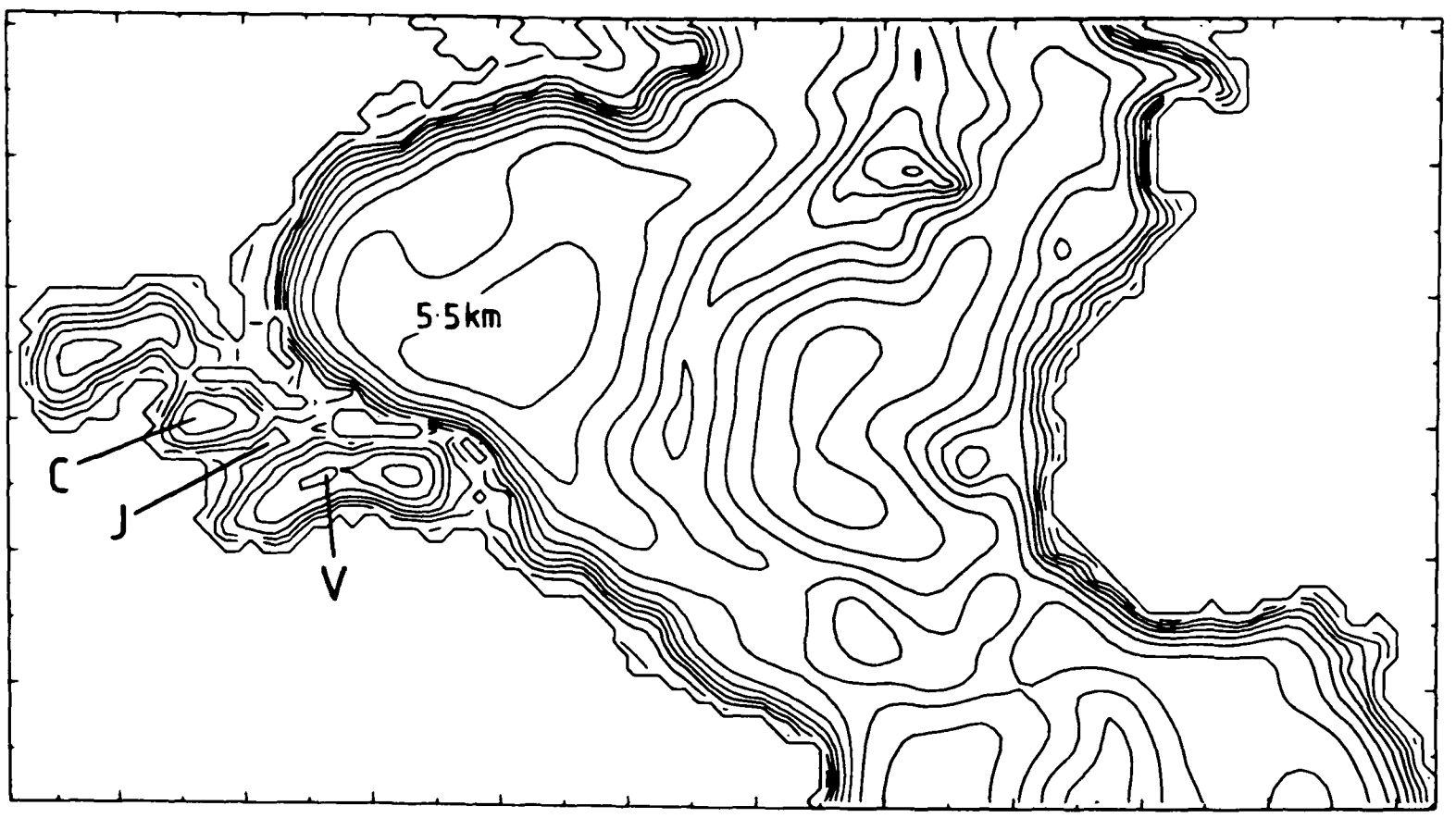

Fig E1 A plot of the North Atlantic bottom topography used. The contour interval is 500 m. The Venezuela basin (V), the Cayman basin (C) and the Jamaica ridge (J) are also shown.

point. Where one of these corresponded to coastline or an island, a value of 400 m was used. At the northern and southern boundaries HN and HS took the value H. The extent of the smoothing, determined by the size of δ, was made dependent on the depth. We wished to preserve as far as possible the shallowness of the shallow topography, since it is this shallowness which blocks the transport variations near the western boundary, but at the same time smooth the data. The degree of smoothing was therefore increased with depth. Thus, close to a topographic ridge, the deeper points decreased their depth more than the shallow points increased their depth. For depths greater than 1500 m, the factor δ was given by:

$$\delta = 0.1 \times (H/4000\ m)^2$$

On the other hand, there are areas, e.g. the Florida Shelf, where the topography is too shallow to be handled by the model. For depths less than 1000 m, δ simply took the value 0.1. Between 1000 m and 1500 m δ was 9/640, the value given by the above formula at 1500 m. The above smoothing operation was applied ten times. Any depths that were then still less than 400 m were set to 400 m. The depth of the North Atlantic after this smoothing operation is shown on Fig E1. The contour interval is 500 m.

Appendix F

The apparent addition to mean transport forced by coupling of modes over topography:

Consider a linear model forced by wind stress patterns A, B, C, D. The model is forced by wind stress A for a season, then wind stress B for a season (with no gradual transition), then wind stress C for a season etc. . Let us assume that the seasons are of equal length. At the end of the first season, the model response at a point is a(1), where a(t) is the model response as a function of time (in units of seasons) at this point for a switched on wind stress pattern A. Similarly for b(t), c(t), and d(t). At the end of the second season of integration the response is b(1)-a(1)+a(2), because wind stress B-A has been applied for one season, and wind stress A has been left switched on. Similarly at the end of the third season the response is c(1)- b(1)+ b(2)- a(2)+ a(3), etc. . At the end of the first year, the annual mean (calculated by adding the response at the end of each season and dividing by four) is:

$$(a(4)+b(3)+c(2)+d(1))/4$$

Similarly at the end of the second year of integration, the mean is:

$$(a(8)+b(7)+c(6)+d(5))/4$$

and so on. If the model takes several years to reach equilibrium

for a given applied wind stress, and the sum of the wind stresses is zero, then the mean response (calculated in the above way) will gradually reach zero, but for the first few years there is no reason why it should be zero, since the responses a, b, c, d added to give the mean are taken at different times.

This argument can be trivially carried over to the case of twelve months of equal length, where we expect a similar result (i.e. the mean will tend to zero with increasing time). In fact the months are not of equal length, but are still all weighted equally by the procedure of adding the response at the end of each month and dividing by twelve. This will result in a slight deviation from zero for the mean, but certainly nothing as large as a quarter of a Sverdrup. This large mean for the baroclinic contribution arises because the model has not reached the stage where the baroclinic response is exactly repeated year after year. This will only happen after several decades of integration for the North Atlantic model of Chapter 3, when the Rossby waves have fully reached across the basin. In fact we have only integrated the model for five years. The basic features of the annual variation would not be changed by increased length of integration, but the anomalous annual mean would eventually be removed.

The extent to which the barotropic response is in equilibrium after a full month's forcing:

This is shown on Fig F1, which shows the response of the homogeneous model of the North Atlantic of Chapter 3 at the Florida Straits as a function of time (days) for the July seasonal wind stress. The response after a month's integration is almost equilibrium. The presence of bottom topography serves

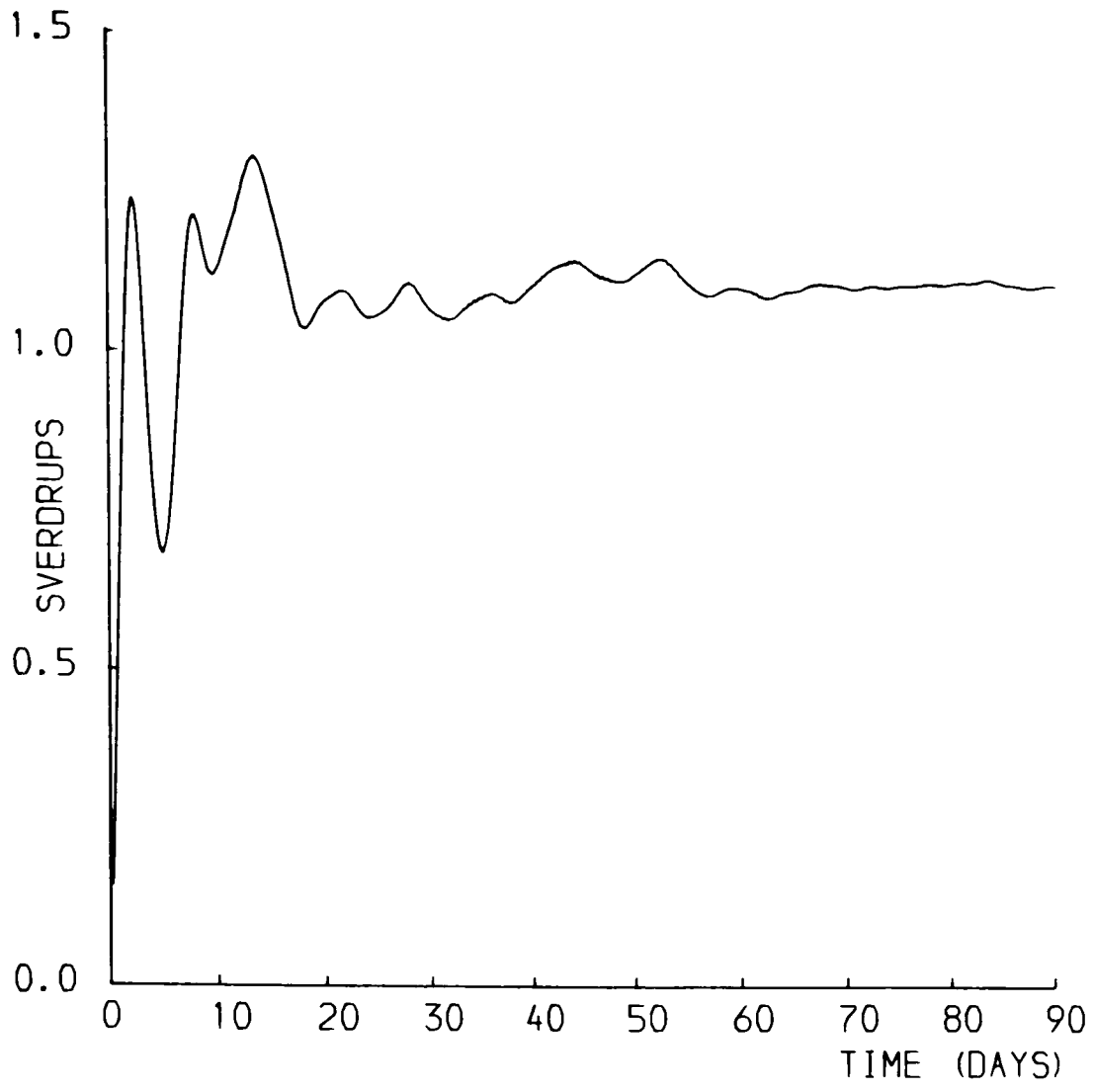

Fig F1 The response of the one layer model at the Florida Straits as a function of time (days) for the July seasonal wind stress.

to remove the basin modes which are present if no bottom topography is used.

References:

Adams,J.K. and V.T.Buchwald (1969) The generation of continental shelf waves. J.Fluid.Mech,35,815-826

Anderson,D.L.T. (1979a) Modelling the seasonal cycle in the Atlantic. In "Seminaire de dynamique des fluides geophysiques et de modelisation numerique applique a l'oceanographie," CNEXO, Paris.

Anderson,D.L.T. (1979b) Basin Models: The general circulation of regions of the world ocean. Dynam.Atmos.Oceans.,3,345-371

Anderson,D.L.T. and P.D.Killworth (1977) Spin-up of a stratified ocean, with topography. Deep-Sea Research,24,709-732

Anderson,D.L.T.,Bryan,K.,Gill,A.E. and R.C.Pacanowski (1979) The transient response of the North Atlantic: Some model studies. J.Geophys.Res.,84[C8], 4795-4815

Anderson,D.L.T. and P.B.Rowlands (1976) The Somali Current response to the Southwest Monsoon: the relative importance of local and remote forcing. J.Mar.Res.,34,395-417

Arakawa,A. and V.R.Lamb (1977) Computational Design of the basic dynamical processes of the UCLA General Circulation Model. Methods in Computational Physics pages 173-265, Academic Press.

Blaha,J. and W.Sturges (1981) Evidence for wind-forced circulation in the Gulf of Mexico. J.Mar.Res., 9(4),711-734

Brooks,I.H. (1979) Fluctuations in the transport of the Florida Current at periods between tidal and two weeks. J.Phys.Oceanogr.,9(5),1048-1053

Bryan,K. (1969) A numerical method for the study of the world ocean. J.Comp.Phys.,4,347-376

Bunker,A.F. and R.A.Goldsmith (1979) Archived time-series of Atlantic Ocean meteorological variables and surface fluxes. Woods Hole Oceanographic Institution, Tech Rep. WHOI79-3,Woods Hole,MA,27pp.

Fuglister,F.C. (1951) Annual variations in current speeds in the Gulf Stream region. J.Mar.Res,10,119-127

Gill,A.E. and Bryan,K. (1971) Effects of geometry on the circulation of a three dimensional southern hemisphere ocean model. Deep-Sea Research,18,685-721

Gill,A.E. and Niiler,P.P (1973) The theory of the seasonal variability in the ocean. Deep-Sea Res.,20,141-177

Gunn,J.T. and D.R.Watts (1982) On the currents and water masses north of the Antilles/Bahamas arc. J.Mar.Res.,40(1),1-18

Hansen,D.V. and R.L.Molinari (1979) Deep currents in the Yucatan Strait. J.Geophys.Res.,84(C1),359-362

Holland,W.R. and A.D.Hirschman (1972) A numerical calculation of the circulation in the North Atlantic Ocean. J.Phys.Oceanogr.,2(4),336-354

Holland,W.R. and P.B.Rhines (1980) An example of eddy-induced ocean circulation. J.Phys.Oceanogr.,10(7),1010-1031

Hsieh,W.W.,Davey,M.K. and R.C.Wajsowicz (1983) The free Kelvin wave in finite difference numerical models. Submitted to J.Phys.Oceanogr.

Kroll,J. and P.P.Niiler (1976) The transmission and decay of barotropic topographic Rossby waves incident on a continental shelf. J.Phys.Oceanogr.,6,432-450

Larsen,J.C. and T.B.Sanford (1985) Florida Current Volume transports from Voltage measurements. Science,227,302-304

Lee,T.N.,Schott,F.A. and R.L.Zantopp (1985) Florida Current: Low-frequency variability as observed with moored current meters during April 1982 to June 1983. Science,227,298-302

Leetmaa,Ants and A.F.Bunker (1978) Updated charts of the mean annual wind stress, convergences in the Ekman layers and Sverdrup transports in the North Atlantic. J.Mar.Res.,36(2),311-322

Leetmaa,A.,Niiler,P.P. and H.Stommel (1977) Does the Sverdrup relation account for the Mid-Atlantic circulation? J.Mar.Res.,35(1),1-10

Longuet-Higgins,M.S. (1949) The electrical and magnetic effects of tidal streams. Mon.Not.R.Astr.Soc.Geophys.Suppl.,5,285-307

Longuet-Higgins,M.S.,Stern,M.E. and H.Stommel (1954) The electric field induced by ocean currents and waves, with applications to the method of towed electrodes. Papers in Physical Oceanography and Meteorology, Massachusetts Institute of Technology and Woods Hole Oceanographic Inst., XIII,1-37

Malkus,W.V.R. and M.E.Stern (1952) Determination of ocean transports and velocities by electromagnetic effects. J.Mar.Res.,11,97-103

Maul,G.A.,Chew,F.,Bushnell,M. and D.A.Mayer (1985) Sea level variation as an indicator of Florida Current Volume transport: Comparisons with direct measurements. Science,227,304-307

Molinari et al (1985) Subtropical Atlantic Climate Studies: Introduction. Science,227,292-294

Molinari,R.L.,Wilson,W.D. and K.D.Leaman (1985) Volume and heat transports of the Florida Current: April 1982 to August 1983. Science,227,295-297

Montgomery,R.B. (1941) Sea level difference between Key-West and Miami, Florida. Jour.Mar.Res.,4,32-37

Morrison,J.M. and W.D.Nowlin Jr. (1982) General distribution of water masses within the eastern Caribbean sea during the Winter of 1972 and the Fall of 1973. J.Geophys.Res.,87(C6),4207-4229

Niiler,P.P. and W.S.Richardson (1973) Seasonal variability of the Florida Current. J.Mar.Res.,31,144-167

Olson,D.B.,Schott,F.A.,Zantopp,R.J. and K.D.Leaman (1984) The mean circulation east of the Bahamas as determined from a recent measurement program and historical XBT data. J.Phys.Oceanogr.,14,1470-1487

Richardson,W.S. and W.J.Schmitz Jr. (1965) A technique for the direct measurement of transport with application to the Straits of Florida. J.Mar.Res.,23,172-185

Roemmich,Dean (1981) Circulation in the Caribbean Sea: a well resolved inverse problem. J.Geophys.Res.,86(C9),7993-8005

Sanford,T.B. (1982) Temperature transport and motional induction in the Florida Current. J.Mar.Res.,40,Suppl.,621-639

Schmitz,W.J.Jr. and W.S.Richardson (1968) On the transport of the Florida Current. Deep-Sea Research,15,679-693

Schopf,P.S.,Anderson,D.L.T. and R.Smith (1981) Beta-dispersion of low-frequency Rossby waves. Dynam.Atmos.Oceans.,5,187-214

Schott,F.A. and R.J.Zantopp (1985) Florida Current: Seasonal and Interannual Variability. Science,227,308-311

Schulman,E.E. and Niiler,P.P. (1970) Topographic effects on the wind driven ocean circulation. Geophys.Fluid.Dyn.,1,439-457

Semtner,A.J. (1974) An Oceanic General Circulation Model with bottom topography. Technical Report No. 9, Department of Meteorology, University of California, Los Angeles.

Spain,P.F.,Dorson,D.L. and H.T.Rossby (1981) PEGASUS: A simple, acoustically tracked, velocity profiler. Deep-Sea Res.,28(12A),1553-1567

Stommel,H.M. (1948) The westward intensification of wind-driven ocean currents. Trans.Amer.Geophys.Union.,29,202-206

Wertheim,G.K. (1954) Studies of the electrical potential between Key West, Florida and Havana, Cuba. Trans.Amer.Geophys.Union,35,872-882

Wise,C.W and R.H.Simpson (1971) The tropical analysis program of the National Hurricane Centre. Weatherwise,164-173

Worthington,L.V. (1977) Intensification of the Gulf Stream after the Winter of 1976-77. Nature,270,415-417

Wu,J. (1980) Wind stress coefficients over sea surface near neutral conditions - A revisit. J.Phys.Oceanogr.,10,727-740

Wunsch,C. and M.Wimbush (1977) Simultaneous pressure, velocity and temperature measurements in the Florida Straits. J.Mar.Res.,35(1),75-104

Veronis,G. and Stommel,H. (1956) The action of variable wind stresses on a stratified ocean. J.Mar.Res.,15,43-75 ~~the barotropic mode.~~